

Scholar@UPRM

Dynamic properties and seismic response of the cable structures and towers of the Arecibo Observatory

Item Type	Dissertation
Authors	Morales Brignac, Juan C.
Download date	2026-05-14 07:53:38
Link to Item	https://hdl.handle.net/20.500.11801/1848

Dynamic Properties and Seismic Response of the Cable Structures and Towers of the Arecibo Observatory

By

Juan Carlos Morales-Brignac

A thesis submitted in partial fulfillment of the requirements for the degree of

Doctor of Philosophy
in Civil Engineering

University of Puerto Rico
Mayagüez Campus
May 2006

Approved by:

Luis E. Suárez-Colche, Ph.D.
President, Graduate Committee

Date

Ricardo López-Rodríguez, Ph.D.
Member, Graduate Committee

Date

José A. Martínez-Cruzado, Ph.D.
Member, Graduate Committee

Date

Felipe J. Acosta-Costa, Ph.D.
Member, Graduate Committee

Date

Héctor Jiménez, Ph.D.
Representative of Graduate Studies

Date

Ismael Pagán-Trinidad, M.S.
Chairperson of the Department

Date

ABSTRACT

This investigation was requested by the staff of the Arecibo Observatory to determine whether the towers and cables that support the suspended platform are capable of resisting a maximum-credible earthquake in the elastic regime. The Arecibo Observatory is one of the most important research centers in the world for astronomic and ionospheric studies and thus maintaining its structural integrity is a top priority. Modal analysis is performed on detailed three-dimensional finite element models to determine the natural response. Three different types of modes are revealed - platform modes, tower modes and cable modes - in addition to strong interactions between them. Very strong interaction modes are recorded in the range of periods between 1.8 and 0.7 seconds. Modal time-history linear analyses are performed to determine the seismic response. Nonlinear direct-integration time history analysis with large displacements yield nearly identical results which validates the modal time-history linear analysis. Five different earthquake records are considered in the final seismic studies. These represent the expected range of seismic hazards for Puerto Rico. The towers are nearly capable of resisting in the elastic regime the seismic loading specified by the UBC-97 building code. However, the top two segments of the towers narrowly exceed their elastic moment capacity. The towers do not tolerate, and could even collapse, if exposed to the higher seismic demands expected in the cities of Ponce and Mayagüez. A preliminary retrofit investigation shows that the use of Fiber Reinforced Polymers (FRP) is the best alternative to boost the moment capacity of the towers to a comfortable level. This alternative requires further research into the capacity, durability and cost of this option. Several alternative locations for the placement of accelerometers are recommended.

RESUMEN

Esta investigación fue solicitada por el personal del Observatorio de Arecibo para determinar si las torres y los cables que sostienen la plataforma suspendida son capaces de resistir un terremoto máximo-probable en el régimen elástico. El Observatorio de Arecibo es uno de los centros de investigación astronómica e ionosférica más importantes del mundo, y la conservación de su integridad estructural es una prioridad. Se utiliza análisis modal para determinar la respuesta vibratoria natural con modelos de elementos finitos en tres dimensiones. Se hallan tres diferentes tipos de modos de vibración – modos de la plataforma, modos de las torres, y modos de los cables – en adición a fuertes interacciones entre ellos. Las interacciones más fuertes se encuentran en el intervalo de periodos entre 1.8 – 0.7 seg. Se utiliza la técnica de superposición modal para hallar la respuesta sísmica. Esta técnica lineal se validó al hallar resultados muy comparables con un análisis no-lineal considerando grandes desplazamientos y basado en técnicas de integración directa. Se utilizaron los registros de cinco diferentes terremotos para el estudio sísmico final. Estos representan la gama de peligrosidad sísmica para Puerto Rico. Las torres estuvieron muy cercanas a cumplir en el régimen elástico con la demanda sísmica especificada por el código UBC-97. Sin embargo, los dos segmentos superiores de las torres no cumplen por un escaso margen. De ser expuestas a las demandas sísmicas esperadas para las ciudades de Ponce y Mayagüez, las torres sufrirían deformaciones plásticas y podrían colapsar. Una investigación preliminar muestra que el uso de polímeros reforzados con fibras (FRP, por sus siglas en inglés) representa la mejor alternativa para cómodamente asegurar la respuesta elástica de las torres durante un sismo máximo-probable. Se requieren investigaciones adicionales con respecto a la capacidad, durabilidad y costo de los FRP. Se recomiendan varias localizaciones en el Observatorio para colocar acelerómetros.

In memory of my grandfathers

José Dionisio Morales and Michael Brignac.

José Dionisio dreamed all his life of pursuing a PhD degree
but never found the opportunity.

Michael barely got the chance to dream
his life having been cut short so very early by pneumonia.

I share this realized dream with you.

ACKNOWLEDGEMENTS

I wish to thank Dr. Luis Suárez, my thesis advisor, for the opportunity to work with him on this project and for being such an excellent role model; Dr. Pierre Schmidt, Dr. Roberto Lorán, and Dr. Dennis Alicea – Dean of Engineering, Provost and Chancellor, respectively - at Turabo University for providing the release time and the financial support required to pursue the PhD degree; Dr. Robert Brown, Dr. Sixto González, Ing. José Maldonado and Ing. Felipe Soberal of the Arecibo Observatory for supporting this research; Dr. Ricardo López, Dr. José Martínez-Cruzado, and Dr. Felipe Acosta for their participation in the graduate committee and for their suggestions; Ing. Ismael Pagán, Department Head of Civil Engineering and Surveying at the University of Puerto Rico, for this opportunity and for his friendship; Dr. Luis Godoy for introducing me to epistemology and for extending my enjoyment of history of science; Ing. Augusto Poitevín, Ing. Gustavo Pacheco, Ing. Edgardo Vélez, Ing. Rolando García, and Ing. Jorge Ayala, fellow PhD classmates and good friends, for their suggestions; Dr. Drianfel Vázquez for providing the SIMQKE artificial earthquake accelerogram compatible with the UBC-97 design spectrum; Ing. Jaffet Martínez of the Puerto Rico Strong Motion Program, for updating the information regarding seismic activity in Puerto Rico between 1999 and 2006; Ing. Nelson Morrison and the CSI technical-support group, for their assistance with the SAP2000 program; Loreen Torres, Marcel Morales and Natalia Morales, my wife and children, for their loving support and for providing all the motivation I ever required; Dr. Juan Enrique Morales and Ruth Brignac, my parents, for their ever-present support of the educational pursuits of their children; Lina Morales, my aunt, for praying for my safety in my trips between San Juan and Mayagüez; Inez Morales and Dr. Ramón Dávila, my sister and my brother in law, for housing me in Hormigueros during preliminary-exams week.

TABLE OF CONTENTS

List of Tables.....	xiii
List of Figures.....	xix
Chapter 1 Introduction.....	1
1.1 Justification.....	1
1.2 Objectives.....	1
1.3 Background of the Structure	2
1.4 Literature Survey.....	7
1.4.1 Software Package vs. Custom-made Programming.....	7
1.4.2 Linear vs. Nonlinear Analysis.....	10
1.4.3 Material Nonlinearities.....	10
1.4.4 Geometric Nonlinearity – Cable-Sag Effect.....	10
1.4.5 Geometric Nonlinearity – Large Displacements.....	12
1.4.6 Fixed Boundary Conditions vs Soil-Structure Interaction.....	13
1.4.7 Earthquake Source for Seismic Study.....	14
1.4.8 Field Measurements.....	15
1.5 Scope of the Study.....	16
1.6 Methodology.....	17
1.7 Preview of the Three Basic Finite Element Models.....	18
1.7.1 Preview of Model A: Uniform Platform, No Tiedown Cables.....	19
1.7.2 Preview of Model B: Uniform Platform, With Tiedown Cables.....	20
1.7.3 Preview of Model C: Distributed Platform, With Tiedown Cables.....	20

1.8 General Organization of this Thesis.....	21
Chapter 2 Static Non-Linear P-Delta Analysis – Model A.....	22
2.1 Finite Element Model Details of Original Model A.....	22
2.1.1 Model Geometry.....	22
2.1.2 Reinforced Concrete Towers.....	23
2.1.3 Tower Saddles.....	27
2.1.4 Concrete Anchors.....	29
2.1.5 Suspended Platform.....	30
2.1.6 Cables.....	33
2.2 Geometric Stiffness Requirement for Cable Structures.....	36
2.3 Case 1: Self-Weight Only (No Preloading of Cables).....	38
2.3.1 Initial Guess on Platform Descent due to Cable Stretch.....	38
2.3.2 Analysis Case Setup.....	39
2.3.3 Results and Validation Checks.....	40
2.3.4 Initial Guess for the Applied Temperatures (Cable Preload).....	46
2.4 Case 2: Achieving Actual Equilibrium State of Structure due to Dead Load.....	47
2.4.1 Iteration of Temperature Values.....	48
2.4.2 Discussion of Results of Case 2.....	50
2.5 Finite Element Model Details of Updated Model A.....	51
2.6 Comparison: Original Model A vs. Updated Model A.....	54
2.7 Major (M_{33}) Bending Moment Distribution in Towers.....	55
2.7.1 Suggested Cause for Bending Distribution.....	55

2.7.2 Verification of Unbalanced Moment at Auxiliary Saddle.....	57
2.7.3 Counterbalancing Effect of Service Cables.....	59
2.7.4 Analytical Estimate of Tension in Service Cables and Estimate of Counterbalancing Moment due to Service Cables.....	61
2.7.5 Finite Element Estimate of Counterbalancing Moment due to Service Cables.....	63
2.7.6 Hypothetical Consideration of Full Projected Concurrency at Main Saddle.....	68
2.7.7 Hypothetical Consideration of Projected Concurrency at Auxiliary Saddle.....	69
2.7.8 Conclusions on the Issue of Auxiliary Saddle Unbalanced Moment.....	73
Chapter 3 Static Non-Linear P-Delta Analysis – Model B.....	74
3.1 Finite Element Model Details.....	74
3.2 Achieving Verticality of Towers.....	78
3.2.1 Iterations on Cable Preload.....	78
3.2.2 Equilibrium Check.....	80
3.2.3 Discussion of Iteration Results.....	81
Chapter 4 Static Non-Linear P-Delta Analysis – Model C.....	83
4.1 Finite Element Model Details.....	83
4.2 Weight Distribution in Platform.....	86
4.3 Maintaining the Platform Level.....	88
4.3.1 Results with Original Weight Distribution.....	89
4.3.2 Redistribution of Weight.....	93
4.4 Conclusions on the Deformed Equilibrium State due to Dead Loads.....	97

Chapter 5 Dynamic Properties	98
5.1 Introductory Concepts.....	98
5.2 Modal Analysis of Model A (Uniform Platform, No Tiedowns).....	99
5.2.1 Results.....	99
5.2.2 Validation of Independent Cable Modes.....	102
5.2.3 Validation of Tower Modes.....	103
5.2.4 Sensitivity Study: Effect of Service Cables.....	105
5.3 Modal Analysis of Model B (Uniform Platform, With Tiedowns).....	106
5.3.1 Results.....	106
5.3.2 Sensitivity Study: Modal Analysis Using I_{cracked} for– Model B.....	114
5.3.3 Sensitivity Study: Modal Analysis Using $I_{\text{effective}}$ for Towers.....	119
5.3.4 Sensitivity Study: Isolation of Platform Modes.....	120
5.3.5 Sensitivity Study: Effect of Bridge and Service Cables.....	125
5.3.6 Conclusions on Modal Analysis of Model B.....	130
5.4 Modal Analysis of Model C (Distributed Platform, With Tiedowns).....	133
5.4.1 Comparison of Modal Results: Calculated mass vs. 50 kip redistrib.....	133
5.4.2 Comparison of Modal Results: Models A, B and C.....	134
5.4.3 Comparison of Several Modal Participating Mass Ratios – Models B and C.....	135
5.4.4 Ranking of Modal Participation Mass Ratios – Model C.....	137
Chapter 6 Initial Studies on Seismic Response	140
6.1 Introduction.....	140
6.2 Uniform Building Code – 1997 (UBC-97) Basis.....	140

6.3 The Loma Prieta Earthquake (October 18, 1989).....	142
6.4 Other Earthquake Records Chosen for Initial Set.....	143
6.5 Modal Time-History Analysis of Loma Prieta Earthquake – Model A	145
6.6 Discussion of Loma Prieta Earthquake Results – Model A.....	148
6.7 Validation Studies – Loma Prieta Earthquake – Model A.....	152
6.7.1 Overturning Moment of Tower T8 per UBC-97.....	153
6.7.2 Overturning Moment of Towers T4 & T12 per UBC-97.....	156
6.7.3 Sensitivity Study: Isolation of Towers.....	159
6.7.4 Examination of Ernst’s Linearized Assumption in Cables.....	160
6.8. Consideration of Large Displacements.....	162
6.8.1 Static P-delta Analysis with Large Displacements Option (Dead Load)..	162
6.8.2 Large-Displacement Non-Linear Direct Integration Case – Loma Prieta	165
6.8.3 Large-Displacement Non-Linear Direct Integration Case – Coalinga....	169
6.9 Results for the Six Earthquake Records: Model A.....	171
6.10 Results for the Six Earthquake Records: Model B.....	173
6.11 Results for the Six Earthquake Records: Model C.....	176
6.12 Two Additional Sensitivity Studies.....	179
6.12.1 Sensitivity Study: Response Using Icracked for Towers.....	179
6.12.2 Sensitivity Study: Response with Bridge and Service Cables.....	181
Chapter 7: Final Studies on Seismic Response.....	184
7.1 Seismic Hazard of the Arecibo Observatory Site.....	184
7.1.1 Overview of Plate Tectonics.....	184

7.1.2 Historical Records of Earthquakes in Puerto Rico.....	186
7.1.3 Selection of Maximum-Credible Earthquakes for Arecibo Site.....	187
7.1.4 SIMQKE Artificial Record Compatible with UBC-97 Design Spectrum	195
7.2 Seismic Response First Run– Unscaled San Salvador-CIG, Northridge- Castaic and Artificial UBC97 Z3, Sb.....	198
7.2.1 Seismic Response First Run – Unscaled Results for Model A.....	198
7.2.2 Seismic Response First Run– Unscaled Results for Model B.....	200
7.2.3 Seismic Response First Run– Unscaled Results for Model C.....	202
7.3 Additional First Run Results for Model C – Unscaled Earthquakes	206
7.3.1 Maximum and Minimum Moments at All Tower Steps.....	206
7.3.2 Biaxial Bending State at All Tower Bases.....	207
7.4 Second Run Results for Model C – Scaled San Salvador and Northridge	208
7.4.1 Maximum and Minimum Moments at All Tower Steps.....	208
7.4.2 Biaxial Bending State at All Tower Bases.....	209
7.5 Third Run Results for Model C – Parkfield and Morgan Hill	210
7.5.1 Maximum and Minimum Moments at All Tower Steps.....	210
7.5.2 Biaxial Bending State at All Tower Bases.....	211
7.6 Recommendation for Accelerometer Locations.....	212
Chapter 8: Failure Criteria.....	214
8.1 Appropriateness of Reinforcement Development Length.....	214
8.2 Introduction to Elastic Failure Criterion for Towers.....	218
8.3 First Run. Unscaled San Salvador, Northridge and Artificial Records.....	223
8.3.1 Elastic Criterion at Base of Towers – First Run.....	223

8.3.2 Elastic Criterion at All Tower Segments– First Run.....	230
8.3.3 Likelihood of Tower Collapse– First Run.....	231
8.4 Second Run. Scaled San Salvador and Northridge.....	240
8.4.1 Elastic Criterion at Base of Towers – Second Run.....	240
8.4.2 Elastic Criterion at All Tower Segments– Second Run.....	244
8.4.3 Likelihood of Tower Collapse– Second Run.....	244
8.5 Third Run. Parkfield and Morgan Hill.....	251
8.5.1 Elastic Criterion at Base of Towers – Third Run.....	251
8.5.2 Elastic Criterion at All Tower Segments– Third Run.....	252
8.5.3 Likelihood of Tower Collapse– Third Run.....	253
8.6 Consideration of Shear Forces in the Towers.....	253
8.7 Consideration of Cable Failure.....	254
Chapter 9 Consideration of Retrofit Alternatives.....	255
9.1 Retrofit Alternatives.....	255
9.2 Feasibility of Retrofitting with Additional Reinforcement.....	257
9.3 Feasibility of Retrofitting with Fiber Reinforced Polymer (FRP).....	259
9.4 Summary.....	260
Chapter 10 Conclusions and Recommendations.....	261
References.....	266

LIST OF TABLES

Table 2.1. Rotation angles for local coordinate systems of frame elements (towers).....	24
Table 2.2. Section properties of tower elements.....	25
Table 2.3. k_2 constants as a function of l/t ratio.....	27
Table 2.4. Values of k_2 constants used to calculate Torsional Constant.....	27
Table 2.5. Section properties of cables.....	34
Table 2.6. Equilibrium check of vertical forces.....	43
Table 2.7. Equilibrium check of horizontal forces.....	43
Table 2.8. T12 Tower - displacements of superstiff saddle.....	44
Table 2.9. T8 Tower - displacements of superstiff saddle.....	44
Table 2.10. T4 Tower - displacements of superstiff saddle.....	45
Table 2.11. T12 – displacements at very stiff platform beam.....	45
Table 2.12. T8 - displacements at very stiff platform beam.....	45
Table 2.13. T4 - displacements at very stiff platform beam.....	46
Table 2.14. Initial guess for backstay temperatures (cable preload).....	46
Table 2.15. Iterations to achieve verticality of towers.....	48
Table 2.16. Summary of tower displacements at the top. Final iteration.....	50
Table 2.17. Summary of error in tensions for the final iteration as compared to values specified in drawings.....	50
Table 2.18. Summary of tensions for two cases of thermal strains.....	51
Table 2.19. Comparison between original Model A vs. updated Model A.....	54
Table 2.20. Analytical calculation of unbalanced moment due to auxiliary cables.....	57

Table 2.21. Bending moment comparison; Analytical vs. FEM.....	58
Table 2.22. Estimate of tension in service cables and counterbalancing moment....	62
Table 2.23. Service cable diameters and tensions in service cables.....	62
Table 2.24. Calculation of net unbalanced moment.....	62
Table 2.25. Iteration Chart – ‘pinned’ constraint at intersection of service cables..	64
Table 2.26. Comparison of ‘major’ bending moments at top and base of towers for models with and without service cables.....	66
Table 2.27. Comparison of ‘minor’ bending moments at top and base of towers for models with and without service cables.....	66
Table 2.28. Solution of the Free Body Diagram (aux. concur. at 1383 ft).....	70
Table 2.29. Solution of the Free Body Diagram of Figure 2.39.....	72
Table 3.1. Rotation of local coordinate systems of frame elements (Tiedown axes coincide with the tower axes.).....	76
Table 3.2. Section properties of tiedown cables.....	77
Table 3.3. Iteration chart for Model B (tiedowns – uniform platform).....	78
Table 3.4. Vertical equilibrium check (Model B).....	81
Table 3.5. Comparison of tension magnitudes; Model A vs. Model B.....	81
Table 4.1. Additional suspended weight added in Gregorian upgrade.....	86
Table 4.2. Invariant preload temperatures in Model C.....	89
Table 4.3. Iteration chart for tiedown preload.....	89
Table 4.4. Displacement and tensions of Model C – original weight distribution...	91
Table 4.5. ‘Major’ M_{33} bending moments – original weight distribution.....	92
Table 4.6. Calculation of new properties - 50 kip weight redistribution.....	94
Table 4.7. Iteration chart for 50 kip weight redistribution.....	94

Table 4.8. Displacements and tensions – 50 kip weight redistribution.....	95
Table 4.9. Comparison of M_{33} bending moments – Model B vs Model C redistributed.....	97
Table 5.1. Comparison of modes and natural periods for three thermal strain cases.....	101
Table 5.2. Comparison of SAP2000 periods against empirical equation (Ren 2005).....	103
Table 5.3. Comparison of tower periods vs. UBC-97 Equation 30-8.....	103
Table 5.4. Comparison of tower T8 periods against a single-tower model.....	104
Table 5.5. Comparison of natural periods with and without service cables.....	105
Table 5.6. Modal results of Model B and comparison with Model A.....	106
Table 5.7. Calculations for $I_{cracked}$	114
Table 5.8. Comparison of ‘cracked’ and ‘gross’ moments of inertia.....	115
Table 5.9. Comparison of equilibrium state between I_{gross} and $I_{cracked}$ – Model B...	116
Table 5.10. Modal analysis results – $I_{cracked}$ – Model B.....	117
Table 5.11. Calculation of $I_{effective}$ and comparison with $I_{cracked}$	119
Table 5.12. Equilibrium displacements and cable tensions: isolation of platform modes.....	121
Table 5.13. Modal analysis comparison – isolation of platform modes.....	122
Table 5.14. Activation of platform modes by cable type.....	124
Table 5.15. Tension values in the cables.....	126
Table 5.16. Section properties of cables.....	128
Table 5.17. Iterations on Model B with bridge to achieve equilibrium under dead load.....	129
Table 5.18. Modal results for Model B including catwalk bridge.....	130

Table 5.19. Comparison of modal results: calculated mass vs. 50 kip redistribution.....	133
Table 5.20. Comparison of natural periods: Models A, B, C.....	134
Table 5.21. Modal participating mass ratios – Model B.....	136
Table 5.22. Modal participating mass ratios – Model C.....	136
Table 5.23. Ranking of participation mass ratios for displacement DOF–Model C	137
Table 5.24. Ranking of participation mass ratios for rotational DOF–Model C.....	137
Table 5.25. Description of modes for Tables 5.21 and 5.22.....	138
Table 6.1. Initial earthquake records and factor used in SAP models.....	143
Table 6.2. Stations where initial set of earthquakes were recorded.....	144
Table 6.3. Loma Prieta earthquake results – Model A (No Ties, Unif. Plat).....	146
Table 6.4. Weight calculation for tower T8.....	153
Table 6.5. Lateral force at each level of tower T8 per UBC-97.....	155
Table 6.6. Weight calculation for tower T4 and T12.....	156
Table 6.7. Lateral force at each level of tower T4 and T12 per UBC-97.....	158
Table 6.8. Modal time-history results - Isolated Towers (no cables nor platform)..	159
Table 6.9. Comparison with static “large displacements” case (DEAD analysis case).....	163
Table 6.10. Comparison of non-linear large displacements vs linear modal results	170
Table 6.11. Results for Loma Prieta, El Centro and Chi Chi earthquakes Model A.....	171
Table 6.12. Results for Kocaeli, San Fernando, and Coalinga earthquakes Model A.....	172
Table 6.13. Results for Loma Prieta, El Centro and Chi Chi earthquakes Model B.....	173

Table 6.14. Results for Kocaeli, San Fernando, and Coalinga earthquakes Model B.....	174
Table 6.15. Results for Loma Prieta, El Centro and Chi Chi earthquakes Model C.....	176
Table 6.16. Results for Kocaeli, San Fernando, and Coalinga earthquakes Model C.....	177
Table 6.17. Seismic response using $I_{cracked}$ – Model B.....	179
Table 6.18. M_{33} moments at different levels in tower T8 – Model B – $I_{cracked}$	181
Table 6.19. Seismic response including bridge, service cable and cable-car cable..	182
Table 7.1. Earthquakes selected for the Arecibo Observatory site.....	196
Table 7.2. Accelerogram data for selected earthquakes.....	197
Table 7.3. Seismic response for Model A (unscaled earthquakes).....	198
Table 7.4. Seismic response for Model B(unscaled earthquakes).....	200
Table 7.5. Seismic response for Model C(unscaled earthquakes).....	202
Table 7.6. Maximum and minimum moments at all tower steps (unscaled).....	206
Table 7.7. Biaxial bending state at all tower bases (unscaled).....	207
Table 7.8. Maximum and minimum moments at all tower steps (scaled).....	208
Table 7.9. Biaxial bending state at all tower bases (scaled).....	209
Table 7.10. Maximum and minimum moments at all tower steps (Third Run).....	210
Table 7.11. Biaxial bending state at all tower bases (Third Run).....	211
Table 8.1. Qualitative summary of elastic criterion test in tower bases.....	229
Table 8.2. Tower capacities in all segments.....	230
Table 8.3. Maximum moments recorded at the bottom of each tower segment.....	230
Table 8.4. Reduced bending moments ($R=2$) at bases of towers.....	232

Table 8.5. Reduced bending moments (R=2) at TSEC1 (bottom).....	234
Table 8.6. Reduced bending moments (R=2) at TSEC2 (bottom).....	236
Table 8.7. Qualitative summary of collapse likelihood in towers.....	238
Table 8.8. Qualitative summary of elastic criterion test in tower bases.....	243
Table 8.9. Max scaled moments at the bottom of each tower segment.....	244
Table 8.10. Reduced moments (R=2) at TSEC1 – Second Run	245
Table 8.11. Reduced moments (R=2) at TSEC2 – Second Run	246
Table 8.12. Reduced moments (R=2) at TSEC3 – Second Run	247
Table 8.13. Reduced moments (R=2) at TSEC4 – Second Run	248
Table 8.14. Reduced moments (R=2) at TSEC5 – Second Run	249
Table 8.15. Reduced moments (R=2) at TSEC6 – Second Run	250
Table 8.16. Maximum moments recorded at the bottom of each tower segment....	252
Table 8.17. Shear capacity and shear forces in the concrete towers.....	253
Table 8.18. Cable breaking strength and maximum tensions.....	254
Table 9.1. Retrofit alternatives.....	256

LIST OF FIGURES

Figure 1.1. Overall view of the Arecibo Observatory (courtesy of NAIC).....	2
Figure 1.2. Sinkhole at onset of construction in the early 1960's. (courtesy of NAIC).....	3
Figure 1.3. Suspended platform and its main components (courtesy of NAIC).....	3
Figure 1.4. Platform is an assembly of built-up beams and columns (photo by author).....	4
Figure 1.5. Tower T8, the tallest (365 ft) of the three towers. (courtesy of NAIC)...	4
Figure 1.6. Cruciform shape of tower cross-section (courtesy of NAIC).....	5
Figure 1.7. Attachment points of cables to platform. T4 cables highlighted. (photo by author).....	5
Figure 1.8. Tiedown cables and platform attachment points (courtesy of NAIC).....	6
Figure 1.9. Catwalk (pedestrian bridge) and supporting cables (photo by author)....	6
Figure 1.10. Four-person capacity cable car accesses the platform (photo by author).....	7
Figure 1.11. Finite element model of Arecibo Observatory– Model A.....	19
Figure 1.12. Finite element model – Model B.....	20
Figure 1.13. Finite element model – Model C.....	20
Figure 2.1. Local axis definitions for tower frame-elements in plan view schematic.....	24
Figure 2.2. Cruciform cross-section. Dimensions in feet.....	25
Figure 2.3. Original steel saddle for attachment of cables.....	27
Figure 2.4. Saddle geometry used in Model A.....	28
Figure 2.5: Cable attachments to saddle (T8 shown).....	28
Figure 2.6. Typical modeling of concrete anchors. A8 shown.....	29

Figure 2.7. Perspective view of platform.....	30
Figure 2.8. Plan view of lower platform.....	31
Figure 2.9. Very stiff beam for main cable attachment at lower platform (T12 shown).....	31
Figure 2.10. Plan view of upper platform.....	32
Figure 2.11. Plan view detail of tiedown attachment points (T12 shown).....	32
Figure 2.12. Typical cable definitions. Section names shown within brackets.....	33
Figure 2.13. Forces on a cable element.....	37
Figure 2.14. Graphical analysis to determine platform descent due to cable stretch..	38
Figure 2.15. Setting up the static non-linear p-delta analysis case.....	39
Figure 2.16. Setting up the p-delta option.....	40
Figure 2.17. Deformed shape with self-weight only (highly exaggerated).....	40
Figure 2.18. Elevation view of auxiliary saddle.....	52
Figure 2.19. Plan view of auxiliary saddle.....	52
Figure 2.20. Finite element model of saddles.....	53
Figure 2.21. Bending moment distribution of Tower T8. Dead-load only.....	55
Figure 2.22. Deformed geometry plot of tower T8.....	55
Figure 2.23. Free Body Diagram of auxiliary saddle to determine unbalanced moment due to auxiliary cables.....	57
Figure 2.24. Meeting point of service cables.....	59
Figure 2.25. Elevation view of main saddle showing service cable (T12 and T4).....	60
Figure 2.26. Photograph of main saddle at tower T8 (Courtesy of Louis Pérez).....	60
Figure 2.27. Free Body Diagram of main saddle.....	61
Figure 2.28. Modification at top of towers to include the service cable.....	63

Figure 2.29. Pin constraint at meeting point of three service cables.....	63
Figure 2.30. Asymmetry in service cables.....	65
Figure 2.31. FEM model with concurrency of cables at 1386.5 ft.....	68
Figure 2.32. M_{33} moment distribution in T8 - All cables concurrent at 1386.5 ft....	68
Figure 2.33. Deformed shape in T8 - All cables concurrent at 1386.5 ft.....	68
Figure 2.34. FEM model-auxiliary cables concurrent at 1383 ft.....	69
Figure 2.35. M_{33} moment distribution in T8 - Aux. concurrency at 1383 ft.....	69
Figure 2.36. Deformed shape in T8 - Aux. concurrency at 1383 ft.....	69
Figure 2.37. Free Body Diagram of hypothetical case (aux. concur. at 1383 ft).....	70
Figure 2.38. Couple moment at top of tower (aux. concur. at 1383 ft).....	71
Figure 2.39. Free Body Diagram of tower at the top (based on FEM model).....	71
Figure 3.1. Perspective view of model with tiedown cables.....	74
Figure 3.2. Detail of tiedown support structure at the platform (T4 shown).....	74
Figure 3.3. Detail of tiedown attachment point at platform level (T4 shown).....	75
Figure 3.4. Detail of tiedown anchor.....	75
Figure 3.5. Drawing of tiedown anchorage.....	76
Figure 3.6. Photo of mechanical jack (by author).....	76
Figure 3.7. Deformed geometry of Model B due to DEAD loading.....	79
Figure 3.8. Base reactions calculated by SAP2000.....	80
Figure 4.1. Perspective view of Model C.....	83
Figure 4.2. Close-up perspective view of platform in Model C.....	83
Figure 4.3. Plan view of platform in Model C.....	84

Figure 4.4. Elevation view of platform in Model C looking towards tower T12.....	84
Figure 4.5. Gregorian Dome.....	85
Figure 4.6. Line Feed Antenna.....	85
Figure 4.7. Deformed shape of towers (2000x mag.) – original weight distribution..	92
Figure 4.8. Deformed Shape of Model C – 50 kip weight redistribution.....	96
Figure 5.1. Typical SAP2000 Version 9 modal analysis case form.....	99
Figure 5.2. Example of platform mode (rotation about North-South axis).....	100
Figure 5.3. Example of tower mode (1 st Flexural mode of tower T8).....	100
Figure 5.4. Example of independent cable mode (fundamental mode of auxiliary backstays in tower T4).....	100
Figure 5.5. Example of interaction mode (tower T4 and T12 in fundamental mode while platform rotates around vertical axis).....	100
Figure 5.6. Plan view of simplified model with service cables.....	105
Figure 5.7. First lateral independent cable mode of tiedowns.....	107
Figure 5.8. Mode 19. Strong rotation of platform about the vertical axes – Strong movement of main and auxiliary cables - Towers and backstays remain quiet.....	108
Figure 5.9. Mode 29. Very similar to Mode 19 (Figure 5.8) but with a weaker rotation of the platform.....	108
Figure 5.10. Mode 30. Weak rotation about North-South axis. Very similar to mode C but weaker. Main and Auxiliary cables displacing vertically and out of phase with each other.....	108
Figure 5.11. Mode 31. Very similar to Mode 19 (Figure 5.8) but with participation of Tower T12.....	108
Figure 5.12. Mode 80. Very similar to mode F (1 st mode of towers T12 and T4 out of phase) but with weaker participation of the towers.....	109
Figure 5.13. Mode 81. Very similar to mode E (1 st mode of towers T12 and T4 in phase) but with weaker participation of the towers.....	109

Figure 5.14. Mode 111. Very strong interaction mode. Creates a 1 st mode type tower deflection (cantilever) but radially (same direction as cables). This direction is typical of even (not odd) modes.....	109
Figure 5.15. Mode 112. Equal to mode 111 except platform rotation is about a North-South axis.....	109
Figure 5.16. ID A. Mode 14. Platform vertical displacement.....	110
Figure 5.17. ID B. Mode 17. Platform rotation about East-West axis.....	110
Figure 5.18. ID C. Mode 18. Platform rotation about East-West axis.....	110
Figure 5.19. ID D. Mode 13. 1 st Mode of Tower T8. This is a cantilever-type mode in the direction perpendicular to cable. Note odd-numbered modes of towers are always normal to cables.....	110
Figure 5.20. ID E. Mode 15. 1 st mode towers T4 and T12 – In Phase. (Platform rotates about vertical axis).	111
Figure 5.21. ID F. Mode 16. 1 st mode Towers T4 and T12 – Out of Phase. Note towers T4 and T12 are identical so their periods coincide.....	111
Figure 5.22. ID G. Mode 18. 2 nd mode of Tower T8. Note similarity to the deformed shape of Figure 2.23. Note that even-numbered tower modes are always in the same direction as the cables.....	111
Figure 5.23. ID H. Mode 137. 2 nd mode of towers T4 and T12 – In Phase.....	111
Figure 5.24. ID I. Mode 138. 2 nd mode towers T4 and T12 – Out of Phase. Cradle motion of platform.....	112
Figure 5.25. ID J. Mode 139. 3 rd mode of tower T8. Note there is no interaction with the platform in this mode.....	112
Figure 5.26. ID K. Mode 258. 3 rd mode of tower T4. Note there is no interaction with the platform.....	112
Figure 5.27. ID L. Mode 260. 3 rd mode of tower T12. Note there is no interaction with the platform.....	112
Figure 5.28. ID M. Mode 259. 4 th mode of tower T8. Note the period is almost identical to the 3 rd modes of T4 and T12(id K, L) but they do not interact.....	113
Figure 5.29. ID N. Mode 385. 4 th mode tower T4.....	113

Figure 5.30. ID O. Mode 410. 4 th mode tower T12. Interaction with tower T4.....	113
Figure 5.31. ID P. Mode 423. 5 th mode of tower T8.....	113
Figure 5.32. Idealization of cross section to determine $I_{cracked}$	114
Figure 5.33. Pin restraints at saddles to isolate the platform modes.....	120
Figure 5.34. Platform rotation about vertical axis – isolation of platform modes.....	123
Figure 5.35. ‘Cradle’ type vibration mode. Motion towards T8. Isolation of platform modes	124
Figure 5.36. ‘Cradle’ type vibration mode. Motion towards T12. Isolation of platform modes	124
Figure 5.37. Model B including bridge, cable-car cable, and three service cables....	125
Figure 5.38. Detail at top of tower T12 to include service and tie-up cable.....	126
Figure 5.39. Schematic of platform rotation modes about the centroidal axes.....	131
Figure 5.40. Schematic of platform “cradle” mode.....	131
Figure 5.41. First four flexural modes of tower T8.....	132
Figure 5.42. Strong interaction modes. Towers T4 and T12 in-phase and out-of-phase.....	139
Figure 6.1. UBC-1997 Elastic design spectrum.....	141
Figure 6.2. U1 (EW) Loma Prieta spectrum for 5% damping ratio vs UBC-97 spectrum.....	142
Figure 6.3. U2 (NS) Loma Prieta spectrum for 5% damping ratio vs UBC-97 spectrum.....	142
Figure 6.4. U3 (Up) Loma Prieta spectrum for 5% damping ratio vs UBC-97 spectrum.....	142
Figure 6.5. U1 Loma Prieta Acceleration Record.....	145
Figure 6.6. U1 El Centro Acceleration Record.....	145

Figure 6.7. U1 Chi Chi Acceleration Record.....	145
Figure 6.8. U1 Kocaeli Acceleration Record.....	145
Figure 6.9. U1 San Fernando Acceleration Record.....	145
Figure 6.10. U1 Coalinga Acceleration Record.....	145
Figure 6.11. Deformed shape (50x mag.) of structure 5.1 sec into Loma Prieta.....	147
Figure 6.12. Tangential displacements [inch] (perpendicular to cables) at Tower T12. All components of Loma Prieta earthquake included – No Tiedowns.....	148
Figure 6.13. U3 displacement [in] at platform corner pointing at Tower T8. All components of Loma Prieta earthquake included – No Tiedowns.....	148
Figure 6.14. M_{33} moment [kip-ft] at TOP of Tower T12. All components of Loma Prieta earthquake included – No Tiedowns.....	149
Figure 6.15. M_{33} moment [kip-ft] at BASE of Tower T8. All components of Loma Prieta earthquake included – No Tiedowns.....	149
Figure 6.16. M_{22} moment [kip-ft] at BASE of Tower T4. All components of Loma Prieta earthquake included – No Tiedowns.....	150
Figure 6.17. Δ Tensions [kip] in main cables of Tower T8. All components of Loma Prieta earthquake included – No Tiedowns.....	151
Figure 6.18. Asymptotic behavior of Ernst’s equivalent modulus for main cables...	161
Figure 6.19. Nonlinear with large displacements – U_x disp. at top of T12 [in]. All components of Loma Prieta earthquake included – (Model B).....	165
Figure 6.20. Linear modal analysis – U_x disp. at top of T12 [in]. All components of Loma Prieta earthquake included – (Model B).....	165
Figure 6.21. Nonlinear with large displacements – z displacement at platform. All components of Loma Prieta earthquake included – (Model B). (Note the 128 inch descent of the platform remains in the analysis).....	166
Figure 6.22. Linear modal analysis – z displacement at platform. All components of Loma Prieta earthquake included – (Model B).....	166
Figure 6.23. Nonlinear with large displacements – M_{33} [kip-ft] at base of T8. All components of Loma Prieta earthquake included – (Model B).....	167

Figure 6.24. Linear modal analysis – M_{33} [kip-ft] at base of T8. All components of Loma Prieta earthquake included – (Model B).....	167
Figure 6.25. Nonlinear with large displacements – Tension T8 Main Cable [kip]. All components of Loma Prieta earthquake included – (Model B). (Note the initial tension of 504 kip remains in the analysis).....	168
Figure 6.26. Linear modal analysis – Tension T8 Main Cable [kip]. All components of Loma Prieta earthquake included – (Model B).....	168
Figure 6.27. Nonlinear with large displacements – M_{33} [kip-ft] at base of T8. All components of Coalinga earthquake included – (Model B).....	169
Figure 6.28. Linear modal analysis – M_{33} [kip-ft] at base of T8. All components of Loma Prieta earthquake included – (Model B).....	169
Figure 6.29. Deformed shape (50x mag.) of structure 5.1 sec into Loma Prieta. Model B (Tiedowns, Uniform Platform).....	175
Figure 6.30. Deformed shape (50x mag.) of structure 5.1 sec into Loma Prieta. Model C (Tiedowns, Dome).....	178
Figure 6.31. Deformed shape (50x mag.) using Icracked 5.6 sec into Loma Prieta. Model B (Tiedowns, Uniform Platform).....	180
Figure 6.32. Deformed shape (50x mag.) of structure 5.1 sec into Loma Prieta. Model B with bridge, service cables, and cable-car cable.....	183
Figure 7.1. Location of Arecibo Observatory with respect to other sites in Puerto Rico.....	184
Figure 7.2. The Puerto Rico Virgin Islands (PRVI) microplate.....	185
Figure 7.3. Response envelope for San Juan (from Irizarry 1999).....	187
Figure 7.4. Response envelope for Mayagüez and Ponce (from Irizarry 1999).....	188
Figure 7.5. Accelerogram of San Salvador – CIG EW record.....	189
Figure 7.6. PSA Spectrum of San Salvador – CIG EW record	189
Figure 7.7. Accelerogram of Northridge - Castaic EW record.....	190
Figure 7.8. PSA spectrum of Northridge - Castaic EW record	190

Figure 7.9. Accelerogram of Parkfield – station097 usaca01.109 EW record.....	191
Figure 7.10. PSA spectrum of Parkfield – station097 usaca01.109 EW record.....	191
Figure 7.11. Response envelope for Dos Bocas and Guajataca Dams (From Llop 2002).....	192
Figure 7.12. Accelerogram of Morgan Hill – Gilroy6 ~EW record.....	193
Figure 7.13. PSA spectrum of Morgan Hill – Gilroy6 ~EW record.....	193
Figure 7.14. Accelerogram of UBC-97 (Z3, “Sb”) compatible SIMQKE artificial earthquake.....	195
Figure 7.15. PSA spectrum of UBC-97 (Z3, “Sb”) compatible SIMQKE artificial earthquake.....	195
Figure 7.16. Deformed shape (50x mag.) of structure 13.5 sec into unscaled Northridge-Castaic.....	199
Figure 7.17. M_{33} moment [kip-ft] at the base of T8 for unscaled Northridge-Castaic – Model A.....	199
Figure 7.18. Deformed shape (50x mag.) of structure 1.5 sec into unscaled San Salvador.....	201
Figure 7.19. M_{33} moment [kip-ft] at the base of tower T8 for unscaled San Salvador – Model B.....	201
Figure 7.20. Deformed shape (50x mag.) of structure 1.5 sec into unscaled San Salvador.....	203
Figure 7.21. M_{33} moment [kip-ft] at base of T8 for unscaled San Salvador – Model C.....	203
Figure 7.22. Deformed shape (50x mag.) of structure 13.5 sec into unscaled Northridge-Castaic.....	204
Figure 7.23. M_{33} moment [kip-ft] at the base of tower T8 for unscaled Northridge-Castaic – Model C.....	204
Figure 7.24. Deformed shape (75x mag.) of structure 5.6 sec into Artificial-SIMQKE.....	205

Figure 7.25. M_{33} moment [kip-ft] at base of T8 in Artificial-SIMQKE – Model C..	205
Figure 8.1. Lap splice at intermediate tower step.....	215
Figure 8.2. Cross section at the top two steps of all the towers.....	215
Figure 8.3. Cross section at all steps of the towers except the top two steps.....	215
Figure 8.4. Nominal interaction diagram for TSEC1 (top step of tower).....	219
Figure 8.5. Nominal interaction diagram for TSEC2.....	219
Figure 8.6. Nominal interaction diagram for TSEC3.....	219
Figure 8.7. Nominal interaction diagram for TSEC4.....	220
Figure 8.8. Nominal interaction diagram for TSEC5 (tower T8 only).....	220
Figure 8.9. Nominal interaction diagram for TSEC6 (tower T8 only).....	220
Figure 8.10. Moment-curvature graph (TSEC6). Axial Load = 17765 kip (San Salvador).....	221
Figure 8.11. Schematic of a biaxial interaction diagram.....	222
Figure 8.12. Orbit plot for biaxial bending – TSEC6 – Axial Load = 17765 kip.....	222
Figure 8.13. Sequence of biaxial combinations for orbit plot at first yield.....	223
Figure 8.14. Orbit plot – San Salvador earthquake – Base of T12.....	224
Figure 8.15. Orbit plot – San Salvador earthquake – Base of T8.....	225
Figure 8.16. Orbit plot – San Salvador earthquake – Base of T4.....	225
Figure 8.17. Orbit plot – Northridge-Castaic earthquake – Base of T12.....	226
Figure 8.18. Orbit plot – Northridge-Castaic earthquake – Base of T8.....	226
Figure 8.19. Orbit plot – Northridge-Castaic earthquake – Base of T4.....	227
Figure 8.20. Orbit plot – Artificial earthquake – Base of T12.....	227
Figure 8.21. Orbit plot – Artificial earthquake – Base of T8.....	228

Figure 8.22. Orbit plot – Artificial earthquake – Base of T4.....	228
Figure 8.23. Orbit plot for likelihood of collapse – Base of T12.....	232
Figure 8.24. Orbit plot for likelihood of collapse – Base of T8.....	233
Figure 8.25. Orbit plot for likelihood of collapse – Base of T4.....	233
Figure 8.26. Orbit plot for likelihood of collapse – (bottom) TSEC1 of T12.....	234
Figure 8.27. Orbit plot for likelihood of collapse – (bottom) TSEC1 of T8.....	235
Figure 8.28. Orbit plot for likelihood of collapse – (bottom) TSEC1 of T4.....	235
Figure 8.29. Orbit plot for likelihood of collapse – (bottom) TSEC2 of T12.....	236
Figure 8.30. Orbit plot for likelihood of collapse – (bottom) TSEC2 of T8.....	237
Figure 8.31. Orbit plot for likelihood of collapse – (bottom) TSEC2 of T4.....	237
Figure 8.32. Orbit plot – scaled San Salvador earthquake – Base of T12.....	240
Figure 8.33. Orbit plot – scaled San Salvador earthquake – Base of T8.....	241
Figure 8.34. Orbit plot – scaled San Salvador earthquake – Base of T4.....	241
Figure 8.35. Orbit plot – scaled Northridge-Castaic earthquake – Base of T12.....	242
Figure 8.36. Orbit plot – scaled Northridge-Castaic earthquake – Base of T8.....	242
Figure 8.37. Orbit plot – scaled Northridge-Castaic earthquake – Base of T4.....	243
Figure 8.38. (Scaled) Orbit plot for likelihood of collapse of TSEC1.....	245
Figure 8.39. (Scaled) Orbit plot for likelihood of collapse of TSEC2.....	246
Figure 8.40. (Scaled) Orbit plot for likelihood of collapse of TSEC3.....	247
Figure 8.41. (Scaled) Orbit plot for likelihood of collapse of TSEC4.....	248
Figure 8.42. (Scaled) Orbit plot for likelihood of collapse of TSEC5.....	249
Figure 8.43. (Scaled) Orbit plot for likelihood of collapse of TSEC6.....	250
Figure 8.44. Orbit plot for base of towers T4 and T12 – Third run.....	251

Figure 8.45. Orbit plot for base of tower T8 – Third run.....	252
Figure 9.1. Schematic of reinforced areas (hatched zones).....	257
Figure 9.2. Orbit plot (at ultimate) of retrofitted TSEC1 with additional rebars.....	258
Figure 9.3. Orbit plot (at yield) of retrofitted TSEC4 with additional rebars.....	259
Figure 9.4. Orbit plot (at yield) of retrofitted TSEC4 with FRP all-around wrap....	260

CHAPTER 1

Introduction

1.1 Justification

This investigation was requested by the staff of the National Astronomy and Ionosphere Center (NAIC) Arecibo Observatory to determine whether the cable structures and towers that support the suspended platform of the Arecibo Observatory are capable of resisting a maximum-credible earthquake in the elastic regime. The Arecibo Observatory is one of the most important research centers in the world for astronomy and ionosphere studies and thus maintaining its structural integrity is a top priority. In addition, the many unique components that form the observatory pose an unusual and challenging problem for its dynamic analysis. The structures of the observatory were designed and built in 1963 before modern seismic provisions became available and enforced in building codes. This contingency, along with the fact that the Arecibo Observatory is likely to be exposed to high seismic activity because Puerto Rico is surrounded by seismic faults as well as faults within the island itself, calls for a seismic assessment of its structures.

1.2 Objectives

1. To create a three-dimensional finite element model of the Arecibo Observatory capable of revealing the dynamic properties and seismic response of this unique structure. This includes the establishment of the deformed equilibrium state due to dead load which serves as the basis from which all further studies are performed.
2. To determine the dynamic properties (mode shapes and natural periods) of the Arecibo Observatory using computational experiments.
3. To computationally determine the bending moments and forces at the towers, and the tension in the cables, due to maximum-credible earthquakes expected at the site of the Arecibo Observatory.
4. To determine if the towers are capable of resisting the maximum-credible earthquake demands in the elastic regime. This stringent requirement (elastic regime) is based on the required positional accuracy of the instrumentation housed in the suspended platform. Plastically deformed towers would result in misalignment of the

instrumented platform and would defeat the scientific mission of the Arecibo Observatory. As a result, the towers shall be considered an integral component of the precise instrumentation systems used for astronomy and ionosphere research. The possibility that reinforcement-development lengths may be inadequate according to present structural codes will be addressed. Additionally, in the instance that the elastic criterion is not met, a preliminary analysis to investigate the likelihood of collapse of the towers will be performed.

5. To consider, if necessary, alternatives for retrofitting the structure and to conduct preliminary feasibility studies to determine appropriateness of the most promising alternatives.
6. To recommend the location of accelerometer transducers in the structure for a future research study being planned by Dr. José Martínez-Cruzado, Director of the Strong Motion Program of the University of Puerto Rico at Mayagüez, and member of the graduate committee

1.3 Background of the Structure

Figure 1.1 shows the primary components of the structure. These include the three reinforced concrete towers, the suspended platform and its supporting cables. The primary reflector is not included in the study as it is an independently supported structure.



Figure 1.1. Overall view of the Arecibo Observatory (courtesy of NAIC)

In Karst landscape, rainwater usually sinks into funnel-shaped depressions of the ground surface called sinkholes, instead of running off in streams. The Observatory is located on a very large sinkhole, roughly the size of the 1000-ft-diameter primary reflector, in Arecibo, Puerto Rico. Figure 2 shows the sinkhole in the early 1960's during excavation for site improvement. The limestone rock typical of Karst landscape is competent.



Figure 1.2. Sinkhole at onset of construction in the early 1960's (courtesy of NAIC)

The 900 ton platform, suspended by 18 cables at a height of 450 feet above the reflector, supports an Azimuth arm, the Gregorian Dome and the Line-Feed Antenna (Figure 1.3). The Azimuth arm is capable of rotating about a vertical centroidal axis. The dome and line-feed antenna can slide along the arm up to a 20° angle (from a vertical axis).

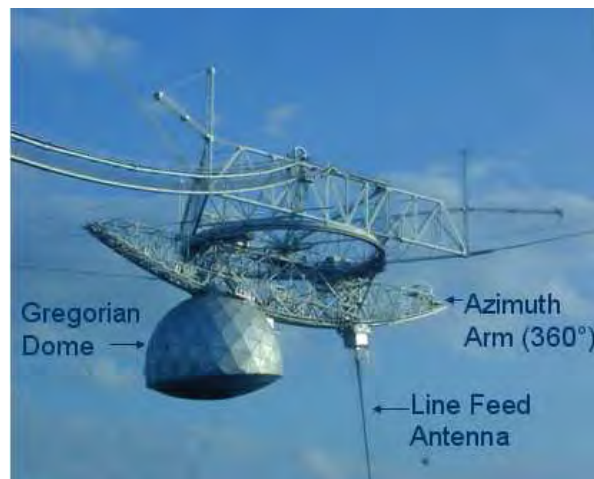


Figure 1.3. Suspended platform and its main components (courtesy of NAIC)

Built-up beams and columns are bolted together to form the suspended platform assembly as shown in Figure 1.4. The lower triangle, however, uses I-beams.



Figure 1.4. Platform is an assembly of built-up beams and columns (photo by author)

The three towers are identified as T12, T8 and T4, based on their position along the perimeter of an imaginary clock. Tower T12 is that located in the North. Each tower has a set of six platform cables and seven backstay cables, as shown in Figure 1.5 (for tower T8). The backstays originate in massive reinforced concrete anchors. Towers T4 and T12 are 265 ft high while tower T8 is 365 ft high. All three tower tops are at the same elevation. The combined volume of reinforced concrete in the three towers (including the footings) is 9,100 cubic yards which represents a combined weight of 35,600,000 pounds.



Figure 1.5. Tower T8, the tallest (365 ft) of the three towers. (courtesy of NAIC)

As shown in Figure 1.6, the towers have a cruciform cross-sectional shape which gives them doubly-strong axes, one of them aligned with the cables. The dimensions change approximately every 60 feet as the towers are stepped in by approximately 3 feet on all sides. The thickness is maintained constant at 6 feet.

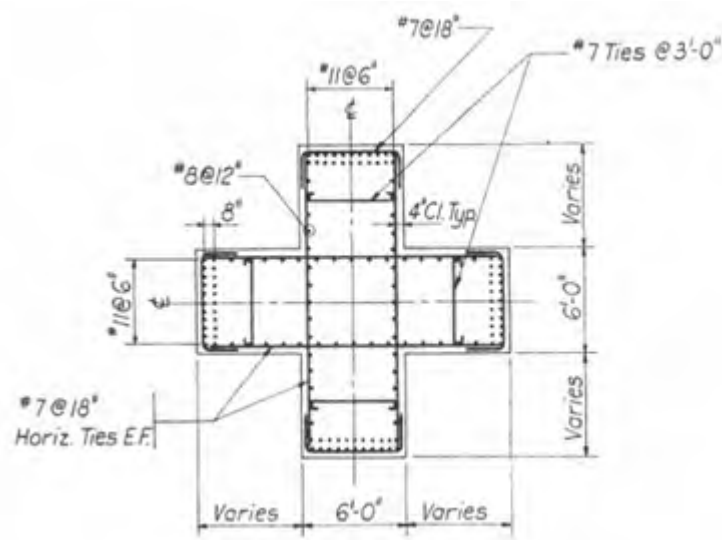


Figure 1.6. Cruciform shape of tower cross-section (courtesy of NAIC)

The six platform-cables per tower are distributed into four, 3.0 inch diameter, main cables that are attached to the platform corners, and two, 3.25 inch diameter, auxiliary cables that are attached to approximately the 2/3 points of the platform (see Figure 1.7).

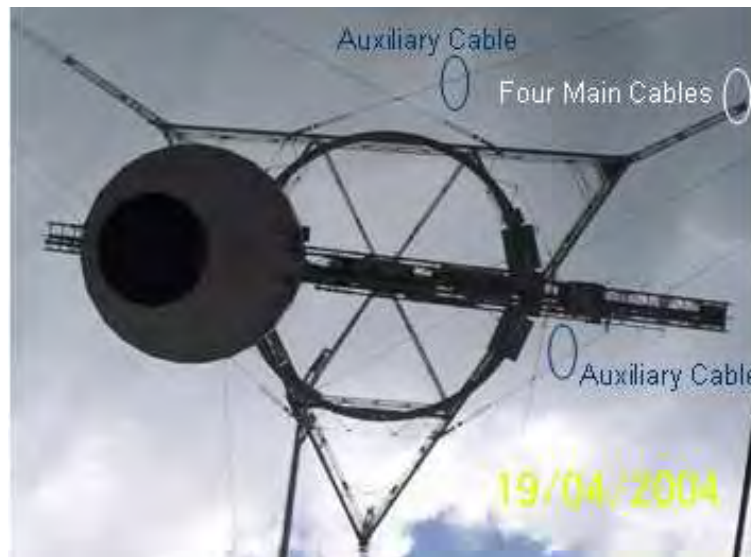


Figure 1.7. Attachment points of cables to platform. T4 cables highlighted (photo by author)

As shown in Figure 1.8, two vertical tiedown cables (each of 1.5 inch diameter) run from each corner extension of the platform down to mechanical jacks located below the primary reflector. The tiedown-cables/jack system allows for adjustment of each extended corner of the platform with millimetric precision. The 66 ft long corner extensions provide the required clearance to allow the azimuth arm to rotate without interfering with the tiedown cables. The corner extensions are supported by a 40 ft mast and supporting cables.

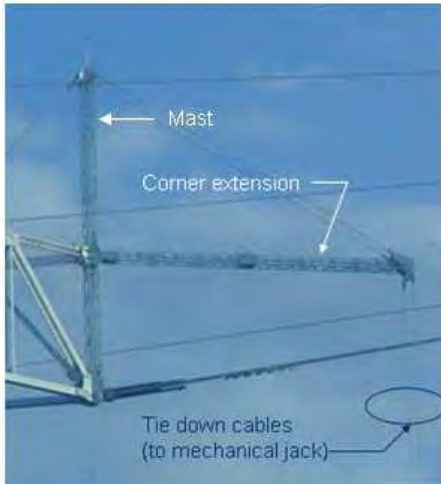


Figure 1.8. Tiedown cables and platform attachment points (courtesy of NAIC)

As shown in Figure 1.9, there is a catwalk (bridge) that permits pedestrian access to the platform. The catwalk is supported at both ends as well as near its midspan where it is restrained by one tie-up cable attached to tower T12 and two ground cables.



Figure 1.9. Catwalk (pedestrian bridge) and supporting cables (photo by author)

A four-person capacity cable-car also permits access to the platform (Figure 1.10)

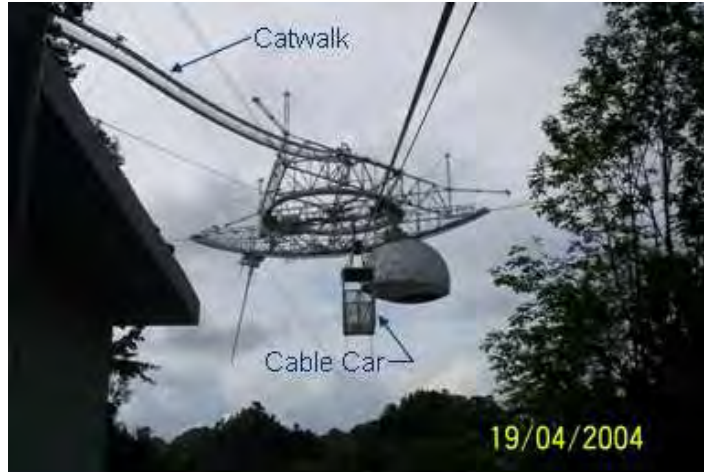


Figure 1.10. Four-person capacity cable car accesses the platform (photo by author)

1.4 Literature Survey

Most of the publications cited in this section are related to suspension bridges and cable-stayed bridges, which are the most closely-related structures to the Arecibo Observatory. The Arecibo Observatory is a one-of-a-kind structure and thus there is not any study dealing with this unique and complex structural system. The objective of the survey is to determine the most appropriate methodology to conduct the study. The following issues are specifically addressed - use of a commercial software package vs. custom-made programming; use of linear vs. non-linear analyses; use of fixed boundary conditions vs. consideration of soil-structure interaction; the earthquake source for the seismic study; and the use of field measurements. At the end of each, a short paragraph summarizes and discusses the manner in which the survey directs the approach that should be taken to conduct the study.

1.4.1 Software Package vs. Custom-Made Programming

Xu (1997) used a finite element (FE) software package to conduct three-dimensional vibration studies of the Tsing Ma suspension bridge in Hong Kong. In addition, Chang (2001), Zhang (2001), Cunha (2001), and Astaneh-Asl (2001) used FE software packages to obtain the three-dimensional dynamic response of cable-stayed bridges. Ren (1999a) and

Ren (1999b) used a software package to analyze a cable-stayed bridge but reduced the problem to two-dimensions to focus on ultimate and elastic-plastic behavior, respectively. Software packages, such as the commercially available SAP2000, offer several advantages. In the initial stages of modeling, the graphical pre-processor facilitates the creation of the geometry as well as the assignment of material properties, section properties, loads and boundary conditions. In the final stages, the graphical post-processor allows for the visualization of deformed shapes, reactions, shear, axial force, and bending moment diagrams, and stresses. The deciding issue on selecting a particular commercial software package rests on the code's ability to perform the desired analysis.

Hangai (1999) and Volokh (2003), on the other hand, used custom-made programming to evaluate simpler three dimensional structures. The origin of Hangai's contribution lies in tensegrity structures which may be thought of as geodesic domes in which compression rods are isolated from each other in a continuous network of tensioned cables. These interesting structures take advantage of the great load-bearing superiority of tension – which is not a function of the member's length - over compression which may cause instability (buckling) problems. Tensegrity structures, however, depend on cable pre-stress to achieve stability. The paper cited additional references which have proposed discrete methods to investigate these “unstable” structures. Hangai's objective was to extend these methods to cover hybrid structures that consisted exclusively of cable elements and rigid bodies. While it did not consider flexural elements, such as beam or frame elements, which are necessary to model the towers of the Arecibo Observatory, it showed that the extended discrete method agreed very well with both theory and experimental data. The example case was very similar to the observatory (a suspended, pyramidal-like platform) and it was verified only for static loading. A similar case (a suspended cube) was examined for vibration but it is only verified by assuring the absence of error during the numerical example. These two cases considered by Hangai vary significantly from a typical tensegrity structure in the sense that they are automatically self-equilibrated by gravity in the act of being suspended from the cables. For this type of structure, the methodology offered in this paper, while proven worthy, can be duplicated by most typical FE software packages with the inclusion of a positive geometric stiffness matrix to a truss or frame element (to account for the tension in the cables) and solving the equations of equilibrium.

Volokh (2003) also relied on custom-made programming to analyze a simpler three-dimensional structure. In this case the objective was to specifically address a reduced basis technique proposed by the authors to nonlinearly solve cable structures. The technique proposed by the authors falls outside the typical capabilities of software packages. The paper addressed simple three-dimensional structures composed of a combination of cable elements (tension) and struts (compression). It did not consider flexural elements, which are required to model the towers of the Arecibo Observatory. Examples offered in the paper were also small enough (of the order of 20 nodes) to handle without a graphical-interface pre-processor. For the comparison case, however, it only considered a simple, horizontal cable with one degree of freedom.

Many other articles available in the literature showed that the majority of cable structures analyzed with custom-made programming are reduced to a single cable. The single-cable isolation permits to focus the research on a specific phenomenon which is typically beyond the capabilities of most commercial software packages. For example, Main (2002) investigated the use of linear viscous dampers to reduce vibration in the cables of cable-stayed bridges. A single, horizontal cable was isolated between fixed boundaries to investigate the benefit of the damper. The cable-isolation approach was used in numerous additional references to investigate issues regarding the behavior of transmission lines, mooring lines and guy wires. The objectives of these investigations, however, fall outside the scope of the present study so no additional references are listed.

In summary, it has been shown that the decision to use a commercial software package is proportional to the magnitude (breadth) of the problem. If the objective of a study is to obtain the overall, three-dimensional dynamic response of a complex structure subjected to loads with arbitrary time variation, then a software package should be selected to manage the complexity of the problem. If, on the other hand, the objective of a study is to focus (achieve depth) on a specific phenomenon, such as the use of oil-dampers in cables to minimize vibration, then the problem is isolated from the overall structure and modeled directly using custom-made programming in most cases. Thus, the selection is reduced to a trade-off between breadth and depth. The Arecibo Observatory study falls in the category of ample breadth. The objective is to determine the overall seismic response in three dimensions of the complex structure; therefore, the recommended approach that can be

inferred from the literature survey is to use a commercial software package such as SAP2000.

1.4.2 Linear vs. Nonlinear Analysis

Xu (1997), Ren (1999a) and Ren (1999b) provided background on the sources of nonlinearities in cable structures. Ren (1999a) stated that nonlinearities arise from two different sources in a general cable structure: (1) material nonlinearities, and (2) geometric nonlinearities. Material nonlinearities refer to nonlinearities in the constitutive relation of the material. Geometric nonlinearities, on the other hand, arise from the changes in geometry that take place as the structure deforms under loading although the behavior of the material may be linearly elastic. The two main sources of geometric nonlinearities are: (a) cable sag effect, and (b) large displacements. Other sources of geometric nonlinearities may be present depending on the specific structure. For example, in the case of cable-stayed bridges, the combined axial load and bending moment interaction for the deck and towers is also a source of geometric nonlinearity. This particular source, however, is not present in the Observatory.

1.4.3 Material nonlinearities

Ren (1999a) and Ren (1999b) included material nonlinearities when studying the response of cable-stayed bridges. In the case of Ren (1999a), material nonlinearities become relevant for the ultimate load-carrying capacity analysis and overall safety evaluation of a long-span cable-stayed bridge under static loading. In the case of Ren (1999b), it addressed the ductility capacity and energy absorption capacity of the bridge under strong seismic ground motions. In both references the breadth of the problem was reduced to two-dimensions in order to achieve depth with respect to the material nonlinearities. None of the three-dimensional studies of cable-stayed or suspension bridges found in the literature survey includes material nonlinearities.

1.4.4 Geometric Nonlinearity – Cable Sag Effect

Inclined cables sag under their own weight. The magnitude of the sag is related to the tension in the cable. Cables that are slack exhibit a large degree of sag while tight cables

show a reduced amount of sag. A typical approach to account for the sag effect on inclined cables (Ren 1999a) is to consider an equivalent straight chord member with an equivalent modulus of elasticity, E_{eq} , given by Ernst's tangent modulus equation,

$$E_{eq} = \frac{E}{1 + \frac{(wL)^2 AE}{12T^3}}, \text{ where, for any consistent set of units,}$$

E = apparent modulus of elasticity of the cable

w = weight per unit length of cable = (specific weight) * (effective area of cable)

L = horizontal projected length of the cable

A = effective area of the cable

T = tension in the cable

Note that E_{eq} approaches E asymptotically as T increases or L decreases (the cable approaches vertical orientation). With Ernst's tangent modulus equation, the cable-sag nonlinearity is handled by linearizing the stiffness of the cable. This model is appropriate as long as the tension in the cable does not vary significantly during the analysis. To account for significant variation in the tension, which could occur during a strong seismic ground motion, Ernst's tangent modulus equation has been modified to a secant model (Ren 1999b) which depends on the tension at the beginning and end of a time step. In this manner, the linearization scheme is updated within each and every time step and the model becomes more accurate. In this case, however, the problem becomes fully nonlinear in the sense that the equations of motion must be solved iteratively at each time step until equilibrium is satisfied.

Ren (1999b) undertook the effort to compare the results of a tangent-linearization case (E_{eq} calculated once) and a secant-linearization case (E_{eq} updated every time step) for the two-dimensional dynamic analysis of a long-span cable-stayed bridge. The conclusion is that there is only a small difference under strong ground motions so the tangent-linearization scheme is deemed appropriate.

Zhang (2001), Xu (1997) and Astaneh-Asl (2001) also used Ernst's tangent modulus. On the other hand, Hangai (1999) ignored it.

1.4.5 Geometric Nonlinearity – Large Displacements

The essence of large-displacement, geometrically-nonlinear analysis is to update the nodal coordinates after every load step. Additional loading is applied to the deformed geometry configuration. On the other hand, in linear analysis the calculations are based on loads applied to the original, undeformed geometry. If the deformations are not large enough then both schemes converge to the same result.

Ren (1999b) included the effects of large displacements while modeling the cable sag effect using Ernst's tangent modulus. The seismic results were compared to a linear analysis and the differences were very small. The conclusion was that consideration of large displacements was not required and linear analysis remained appropriate. In addition, Ren (1999b) observed that Fleming (1979) and Nazmy (1990) also reached the same conclusion for cable-stayed bridges. This is the case while the cables are in a high state of tension and while there is no significant variation in the state of tension.

Chang (2001) cited Fleming (1980) as a basis to proceed with a linear dynamic analysis of a long-span cable-stayed bridge and ignored large displacements. In this case the analysis was limited to the free vibration response. This study adds more credence to the linear approach by showing that the calculated natural frequencies and mode shapes agreed well with field measurements.

Hangai (1999), which addressed simple hybrid structures consisting of cables and rigid bodies (pyramidal-like structure suspended by cables), ignored both large displacements and cable-sag effects and still obtained good agreement with experimental results. The experimental results, however, were only performed for the static case.

A key requirement to obtain the dynamic properties and seismic response of cable structures is to first obtain the deformed equilibrium state due to dead loads. This is accomplished by running a p-delta static analysis to create the geometric stiffness matrices of all the structural elements. The 'geometric' stiffness of a structural element differs from the 'mechanical' stiffness in that it is a function of the load while the 'mechanical' stiffness is only based on the physical properties (area moment of inertia, elastic modulus, etc.) of the element. Cable elements derive practically all their lateral stiffness from their state of tension rather than from their physical properties. Ren (1999b) ran a model of a cable-stayed bridge with and without the contribution of the geometric stiffness and concluded that the

contribution of the geometric stiffness of the cables is essential to obtain accurate results. In addition, Ren (1999a) and Ren (1999b) concluded that large displacements may be ignored in the static p-delta analysis required to reach equilibrium state due to dead loads.

In summary, all references indicate that a linearized dynamic analysis using the small-strain assumption is appropriate for highly tensioned cable structures similar to the Arecibo Observatory.

1.4.6 Fixed Boundary Conditions vs. Soil-Structure Interaction

Soil-structure interaction is of importance for structures founded in soft soils or for very massive, short-period structures, neither of which represents the Arecibo Observatory. Most of the cable-stayed bridge studies cited previously ignored soil-structure interaction; specifically, Xu (1997), Chang (2001), Zhang (2001), Astaneh-Asl (2001), Ren (1999a), and Ren (1999b), assumed fixed boundary conditions at the bridge-tower bases, thus ignoring soil-structure interaction effects. The only exception was Mylonakis (2001) but soil-structure interaction was considered because the study specifically addressed soft soils. Chopra (2000) stated in page 463 of his book “While the underlying soil can be assumed as rigid in the analysis of many structures, soil-structure interaction should be considered in the analysis of structures with very short natural periods, such as nuclear containment structures”.

The soil where the Arecibo Observatory towers are founded is competent limestone rock typical of Karst landscape which closely approximates a rigid support. It is noted that the existence of competent soil characteristics was a prerequisite for the chosen site of the radio-telescope. In addition, the tall and relatively slender towers of the Arecibo Observatory have very high natural periods on the order of 2 seconds, unlike the short-period nuclear containment structures mentioned by Chopra (2000). The combination of these factors diminishes the importance of soil-structure interaction concerns.

In summary, the references indicate that soil-structure interaction effects may be safely disregarded in well-founded, long-period structures. It is noted that an assessment of the rock capacity under the existing foundation is beyond the scope of this thesis.

1.4.7 Earthquake Source for the Seismic Study

In a two-dimensional study of a cable-stayed bridge in China, Ren (1999b) used three strong earthquake records of the Great Hanshin earthquake of 1995 in Japan (also known as the Kobe earthquake). The acceleration records were not scaled for the study and included Peak Ground Accelerations (PGA) as high as 0.83g (recorded in the Kobe station). The records were input in the longitudinal directions, in the vertical direction and in the combined longitudinal and vertical directions.

Astaneh-Asl (2001), in a three-dimensional study of a curved cable-stayed bridge design between San Francisco and Oakland, California, used only an artificial earthquake record compatible with a design spectrum similar to the one recommended by the American Association of State Highway and Transportation Officials (AASHTO). The study stated “The ground motions used in the seismic design and analysis were three orthogonal components (east-west, north-south, and vertical) of acceleration time history developed for Pier E3 of the existing East Bay Crossing of the San Francisco-Oakland Bay Bridge. Pier E3 is about 200 meters from the location of the main tower of the proposed bridge.” Citing from the conclusions, “The response of the bridge to the magnitude 7.3 artificial earthquake was essentially elastic. The ground motions used in the analysis were generated to represent the maximum-credible earthquake emanating from the nearby Hayward Fault when it ruptures.”

Button (2002) investigated the effect of vertical motions on the seismic response of highway bridges using records scaled to design spectra. The study stated that current seismic design requirements do not attempt to account for vertical motion effects. In the cases where vertical effects were explicitly included in the design, they were typically represented by a response spectrum with ordinates arbitrarily set at two-thirds those of the horizontal response spectrum considered for the site. Button pointed out that recent studies showed that this ratio grossly underestimated the severity of the vertical component in the near-fault region. The paper pointed out that it has been commonly assumed that vertical ground motions do not have a significant impact on the response of a bridge and, as a consequence, current bridge design codes do not explicitly address the response to vertical motions. It indicates that this is certainly not a valid assumption for bridge sites located within 20 km of a fault and even up to 60 km from a major fault. Button recommends the inclusion of a vertical component of motion as a function of the distance to the fault in the design and analysis process.

Mylonakis (2001) considered nonuniform seismic excitations in soft soils. He stated that the causes of spatial variability are generally attributed to four main factors: (1) loss of coherency of the seismic waves due to inhomogeneity of the ground material and finite size of the seismic source (coherency effect); (2) propagating wave nature of seismic excitation leading to different arrival times at the supports (wave-passage effect); (3) loss of wave amplitude with increasing distance from the fault due to geometric and material energy dissipation (attenuation effect); and (4) variable ground conditions in the horizontal direction leading to different wave amplifications and, thereby, different surface motions along the structure (site response effect). Mylonakis (2001) stated that the attenuation effect is known to be of secondary importance and that research has concentrated on the coherency effect and the wave passage effect. Citing from the introduction, "...the dynamic response of multiply excited structures tends to be smaller than under uniform excitation due to the destructive interference ("cancellation") of the time histories of ground motions at the various supports."

Based on this literature survey, three different scenarios will be considered in this thesis:

1. Consideration of unscaled maximum-credible earthquake records, even if the recorded PGA is higher than specified by code design spectra. This is the most stringent case, although it may be conservative.
2. Consideration of scaled maximum-credible earthquake records. Scaling would be based on the 0.3g PGA value recommended by the 1997 UBC.
3. Consideration of an artificial earthquake compatible with the UBC-97 design spectrum.

The records should include the three orthogonal components as recommended. The literature survey used for earthquake selection is fully discussed in Chapter 7.

1.4.8 Field Measurements

While field measurements provide the definitive confirmation to a numerical simulation, obtaining them is a costly and complex endeavor. Xu (1997) and Chang (2001) used field measurements to compare mode shapes and natural frequencies of bridges; however, these were obtained from an independent and separate experimental study.

Field measurements of mode shapes and natural frequencies for the Arecibo Observatory do not exist. However, the cable tensions specified in the drawings have been confirmed by field measurements performed as part of the conservation and maintenance program of the structure. At present, the Puerto Rico Strong Motion Program, based on the Civil Engineering Department at the University of Puerto Rico in Mayagüez, is planning a separate research project to instrument the Arecibo Observatory site. One of the objectives of this thesis is to recommend the placement locations of the accelerometers. If there is sufficient funding to instrument the towers, then field measurements should be available within the next five years. These will provide the data to estimate the lower natural frequencies, damping ratios and mode shapes. They can then be compared against the results of the present computational investigation.

In summary, the cable tensions specified in the drawings have been confirmed by field measurements, but the acquisition of field data to estimate the natural frequencies and mode shapes, merits a separate study due to the complexity and cost of the endeavor.

1.5 Scope of the Study

This research project focuses on the overall dynamic response to an earthquake excitation of the towers-platform-cables system by means of computational simulations in three dimensions using the commercial software package SAP2000, Version 9. The suspended platform, a 3D truss structure that is considerably stiffer than the cables on which it hangs, will be modeled as a collection of rigid bodies since only its overall dynamic response is desired. The effect of seismic loading on the individual components of the platform (dome, azimuth arm, etc), and on the instruments housed on the platform, is beyond the scope of this study. A separate study could use the displacement histories at the three corners of the platform (obtained from the present study) as the input to a detailed model of just the platform. The issue of geometric nonlinearity will be addressed by comparing the results of a linear versus a non-linear (“large displacements”) case. The expectation, based on the literature survey, is that the linear assumption will be proven accurate, i.e., there should be no significant differences between the two cases. In the case that there was a significant difference, the analysis of the Arecibo Observatory must take the large-

displacement, geometric non-linearities into account. Material nonlinearities, however, are outside the scope of this study. Soil structure interaction will not be considered since the towers are long-period structures and the limestone rock is competent. Field measurements of the dynamic properties (natural frequencies, damping ratios and mode shapes) are also outside the scope of this project; however, the tensions specified in the drawings have been validated by field measurements and so they are reliable. Possible failure scenarios are limited to the failure of cables and to the failure of the reinforced concrete towers, as defined in the objectives.

1.6 Methodology

1. Obtain the necessary documentation from the offices of the Arecibo Observatory to accurately model the structural system.
2. Create the finite element models with the program SAP2000, version 9.
3. Achieve the deformed equilibrium state due to dead load by running a non-linear p-delta analysis. Subsequent modal analysis, and non-linear direct-integration time-history analyses, must start from this state. Achieving the deformed equilibrium state due to dead load will be one of the most difficult tasks in this project, as it is a trial-and-error process.
4. Create several models with increasing degrees of difficulty. This will allow for gradual immersion into the research project.
5. Perform validation checks of the models at all stages to assure reliability of results.
6. Perform sensitivity studies of various parameters to investigate the effects of various assumptions.
7. Obtain appropriate acceleration records in the three orthogonal directions to represent maximum-credible earthquakes for the Arecibo Observatory site.
8. Perform initial seismic simulations and validate the results. Among these, validate the linearized assumption for cable behavior that is based on Ernst's tangent modulus. Also, validate the linear time-history analysis by comparing the results against a large-displacement non-linear direct-integration time-history analysis.

9. Perform final seismic simulations to determine the response when the structure is subjected to maximum-credible earthquakes.
10. Determine the likelihood of failure of the towers and cables of the Arecibo Observatory when subjected to maximum-credible seismic loading.
11. Consider retrofit alternatives, if required.

1.7 Preview of the Three Basic Finite Element Models

The seismic response simulation of the Arecibo Observatory will be conducted with three finite element models of increasing complexity. The first model (Model A) models the platform as two rigid equilateral triangles and assumes that the platform weight is uniformly distributed in the triangles. This model does not include the dome, azimuth arm nor the line feed antenna. Neither does it include the vertical tiedown cables. Model A is also referred to as the “Uniform Platform, No Tiedowns” model throughout the thesis. The second model (Model B) is essentially identical to Model A but includes the vertical tiedown cables. Model B is also referred to as the “Uniform Platform, Tiedowns” model throughout the thesis. The third model (Model C) explicitly models the azimuth arm, the Gregorian dome and the line feed antenna, in addition to the triangular platform. Model C distributes the appropriate weight to each of the components and it is also referred to as the “Distributed Platform, Tiedowns” or “Dome, Tiedowns” model throughout the thesis. Figures of the three models are presented in the following subsections as a preview. Variations from these geometries are undertaken throughout the thesis in sensitivity studies to address different assumptions.

1.7.1 Preview of Model A: Uniform Platform, No Tiedown Cables

The first model (Model A), shown in Figure 1.11, models the platform as two rigid equilateral triangles and assumes the platform weight is uniformly distributed in the triangles. This model does not include the dome, azimuth arm nor the line feed antenna. Neither does it include the vertical tiedown cables. Model A is also referred to as the “Uniform Platform, No Tiedowns” model throughout the thesis. Model A allows for a more gradual investigation into the static behavior of the structure to determine the equilibrium configuration state due to dead load in a non-linear p-delta analysis. The model is thoroughly validated to obtain a high degree of reliability in the results. Two versions of Model A were constructed. The original version assumed a geometry for the auxiliary saddle, since that detail was not available during model construction. Note that the “saddle” is the component atop each tower used to fasten the backstay and platform cables. The ‘auxiliary saddle’ is used to fasten the auxiliary cables while the ‘main saddle’ is used to fasten the main cables. The updated version of Model A incorporated the correct auxiliary saddle geometry. It is shown that the results of the two models (original and updated saddles) are almost identical in most respects. The original version is only used at the beginning of the thesis but its results are fully documented because it accomplished its primary objective of obtaining (and thoroughly validating) the deformed equilibrium state of the structure due to dead load. This step was one of the most important in the thesis as it assures that the cables include their geometric stiffness terms. Both versions of Model A are fully discussed in Chapter 2.

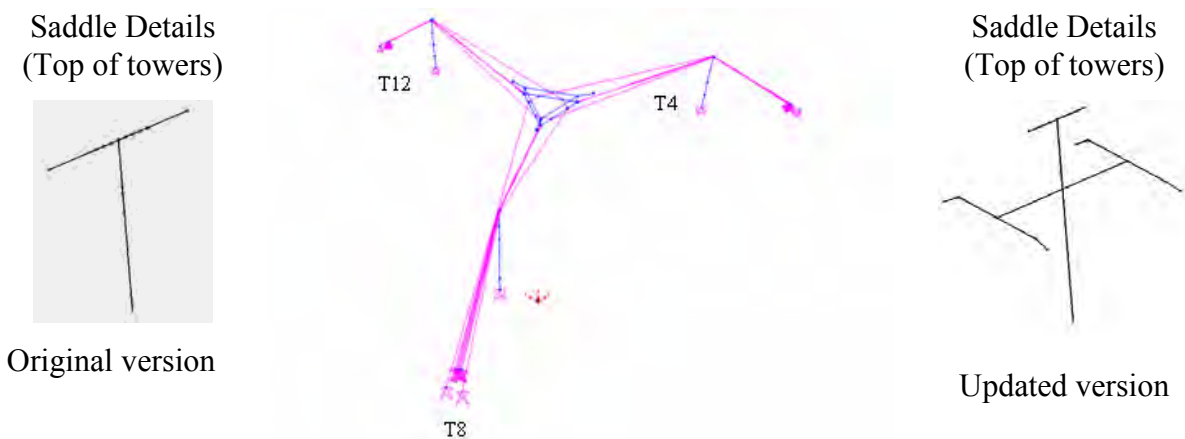


Figure 1.11. Finite element model of Arecibo Observatory— Model A

1.7.2 Preview of Model B: Uniform Platform, With Tiedown Cables

The second model, referred to as Model B and shown in Figure 1.12, is essentially identical to Model A but includes the tiedown cables. This model is fully discussed in Chapter 3. Model B is also referred to as the “Uniform Platform, With Tiedowns” model.

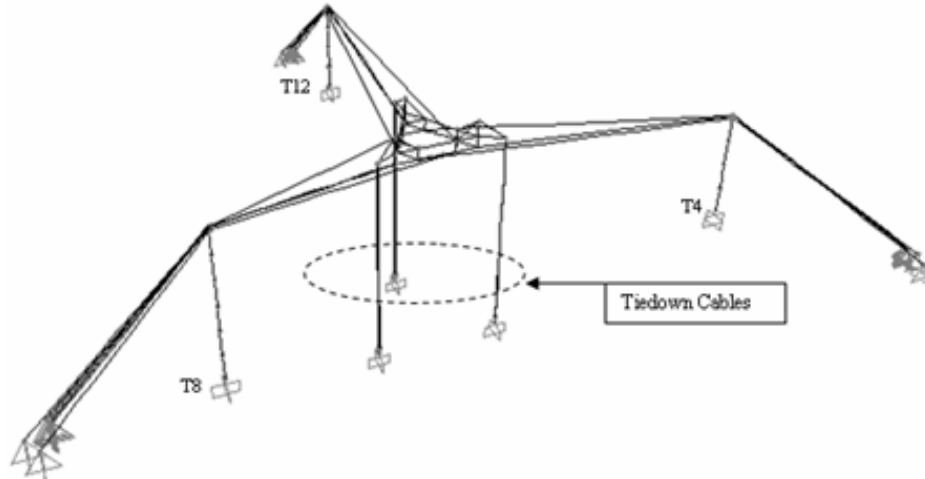


Figure 1.12: Finite element model – Model B

1.7.3 Preview of Model C: Distributed Platform, With Tiedown Cables

The third model (Model C), shown in Figure 1.13, explicitly includes the azimuth arm, the Gregorian dome and the line feed antenna. It is modeled in a worst-case condition with the azimuth arm pointing at tower T8 while the Gregorian dome is at the extreme end (20° position), and the line feed antenna is at stow position. Model C distributes the appropriate weight to each of the platform components and is also referred to as the “Distributed Platform, with Tiedowns” or “Dome, With Tiedowns” model throughout the thesis. Model C is described in detail in Chapter 4.

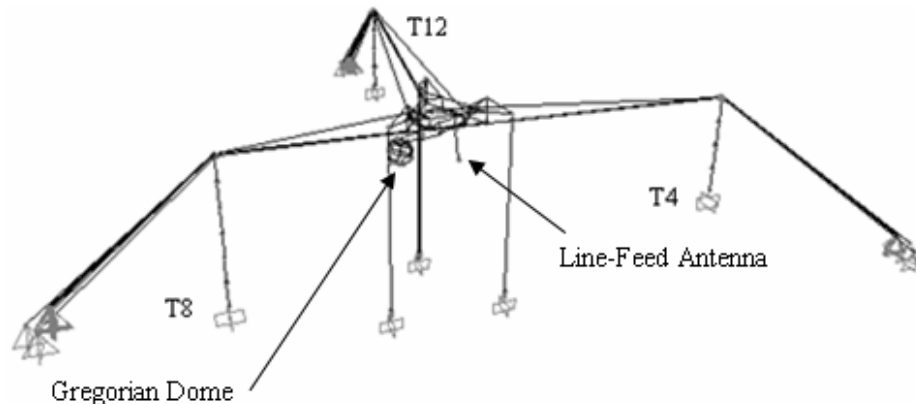


Figure 1.13. Finite element model – Model C

1.8 General Organization of this Thesis

The Arecibo Observatory is a complex structure which requires sophisticated structural analysis procedures in three dimensions to determine its response. Rather than attempting to model every detail of the structure, and run the most complex non-linear analysis procedures in one single shot, the selected approach was one of gradual immersion. In this manner the behavior of the structure could be investigated at a pace that allowed for the implementation of validation procedures that assured the reliability and accuracy of the results. This gradual approach also allowed for the determination of sensitive areas of the structure and assisted in the decision-making process regarding the importance of particular features of the design.

The body of the thesis is divided into three major parts. The first part, which includes Chapters 2 through 4, addresses the creation of the finite element models and the application of self-weight (dead load) to the model using the non-linear p-delta analysis option to achieve the deformed equilibrium state due to dead load. Chapter 2 addresses both versions of Model A; Chapter 3 considers Model B; and Chapter 4 is devoted to Model C. P-delta effects, usually ignored in many typical structural applications, are of primary importance in cable structures. The reason is that cables elements derive practically all their lateral stiffness from their state of tension (defined by the ‘geometric’ stiffness matrix) rather than from their physical properties (defined by the ‘mechanical’ stiffness matrix). Tension in the cables is generated during the p-delta analysis as the self-weight is gradually applied to the model. The cables tighten as a reaction to the applied weight. The ‘structural’ or ‘total’ stiffness matrix of the structure is calculated at the end of the P-delta analysis and is defined as the sum of the ‘mechanical’ and the ‘geometric’ stiffness components.

The second part, Chapter 5, is devoted to calculating the dynamic properties of the system. Mode shapes and natural periods of the structure are determined by using modal decomposition or modal analysis. Mode shapes and periods are determined based on the stiffness matrix generated at the end of the p-delta analysis case, so as to include the geometric stiffness terms.

The third part of the thesis, Chapter 6 through Chapter 10, considers the seismic response of the system (Chapters 6 and 7), the failure criteria (Chapter 8), and an introduction to retrofit alternatives (Chapter 9). Chapter 10 contains the conclusions.

CHAPTER 2

Static Non-Linear P-Delta Analysis – Model A

2.1 Finite Element Model Details of Original Model-A

Model A assumes that the platform's mass is uniformly distributed in the triangular chords of the platform. In addition it does not include tiedown cables. This section addresses the original version. The updated version of Model A is addressed in section 2.5.

2.1.1 Model Geometry

The geometry of the model was obtained from the drawings supplied by the Arecibo Observatory. A rectangular coordinate system was used. The x and y axes are defined in the horizontal plane with 'x' pointing East while 'y' points North (towards tower T12). The z-coordinate points up. The origin of the coordinate system is located exactly under the centroid of the platform at sea level. All z-coordinate values in the model correspond to the elevation above sea level specified in the drawings. This configuration facilitates verification of the data against the drawings.

The (x,y,z) coordinates for all the nodes in the system were determined with AutoCAD and transferred to SAP2000. The "array" command was used in AutoCAD to take advantage of polar symmetry since the towers are separated by 120°.

The overall dimensions of the structure are:

Plan View

- The platform corners are located at a radius of 124.71 ft from the origin. The origin is defined under the centroid of the platform at sea level.
- The tower centerlines are located at a radius of 700 ft from the origin.
- The frontal face of the T12, T8, and T4 backstay anchors are located at a radius of 1080 ft, 1090 ft, and 1155 ft from the origin, respectively.

Elevation View

- The bottom chords of the platform are located at an elevation of 1256.128 ft. The platform must be drawn above this level (approximately 10 feet) to allow it to descend to the specified value as it achieves equilibrium under dead loading in the p-delta analysis.
- The upper chord of the platform is 30 ft above the lower chord.
- The elevations of each step of towers T4 and T12 are: 1133 ft, 1195.5 ft, 1258 ft, 1320.5 ft, and 1383 ft.
- The elevations of each step of tower T8 are: 1018 ft, 1979 ft, 1140 ft, 1201 ft, 1262 ft, 1323 ft, and 1383 ft.
- The elevations of backstay anchors at the working points of A12, A8 and A4 are 1114 ft, 1195 ft, and 1060 ft, respectively.

Additional dimensions are provided in the following sections, as required.

2.1.2 Reinforced Concrete Towers

The towers have a cruciform shape (Figure 1.6) and are stepped in approximately every 60 feet in height (Figure 1.5). Each ~ 60 ft segment is modeled with a single frame object (subdivided into 10 finite elements for the analysis). Towers T12 and T4 use four frame objects (one per segment) while tower T8, the highest one, uses six frame objects.

The local coordinate systems of the tower frames were rotated counterclockwise (CCW) about the local “1” axis to achieve proper orientation for the section properties. The local “1” axis of all towers points up and is coincident with the longitudinal axis of the towers as well as with the global z-axis of SAP2000. The rotation of the axis was achieved by specifying the angles listed in Table 2.1. As shown in Figure 2.1, the local axis 2 of all towers points radially outwards for all objects while the local axis 3 of all the towers is tangential, positive counterclockwise (CCW).

Table 2.1. Rotation angles for local coordinate systems of frame elements (towers)

Tower	Rotation Angle (about "1" axis which coincides with Global Z)
T12	90°
T8	210°
T4	330°

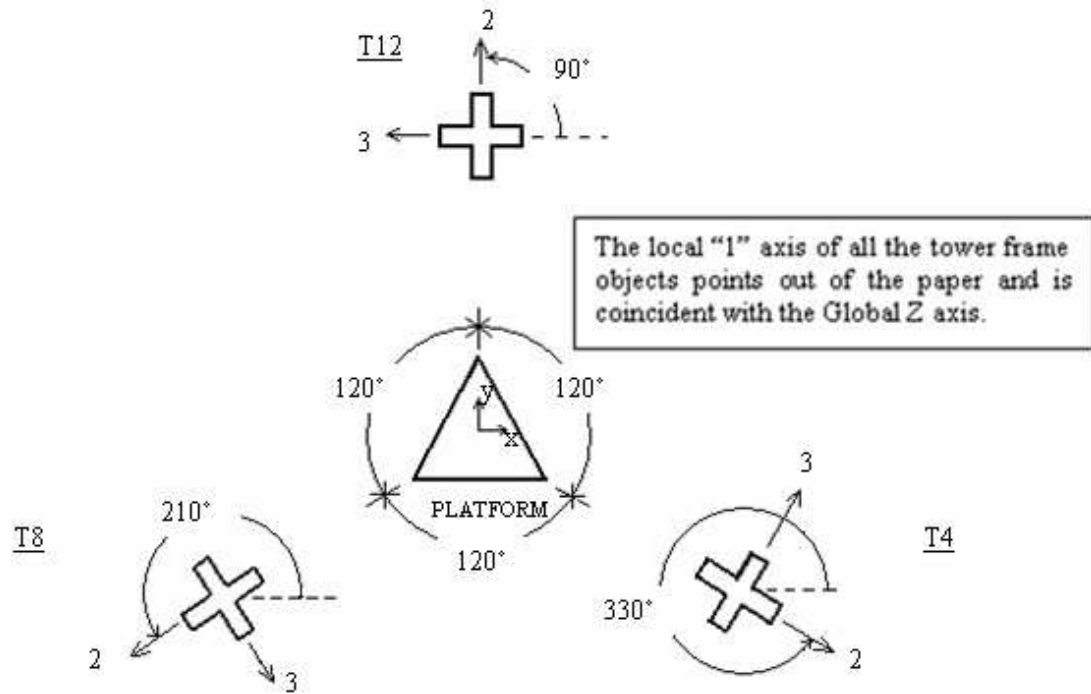


Figure 2.1. Local axis definitions for tower frame-elements in plan view schematic

The material properties [CONC] used for the concrete towers are as follows:

- Concrete unit weight = 150 pcf [default value]
- Concrete unit mass = (concrete unit weight)/g [default value]
- $E = 57 \cdot \sqrt{f'c} = 57(\sqrt{3000 \text{ psi}}) = 3122 \text{ ksi}$
 - 3000 psi concrete strength is specified in the drawings
- Poisson's ratio = 0.2

The section properties of the tower elements, summarized in Table 2.2, were calculated in Excel for each element of each tower. Note that the sections are listed from top to bottom of the towers. Due to the symmetry of the cross section, the same values for Moment of Inertia and Shear Areas are used in both the “2” and “3” local directions for each frame element. The ‘a’ and ‘b’ dimensions are defined in Figure 2.2.

Table 2.2. Section properties of the tower elements

a [ft]	b [ft]	Total Area [ft ²]	Shear Area [ft ²]	Moment of Inertia (Gross) [ft ⁴]	Torsional Constant [ft ⁴]	Section Name	Notes
1.5	9	72	45	419	401	TSEC1	T4, T8, T12
3.5	13	120	65	1225	744	TSEC2	T4, T8, T12
6	18	180	90	3132	1230	TSEC3	T4, T8, T12
9	24	252	120	7236	2109	TSEC4	T4, T8, T12
12	30	324	150	13932	2992	TSEC5	T8 Only
15	36	396	180	23868	4094	TSEC6	T8 Only

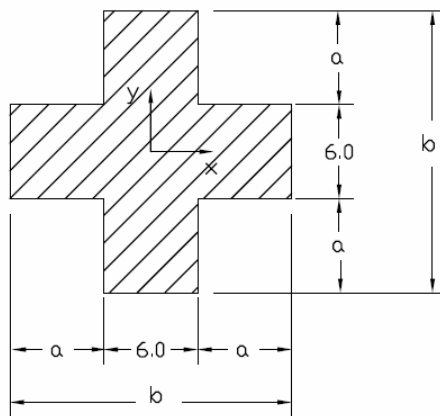


Figure 2.2. Cruciform cross-section. Dimensions in feet.

The entries of Table 2.2 are defined as follows:

b = maximum dimension of the cruciform shape

$$a = (b - 6)/2$$

$$\text{Total Area} = b^2 - 4*a^2$$

$$\text{Shear Area} = 5/6*(b*6.0)$$

The equation assumes that only the rectangular section in the direction of the shear force is effective in resisting shear deformation. This situation is similar to an I-beam resisting shear in the weak-axis direction - the two flanges resist the shear deformation while the web (centrally located as in the case of the cruciform shape) is ignored. The behavior in shear of these shapes is essentially the same as for the rectangle (shape factor of 5/6).

The shear area is a “corrected area” introduced in finite element analysis to account for the difference in the constant rate of shear stress assumed in Timoshenko Beam Theory, used in the formulation of the “frame” finite elements in SAP2000, and the parabolic variation of the actual state of stress, as predicted by equilibrium equations (Reddy 1993). It is significant only in “short beam” cases in which shear, rather than flexure, governs.

$$\text{Moment of Inertia (Gross)} = I_g = 1/12*b^4 - 4[1/12*a^4 + a^2(a/2 + 3)^2]$$

This calculation ignores the contribution of steel re-bar. As a result the towers are very slightly less stiff. The effect of a cracked section, which will soften the sections ($I_{\text{cracked}} < I_{\text{gross}}$), is addressed in Chapters 5 and 7. At that point, the calculation of I_{crack} will include the contribution of steel re-bar. It is expected that the moments generated during a strong seismic event will crack the concrete sections.

$$\text{Torsional Constant} = J = (k_2)_H * b * 6^3 + 2 * (k_2)_V * a * 6^3 \text{ (see Fig. 2.2 for definition of 'a' and 'b')}$$

For open sections developed from rectangular strips (I-beams, channels, angles, cruciforms, for example), the torsional constant is expressed as $J = \sum k_2 * l * t^3$ (Salmon

1996) where k_2 is a constant (see Table 2.3), l is the length of the strip, and t is the width of the strip.

Table 2.3. k_2 constants as a function of l/t ratio

l/t	1.0	1.2	1.5	2.0	2.5	3.0	4.0	5.0	∞
k_2	0.141	0.166	0.196	0.229	0.249	0.263	0.281	0.291	0.333

The constants used in the model are given in Table 2.4:

Table 2.4. Values of k_2 Constants used to calculate Torsional Constant

Section Name	$(a/t)_H$ [adim]	$(k_2)_H$ [adim]	$(b/t)_V$ [adim]	$(k_2)_V$ [adim]
TSEC1	$1.5/6 = 0.25$	0.141	$9/6 = 1.5$	0.196
TSEC2	$3.5/6 = 0.58$	0.141	$13/6 = 2.17$	0.236
TSEC3	$6/6 = 1.0$	0.141	$18/6 = 3.0$	0.263
TSEC4	$9/6 = 1.5$	0.196	$24/6 = 4.0$	0.281
TSEC5	$12/6 = 2.0$	0.229	$30/6 = 5.0$	0.291
TSEC6	$15/6 = 2.5$	0.249	$36/6 = 6.0$	0.333

2.1.3 Tower Saddles

The tower saddles provide the attachment points for cables at the top of the towers. There are two saddles per tower; the main saddle (Figure 2.3) which dates from the original construction in 1963 and the auxiliary saddle which was added in the Gregorian upgrade of 1992. The details of the auxiliary saddle were not available for this model.

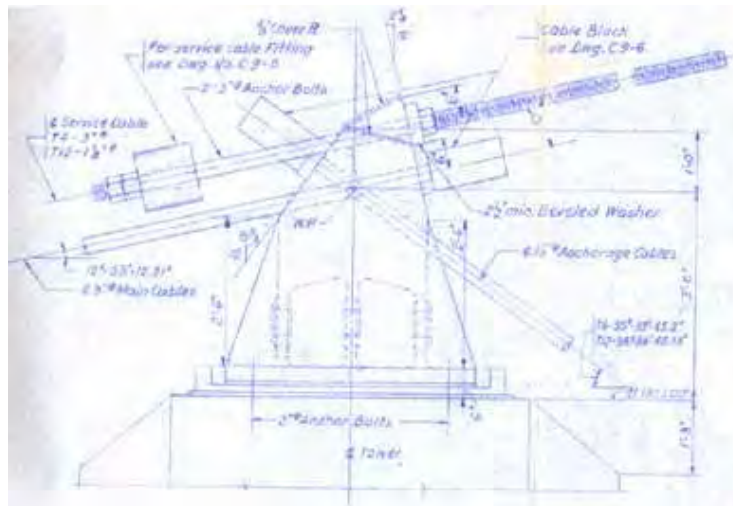


Figure 2.3. Original steel saddle for attachment of cables

Both saddles were modeled within a very stiff “T” frame of negligible weight as shown in Figure 2.4. The main saddle is represented by the nine interior nodes in the horizontal portion of the tee which are used to connect the backstays and main cables in alternate fashion, as shown in Figure 2.5. This geometry is accurate, including the 3.5 ft offset above the concrete towers. On the other hand, the auxiliary saddle is assumed to be represented by the two exterior nodes which are used to connect auxiliary platform and backstay cables.

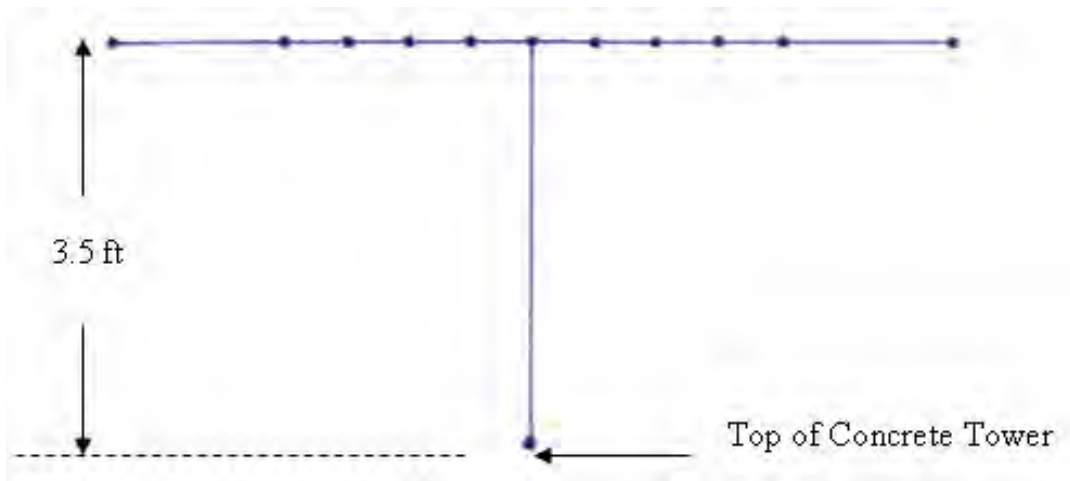


Figure 2.4. Saddle geometry used in Model A

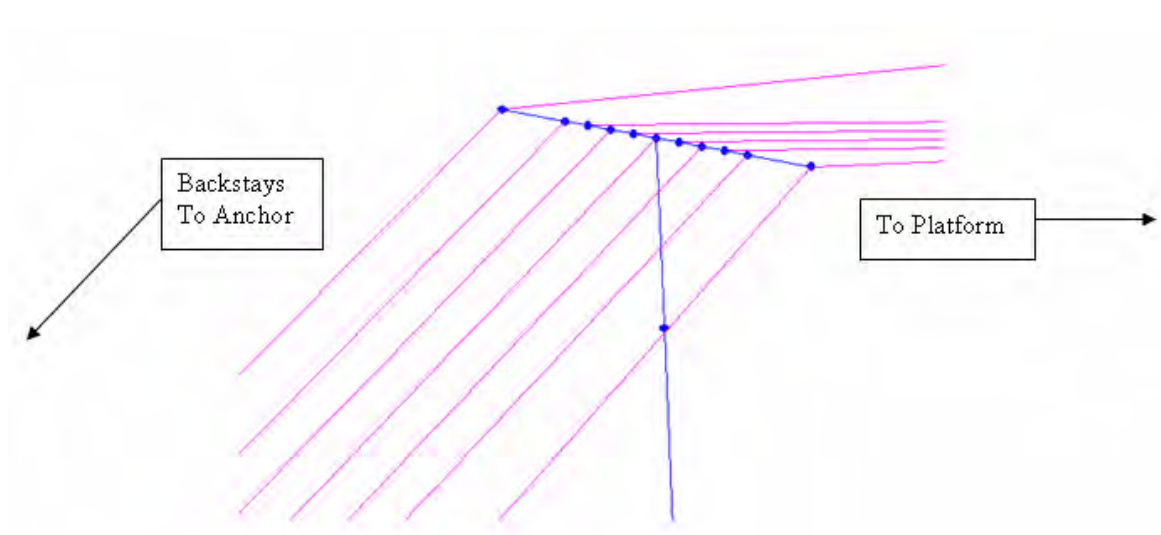


Figure 2.5. Cable attachments to saddle (T8 shown)

2.1.4 Concrete Anchors

The concrete anchors are assumed rigid. They are modeled as special joints unto which the cable ends connect. Joint coordinates were obtained from the drawings. The joints are pinned, i.e., they are restrained against displacements but maintain all the rotational degrees of freedom. The middle five joints anchor the main backstays while the two exterior joints anchor the auxiliary backstays. Figure 2.6 shows a typical anchor (A8 shown).

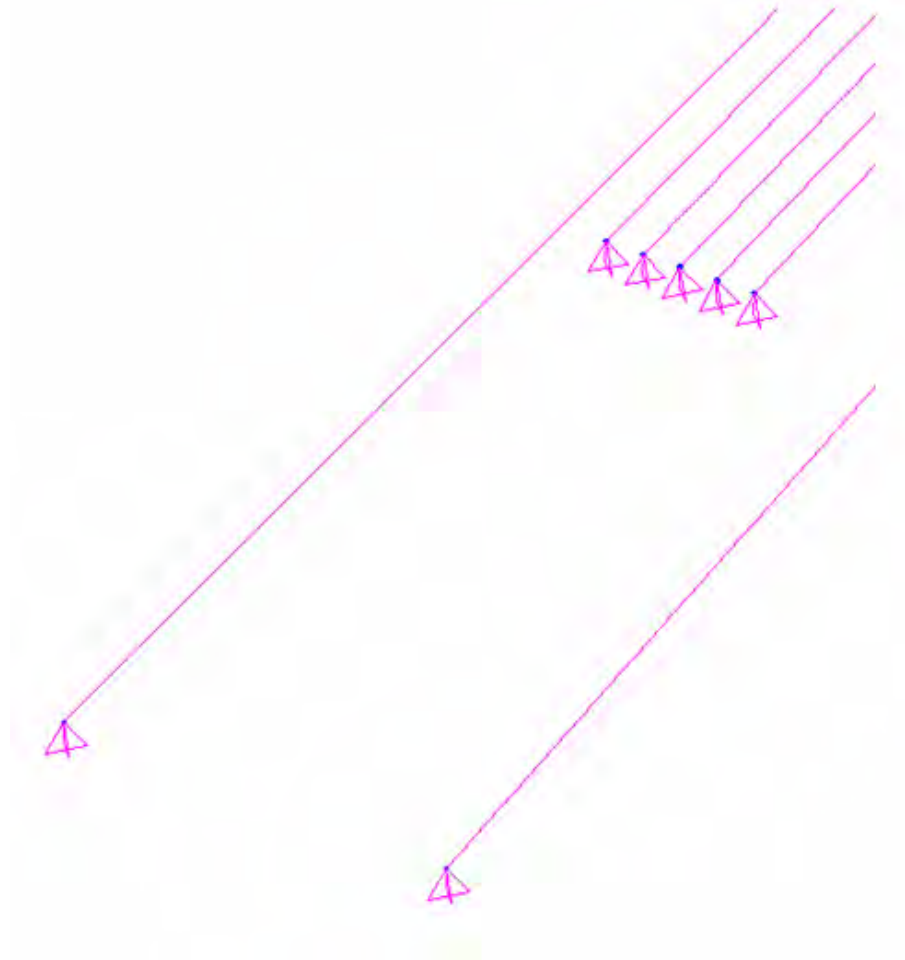


Figure 2.6. Typical modeling of concrete anchors. A8 shown.

2.1.5 Suspended Platform

The suspended platform is assumed to behave as a rigid body since its stiffness is considerably greater than that of the cables supporting it. The rigid body assumption is also considered adequate since the importance of the platform in this study is its overall effect on the behavior of the cable structures that support it. Rigid body behavior is accomplished by using very stiff properties for the elements.

The platform is modeled as two equilateral triangles, one on top of the other, connected by vertical elements at each vertex as shown in Figure 2.7. The length of each side of the triangles is 216 ft, and the separation between the two triangles is 30 feet, as specified in the drawings. All structural details of the platform have been omitted since it is assumed rigid. The load-transfer cables (specified in the drawings) were included to react the tension in the auxiliary cables. The auxiliary cables connect to the lower platform at the end nodes of the load-transfer cables. The entire weight of the platform (1764 kip) is distributed uniformly over the three sides of the lower platform elements.

Although they were not used in the analysis of Model A, the corner extensions were included in the model in anticipation of the need to attach the tiedown cables (see Figure 1.8).

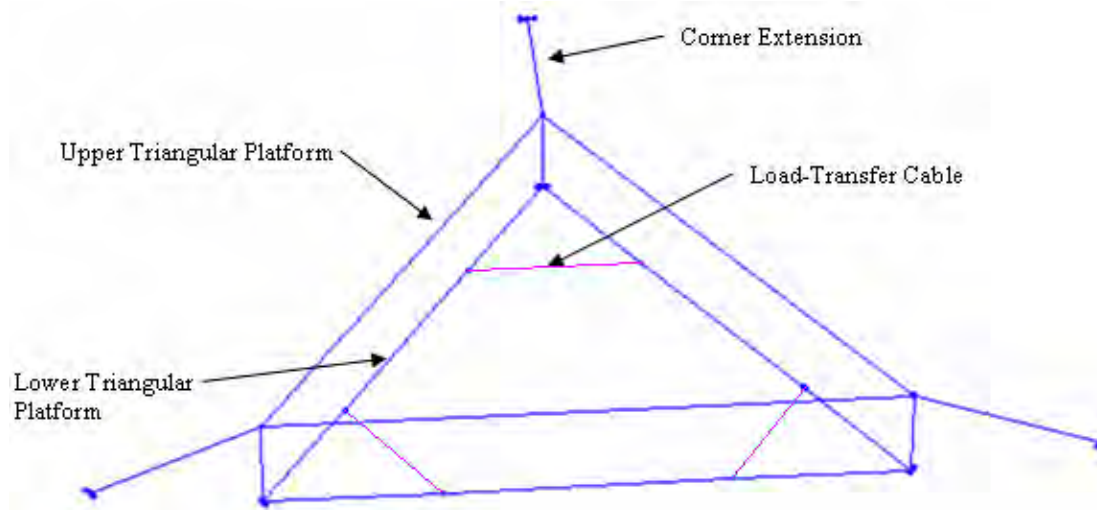


Figure 2.7. Perspective view of platform

The lower platform triangle is modeled with three elements per side. The nodes of the interior element provide the attachment points to the auxiliary cables. Note that load-transfer cables are attached between these points, as noted previously, to react the tension in the auxiliary cables. The load-transfer cables reduce the tendency of the platform to deform in the horizontal plane.

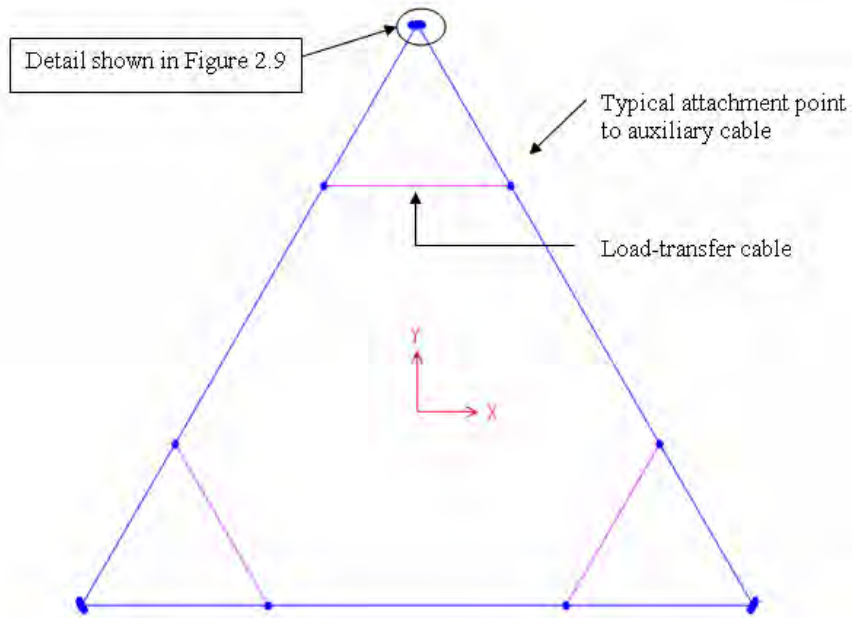


Figure 2.8. Plan view of lower platform

The main cables are connected to the platform by a very stiff, massless beam defined at each vertex (see Figure 2.9).

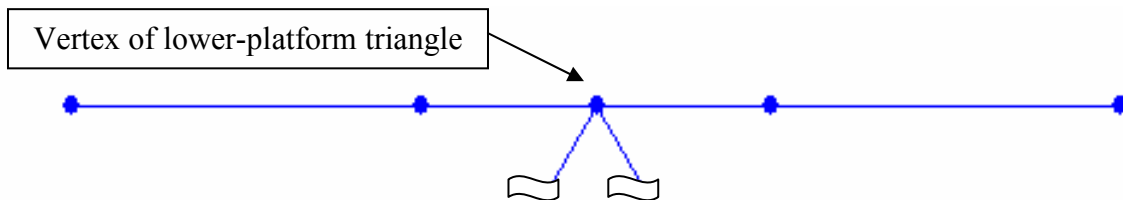


Figure 2.9. Very stiff beam for main cable attachment at lower platform (T12 shown)

The upper platform, as well as the three vertical columns used to connect the lower and upper platforms, are modeled with very stiff, massless elements. Corner extensions are

modeled at each vertex in anticipation of the need to provide attachment points for the tiedown cables (see Figures 2.10 and 2.11), but are not used in the analysis because tiedown cables are not addressed with this model.

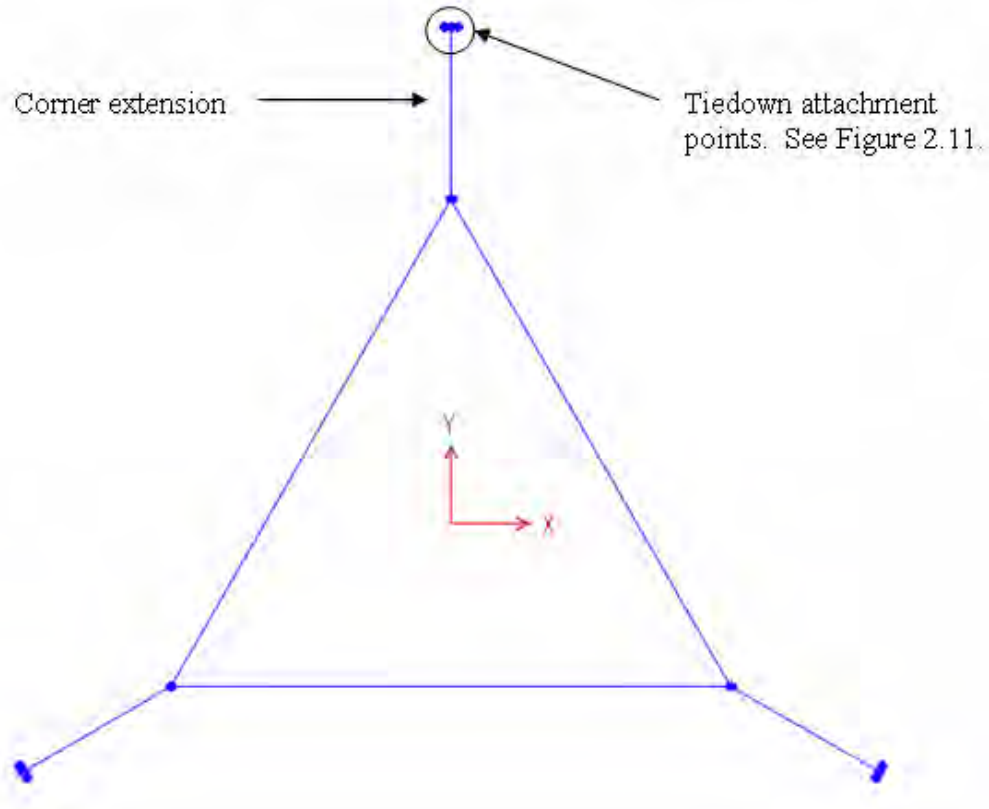
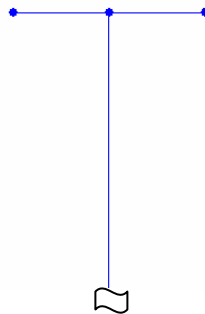


Figure 2.10. Plan view of upper platform



**Figure 2.11. Plan view detail of tiedown attachment points (T12 shown)
(tiedowns not used in analysis of Model A)**

2.1.6 Cables

Figure 2.12 identifies all the cables in the model using T12 as a reference. The same pattern is repeated for each tower. The section name used in SAP2000 is shown within brackets. End release assignments are shown on the left.

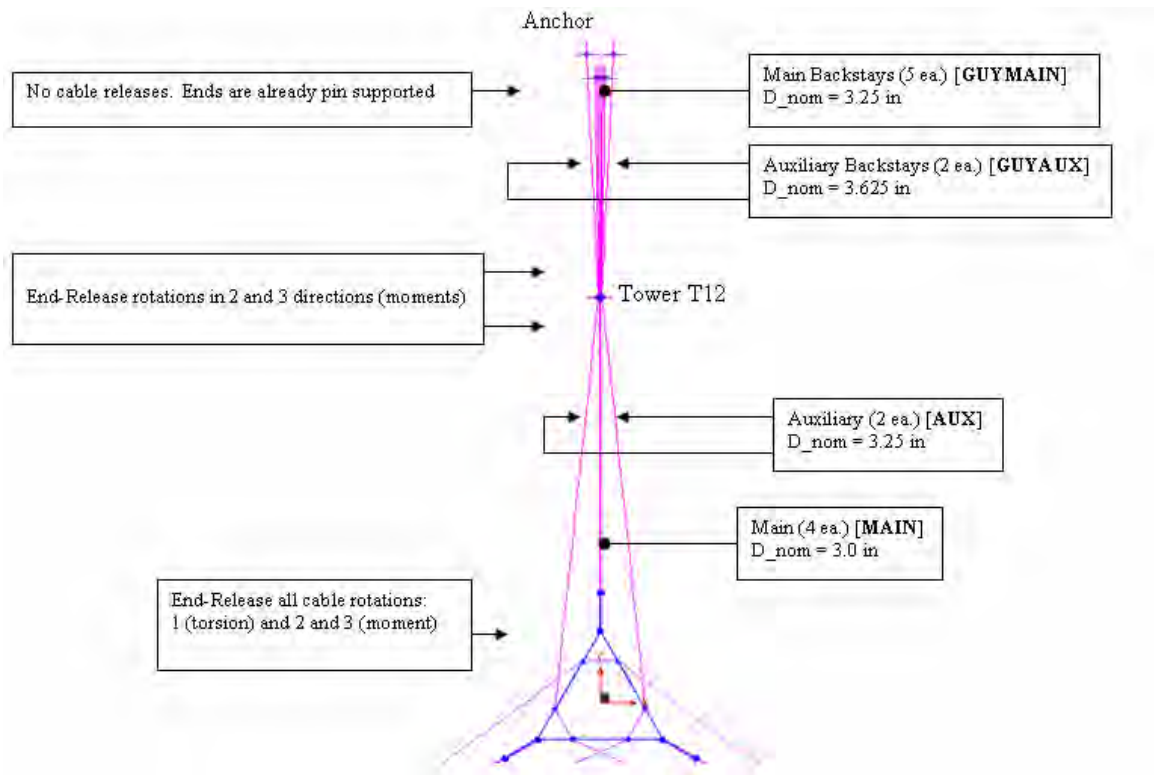


Figure 2.12. Typical cable definitions. Section names shown within brackets (End-release assignments shown on the left)

Cables are modeled as “cable” elements in version 9 of SAP2000. This is the first version that includes a specific cable element in its library of finite elements. Previous versions of SAP2000 did not distinguish cable elements from “frame” elements. The cable length is entered in the “undeformed geometry” state by defining the cables as straight lines between two points. Cable parameters (maximum sag, tensions at each end due to self-weight) are automatically calculated by the program.

The first step in creating the cables is defining the cartesian coordinates of special joints at each end of each cable. Then cables are drawn between the special joints.

The material properties [**STEELCAB**] used for the cables are:

Cable specific weight = $\gamma = 490 \text{ lb/ft}^3$ [default value for steel]

Cable mass density = (cable unit weight)/g [default value]

$E = 24E6 \text{ psi}$ [wire “strand” cable] (See Ernst’s Modulus discussion below)

Poisson’s ratio = 0.3

Table 2.5 summarizes the section properties.

Table 2.5. Section properties of cables

Section Name used in SAP2000	Nominal Diameter [in]	Effective Area [in²]	Effective Diameter [in]	Effective Moment of Inertia [in⁴]	Weight per Unit Length [lb/in]
MAIN	3.0	5.44	2.6318	2.355	1.54
AUX	3.25	6.38	2.8501	3.2392	1.81
GUYMAIN	3.25	6.38	2.8501	3.2392	1.81
GUYAUX	3.625	7.95	3.1815	5.0295	2.25
TIEDOWN	1.5	1.36	1.3159	0.1472	0.38

where,

The nominal diameter is read from the drawings.

The effective area is calculated as: $A_{eff} = \frac{0.77\pi D_{nominal}^2}{4}$ [in²]

The effective diameter is automatically calculated by SAP2000 as: $D_{eff} = \sqrt{\frac{4A_{eff}}{\pi}}$ [in]

The effective moment of inertia about any centroidal-axis in the cross sectional plane is automatically calculated as: $I_{eff} = \frac{\pi D_{eff}^4}{64}$ [in⁴]. It is nearly zero but it is included to avoid computational problems.

The weight per unit length is calculated as: $w = \left(\frac{490}{12^3}\right)(A_{eff})$ [lb/in]

The drawings indicate that all cables are of the “strand” type as compared to “rope” type. In the “strand” type, individual wires are assembled to the desired diameter in one step only. In the “rope” type, individual wires are first wound into smaller-diameter subassemblies and then several of these subassemblies are wound together to form the desired cable diameter. “Strand” utilizes the available area ($\pi D^2/4$) more efficiently than “rope”, i.e., “strand” packs the wires more efficiently. On average, the area of metal in “strand” is 77% of the available area (the remaining 23% is voids) compared to 61% metal area for “rope”. As a result, the weight per unit length of “strand” is higher than for “rope”. In addition, the apparent modulus of elasticity is 24E6 psi for “strand” compared to 22E6 psi for “rope” (see Roebbling 1997).

Ernst’s Modulus of Elasticity

According to Ren (1999a), a typical linearized approach to account for the sag effect of cables is to consider an equivalent straight chord member with an equivalent modulus of elasticity, E_{eq} , given by Ernst’s tangent modulus equation:

$$E_{eq} = \frac{E}{1 + \frac{(wL)^2 AE}{12T^3}}$$

where, for any consistent set of units,

E = Apparent modulus of elasticity (24E6 psi for wire ‘strand’)

w = weight per unit length = (Specific weight) * (Effective Area)

L = horizontal projected length of the cable

A = Effective area of the cable

T = Tension in the cable

Note that as T increases or L decreases (cable inclination approaches verticality), the value of E_{eq} asymptotically approaches E . In the case of the Arecibo Observatory it is shown (see example below) that, due to the very high state of tension in the cables, there is only a 1% difference between moduli so, for all practical purposes, $E_{eq} = E$. Therefore the model uses an elastic modulus $E = 24E6$ psi for all cables throughout the analyses.

Example Case: Main Cable (proves that $E_{eq} \approx E$)

$$A_{eff} = 5.44 \text{ in}^2$$

$$E = 24E6 \text{ lb/in}^2$$

$$w = \gamma * A_{eff} = 490/(12^3) \text{ lb/in}^3 * 5.44 \text{ in}^2 = 1.543 \text{ lb/in}$$

$$L = \text{sqrt}[(588 \text{ ft})^2 - (1386.5 \text{ ft} - 1264.9 \text{ ft})^2] = 575 \text{ ft} = 6900 \text{ in}$$

$$T = 480000 \text{ lb [specified in drawings]}$$

Substituting,

$$E_{eq} = \frac{24E06}{1 + \frac{[(1.543)(6900)]^2 (5.44)(24E06)}{12(480000)^3}}$$

$$E_{eq} = 23.74E6 \text{ psi}$$

$$\text{Percent difference (between } E_{eq} \text{ and } E) = 1.1 \%$$

Due to the very high state of tension in the cables it can be concluded that the magnitude of E_{eq} has approached E asymptotically; therefore, $E_{eq} = E = 24E6$ psi.

2.2 Geometric Stiffness Requirement for Cable Structures

This section introduces the concept of geometric stiffness which is critical in the study of cables. It follows Wilson (2000). The ‘geometric’ stiffness of a structural element differs from the ‘mechanical’ stiffness in that it is a function of the load while the ‘mechanical’ stiffness is only based on the physical properties of the element. The total structural stiffness matrix is obtained by adding the geometric and the mechanical stiffness matrices. The geometric stiffness can be either positive or negative. The positive geometric stiffness case is represented by a tensioned cable, where its lateral stiffness increases with increased levels of tension. On the other hand, the negative geometric stiffness case is represented by a slender rod in compression, where its lateral stiffness is reduced with increased levels of compression, so that a small lateral load may cause the rod to buckle. The fundamental equations for the geometric stiffness of a cable are easily derived. The key to the derivation is to base it on the deformed geometry.

Consider the cable element shown in Figure 2.13. Originally, the cable is horizontal with an initial tension T . When subjected to lateral displacements v_i and v_j , the additional forces F_i and F_j (assumed positive in the up direction) must be developed to satisfy equilibrium in the deformed shape. It is assumed that displacements are small so they do not change the tension in the cable, and the tension can be considered to act horizontally.

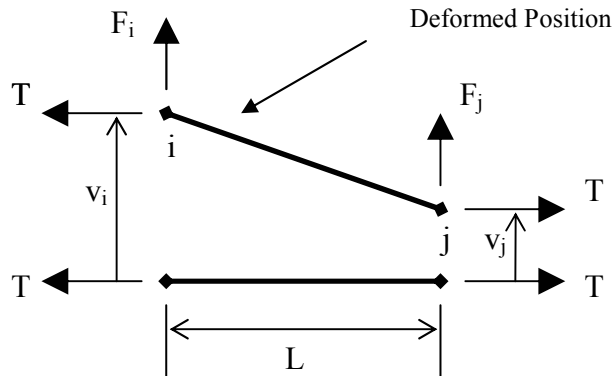


Figure 2.13. Forces on a cable element

The following equation results from $\sum M_j = 0$:

$$F_i = \frac{T}{L}(v_i - v_j)$$

The following equation is apparent from $\sum F_y = 0$:

$$F_j = -F_i$$

These two equations can be combined into the following matrix equation:

$$\begin{Bmatrix} F_i \\ F_j \end{Bmatrix} = \frac{T}{L} \begin{bmatrix} 1 & -1 \\ -1 & 1 \end{bmatrix} \begin{Bmatrix} v_i \\ v_j \end{Bmatrix}$$

The 2x2 stiffness matrix shown above is not a function of the mechanical properties. It is only a function of the load and the length of the element. This is the reason it is termed the ‘geometric’ stiffness matrix. It is only important when it is large compared to the mechanical stiffness of the structural system. The four terms of the 2x2 geometric stiffness matrix would be added to the “ $12EI/L^3$ ” terms in the mechanical stiffness matrix. For the derivation of a consistent geometric stiffness matrix for beam elements see Cook (2002).

2.3 Case 1: Self-Weight Only (No Preloading of Cables)

In this initial case the self-weight of the structure is applied in a non-linear p-delta analysis. This is the step in which the ‘geometric’ stiffness matrix of the cables is developed. In fact, the geometric stiffness matrix of all the structural elements is created in this step; however, only for cables is it large compared to the mechanical stiffness. A full validation of the results is included as it is this process that builds reliability in the results and assures that the subsequent analyses are well founded. In the next case, case 2, thermal strains will be applied to the backstays to simulate the jacking operation performed during construction to maintain the towers straight and vertical. Jacking was performed as the platform was raised from the ground, and during maintenance procedures.

2.3.1 Initial Guess on Platform Descent due to Cable Stretch

Cables will stretch during the non-linear p-delta analysis as the self-weight of the structure is applied. As a result the platform will descend. It can be shown that a 3.0 inch diameter main cable will stretch approximately 1.9 feet (using $u = TL/AE$) based on the nominal tension value specified in the drawings. The vertical drop associated with this stretch may be obtained with AutoCAD (see Figure 2.14), as follows: the initial length ($L_{initial}$) is swept into an arc; the stretched length (L_{final}) is drawn at the angle specified in the drawings; a vertical line is drawn from the end of the stretched line up to the arc and measured (8.777 ft). The vertical distance represents the descent of the platform.

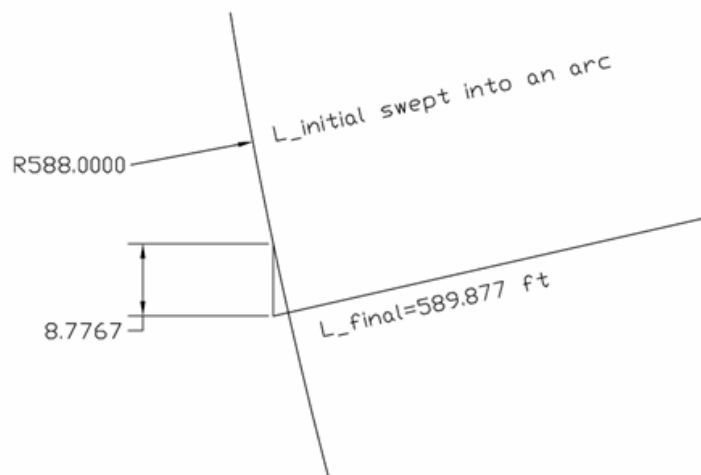


Figure 2.14. Graphical analysis to determine platform descent due to cable stretch

The platform descent is estimated at 8.777 ft. This is the amount by which the platform must be raised to allow it to descend to the specified height of 1256.128 ft.

Calculation of z-coordinate (lower chord) = 1256.128 ft + 8.777 ft = 1264.905 ft.

This value (1264.905 ft) establishes the elevation at which the lower platform must be drawn in the model.

2.3.2 Analysis Case Setup

The static non-linear p-delta analysis option is set in the ‘Define Analysis Cases’ of the SAP2000 environment. The dialog box that appears is shown in Figure 2.15. Note the load name is DEAD with a scale factor of 1.0 to apply self-weight. Also note the ‘Static’ analysis case type is selected along with the ‘Nonlinear’ type.

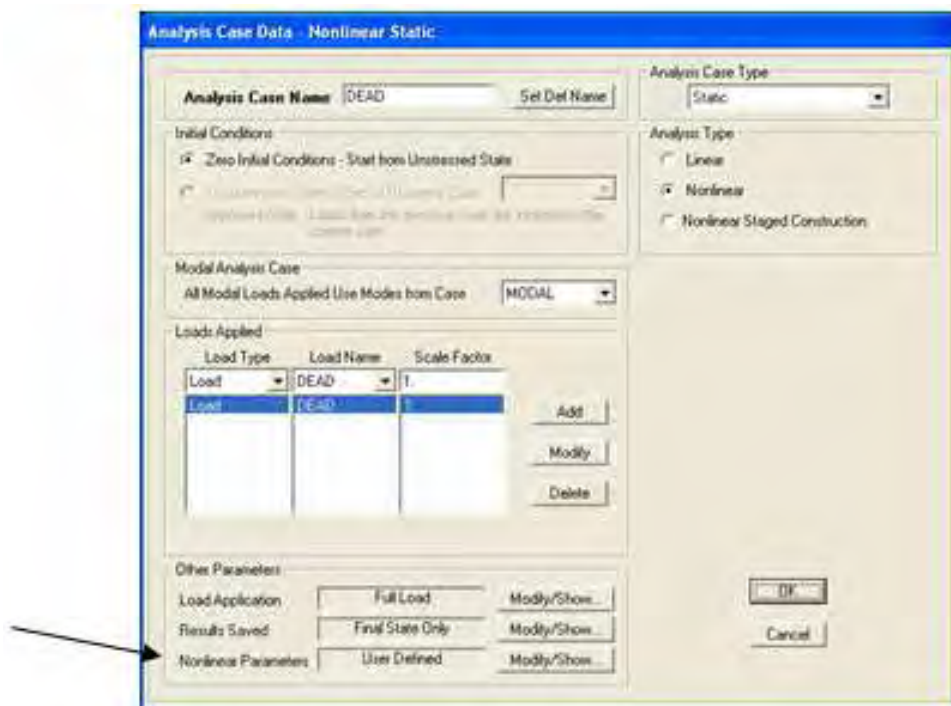


Figure 2.15. Setting up the static non-linear p-delta analysis case

To establish that it is a p-delta analysis the Modify/Show button for ‘Nonlinear parameters’ (Figure 2.15) must be activated. The dialog box that appears is shown in Figure 2.16.

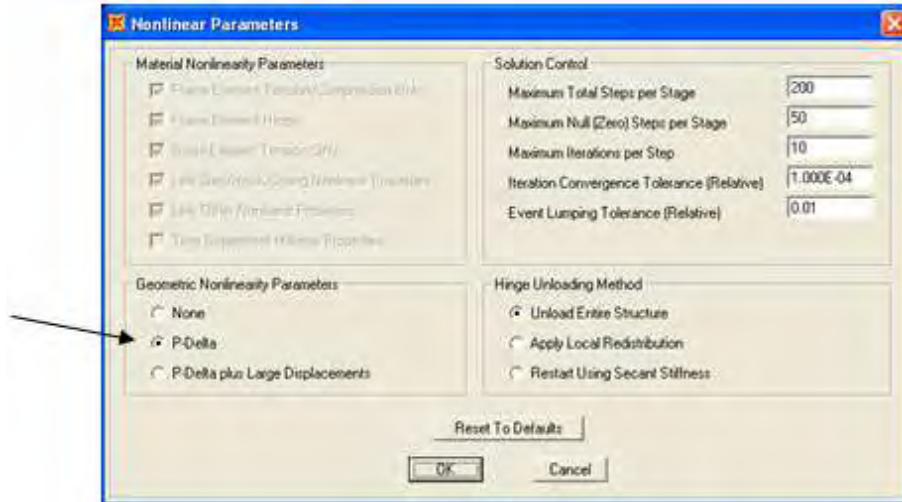


Figure 2.16. Setting up the p-delta option.

2.3.3 Results and Validation Checks (Self-Weight Only)

The deformed shape (highly exaggerated) is shown in Figure 2.17. Note the platform has descended as expected. In addition, the tower tops are flexing inward due to the weight of the platform. This will be corrected in the next section using thermal strains that simulate the hydraulic jacking action which physically applies preload to the cables.



Figure 2.17. Deformed shape with self-weight only (highly exaggerated)

Validation Check 1 – A rigorous data check of the Excel spreadsheets exported from the model as well as data checks within the graphic environment of SAP2000 was carried out. The following tasks were performed:

- i. Confirm cartesian coordinates and labels of all the joints.
- ii. Confirm frame object connectivity as well as their labels.
- iii. Confirm local axes assignments for the tower frame objects.
- iv. Confirm cable object connectivity as well as their labels.
- v. Confirm restraints. Pinned at the anchors and fixed at the tower supports.
- vi. Confirm material properties
 - CONC for concrete towers
 - STEELCAB for all the cables
 - CORRSTIFF4 to assign the proper weight to the lower platform frame objects.
 - STIFFNOWT4 very stiff, almost massless material used in all the very stiff objects. The number 4 at the end of the name refers to the order of magnitude of the change in the properties (elastic modulus increased by 10^4 and mass reduced by 10^{-4}). The SAP2000 manual recommends this order of magnitude to avoid singularities in the solution.
- vii. Confirm the section properties
 - TSEC1, TSEC2, TSEC3, TSEC4, TSEC5, TSEC6 to model the six steps in the concrete towers. These sections use the material CONC.
 - MAIN, AUX, GUYMAIN, GUYAUX to model the main, auxiliary, main backstays, and auxiliary backstays cables. These sections use the material STEELCAB.
- viii. Confirm that the frame autosubdivision assignments to tower objects is equal to ten (ten finite elements per tower step).

- ix. Confirm that the autosubdivision assignment for cables is equal to ten.
- x. Confirm that the compression limit for cables is equal to zero (no compression allowed).
- xi. Confirm the parameters of the non-linear, p-delta analysis case.

These validation checks were performed on the Excel spreadsheets exported from the model as well as data checks within the graphic environment of SAP2000.

Validation Check 2 - Equilibrium check. The sum of the vertical reactions at the supports must equal the self weight of the structure ($\Sigma R_z = |W|$). The horizontal reactions at all the supports must total zero ($\Sigma F_x = \Sigma F_y = 0$) since the only applied load is vertical (self-weight only).

Table 2.6. Equilibrium check of vertical forces

Weight of all cables	470.92 kip
Weight of lower platform	1764.0 kip
Weight of concrete towers	23,986.8 kip
Weight of very stiff elements (essentially “weightless”)	3.38 kip
TOTAL SELF WEIGHT (Add above weights)	26,225.14 kip
Magnitude of vertical reactions at all model supports: 3 fixed tower bases and 3 pinned anchors. (Σ Reactions in Global z direction)	26,266.7kip
PERCENT DIFFERENCE	0.16%

Table 2.6 shows there is a 42 kip mismatch (0.16% difference) which is acceptable considering the size and weight of the structure (over 26,000 kip) and the fact that the forces were obtained from a nonlinear numerical analysis.

Table 2.7. Equilibrium check of horizontal forces

Σ Reactions in Global x direction (should equal 0)	3.20 kip
Σ Reactions in Global y direction (should equal 0)	-0.002 kip

Table 2.7 shows a 3.2 kip difference in the x-direction equilibrium which is acceptable considering the magnitude of the forces involved (weight of the structure over 26,000 kip), the size of the structure, and the fact that a nonlinear numerical analysis was performed. The 0.002 kip difference in the y-direction is excellent.

Validation Check 3 - Check the very stiff saddle on top of the towers (see Figure 2.4) and the very stiff beam at the platform (see Figure 2.9) to verify they are acting like rigid bodies as planned. Results are included for each of the three towers in Tables 2.8-2.10

Table 2.8. T12 Tower - displacements of very stiff saddle (See Fig. 2.4)

JOINT	Ux [in]	Uy [in]	Uz [in]
22	-0.08433	-19.00512	-0.20839
23	-0.08433	-19.00627	-0.20956
24	-0.08433	-19.00669	-0.20999
25	-0.08433	-19.00711	-0.21041
26	-0.08433	-19.00753	-0.21084
27	-0.08433	-19.00794	-0.21126
28	-0.08433	-19.00836	-0.21168
29	-0.08433	-19.00878	-0.21211
30	-0.08433	-19.00920	-0.21253
31	-0.08433	-19.00961	-0.21296
32	-0.08433	-19.01077	-0.21413

Since almost identical results are obtained at each node, rigid body behavior is validated in the saddle of tower T12. In the case of Uy and Uz, the small variations in the displacements produces a straight-line deflected shape. The same conclusions can be reached in towers T8 and T4, the displacements of which are tabulated in Table 2.9 and 2.10.

Table 2.9. T8 Tower - displacements of very stiff saddle (See Fig. 2.4)

JOINT	Ux [in]	Uy [in]	Uz [in]
33	13.35390	7.76760	-0.27736
34	13.35339	7.76731	-0.27678
35	13.35321	7.76720	-0.27657
36	13.35303	7.76709	-0.27636
37	13.35284	7.76699	-0.27615
38	13.35266	7.76688	-0.27594
39	13.35248	7.76678	-0.27574
40	13.35229	7.76667	-0.27553
41	13.35211	7.76656	-0.27532
42	13.35193	7.76646	-0.27511
43	13.35142	7.76616	-0.27453

Table 2.10. T4 Tower - displacements of very stiff saddle (See Fig. 2.4)

JOINT	Ux [in]	Uy [in]	Uz [in]
44	-19.10736	10.97916	-0.21090
45	-19.10683	10.97885	-0.21027
46	-19.10664	10.97874	-0.21004
47	-19.10644	10.97863	-0.20981
48	-19.10625	10.97852	-0.20958
49	-19.10606	10.97841	-0.20935
50	-19.10587	10.97830	-0.20912
51	-19.10568	10.97819	-0.20889
52	-19.10549	10.97808	-0.20867
53	-19.10530	10.97797	-0.20844
54	-19.10476	10.97766	-0.20780

The results for the very stiff beams at the corners of the platform are given in Tables 2.11 through 2.13. The displacements shown in the tables confirm the intended rigid body behavior. When there are small differences, a plot of the deformed shape shows a straight line.

Table 2.11. T12 – displacements at very stiff platform beam (See Fig. 2.9)

JOINT	Ux [ft]	Uy [ft]	Uz [ft]
81	-0.30713	-0.01369	-19.49643
82	-0.30713	-0.01369	-19.49594
72 (Vtx.)	-0.30713	-0.01369	-19.49570
83	-0.30713	-0.01369	-19.49546
84	-0.30713	-0.01369	-19.49497

Table 2.12. T8 - displacements at very stiff platform beam (See Fig. 2.9)

JOINT	Ux [ft]	Uy [ft]	Uz [ft]
85	-0.30721	-0.01365	-19.43909
86	-0.30721	-0.01365	-19.43930
75 (Vtx.)	-0.30721	-0.01365	-19.43940
87	-0.30721	-0.01365	-19.43950
88	-0.30721	-0.01365	-19.43971

Table 2.13. T4 - displacements at very stiff platform beam (See Fig. 2.9)

JOINT	Ux [ft]	Uy [ft]	Uz [ft]
89	-0.30721	-0.01374	-19.53620
90	-0.30721	-0.01374	-19.53648
78(Vtx.)	-0.30721	-0.01374	-19.53662
91	-0.30721	-0.01374	-19.53677
92	-0.30721	-0.01374	-19.53705

It can be concluded that the results are reasonable and the investigation can proceed to the next step which is to iterate on the cable preload to achieve verticality of towers. The negative strains are induced with a negative temperature load. Before proceeding with the iterations, the initial guess on temperatures is calculated.

2.3.4 Initial Guess for the Applied Temperatures (Cable Preload)

The elongation of a one-dimensional bar due to a temperature difference is given by the following equation

$$v = \alpha \Delta T L, \text{ or rearranging, } \Delta T = v/(\alpha L)$$

where, for any consistent set of units,

v = Elongation experienced by the bar (use the radial displacement at the top of tower

T8 calculated with SAP2000 in Case1: self-weight case)

α = Coefficient of thermal expansion [1/°F]

ΔT = Temperature difference [°F] (Applied as a negative value to create compressive strains)

L = Length of the bar

Table 2.14. Initial guess for backstay temperatures (cable preload)

Tower ID	v [ft]	L [ft]	α [1/°F]	ΔT [°F]
T12	1.6	467	6.5E-06	527
T8	1.3	435	6.5E-06	460
T4	1.9	560	6.5E-06	522

2.4 Case 2: Achieving Actual Equilibrium State of Structure due to Dead Load

The results of case 1 indicate the non-linear p-delta analysis is generating reliable results. However, case 1 did not consider cable preload which is necessary to achieve the actual equilibrium state of the structure. The correct deformed equilibrium condition under dead loads is defined by the following three criteria:

1. The three towers are vertical, i.e., the x and y displacements at the top of each tower converge to zero. Axial shortening is not zero since weight and the vertical component of the cable tensions will compress the towers.

This criterion governs the amount of preload to be added to the backstays. Preload must be large enough to bring the towers back to vertical after adding the self-weight of the platform and cables. Note that if the backstays are not preloaded the three towers flex radially inwards as shown in Figure 2.17. In reality, preload is added with hydraulic jacks at the concrete anchors. In the model, preload is added as a negative temperature strain per recommendations of the software developer.

2. The magnitude of the tension in each cable must be equal to the tension values specified in the drawings.

This constraint clashes with the first (verticality of towers) in the sense that it may be impossible to satisfy both of them simultaneously in the model. The structure is indeterminate to a very high degree and small uncertainties in material or section properties may lead to different tensions. The emphasis in the analysis will be on achieving criterion 1 and then determining the difference in tension as compared to the drawings.

3. The elevation of the platform at the end of the p-delta analysis should match the elevation specified in the drawings. The platform descends during the p-delta analysis as cables stretch due to the applied self-weight. A preliminary estimate of the descent was calculated graphically in Figure 2.14.

2.4.1 Iteration of Temperature Values

Cable preload is achieved by applying negative thermal strains to the cables. This is accomplished by applying negative temperatures in the DEAD analysis case and setting the reference temperature to zero. Fifteen iterations were required to achieve verticality of the towers. The summary of the iterations is shown in Table 2.15. The tensions specified in the drawings have been included (for reference) in the first column.

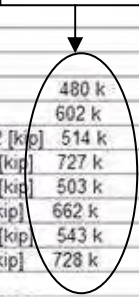
Table 2.15. Iterations to achieve verticality of towers

ARECIBO OBSERVATORY ITERATION CHART - CABLE PRELOAD PAGE 1									
INPUT	NO TEMP	TEMP 1	TEMP 2	TEMP 3	TEMP 4	TEMP 5	TEMP 6	TEMP 7	
TEMP MAIN [F]	0	0	0	0	0	0	0	0	0
TEMP AUX [F]	0	-100	-200	-300	-250	-250	-250	-250	-250
TEMP GUYMAIN T12 [F]	0	-527	-527	-527	-550	-527	-475	-500	
TEMP GUYAUX T12 [F]	0	-527	-527	-527	-600	-475	-475	-500	
TEMP GUYMAIN T8 [F]	0	-460	-460	-460	-500	-460	-475	-465	
TEMP GUYAUX T8 [F]	0	-460	-460	-460	-560	-400	-475	-465	
TEMP GUYMAIN T4 [F]	0	-522	-522	-522	-600	-522	-475	-500	
TEMP GUYAUX T4 [F]	0	-522	-522	-522	-650	-480	-475	-500	
INITIAL Z OFFSET [ft]	8.777	8.777	8.777	8.777	8.777	8.777	8.777	8.777	8.777
OUTPUT									
PLATFORM UZ [ft]	-19.5	-11.1	-10.5	-10	-9.2	NO GOOD	-10.7	-10.5	
UX T12 TOWER [in]	-0.08159	0.00951	0.00864	0.0076	0.03561	NO GOOD	-0.02534	-0.00665	
UY T12 TOWER [in]	-18.40276	0.95898	0.73833	0.51761	2.062	NO GOOD	-1.32918	-0.38838	
UX T8 TOWER [in]	12.9986	-0.13325	0.02225	0.1779	-1.60625	NO GOOD	-0.37878	-0.06408	
UY T8 TOWER [in]	7.5609	-0.07568	0.01498	0.10559	-0.97585	NO GOOD	-0.21443	-0.0356	
UX T4 TOWER [in]	-18.49694	0.79042	0.56886	0.34706	4.0184	NO GOOD	-1.33133	-0.37784	
UY T4 TOWER [in]	10.62844	-0.44435	-0.31675	-0.18932	-2.31674	NO GOOD	0.74257	0.21151	
TENSION MAIN [kip]	480 k	554	521	492	462	477	NO GOOD	477	477
TENSION AUX [kip]	602 k	365	504	579	655	627	NO GOOD	614	616
TENSION GUYMAIN T12 [kip]	514 k	418	499	504	510	497	NO GOOD	501	504
TENSION GUYAUX T12 [kip]	727 k	470	625	630	636	687	NO GOOD	620	626
TENSION GUYMAIN T8 [kip]	503 k	403	450	454	460	443	NO GOOD	457	457
TENSION GUYAUX T8 [kip]	662 k	453	564	569	575	635	NO GOOD	574	572
TENSION GUYMAIN T4 [kip]	543 k	405	499	504	509	505	NO GOOD	500	503
TENSION GUYAUX T4 [kip]	728 k	463	624	629	635	701	NO GOOD	619	626
ERROR									
error in platform offset [ft]	-10.723	-2.323	-1.723	-1.223	-0.423	NO GOOD	-1.923	-1.723	
error in ux T12 tower [in]	-0.08159	0.00951	0.00864	0.0076	0.03561	NO GOOD	-0.02534	-0.00665	
error in uy T12 tower [in]	-18.40276	0.95898	0.73833	0.51761	2.062	NO GOOD	-1.32918	-0.38838	
error in ux T8 tower [in]	12.9986	-0.13325	0.02225	0.1779	-1.60625	NO GOOD	-0.37878	-0.06408	
error in uy T8 tower [in]	7.5609	-0.07568	0.01498	0.10559	-0.97585	NO GOOD	-0.21443	-0.0356	
error in ux T4 tower [in]	-18.49694	0.79042	0.56886	0.34706	4.0184	NO GOOD	-1.33133	-0.37784	
error in uy T4 tower [in]	10.62844	-0.44435	-0.31675	-0.18932	-2.31674	NO GOOD	0.74257	0.21151	
error in tension main [kip]	480 k	74	41	12	-18	-3	NO GOOD	-3	-3
error in tension aux [kip]	602 k	-237	-98	-23	53	25	NO GOOD	12	14
error in tension guymain T12 [kip]	514 k	-96	-15	-10	-4	-17	NO GOOD	-13	-10
error in tension guyaux T12 [kip]	727 k	-257	-102	-97	-91	-40	NO GOOD	-107	-101
error in tension guymain T8 [kip]	503 k	-100	-53	-49	-43	-60	NO GOOD	-46	-46
error in tension guyaux T8 [kip]	662 k	-209	-98	-93	-87	-27	NO GOOD	-88	-90
error in tension guymain T4 [kip]	543 k	-138	-44	-39	-34	-38	NO GOOD	-43	-40
error in tension guyaux T4 [kip]	728 k	-265	-104	-99	-93	-27	NO GOOD	-109	-102
PERCENT ERROR (TENSIONS)									
percent error in tension main [kip]	480 k	15.4	8.5	2.5	-3.8	-0.6	NO GOOD	-0.6	-0.6
percent error in tension aux [kip]	602 k	-39.4	-16.3	-3.8	8.8	4.2	NO GOOD	2.0	2.3
percent error in tension guymain T12 [kip]	514 k	-18.7	-2.9	-1.9	-0.8	-3.3	NO GOOD	-2.5	-1.9
percent error in tension guyaux T12 [kip]	727 k	-35.4	-14.0	-13.3	-12.5	-5.5	NO GOOD	-14.7	-13.9
percent error in tension guymain T8 [kip]	503 k	-19.9	-10.5	-9.7	-8.5	-11.9	NO GOOD	-9.1	-9.1
percent error in tension guyaux T8 [kip]	662 k	-31.6	-14.8	-14.0	-13.1	-4.1	NO GOOD	-13.3	-13.6
percent error in tension guymain T4 [kip]	543 k	-25.4	-8.1	-7.2	-6.3	-7.0	NO GOOD	-7.9	-7.4
percent error in tension guyaux T4 [kip]	728 k	-36.4	-14.3	-13.6	-12.8	-3.7	NO GOOD	-15.0	-14.0
NOTES:									
1. Case TEMP5. Auxiliary Backstays of T4 went slack. Periods of 80 sec.									

Table 2.15. Continuation

ARECIBO OBSERVATORY ITERATION CHART - CABLE PRELOAD PAGE 2									
INPUT	TEMP 8	TEMP 9	TEMP 10	TEMP 11	TEMP 12	TEMP 13	TEMP 14	TEMP 15	
TEMP MAIN [F]	0	0	0	0	0	0	0	0	0
TEMP AUX [F]	-250	-250	-250	-240	-235	-235	-235	-235	-235
TEMP GUYMAIN T12 [F]	-505	-505	-505	-505	-485	-500	-502.5	-505	
TEMP GUYAUX T12 [F]	-505	-515	-525	-525	-525	-525	-525	-525	
TEMP GUYMAIN T8 [F]	-470	-455	-455	-455	-455	-455	-455	-455	
TEMP GUYAUX T8 [F]	-470	-465	-475	-475	-480	-477.5	-477.5	-477.5	
TEMP GUYMAIN T4 [F]	-505	-505	-505	-505	-505	-505	-505	-505	
TEMP GUYAUX T4 [F]	-505	-515	-525	-525	-535	-522.5	-520	-517.5	
INITIAL Z OFFSET [ft]	8.777	8.777	8.777	8.777	8.777	8.777	8.777	8.777	
OUTPUT									
PLATFORM UZ [ft]	-10.4	-10.4	-10.4	-10.4	-10.5	-10.5	-10.5	-10.5	
UX T12 TOWER [in]	-0.00601	0.00108	0.0015	0.0016	0.00283	0.00081	0.00035	-0.00001	
UY T12 TOWER [in]	-0.20298	-0.0736	0.04985	0.07193	-0.42609	-0.04368	0.02013	0.00699	
UX T8 TOWER [in]	-0.20884	0.14	0.04514	0.02957	-0.02474	-0.00325	-0.00387	-0.00037	
UY T8 TOWER [in]	-0.11978	0.08168	0.02613	0.01707	-0.02683	-0.00363	-0.00212	-0.00004	
UX T4 TOWER [in]	-0.19148	-0.05808	0.06597	0.08817	0.22761	0.06764	0.03565	0.00034	
UY T4 TOWER [in]	0.10418	0.03513	-0.03632	-0.04905	-0.13803	-0.03952	-0.02012	-0.00006	
TENSION MAIN [kip]	480 k	477	477	480	482	482	482	482	
TENSION AUX [kip]	602 k	617	616	617	609	604	605	605	
TENSION GUYMAIN T12 [kip]	514 k	505	501	498	498	489	496	496	
TENSION GUYAUX T12 [kip]	727 k	627	636	645	645	657	648	646	
TENSION GUYMAIN T8 [kip]	503 k	457	454	450	450	448	449	449	
TENSION GUYAUX T8 [kip]	662 k	573	580	589	588	592	590	590	
TENSION GUYMAIN T4 [kip]	543 k	504	501	498	498	495	498	499	
TENSION GUYAUX T4 [kip]	728 k	627	636	646	645	654	642	640	
ERROR									
error in platform offset [ft]		-1.623	-1.623	-1.623	-1.623	-1.723	-1.723	-1.723	-1.723
error in ux T12 tower [in]		-0.00601	0.00108	0.0015	0.0016	0.00283	0.00081	0.00035	-0.00001
error in uy T12 tower [in]		-0.20298	-0.0736	0.04985	0.07193	-0.42609	-0.04368	0.02013	0.00699
error in ux T8 tower [in]		-0.20884	0.14	0.04514	0.02957	-0.02474	-0.00325	-0.00387	-0.00037
error in uy T8 tower [in]		-0.11978	0.08168	0.02613	0.01707	-0.02683	-0.00363	-0.00212	-0.00004
error in ux T4 tower [in]		-0.19148	-0.05808	0.06597	0.08817	0.22761	0.06764	0.03565	0.00034
error in uy T4 tower [in]		0.10418	0.03513	-0.03632	-0.04905	-0.13803	-0.03952	-0.02012	-0.00006
error in tension main [kip]	480 k	-3	-3	-3	0	2	2	2	2
error in tension aux [kip]	602 k	15	14	15	7	2	3	3	3
error in tension guymain T12 [kip]	514 k	-9	-13	-16	-16	-25	-18	-18	-17
error in tension guyaux T12 [kip]	727 k	-100	-91	-82	-82	-70	-79	-81	-82
error in tension guymain T8 [kip]	503 k	-46	-49	-53	-53	-55	-54	-54	-54
error in tension guyaux T8 [kip]	662 k	-89	-82	-73	-74	-70	-72	-72	-72
error in tension guymain T4 [kip]	543 k	-39	-42	-45	-45	-48	-45	-44	-43
error in tension guyaux T4 [kip]	728 k	-101	-92	-82	-83	-74	-86	-88	-90
PERCENT ERROR (TENSIONS)									
percent error in tension main [kip]	480 k	-0.6	-0.6	-0.6	0.0	0.4	0.4	0.4	0.4
percent error in tension aux [kip]	602 k	2.5	2.3	2.5	1.2	0.3	0.5	0.5	0.5
percent error in tension guymain T12 [kip]	514 k	-1.8	-2.5	-3.1	-3.1	-4.9	-3.5	-3.5	-3.3
percent error in tension guyaux T12 [kip]	727 k	-13.8	-12.5	-11.3	-11.3	-9.6	-10.9	-11.1	-11.3
percent error in tension guymain T8 [kip]	503 k	-9.1	-9.7	-10.5	-10.5	-10.9	-10.7	-10.7	-10.7
percent error in tension guyaux T8 [kip]	662 k	-13.4	-12.4	-11.0	-11.2	-10.6	-10.9	-10.9	-10.9
percent error in tension guymain T4 [kip]	543 k	-7.2	-7.7	-8.3	-8.3	-8.8	-8.3	-8.1	-7.9
percent error in tension guyaux T4 [kip]	728 k	-13.9	-12.6	-11.3	-11.4	-10.2	-11.8	-12.1	-12.4
NOTES:									
2. Case TEMP9. Start to use different temperatures for main backstays and auxiliary backstays. It did not bomb like case TEMP5. The trend looks good. Continue it.									

From drawings



2.4.2 Discussion of Results of Case 2

1. Verticality was achieved in the three towers in the 15th iteration. As shown in Table 2.16, the largest error is just 0.00699 inch (in tower T12) which is negligible. However, tensions did not match the values of the drawings. Verticality of towers and correct tensions could not be achieved simultaneously as it was suspected.

Table 2.16. Summary of tower displacements at the top. Final iteration.

Tower Displacements at Top	TEMP 15
UX T12 TOWER [in]	-0.00001
UY T12 TOWER [in]	0.00699
UX T8 TOWER [in]	-0.00037
UY T8 TOWER [in]	-0.00004
UX T4 TOWER [in]	0.00034
UY T4 TOWER [in]	-0.00006

2. All the guys (backstays) are undertensioned as summarized in Table 2.17. Any additional thermal strains on the backstays to increase tension would bend the towers away from verticality (radially outwards). While the mismatch is significant (average of 10%), it is still better than expected considering the very high degree of indeterminacy of the structure and uncertainties in material and section properties.

Table 2.17. Summary of errors in tension for the final iteration as compared to values specified in drawings

	Drawings	TEMP 15	% DIFF
TENSION MAIN [kip]	480	482	0.4
TENSION AUX [kip]	602	605	0.5
TENSION GUYMAIN T12 [kip]	514	497	-3.3
TENSION GUYAUX T12 [kip]	727	645	-11.3
TENSION GUYMAIN T8 [kip]	503	449	-10.7
TENSION GUYAUX T8 [kip]	662	590	-10.9
TENSION GUYMAIN T4 [kip]	543	500	-7.9
TENSION GUYAUX T4 [kip]	728	638	-12.4

3. As it can be observed from Table 2.17, a very small mismatch (0.5%) was achieved in the tensions of main (MAIN) and auxiliary (AUX) cables. This isolates the mismatch in tensions to the backstays.

4. Most of the tension in the cables is generated just from self-weight (case NO TEMP) as shown in Table 2.18. The increase in backstay tension due to thermal strains is on the order of 25% (average). Except for the main cables, all other cables saw an increase in tension. The main cables relaxed as the auxiliary cables were thermally strained (thus attracting a higher share of the load).

Table 2.18. Summary of tensions for two cases of thermal strains (NO TEMP = No thermal strains. Towers flex radially inwards) (TEMP 15 = Final iteration. Towers achieve straightness.)

	NO TEMP	TEMP 15	% DIFF
TENSION MAIN [kip]	554	482	-14.9
TENSION AUX [kip]	365	605	39.7
TENSION GUYMAIN T12 [kip]	418	497	15.9
TENSION GUYAUX T12 [kip]	470	645	27.1
TENSION GUYMAIN T8 [kip]	403	449	10.2
TENSION GUYAUX T8 [kip]	453	590	23.2
TENSION GUYMAIN T4 [kip]	405	500	19.0
TENSION GUYAUX T4 [kip]	463	638	27.4

5. The platform descended 10.5 feet rather than the 8.8 feet predicted. The 1.7 ft mismatch represents a 1.3% difference in the vertical component of the length of the main cables, i.e., there is a vertical difference of 130 ft from the top of the towers to the platform). The platform z coordinate was not changed during the iterations. The 1.3% difference in the original guess is considered acceptable for the purpose of this base case. Iterations on the platform elevations are conducted in the tiedown case.

2.5 Finite Element Model Details of Updated Model A

This model is essentially a copy of the original Model A but corrects a modeling assumption made due to the unavailability of some drawings during the initial stages of the investigation. The modification is in the auxiliary saddle (the part that secures the auxiliary cables at the top of the towers). In addition, the modulus of elasticity of very stiff components (rigid body assumption) was reduced to avoid numerical instabilities which were causing some difficulty in the convergence of the non-linear p-delta analysis. Rigid body response is still assured.

The elevation and plan views of the auxiliary saddle are shown in Figures 2.18 and 2.19, respectively. The main saddle is included in Figure 2.18. The main saddle serves as the attachment point for the main cables at the top of the towers and dates back to the 1960's (original construction). The auxiliary saddle was added in the Gregorian upgrade of 1992 to support the additional weight of the Gregorian dome and its appurtenances.

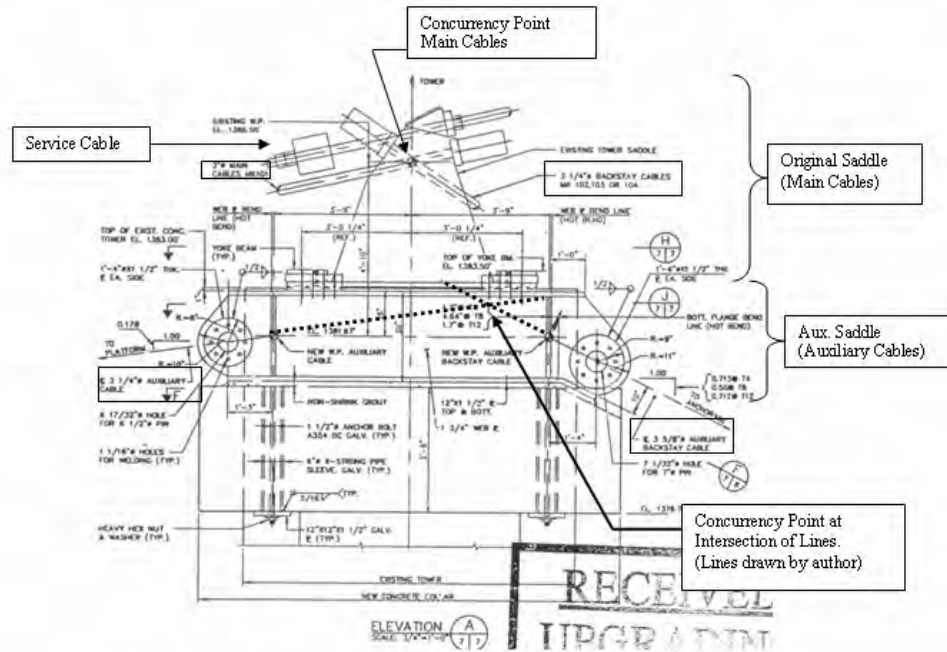


Figure 2.18. Elevation view of auxiliary saddle

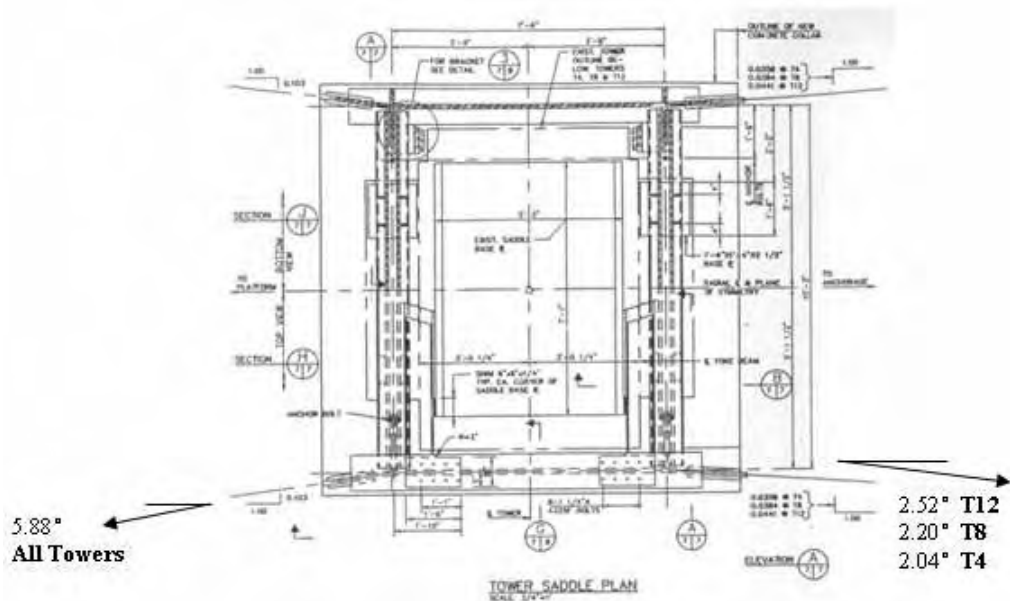
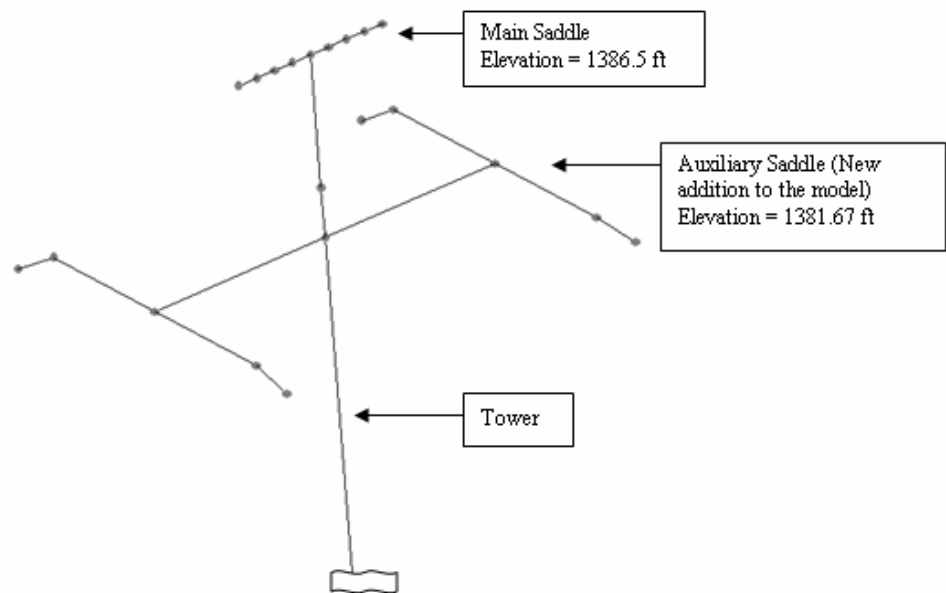


Figure 2.19. Plan view of auxiliary saddle

A noteworthy observation from Figure 2.18 is the offset in the projected concurrency point of the auxiliary cables which does not coincide with that of the main cables. Neither does it coincide with the projected centerline axis of the tower.

NOTE: In all cases hereon, the phrase **“concurrency point”** is meant as the **“projected concurrency point”** of the cables. The projection is directed unto the elevation view looking at each tower in a direction perpendicular to the cables, as shown in Figure 2.18.

Figure 2.20 shows the detail of the finite element model at the top of tower T12. The main saddle has been modeled at the concurrency point of the cables at an elevation of 1386.5 ft (same as original Model A). The auxiliary saddle is tied to the tower at the working point elevation of 1381.67 ft. Both saddles are modeled as rigid bodies with very stiff properties.



**Figure 2.20. Finite element model of saddles
(Cables not shown for clarity)**

2.6 Comparison: Original Model A vs. Updated Model A

Table 2.19 documents the results of both models. Note the same input was used in both cases. Also note there is minimal difference between results. Cable tensions are very similar and tower displacements are approximately zero. Iteration was not performed on this model as the purpose was to show acceptable similarity with the thoroughly validated original model while maintaining the same input. This objective has been achieved and the model is considered validated in this aspect.

Table 2.19. Comparison between original Model A vs. updated Model A

INPUT	ORIGINAL Model A (Case TEMP15)	UPDATED Model A (Same Input as TEMP15)	Percent Difference [%]
TEMP MAIN [F]	0	0	0 (same input)
TEMP AUX [F]	-235	-235	0 (same input)
TEMP GUYMAIN T12 [F]	-505	-505	0 (same input)
TEMP GUYAUX T12 [F]	-525	-525	0 (same input)
TEMP GUYMAIN T8 [F]	-455	-455	0 (same input)
TEMP GUYAUX T8 [F]	-477.5	-477.5	0 (same input)
TEMP GUYMAIN T4 [F]	-505	-505	0 (same input)
TEMP GUYAUX T4 [F]	-517.5	-517.5	0 (same input)
INITIAL Z OFFSET [ft]	8.777	8.777	0 (same input)
OUTPUT			
PLATFORM UZ [ft]	-10.5	-10.6	0.9%
TENSION MAIN [kip]	482	488	1.2%
TENSION AUX [kip]	605	602	-0.5%
TENSION GUYMAIN T12 [kip]	497	497	0.0%
TENSION GUYAUX T12 [kip]	645	645	0.0%
TENSION GUYMAIN T8 [kip]	449	450	0.2%
TENSION GUYAUX T8 [kip]	590	590	0.0%
TENSION GUYMAIN T4 [kip]	500	499	-0.2%
TENSION GUYAUX T4 [kip]	638	638	0.0%
ERROR IN VERTICALITY OF TOWERS			
verticality error in ux T12 tower [in]	-0.00001	0.00006	N/A
verticality error in uy T12 tower [in]	0.00699	0.10069	N/A
verticality error in ux T8 tower [in]	-0.00037	0.04539	N/A
verticality error in uy T8 tower [in]	-0.00004	0.03619	N/A
verticality error in ux T4 tower [in]	0.00034	0.00911	N/A
verticality error in uy T4 tower [in]	-0.00006	0.0003	N/A

2.7 Major (M_{33}) Bending Moment Distribution in Towers

The bending moment distribution of Tower T8 due to dead load and cable preload is shown in Figure 2.21. The accompanying deformed shape is shown in Figure 2.22 (highly exaggerated – 2000x Magnification). Similar distributions are also found in towers T4 and T12. Note the moment reversal at approximately 1/3 of the way from the top. There is good correlation between the moment diagram and the deformed geometry plot, as expected.

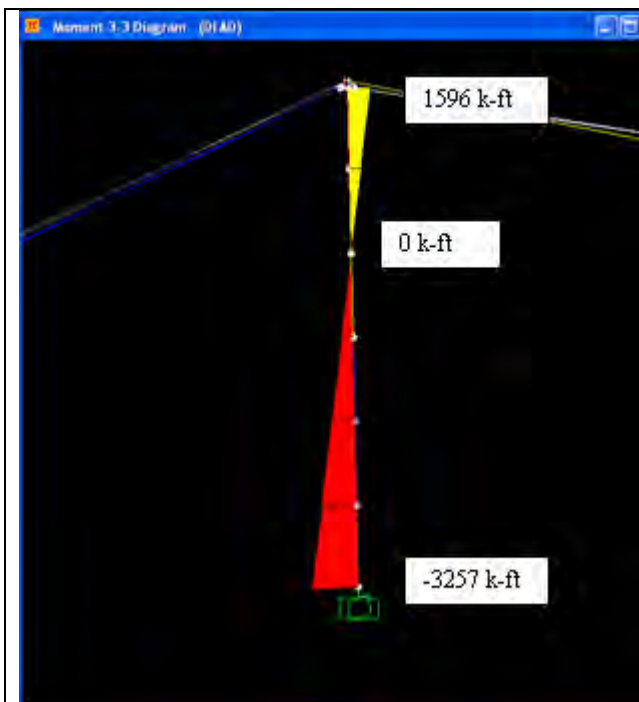


Figure 2.21. Bending moment distribution of tower T8. Dead load only.

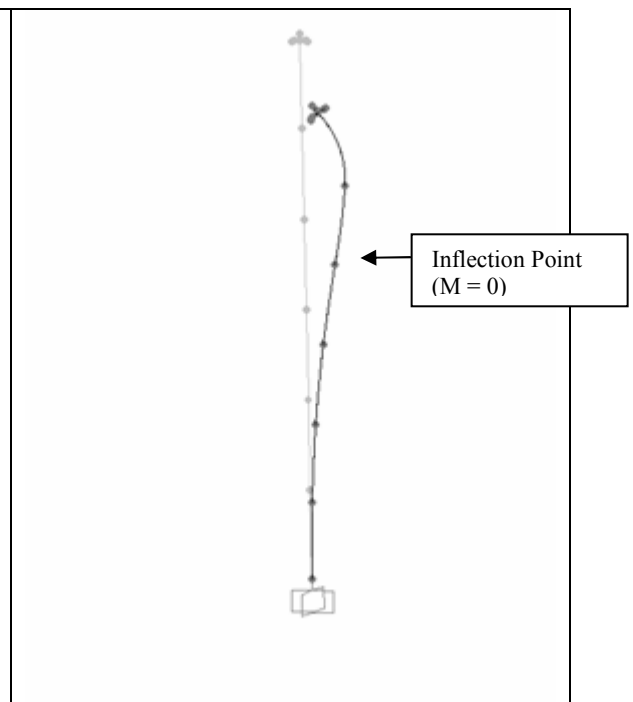


Figure 2.22. Deformed geometry plot of tower T8 Dead load only (2000x Mag.)

2.7.1 Suggested Cause for Bending Distribution

The distribution shown in Figure 2.21 was unexpected. A closer inspection of the auxiliary saddle drawing in Figure 2.18 reveals that there is an offset in the concurrency points (note it is a projected offset) of the cables. There is both a vertical and horizontal

offset. As a result, an unbalanced moment at the top is generated. This seems to be the cause for the unexpected bending distribution shown in Figure 2.21. The expectation was a cantilever-like distribution with zero moment at the top and a maximum at the base which would correlate with the stepped design of the towers (weakest at the top and strongest at the bottom). This issue merits validation to assure that the results are reliable. The following points are addressed:

1. Is the bending moment distribution predicted by finite element model correct? Validate the results. Analytically determine the unbalanced moment magnitude.
2. Is the finite element model omitting any features which could provide a counterbalancing effect? Consider (analytically and with FEM) the counterbalancing effect of the service cables.
3. What if all the cables had been concurrent at the main saddle point (elevation of 1386.5 ft)? Establish computationally that a cantilever-like distribution of bending moments is indeed achieved when all cables are concurrent at the same point.
4. What if the auxiliary cables had been concurrent at the base of the main saddle on the centerline of the tower (elevation of 1383 ft)? This model isolates the unbalanced moment to the contribution of just the vertical offset in concurrency points.
5. Reach a conclusion.

The second validation step will provide an initial sense for the effect of including service cables in the model. These cables support the catwalk and cable car systems and are of secondary importance in the structure. Their effect, however, is investigated as the degree of complexity of the analysis is gradually increased. Step 2 in the validation process will provide the first glimpse into their behavior and effect on the structure.

2.7.2 Verification of Unbalanced Moment at Auxiliary Saddle

Assume that the tower resistance is replaced by the three reactions shown at the center of the auxiliary saddle in Figure 2.23. T_1 represents the tension in the main auxiliary cable (to platform) while T_2 represents the tension in the guy auxiliary cable (backstay). θ_1 and θ_2 represent the angles of T_1 and T_2 , respectively, measured from the horizontal. Assume that there is no shear force, no axial force, nor a bending moment transmitted from the top saddle since the objective is to only determine the unbalanced moment due to the horizontal offset in the auxiliary cables.

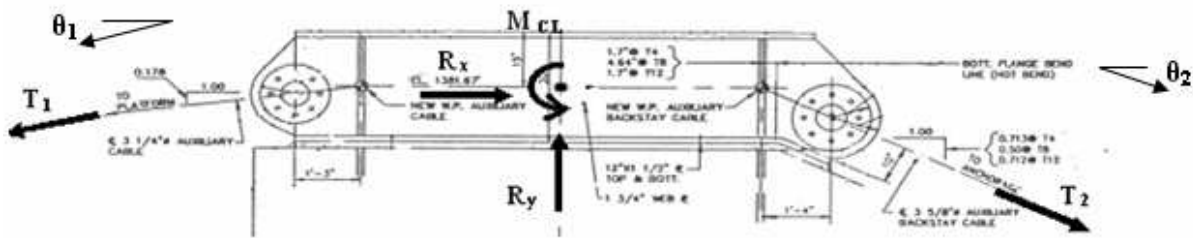


Figure 2.23. Free Body Diagram of auxiliary saddle to determine unbalanced moment due to auxiliary cables

Table 2.20 presents the data and the solution of the equations of equilibrium for each of the three towers. A clockwise unbalanced moment due to the horizontal offset is predicted. The counterclockwise reaction M_{CL} is given in the last row of Table 2.20. Note the forces in the x direction are essentially balanced so there is no direct shear demand placed on the towers. R_y represents the axial compressive force transferred to the towers.

Table 2.20. Analytical calculation of unbalanced moment due to auxiliary cables

	Tower T12	Tower T8	Tower T4
T1 per cable [kip] from dwgs. (2 cables)	602	602	602
T2 per cable [kip] from dwgs. (2 cables)	727	662	728
Theta_1 [deg] from dwgs. (2 cables)	10	10	10
Theta_2 [deg] from dwgs. (2 cables)	35.5	26.6	35.5
T1x per cable [kip] (2 cables)	592.9	592.9	592.9
T1y per cable [kip] (2 cables)	104.5	104.5	104.5
T2x per cable [kip] (2 cables)	591.9	591.9	592.7
T2y per cable [kip] (2 cables)	422.2	296.4	422.8
Rx [kip]	-2.0	-1.8	-0.4
Ry [kip]	1053.4	801.9	1054.6
Arm for T1x [ft]	0.23	0.23	0.23
Arm for T1y [ft]	5.03	5.03	5.03
Arm for T2x [ft]	0.81	0.63	0.81
Arm for T2y [ft]	4.89	5.00	4.89
M_CL [kip-ft]	2382	1439	2387

The following equilibrium equations are used in Table 2.20

- $R_x = 2*(T_{2x} - T_{1x})$
- $R_y = 2*(T_{2y} + T_{1y})$
- $M_{CL} = 2*(T_{1x}*ArmForT_{1x} - T_{1y}*ArmForT_{1y} - T_{2x}*ArmForT_{2x} + T_{2y}*ArmForT_{2y})$

where tensions are assumed to act at the center of the hole and are defined as,

- $T_{nx} = T_n \cos \theta$ (Neglect off-radial angles in Fig. 2.19 since $\cos(5.88^\circ) = 0.995 \approx 1$)
- $T_{ny} = T_n \sin \theta$ (Neglect off-radial angles in Fig. 2.19 since $\cos(5.88^\circ) = 0.995 \approx 1$)

and where the moment arms (in units of feet) are defined as

- Arm for $T_{1x} = 1.3\sin(\theta_1)$
- Arm for $T_{1y} = 1.3\cos(\theta_1) + 3.75$
- Arm for $T_{2x} = 1.4\sin(\theta_2)$
- Arm for $T_{2y} = 1.4\cos(\theta_2) + 3.75$

Table 2.21 shows a comparison between the unbalanced moment calculated analytically in Table 2.20 versus the results obtained with the full finite element model. As it can be observed, the results are very similar (there is a 10% difference, approximately). Given the close proximity of both results it is concluded that the finite element results are reliable.

Table 2.21. Bending moment comparison; Analytical vs. FEM

	Tower T12	Tower T8	Tower T4
ANALYTICAL Calculation of Bending Moment [kip-ft]	2382	1439	2387
FINITE ELEMENT Calculation of Bending Moment [kip-ft]	2714	1596	2745
% Difference	12.2%	9.8%	13.0%

2.7.3 Counterbalancing Effect of Service Cables

Service cables, ignored in all previous analysis, were designed to independently support the pedestrian bridge and the cable-car. One service cable runs from each tower and are all joined near the platform as shown in Figure 2.24. The bridge and the cable car are supported from this point. This design feature effectively decouples the platform from the bridge and the cable car, which is beneficial to the operation of the radio telescope as it effectively insulates the platform and its instrumentation. Loads from the bridge or cable car are not transmitted to the platform; instead, they are routed directly to the towers through the service cables. In terms of structural dynamics, this design should effectively decouple the bridge and cable car from the dynamic response of the platform and its supporting structure.

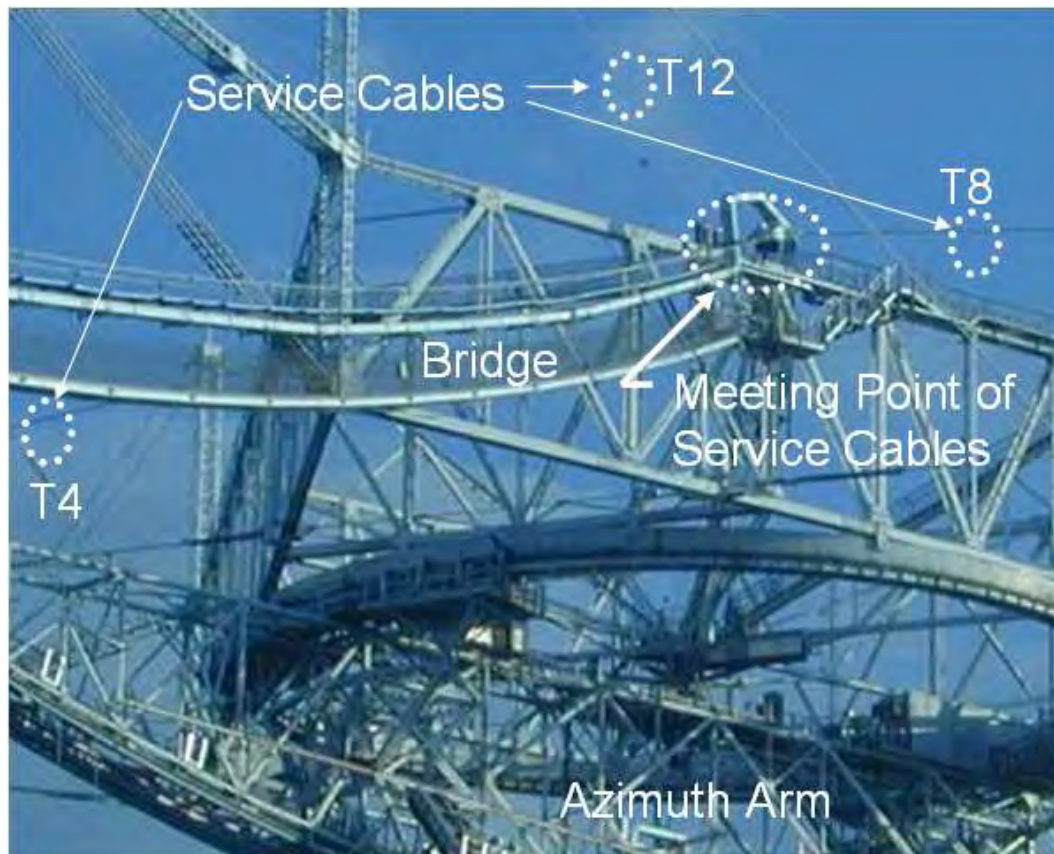


Figure 2.24. Meeting point of service cables

Service cables are attached at the top of the main saddle as shown in Figure 2.25. A photograph is also shown in Figure 2.26. Note the service cable is offset 10 inches from the main-cable concurrency point so as to create a counterclockwise moment that will counterbalance the clockwise unbalanced moment generated at the auxiliary saddle (reported in Table 2.20).

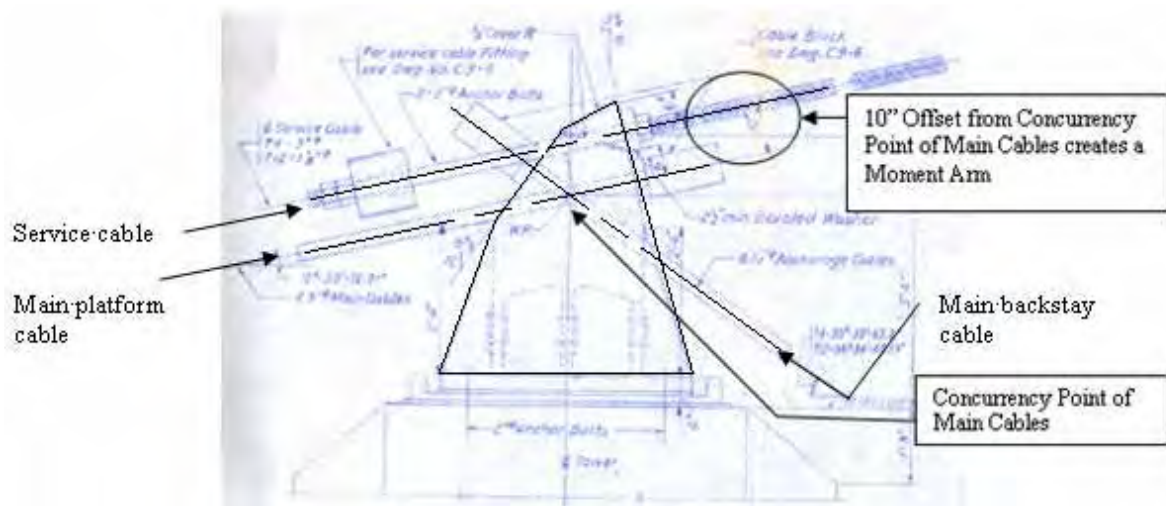


Figure 2.25. Elevation view of main saddle showing service cable (T12 and T4) (A similar drawing is available for tower T8, which has a shallower backstay angle)

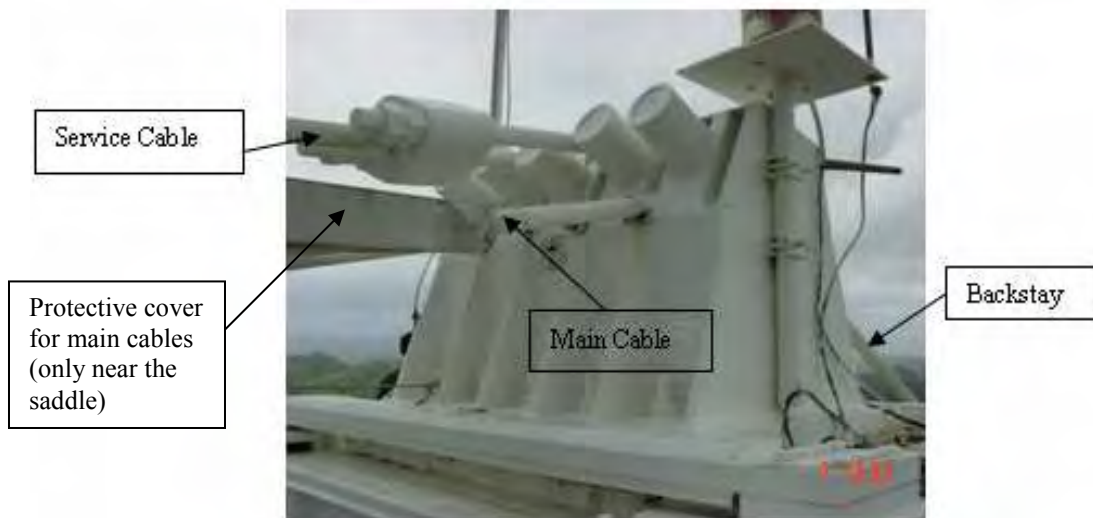


Figure 2.26. Photograph of main saddle at tower T8 (courtesy of Louis Pérez)

2.7.4 Analytical Estimate of Tension in Service Cables and Estimate of Counterbalancing Moment due to Service Cables

Assume that the tower resistance is replaced by the three reactions shown at the centerline of the tower in Figure 2.27. Note that the reactions are assumed to be acting at the working point elevation of the auxiliary saddle (1381.67 ft) to allow a direct comparison with the unbalanced moment of Figure 2.23. T_3 represents the tension in the main cables while T_4 represents the tension in the main backstays. T_{SC} represents the tension in the service cable. θ_3 and θ_4 are the angles of T_3 and T_4 , respectively, measured from the horizontal. The angle θ_{SC} between T_{SC} and the horizontal is taken equal to θ_3 . M represents the counterbalancing moment.

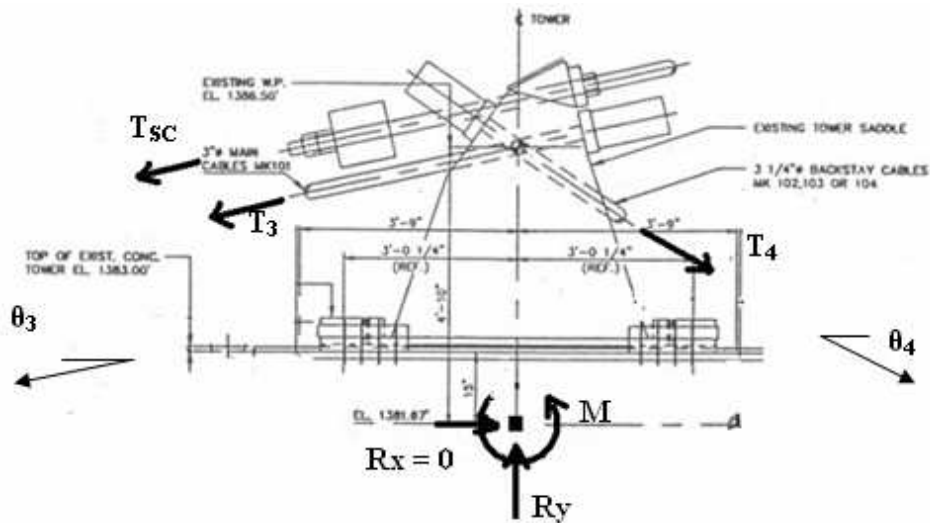


Figure 2.27. Free Body Diagram of main saddle

For this calculation there was no information available about the tension in the service cables. Therefore it will be assumed that the magnitude of T_{SC} is such that it perfectly balances the cable forces in the horizontal direction. This criterion is based on the auxiliary saddle design where it was shown that $R_x = 0$ (see Table 2, $R_x \sim 0$). In other words, it is assumed that no horizontal shear force is passed on to the towers which is a reasonable assumption. This, in turn, permits to calculate T_{SC} from the equilibrium equations.

The results of the analysis are summarized in Table 2.22. This table is similar to Table 2.20, i.e., it presents the data, the reactions and T_{SC} from the solution of the static equilibrium equations.

Table 2.22. Estimate of tension in service cables and counterbalancing moment

	Tower T12	Tower T8	Tower T4
T3 per cable [kip] from dwgs. (4 cables)	480	480	480
T4 per cable [kip] from dwgs. (5 cables)	514	503	543
Theta 3 [deg] from dwgs.	12.9	12.9	12.9
Theta 4 [deg] from dwgs.	35.6	26.2	35.6
T3x [kip] (4 cables)	467.9	467.9	467.9
T3y [kip] (4 cables)	107.2	107.2	107.2
T4x [kip] (5 cables)	417.9	451.3	441.5
T4y [kip] (5 cables)	299.2	222.1	316.1
(Tsc)x [kip] (1 cable)	218.1	385.1	336.0
Ts c [kip]	224	395	345
Rx [kip]	0.0	0.0	0.0
Ry [kip]	1924.7	1539.0	2009.1
Arm for T3x [ft]	4.83	4.83	4.83
Arm for T4x [ft]	4.83	4.83	4.83
Arm for Tscx [ft]	5.93	5.93	5.93
M [kip-ft]	240	424	370

The tension values for T_{SC} in Table 2.22 seem reasonable: they are comparable to the tension from other cables with the same diameter. The diameters of the service cables and their tension values are included in Table 2.23. In a general sense, the tensions correlate well with the service cable diameters, i.e., the larger diameter cables are specified for the more heavily loaded service cables.

Table 2.23. Service cable diameters and tensions in service cables

	Tower T12	Tower T8	Tower T4
Diameter of Service Cable [in]	1.875	3.25	3.0
Tension in Service Cable [kip]	224	395	345

The magnitude of the counterbalancing moment (last row in Table 2.22) is relatively small. For towers T12 and T4 it is basically an order of magnitude lower than the unbalanced moment. The net unbalanced moment calculation is included in Table 2.24.

Table 2.24. Calculation of net unbalanced moment

	Tower T12	Tower T8	Tower T4
CCW Counterbalance Moment due to Offset in Service Cable [kip-ft]	-240	-424	-370
CW Unbalanced Moment due to Offset in Auxiliary Saddle [kip-ft]	2382	1439	2387
Net CW Unbalanced Moment [kip-ft]	2142	1015	2017

These results prove that the service cables provide a counterbalancing moment but it is small. For example, for tower T12, the counterbalancing moment of 240 kip-ft is nearly an order of magnitude lower than the unbalanced moment of 2382 kip-ft. Therefore, the unbalanced moment in the auxiliary saddle is only partially cancelled by the service cables. The net moment at the top of the towers may be significant, depending on the capacity of the towers. In the next section the exercise is repeated but with a finite element analysis.

2.7.5 Finite Element Estimate of the Counterbalancing Moment due to Service Cables

The finite element model was modified to include the service cables. It is a simplified model whose primary objective is to obtain a general idea of the effect of the service cables in providing relief to the unbalanced moment at the auxiliary saddle. The analytical calculations of the previous section predict a small effect. In addition, this model provides an initial sense for the general effect of service cables in the model. An additional joint (and element) was added as shown in Figure 2.28

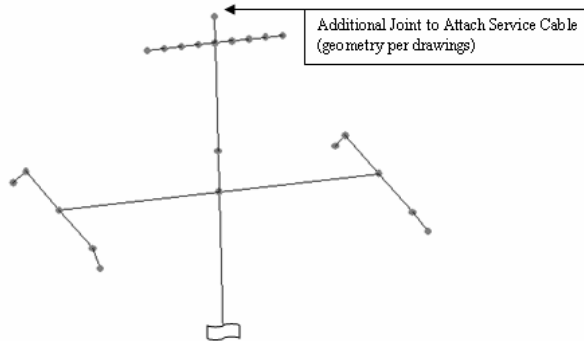


Figure 2.28. Modification at top of towers to include the service cable

The three service cables intersect near the platform in a single joint. A pin restraint is assigned at the joint (see Figure 2.29) to allow control of the tension in the service cables. Note that the pin restraint effectively models the situation without including the bridge and cable car specifications at this preliminary stage.

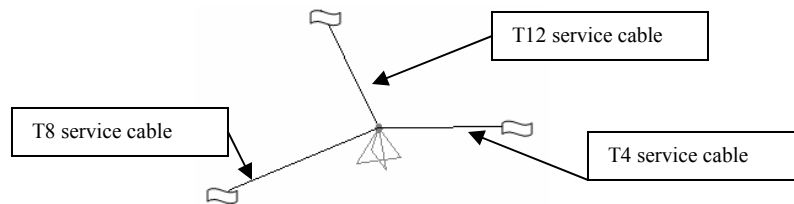


Figure 2.29. Pin constraint at meeting point of three service cables

The results of iteration to achieve verticality of towers are shown in Table 2.25.

Table 2.25. Iteration chart - pinned constraint at intersection of service cables

SERVICE CABLES - PINNED MEETING JOINT - NO TIEDOWNS - LEVEL PLATFORM ITERATION CHART
1764K PLATFORM WEIGHT

INPUT	PINNED Serv Cables TEMP1	PINNED Serv Cables TEMP2	PINNED Serv Cables TEMP3	PINNED Serv Cables TEMP4	PINNED Serv Cables TEMP5	PINNED Serv Cables TEMP6
TEMP MAIN [F]	0	0	0	0	0	0
TEMP AUX [F]	-235	-235	-240	-240	-240	-240
TEMP GUYMAIN T12 [F]	-505	-505	-510	-530	-530	-520
TEMP GUYAUX T12 [F]	-525	-575	-585	-590	-590	-590
TEMP GUYMAIN T8 [F]	-455	-465	-465	-465	-465	-495
TEMP GUYAUX T8 [F]	-477.5	-530	-530	-530	-530	-530
TEMP GUYMAIN T4 [F]	-505	510	-525	-535	-535	-520
TEMP GUYAUX T4 [F]	-517.5	-575	-575	-590	-590	-580
TEMP SERV CABL T12 [F]	-700	-700	-680	-660	-660	-660
TEMP SERV CABL T8 [F]	-450	-450	-250	-350	-350	-425
TEMP SERV CABL T4 [F]	-450	-450	-420	-420	-420	-420
INITIAL Z OFFSET [ft]	8.777	8.777	8.777	8.777	8.777	8.777
OUTPUT						
PLATFORM UZ [ft]	-11.3	-11.0	-10.7	-10.6	-10.6	-10.9
UX T12 TOWER [in]	-0.47789	-0.48461	-0.48368	-0.46383	-0.46259	-0.46339
UY T12 TOWER [in]	-1.08124	-0.50449	-0.27427	0.33304	0.33653	-0.06835
UX T8 TOWER [in]	0.45131	-0.22255	-0.44272	-0.32125	-0.32197	-0.7025
UY T8 TOWER [in]	3.1364	2.83335	1.43201	2.13782	2.13322	2.44178
UX T4 TOWER [in]	-1.49343	-0.72818	-0.3043	0.12712	0.12983	-0.50587
UY T4 TOWER [in]	1.96089	1.55586	1.25042	1.03714	1.03379	1.33809
TENSION MAIN [kip]	480 k	484	484	482	482	489
TENSION AUX [kip]	602 k	594	593	600	601	603
TENSION GUYMAIN T12 [kip]	514 k	523	510	510	516	515
TENSION GUYAUX T12 [kip]	727 k	675	722	729	719	731
TENSION GUYMAIN T8 [kip]	503 k	502	491	468	479	504
TENSION GUYAUX T8 [kip]	662 k	651	685	665	680	668
TENSION GUYMAIN T4 [kip]	543 k	542	530	536	536	535
TENSION GUYAUX T4 [kip]	728 k	686	738	727	735	738
TENSION SERV CAB T12 [kip]	224 k	225	229	224	221	219
TENSION SERV CAB T8 [kip]	403 k	407	592	239	330	406
TENSION SERV CAB T4 [kip]	346 k	348	360	343	350	339
ERROR						
error in platform offset [ft]	-2.523	-2.223	-1.923	-1.823	-1.823	-2.123
verticality error in ux T12 tower [in]	-0.47789	-0.48461	-0.48368	-0.46383	-0.46259	-0.46339
verticality error in uy T12 tower [in]	-1.08124	-0.50449	-0.27427	0.33304	0.33653	-0.06835
verticality error in ux T8 tower [in]	0.45131	-0.22255	-0.44272	-0.32125	-0.32197	-0.7025
verticality error in uy T8 tower [in]	3.1364	2.83335	1.43201	2.13782	2.13322	2.44178
verticality error in ux T4 tower [in]	-1.49343	-0.72818	-0.3043	0.12712	0.12983	-0.50587
verticality error in uy T4 tower [in]	1.96089	1.55586	1.25042	1.03714	1.03379	1.33809
error in tension main [kip]	4	4	2	2	2	9
error in tension aux [kip]	-8	-9	-2	-1	0	1
error in tension guymain T12 [kip]	9	-4	-4	2	2	1
error in tension guyaux T12 [kip]	-52	-5	2	-7	-8	4
error in tension guymain T8 [kip]	-1	-12	-35	-24	-24	1
error in tension guyaux T8 [kip]	-11	23	3	18	11	6
error in tension guymain T4 [kip]	-1	-13	-7	-6	-7	-8
error in tension guyaux T4 [kip]	-42	10	-1	7	7	10
error in tension ServCable T12 [kip]	1	5	0	-3	-3	-5
error in tension ServCable T8 [kip]	4	189	-164	-73	-73	3
error in tension ServCable T4 [kip]	2	14	-3	4	4	-7
PERCENT ERROR (CABLE TENSIONS)						
percent error in tension main [kip]	0.8	0.8	0.4	0.4	0.4	1.9
percent error in tension aux [kip]	-1.3	-1.5	-0.3	-0.2	0.0	0.2
percent error in tension guymain T12 [kip]	1.8	-0.8	-0.8	0.4	0.4	0.2
percent error in tension guyaux T12 [kip]	-7.2	-0.7	0.3	-1.0	-1.1	0.6
percent error in tension guymain T8 [kip]	-0.2	-2.4	-7.0	-4.8	-4.8	0.2
percent error in tension guyaux T8 [kip]	-1.7	3.5	0.5	2.7	1.7	0.9
percent error in tension guymain T4 [kip]	-0.2	-2.4	-1.3	-1.1	-1.3	-1.5
percent error in tension guyaux T4 [kip]	-5.8	1.4	-0.1	1.0	1.0	1.4
percent error in tension ServCable T12 [kip]	0.4	2.2	0.0	-1.3	-1.3	-2.2
percent error in tension ServCable T8 [kip]	1.0	46.9	-40.7	-18.1	-18.1	0.7
percent error in tension ServCable T4 [kip]	0.6	4.0	-0.9	1.2	1.2	-2.0

Several observations can be made from Table 2.25.

1. The iterations do not converge to zero displacement at the top of the towers. For example, Tower T12 always shows a displacement along the x-axis on the order of -0.5 inch (see the row UX T12 TOWER [in]) which cannot be corrected by variations in the preloading scheme. The same situation occurs with towers T12 and T4. There is always a skew in the towers due to the asymmetry of the service cables (see Figure 2.30). The off-radial (tangential) tension component is resisted only by the towers – not by a backstay (see arrows on Figure 2.30) and so tower deformation takes place.

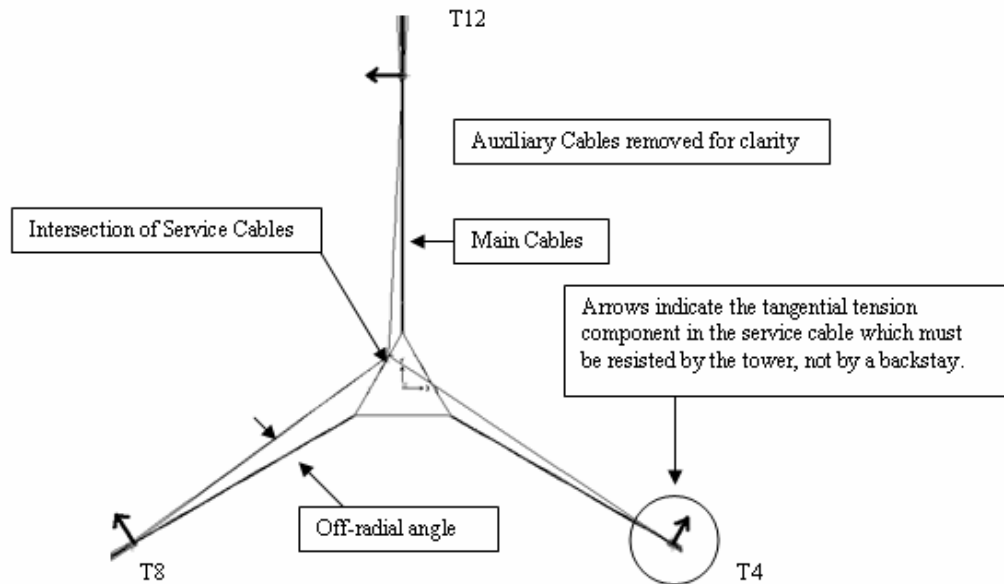


Figure 2.30. Asymmetry in service cables

2. As a result of the skew in the towers, a minor-axis (M_{22}) bending moment component is also generated in the towers and must be checked. Bending occurs in the direction of the arrows shown in Figure 2.30.
3. In the presence of service cables, backstays must be retightened to support the additional load. **Backstay tensions converged to the values specified in the drawings to within approximately 1%. The service cables have been shown to be the missing key to achieving backstay tensions as specified in the drawings.** Recall from section 2.4.2 (point 2) that in the absence of service cables, backstay tensions were approximately 10% lower than the values specified in the drawings.

A comparison of the major bending moments (M_{33}) is shown in Table 2.26. Note that when the effect of the service cables is accounted for, the bending moments at the top of the towers (first three rows) show a decrease in magnitude in all cases. This was expected because the service cables partially cancel out the unbalanced moment in the auxiliary saddle. The difference is somewhat higher than the analytical prediction (see Table 2.24 – first row) but a general trend has been established. Also note from Table 2.26 that the bending moments at the base of the towers increase in the presence of the service cables.

Table 2.26. Comparison of ‘major’ bending moments at top and base of towers for models with and without service cables

	NO Service Cables	WITH Service Cables (PINNED Joint)	Difference [kip-ft]	Percent Difference
TOP of Tower T12 - M33 Moment [kip-ft]	2714	2239	475	18%
TOP of Tower T8 - M33 Moment [kip-ft]	1596	731	865	54%
TOP of Tower T4 - M33 Moment [kip-ft]	2745	1994	751	27%
BASE of Tower T12 - M33 Moment [kip-ft]	-2982	-3358	376	13%
BASE of Tower T8 - M33 Moment [kip-ft]	-3257	-5375	2118	65%
BASE of Tower T4 - M33 Moment [kip-ft]	-3571	-9171	5600	157%

Table 2.27 presents a similar comparison but for the minor bending moments (M_{22}). As expected, the minor moments are essentially zero in the case with no service cables and increase when service cables are included due to the loading asymmetry.

Table 2.27. Comparison of ‘minor’ bending moments at top and base of towers for models with and without service cables

	NO Service Cables	WITH Service Cables (PINNED Joint)
TOP of Tower T12 - M22 Moment [kip-ft]	0	54
TOP of Tower T8 - M22 Moment [kip-ft]	-3	-231
TOP of Tower T4 - M22 Moment [kip-ft]	0	108
BASE of Tower T12 - M22 Moment [kip-ft]	-3	2667
BASE of Tower T8 - M22 Moment [kip-ft]	-52	-15906
BASE of Tower T4 - M22 Moment [kip-ft]	28	5210

The M_{22} moment in tower T8 is very significant and it merits validation. The T8 service cable runs in essentially the same direction as its auxiliary cable, and therefore, the moment M_{22} can be calculated as follows:

- Service Cable Tension in T8 = 406 kip (see Table 2.25)
- Radial Component of T8 Service Cable Tension = $406 \text{ kip} * \cos(12.9^\circ) = 396 \text{ kip}$
(See Figure 2.25 for the angle)
- Off-radial angle = $\arctan(0.103/1.0) = 5.88^\circ$ (see Figures 2.19 and 2.30)
- Off-radial Unbalanced Force Component = $396 \text{ kip} * \sin(5.88^\circ) = 41.6 \text{ kip}$
- Height of Tower T8 = Moment Arm = 370 ft
- M_{22} Moment at base = $41.6 \text{ kip} * 370 \text{ ft} = 15,400 \text{ kip-ft}$ (compared to 15,906 kip-ft)

The previous analytical calculation validates the magnitude of the M_{22} moment at the base of tower T8. Note that the moment arises because the off-radial (tangential) component of 41.6 kip is not balanced by any of the symmetrical backstay cables. Only the tower is capable of resisting it. Depending on the capacity of the towers, the magnitude of this moment may represent another significant finding in the stress state of the Arecibo Observatory towers. Note that tower T8 is the worst case (in terms of M_{22}) on three accounts; first, it has the largest service cable tension (see Table 2.23); second, it has the largest off-radial angle of the three service cables (see Figure 2.30), and third, it has the largest moment arm since tower T8 is 100 ft taller than both T4 and T12.

2.7.6 Hypothetical Consideration of Full Projected Concurrency at Main Saddle

Figure 2.31 shows a modified model that considers full concurrency at the elevation of the main saddle. The connecting beam of the auxiliary cables was kept at an elevation of 1381.67 ft. Vertical frame elements were placed at the ends to achieve the specified elevation of 1386.5 ft at which main cables are concurrent.

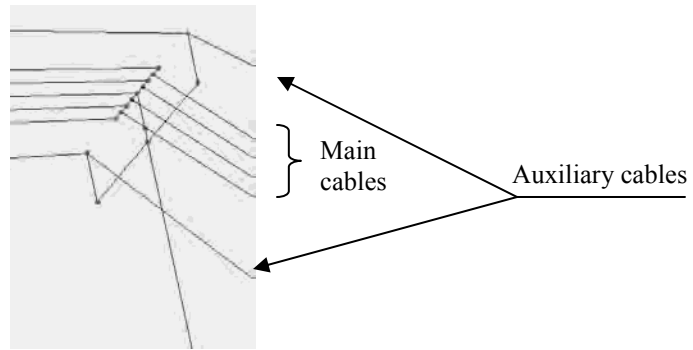
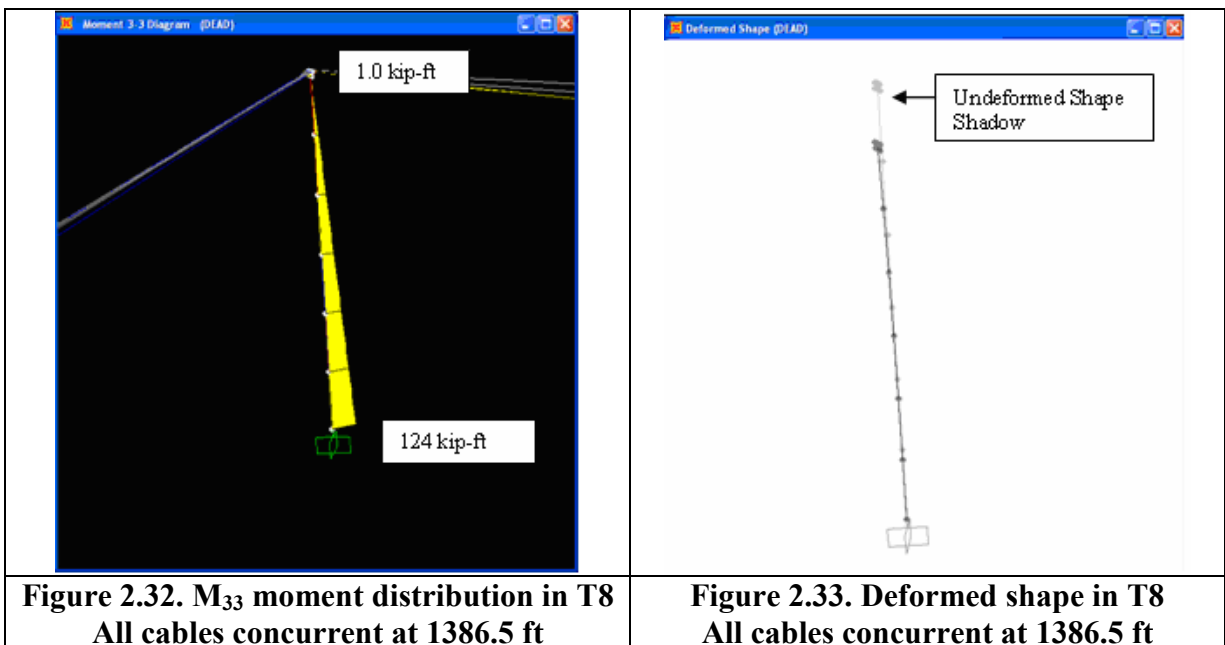


Figure 2.31. FEM Model with concurrency of cables at 1386.5 ft

The M_{33} bending moment distribution and the deformed shape (2000x Mag.) are shown in Figures 2.32 and 2.33, respectively. Note that the unbalanced moment disappears (compare with Figure 2.21). A negligible bending moment is recorded at the base of the tower. Now the tower is essentially straight in its deformed shape (compare with Figure 2.22). The effect of achieving concurrency is effectively demonstrated with this analysis.



2.7.7 Hypothetical Consideration of Projected Concurrency at Auxiliary Saddle

Figure 2.34 considers partial concurrency at the elevation of the auxiliary saddle. In this case, the auxiliary cables are only concurrent with the centerline of the towers. Therefore, there is only the effect of the vertical offset between the concurrency point of the main cables and the concurrency point of the auxiliary cables. The connecting beam of the auxiliary cables was raised to 1383 ft which would correspond to a potentially feasible location of the concurrency point at the centerline of the towers (elevate the platform-side clevis by ~6 inches and lower the backstay-side clevis by ~6 inches - see Figure 2.18).

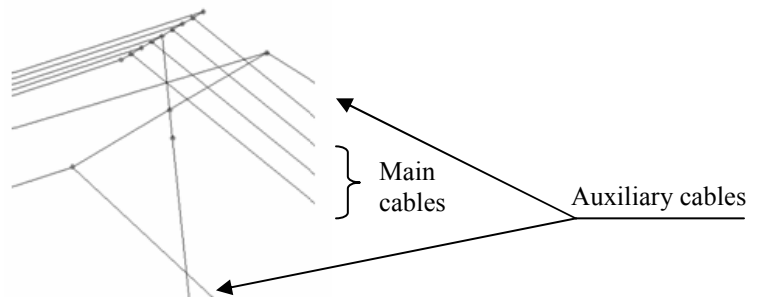
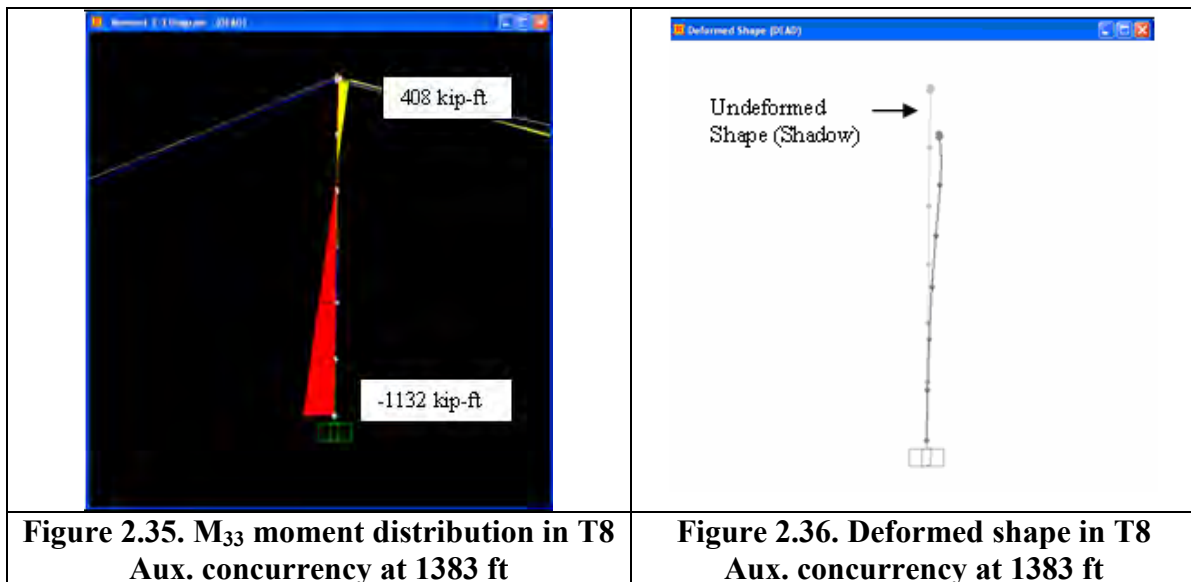
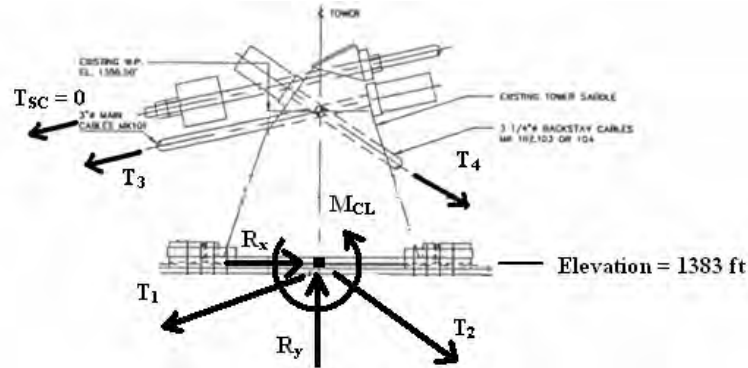


Figure 2.34. FEM model-auxiliary cables concurrent at 1383 ft

The M_{33} bending moment distribution and the deformed shape (2000x Mag.) are shown in Figures 2.35 and 2.36, respectively. Note that there is an unbalanced moment but it is reduced by a factor of three compared to Figure 2.21. The vertical offset still creates an unbalanced moment but of a lesser magnitude. It is comparable to the moment generated by the service cables.



The cause of the unbalanced moment can be understood by analyzing the free body diagram of the system as shown in Figure 2.37.



**Figure 2.37. Free Body Diagram of hypothetical case (aux. concur. at 1383 ft)
(Tension magnitudes from finite element model)**

The solution of the equilibrium equations for the set of forces in Figure 2.37 is shown in Table 2.28. The values of the tensions have been read directly from the FEM model. The angles are as specified in the drawings. The components are calculated in both the x and y directions. The sum of forces in the x direction results in a -10.2 kip force which is transferred as a shear force to the towers. The horizontal tension components in the cables are not balanced at each level. $T_{2x} - T_{1x} = -128.6$ kip and $T_{4x} - T_{3x} = 118.4$ kip. The net forces ($T_{2x} - T_{1x}$) and ($T_{4x} - T_{3x}$) gives rise to a couple as shown in Figure 2.38.

Table 2.28. Solution of the Free Body Diagram (aux. concur. at 1383 ft)

	Tower T8
T1 per cable [kip] from dwgs. (2 cables)	601
T2 per cable [kip] from dwgs. (2 cables)	590
T3 per cable [kip] from dwgs. (4 cables)	489
T4 per cable [kip] from dwgs. (5 cables)	451
Theta 1 [deg] from dwgs.	10
Theta 2 [deg] from dwgs.	26.6
Theta 3 [deg] from dwgs.	12.9
Theta 4 [deg] from dwgs.	26.1
T1x [kip] (2 cables)	591.9
T1y [kip] (2 cables)	104.4
T2x [kip] (2 cables)	527.6
T2y [kip] (2 cables)	264.2
T3x [kip] (4 cables)	476.7
T3y [kip] (4 cables)	109.2
T4x [kip] (5 cables)	405.0
T4y [kip] (5 cables)	198.4
Rx [kip]	-10.2
T2x - T1x [kip] (Aux. Cables)	-128.6
T4x - T3x [kip] (Main Cables)	118.4
Moment Arm [ft]	3.5
Couple Moment [kip-ft]	432.3

The generated moment is $118.4 \text{ kip} * 3.5 \text{ ft} = 414 \text{ kip-ft}$ which validates the value shown in the bending moment distribution of Figure 2.35.

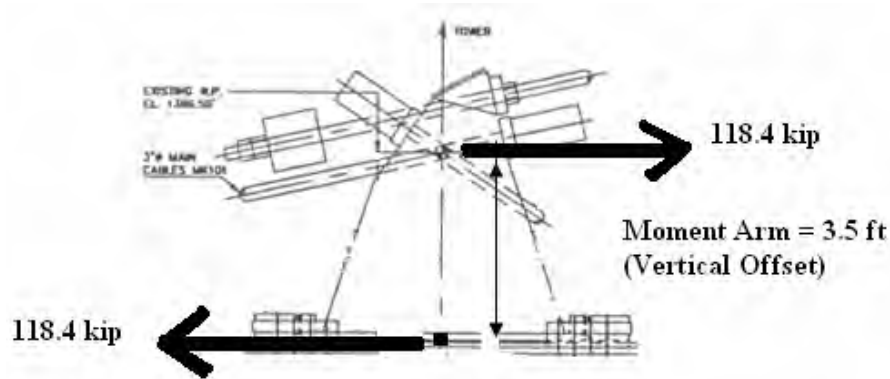


Figure 2.38. Couple moment at top of tower (aux. concurr. at 1383 ft)

This analysis has shown that the vertical offset in concurrency points leads to a couple moment. Although horizontal equilibrium is maintained for the entire free body diagram, the cables are not balanced at each level which leads to the couple. Note that this couple can not be predicted based purely on the static equilibrium equations. Rather one needs to know the equilibrium state after accommodating the multiple redundancies in the system.

Returning to section 2.7.2, this couple moment should explain the augmented values in the middle row of Table 2.21 (FEM results). The finite element model predicted a higher unbalanced moment than that calculated analytically. The analytical model did not consider the couple due to the vertical offset. The following free body diagram (Figure 2.39) has been set up to prove this point.

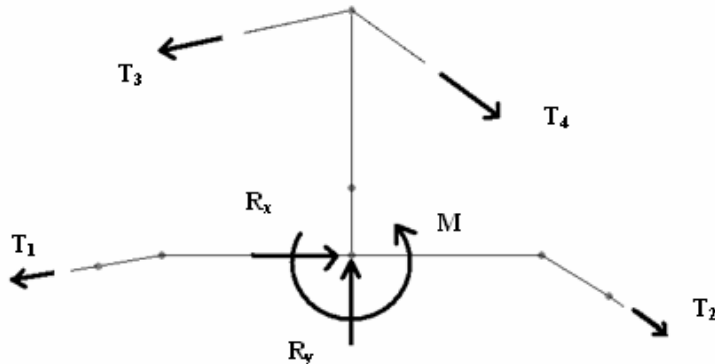


Figure 2.39. Free Body Diagram of tower at the top (based on FEM model) (Includes main and auxiliary saddles)

The system shown in Figure 2.39 has been solved in Table 2.29 below. Note that indeed a couple is developed since the horizontal tension components in the cables are not balanced at each level. $T_{2x} - T_{1x} = -135.5$ kip while $T_{4x} - T_{3x} = 113.8$ kip. A figure similar to Figure 2.38 could be drawn for this case with an almost equal horizontal force of 113.8 kip. Note that the total sum of forces in the x direction (R_x) results in a -21.7 kip force which is transferred as a shear force. This value was confirmed in the SAP2000 model by inspection of the V22 shear component.

Table 2.29. Solution of the Free Body Diagram of Figure 2.39

	Tower T12
T1 per cable [kip] from dwgs. (2 cables)	602
T2 per cable [kip] from dwgs. (2 cables)	645
T3 per cable [kip] from dwgs. (4 cables)	488
T4 per cable [kip] from dwgs. (5 cables)	496
Theta_1 [deg] from dwgs.	10
Theta_2 [deg] from dwgs.	35.5
Theta_3 [deg] from dwgs.	12.9
Theta_4 [deg] from dwgs.	35.6
T1x [kip] (2 cables)	592.9
T1y [kip] (2 cables)	104.5
T2x [kip] (2 cables)	525.1
T2y [kip] (2 cables)	374.6
T3x [kip] (4 cables)	475.7
T3y [kip] (4 cables)	108.9
T4x [kip] (5 cables)	403.3
T4y [kip] (5 cables)	288.7
Rx [kip]	-21.7
T2x - T1x [kip] (Aux. Cables)	-135.5
T4x - T3x [kip] (Main Cables)	113.8

These results confirm that the vertical offset in concurrency points creates an unbalanced couple moment that must be resisted by the towers and explains the difference seen in Table 2.21. It is also evident that the couple moment can not be predicted based purely on static equilibrium (rigid body assumption). It can only be calculated by taking into account the stiffness properties of all the members and the multiple redundancies in the structure. This would be an extremely difficult task if performed analytically. Only through a computational model (finite element analysis, for example) is it feasible. In the absence of a numerical analysis it would seem reasonable to assume that horizontal forces are balanced at the auxiliary saddle as shown in Table 2.20.

2.7.8 Conclusions on the Issue of Auxiliary Saddle Unbalanced Moment

1. The geometry of the auxiliary saddle creates an unbalanced moment at the top of the towers by virtue of offsets in the projected concurrency points of the cables. There is both a horizontal and a vertical offset present. The unbalanced moment demand is on the order of 2000 kip-ft for towers T12 and T4 and 1000 kip-ft for tower T8. These values already include the reduction due to the counterbalance moment provided by the service cables. This unbalanced moment acts at the top of the towers – its weakest segment. The values cited are due to the dead loads and pretension; they do not include the contributions to seismic loads.
2. The previous result indicates that the top of the towers should be monitored in the seismic analysis stage of the thesis.
3. Service cables create a moment demand on the order of $M_{22} = 16,000$ kip-ft at the base of Tower T8. This moment acts in the ‘minor’ direction of the towers which tends to bend the towers in a direction perpendicular to the cables. This value is based on a simplified model of the service cables; however, it should be reasonably accurate for the case of dead loading.
4. Both the M_{22} and the M_{33} moment components at the base of the towers should be closely monitored during the seismic analysis stage.
5. The inclusion of service cables in the analysis improves the accuracy of the bending moment results in the towers. They also assist in achieving the expected tension magnitudes in the cables (as specified in the drawings). Without the service cables the backstays can only reach 90% of the expected values. The expected values are reached with the additional backstay tightening required to compensate for the service cables.

CHAPTER 3

Static Non-Linear P-Delta Analysis – Model B

3.1 Finite Element Model Details

As mentioned in the methodology section, models with increasing degrees of difficulty are developed throughout the investigation to allow for gradual immersion into the project. Now that the equilibrium state due to dead loads has been established and validated for Model A (see Chapter 2), the next step is to modify Model A so as to include the vertical tiedown cables. The modified model is named Model B and is shown in Figure 3.1. Tiedown cables keep the platform leveled at all times and provide vertical stiffness.

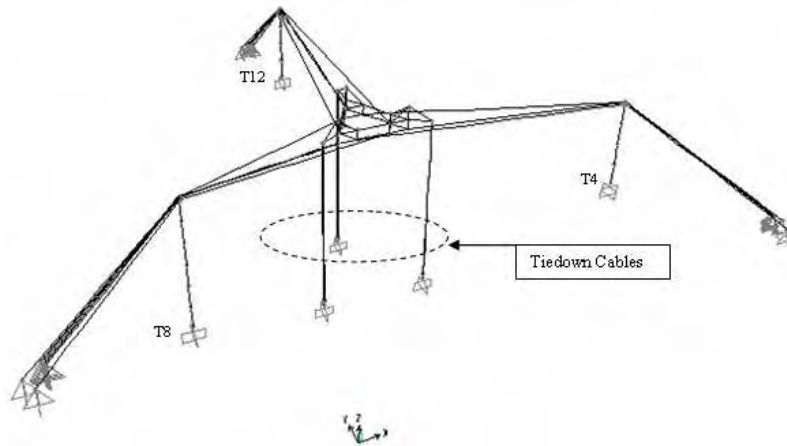


Figure 3.1. Perspective view of model with tiedown cables

The supporting structure of the tiedowns at the platform (see Figure 3.2) was modeled according to the dimensions specified in the drawings. The corner extensions are 66 ft long while the mast is 40 ft high. They are modeled as rigid bodies with very stiff properties.

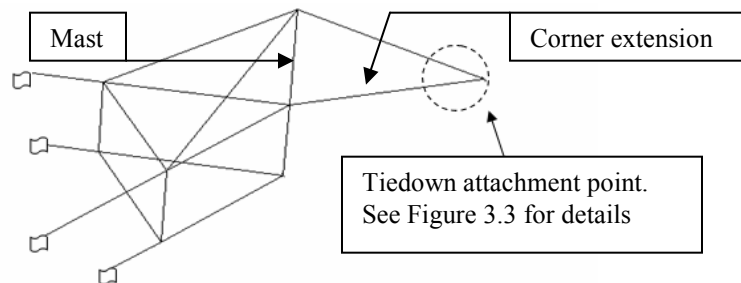


Figure 3.2. Detail of tiedown support structure at the platform (T4 shown) (cables not shown for clarity)

The detail of the tiedown attachment point at platform elevation is shown in Figure 3.3. The 3.5 ft long connecting bar is modeled as a rigid body with very stiff properties. Note that the tiedown cables are specified in pairs at each platform corner.

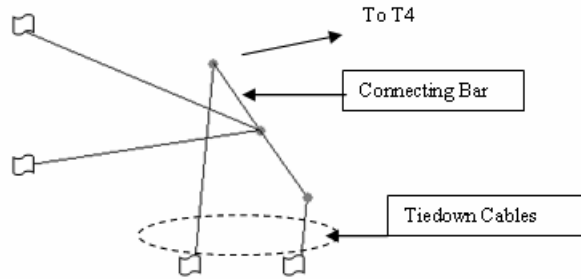


Figure 3.3. Detail of tiedown attachment point at platform level (T4 shown)

The tiedown attachment point at ground level is shown in Figure 3.4. The bottom element represents a 10 ft x 10 ft x 8.5 ft (height) concrete block. The elements immediately above represent the mechanical jack used to adjust the tension in the tiedown cables.

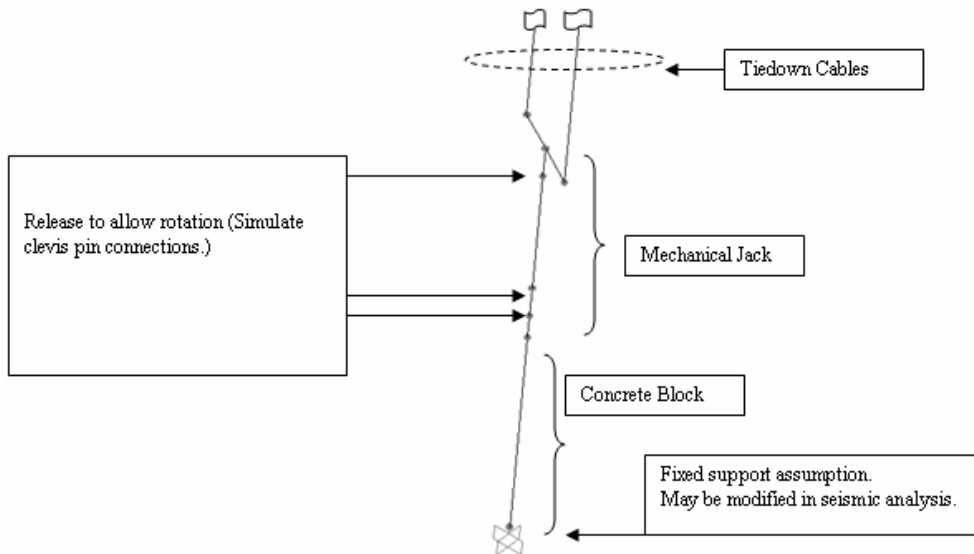


Figure 3.4. Detail of tiedown anchor

Although the concrete block rests on its foundation to provide a fail-safe mechanism (if the tiedown tension exceeds the weight of the concrete block, the block lifts), the model assumes a fixed constraint. This may be modified in the seismic analysis stage with a non-linear link (compression only) depending on the tension level achieved in the tiedown. The fixed support assumption is appropriate while tiedown tension levels are maintained below the block weight, i.e., when the tiedown tension is less or equal than 65 kip.

Figure 3.5 shows the drawing of the tiedown anchorage. Figure 3.6 is a photo of the mechanical jack.

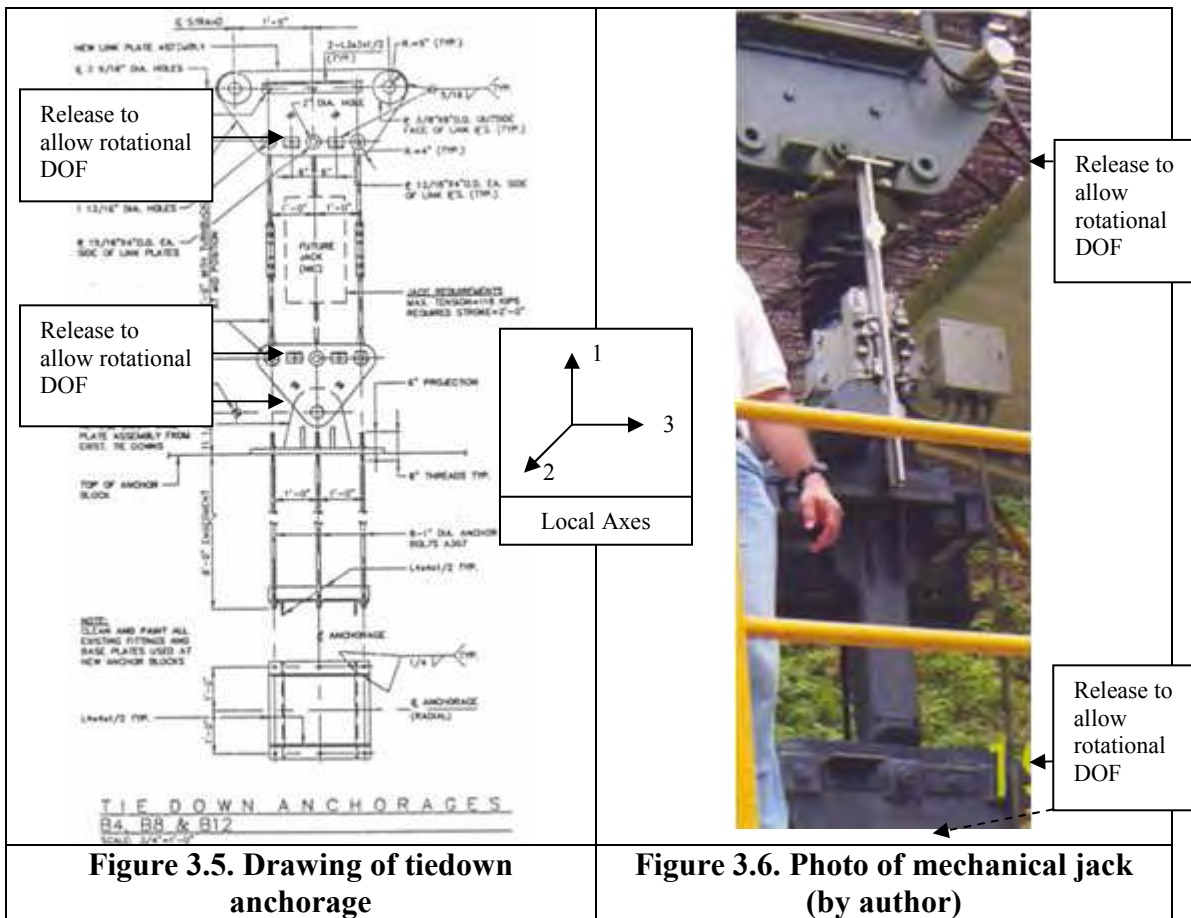


Figure 3.5. Drawing of tiedown anchorage

Figure 3.6. Photo of mechanical jack (by author)

The local axes of the tiedown anchors were rotated to permit the release of the degree of freedom offered by the clevis-pin connections (see Figures 3.4 to 3.6). The new local axes coincide with the axes of the concrete towers. The rotation angles (about the “1” or longitudinal axis) are given in Table 3.1. The “2” direction, which coincides with the out-of-plane direction in Figure 3.5, is the direction about which the rotational degree of freedom is released to simulate the clevis-pin connections.

Table 3.1. Rotation of local coordinate systems of frame elements (Tiedown anchor axes coincide with the tower axes.)

Tiedown Anchor	Rotation Angle (about “1” axis which coincides with Global Z)
T12	90°
T8	210°
T4	330°

The material properties [STEELCAB] used for the cables are the same ones defined in section 2.1.6. These are repeated here for completeness:

- Cable unit weight = 490 pcf [default value for steel]
- Cable unit mass = (cable unit weight)/g [default value]
- E = 24E6 psi [wire “strand” cable]
- Poisson’s ratio = 0.3

The section properties for the tiedown cables are summarized in Table 3.2 below. These are repeated from section 2.1.6.

Table 3.2. Section properties of tiedown cables

Section Name used in SAP2000	Nominal Diameter [in]	Effective Area [in²]	Effective Diameter [in]	Effective Moment of Inertia [in⁴]	Weight per Unit Length [lb/in]
TIEDOWN	1.5	1.36	1.3159	0.1472	0.38

The properties for all other parts are the same ones used for Model A except for the weight of the platform. The platform weight used for model A was $W = 1764$ kip. This value included 144 kip due to tension in the tiedown cables (24 kip per tiedown cable). Since Model B explicitly includes tiedowns, the weight of the platform is reduced accordingly. Therefore,

$$W_{\text{platform}} = 1764 \text{ kip} - 144 \text{ kip} = 1620 \text{ kip}$$

The following values for specific weight and mass density are used:

$$\text{Volume of Platforms} = 2 \text{ triangles} * 5 \text{ ft} * 5 \text{ ft} * 216 \text{ ft/side} * 3 \text{ sides/triangle} = 32,400 \text{ ft}^3$$

$$\text{Specific Weight of Platform} = \gamma = W/V = 1,620,000 \text{ lb} / 32,400 \text{ ft}^3 = \underline{50 \text{ lb/ft}^3}$$

$$\text{Mass Density of Platform} = \rho = \gamma/g = 50 \text{ lb/ft}^3 / 32.2 \text{ ft/s}^2 = \underline{1.55 \text{ lb.s}^2/\text{ft}^4}$$

The initial estimate for the tiedown temperature (for thermal strain) is

$$\Delta T = v/(\alpha L) = -11 \text{ ft} / [(6.5E-06 /^\circ\text{F})*(500 \text{ ft})] = -3384 \text{ }^\circ\text{F} \approx \underline{\underline{-3500 \text{ }^\circ\text{F}}}$$

3.2 Achieving Verticality of Towers

3.2.1 Iterations on Cable Preload

Eight iterations were performed to achieve verticality of the towers. The summary of the iterations is shown in Table 3.3.

Table 3.3. Iteration chart for Model B (tiedowns – uniform platform)

ITERATION CHART - MODEL B - UNIFORM PLATFORM - INCLUDES TIEDOWNS
1620K PLATFORM WEIGHT

INPUT	STAGE 2-B TEMP1	STAGE 2-B TEMP2	STAGE 2-B TEMP3	STAGE 2-B TEMP4	STAGE 2-B TEMP5	STAGE 2-B TEMP6	STAGE 2-B TEMP7	STAGE 2-B TEMP8
TEMP MAIN [F]	0	0	0	0	0	0	0	0
TEMP AUX [F]	-235	-235	-235	-235	-235	-235	-235	-235
TEMP GUYMAIN T12 [F]	-505	-505	-505	-505	-505	-505	-505	-505
TEMP GUYAUX T12 [F]	-525	-525	-525	-525	-525	-530	-540	-540
TEMP GUYMAIN T8 [F]	-455	-455	-455	-455	-460	-465	-465	-465
TEMP GUYAUX T8 [F]	-477.5	-477.5	-477.5	-477.5	-485	-485	-487.5	-487.5
TEMP GUYMAIN T4 [F]	-505	-505	-505	-505	-505	-515	-515	-515
TEMP GUYAUX T4 [F]	-517.5	-517.5	-517.5	-517.5	-517.5	-520	-520	-520
TEMP TIEDOWNS [F]	-3500	-3100	-3275	-3275	-3275	-3325	-3315	-3300
INITIAL Z OFFSET [ft]	8.777	8.777	8.777	10.872	10.872	10.872	10.872	10.872
OUTPUT								
PLATFORM UZ [ft]	-11.4	-10.4	-10.8	-10.9	-11.0	-11.0	-11.0	-11.0
UX T12 TOWER [in]	-0.00245	0.00249	0.00035	0.00074	-0.00215	-0.00085	-0.00041	-0.00021
UY T12 TOWER [in]	-0.62786	0.38243	-0.05978	-0.02192	-0.16255	-0.15534	-0.02694	0.01054
UX T8 TOWER [in]	0.5579	-0.15711	0.15587	0.11723	0.09153	0.03302	-0.04323	-0.06977
UY T8 TOWER [in]	0.33867	-0.07706	0.1049	0.06934	0.055	0.0154	-0.02584	-0.04129
UX T4 TOWER [in]	-0.71988	0.29525	0.14906	-0.08744	-0.23003	0.00368	0.00609	0.0438
UY T4 TOWER [in]	0.42291	-0.1599	0.0952	0.04951	0.1289	-0.00716	-0.00782	-0.02948
TENSION MAIN [kip]	511	480	494	493	496	497	497	496
TENSION AUX [kip]	616	596	605	605	607	609	609	608
TENSION GUYMAIN T12 [kip]	514	491	500	499	503	502	499	498
TENSION GUYAUX T12 [kip]	727	664	638	649	648	652	658	667
TENSION GUYMAIN T8 [kip]	503	445	455	453	458	461	457	456
TENSION GUYAUX T8 [kip]	662	607	582	593	595	593	600	599
TENSION GUYMAIN T4 [kip]	543	515	492	502	501	504	510	509
TENSION GUYAUX T4 [kip]	728	656	630	642	640	643	641	640
TENSION TIEDOWN T12 [kip]	24	35.5	17.5	25.5	21.5	24	24.9	24.8
TENSION TIEDOWN T8 [kip]	24	35.5	17.5	25.5	21.5	24	24.9	24.8
TENSION TIEDOWN T4 [kip]	24	35.5	17.5	25.5	21.5	24	24.9	24.8
ERROR								
error in platform offset [ft]	-2.623	-1.623	-2.023	-0.028	-0.128	-0.128	-0.128	-0.128
verticality error in ux T12 tower [in]	-0.00245	0.00249	0.00035	0.00074	-0.00215	-0.00085	-0.00041	-0.00021
verticality error in uy T12 tower [in]	-0.62786	0.38243	-0.05978	-0.02192	-0.16255	-0.15534	-0.02694	0.01054
verticality error in ux T8 tower [in]	0.5579	-0.15711	0.15587	0.11723	0.09153	0.03302	-0.04323	-0.06977
verticality error in uy T8 tower [in]	0.33867	-0.07706	0.1049	0.06934	0.055	0.0154	-0.02584	-0.04129
verticality error in ux T4 tower [in]	-0.71988	0.29525	0.14906	-0.08744	-0.23003	0.00368	0.00609	0.0438
verticality error in uy T4 tower [in]	0.42291	-0.1599	0.0952	0.04951	0.1289	-0.00716	-0.00782	-0.02948
error in tension main [kip]	31	0	14	13	16	17	17	16
error in tension aux [kip]	14	-6	3	3	5	7	7	6
error in tension guymain T12 [kip]	0	-23	-14	-15	-11	-12	-15	-16
error in tension guyaux T12 [kip]	-63	-89	-78	-79	-75	-69	-60	-62
error in tension guymain T8 [kip]	-36	-58	-48	-50	-45	-42	-46	-47
error in tension guyaux T8 [kip]	-55	-80	-69	-69	-67	-69	-62	-63
error in tension guymain T4 [kip]	-28	-51	-41	-42	-39	-33	-33	-34
error in tension guyaux T4 [kip]	-72	-98	-86	-88	-85	-87	-87	-88
error in tension tiedown T12 [kip]	11.5	-6.5	1.5	-2.5	0	0.9	0.8	0.1
error in tension tiedown T12 [kip]	11.5	-6.5	1.5	-2.5	0	0.9	0.8	0.1
error in tension tiedown T12 [kip]	11.5	-6.5	1.5	-2.5	0	0.9	0.8	0.1
PERCENT ERROR (CABLE TENSIONS)								
percent error in tension main [kip]	6.5	0.0	2.9	2.7	3.3	3.5	3.5	3.3
percent error in tension aux [kip]	2.3	-1.0	0.5	0.5	0.8	1.2	1.2	1.0
percent error in tension guymain T12 [kip]	0.0	-4.5	-2.7	-2.9	-2.1	-2.3	-2.9	-3.1
percent error in tension guyaux T12 [kip]	-8.7	-12.2	-10.7	-10.9	-10.3	-9.5	-8.3	-8.5
percent error in tension guymain T8 [kip]	-7.2	-11.5	-9.5	-9.9	-8.9	-8.3	-9.1	-9.3
percent error in tension guyaux T8 [kip]	-8.3	-12.1	-10.4	-10.4	-10.1	-10.4	-9.4	-9.5
percent error in tension guymain T4 [kip]	-5.2	-9.4	-7.6	-7.7	-7.2	-6.1	-6.1	-6.3
percent error in tension guyaux T4 [kip]	-9.9	-13.5	-11.8	-12.1	-11.7	-12.0	-12.0	-12.1
percent error in tension tiedown T12 [kip]	47.9	-27.1	6.3	-10.4	0.0	3.7	3.3	0.4
percent error in tension tiedown T8 [kip]	47.9	-27.1	6.3	-10.4	0.0	3.7	3.3	0.4
percent error in tension tiedown T4 [kip]	47.9	-27.1	6.3	-10.4	0.0	3.7	3.3	0.4

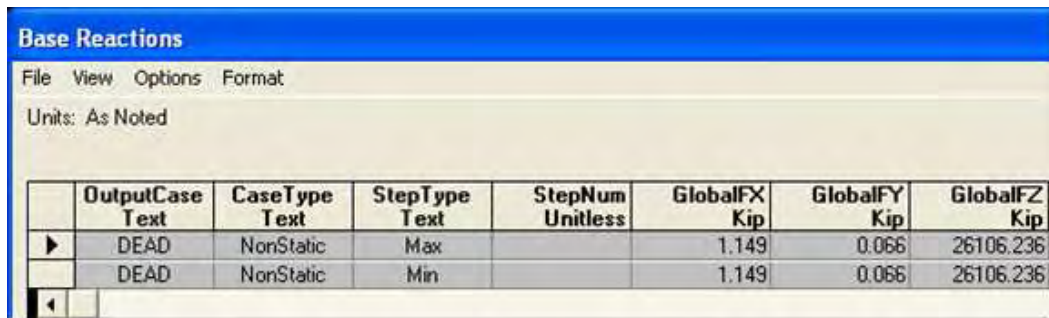
A plot of the deformed geometry (at a highly exaggerated scale) is shown in Figure 3.7. Note that the platform has descended and the tiedown cables are tight and vertical as expected. All the inclined cables are sagging (at a highly exaggerated scale) under their own weight. Deformed geometry plots are a visual way, yet very effective one, of checking for any shortcomings in the model.



Figure 3.7. Deformed geometry of Model B due to DEAD loading

3.2.2 Equilibrium Check

The sum of the vertical reactions at the supports must equal the weight of the structure ($\sum R_z = |W|$). In addition, the horizontal reactions at all the supports must total zero ($\sum F_x = \sum F_y = 0$) since no external forces are applied in the horizontal direction. The thermal strains inherently balance out to zero in terms of reaction forces since they are displacement-limited. The reactions calculated by SAP2000 are shown in the window of the program displayed in Figure 3.8.



The screenshot shows the 'Base Reactions' window in SAP2000. It includes a menu bar (File, View, Options, Format), a unit setting of 'As Noted', and a table with the following data:

	OutputCase Text	CaseType Text	StepType Text	StepNum Unitless	GlobalFX Kip	GlobalFY Kip	GlobalFZ Kip
▶	DEAD	NonStatic	Max		1.149	0.066	26106.236
	DEAD	NonStatic	Min		1.149	0.066	26106.236

Figure 3.8. Base reactions calculated by SAP2000

In terms of the global x-direction, the 1.149 kip difference (it should be zero) is acceptable, considering the size and weight of the structure (over 26,000 kip) and the fact that a nonlinear numerical analysis was carried out. The 0.066 kip difference in the global y-direction (which also should be zero) is very good. Equilibrium in the vertical direction is checked next.

Table 3.4 includes the calculation of the total weight of the structure and the comparison with the results in terms of the reactions in the z direction. There is a 10.9 kip mismatch (0.04% difference) which is deemed acceptable considering the size and weight of the structure (over 26, 000 kip) and the fact that the reactions were obtained from a nonlinear numerical analysis.

Table 3.4. Vertical equilibrium check (Model B)

Weight of all cables (except tiedowns)	470.92 kip
Weight of tiedown cables 6 cab*520 ft/cab*.38 lb/in*12 in/ft*1 kip/1000 lb	14.2 kip
Weight of platform	1620.0 kip
Weight of concrete towers	23986.8 kip
Weight of very stiff and very light elements	3.4 kip
TOTAL SELF WEIGHT (Add above weights)	26095.3 kip
Vertical Base Reaction calculated by SAP2000 (from Figure 3.8)	26106.2 kip
Difference	10.9 kip
PERCENT DIFFERENCE	0.04%

3.2.3 Discussion of Iteration Results

1. Verticality was achieved in all towers. The largest error is just 0.07 inches.
2. Table 3.5 below compares the magnitude of the tensions. It shows the values specified in the drawings, the results of Model A, which does not include tiedowns, and the results of the current Model B, which includes tiedowns. The last column shows that there is no more than 3% difference between Model A and Model B with respect to the tensions in the cables.

Table 3.5. Comparison of tension magnitudes; Model A vs. Model B

	Drawings	Model A (No Tiedowns)	Model B (With Tiedowns)	% DIFF (Model A vs Drawings)	% DIFF (Model B vs Drawings)	% DIFF (Model B vs Model A)
TENSION MAIN [kip]	480	482	496	0.4%	3.3%	2.9%
TENSION AUX [kip]	602	605	608	0.5%	1.0%	0.5%
TENSION GUYMAIN T12 [kip]	514	497	498	-3.3%	-3.1%	0.2%
TENSION GUYAUX T12 [kip]	727	645	665	-11.3%	-8.5%	3.1%
TENSION GUYMAIN T8 [kip]	503	449	456	-10.7%	-9.3%	1.6%
TENSION GUYAUX T8 [kip]	662	590	599	-10.9%	-9.5%	1.5%
TENSION GUYMAIN T4 [kip]	543	500	509	-7.9%	-6.3%	1.8%
TENSION GUYAUX T4 [kip]	728	638	640	-12.4%	-12.1%	0.3%
TENSION TIEDOWN T12 [kip]	24	N/A	24.1	N/A	0.4%	N/A
TENSION TIEDOWN T8 [kip]	24	N/A	24.1	N/A	0.4%	N/A
TENSION TIEDOWN T4 [kip]	24	N/A	24.1	N/A	0.4%	N/A

3. Note that both Model A and Model B underpredict the tension in the backstays (guys) when compared to the tensions specified in the drawings. The order is approximately 10%. It was shown in section 2.7.5 that the inclusion of service cables corrects this situation. The additional tightening required to compensate for the service cables increases the backstay tensions up to the level specified in the drawings.
4. Note in the last column that the percent difference between Model A and Model B is of the order of 3% which can be considered essentially negligible. This finding shows that, as expected, the removal of 144 kip from the dead weight of the platform and the addition of 144 kip of tension in the tiedown cables ($24.1 \text{ kip/cable} * 6 \text{ cables} \approx 144 \text{ kip}$) results in essentially the same state of equilibrium.
5. The initial vertical offset of the platform was successfully varied in Model B. An initial upwards offset is required since the platform descends as the cables stretch due to their self-weight and the weight of the platform. The elevation error improved to just 0.128 ft (1.5 inch) compared to a 1.7 ft error for Model A. The fact that cable tensions are very similar in both cases indicates that variations in the platform elevation of the order of 2 feet are not significant.

CHAPTER 4

Static Non-Linear P-Delta Analysis – Model C

4.1 Finite Element Model Details

A more sophisticated model of the platform was created in Model C. The model considers the triangular platform, the azimuth arm pointing at tower T8, the Gregorian dome at a 20° angle and the line feed antenna in stow position. This particular orientation was requested by Ing. José Maldonado, the former Director of Facilities and Utilities at the Arecibo Observatory, as it presents the worst unbalanced condition of the platform. Figure 4.1 shows a perspective view of the entire model while Figure 4.2 focuses on the platform.

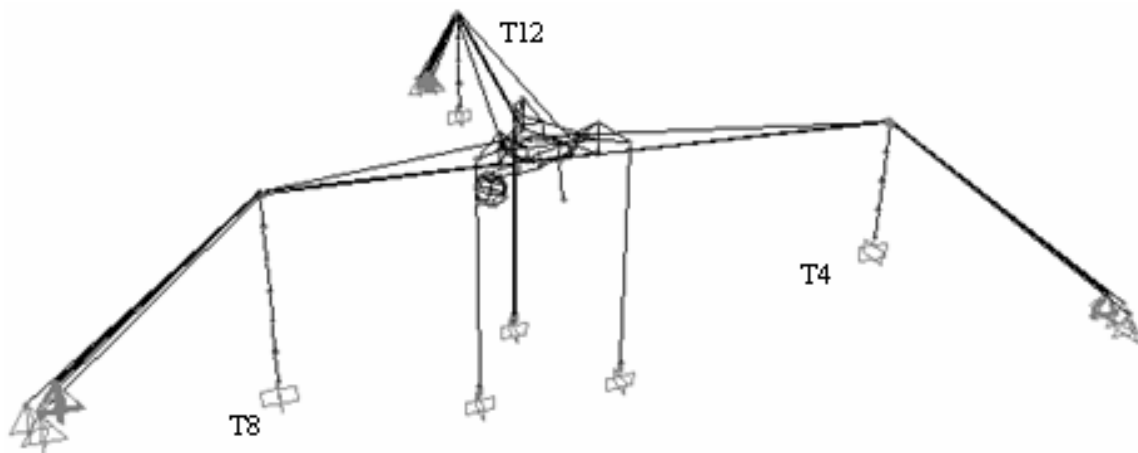


Figure 4.1. Perspective view of Model C

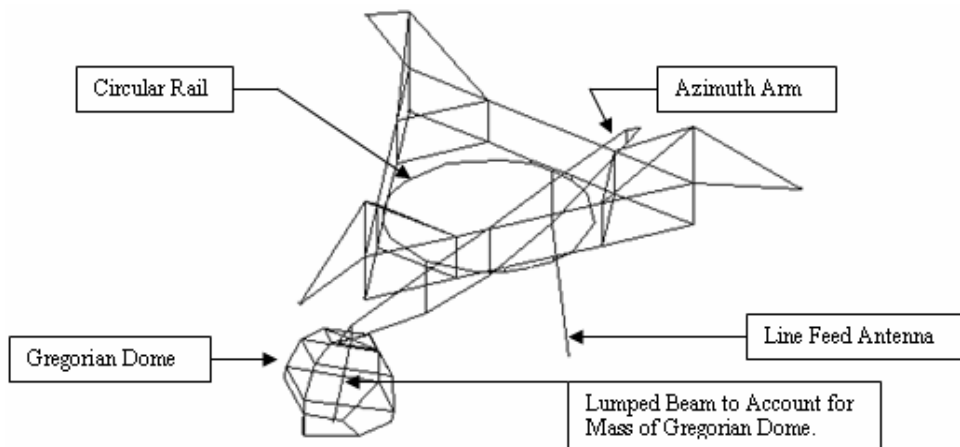


Figure 4.2. Close-up perspective view of platform in Model C

The circular rail is modeled as an 18-sided polygon with six attachment points to the lower platform as shown in plan view in Figure 4.3. The attachment points are located at the intersection of the rail with the triangular platform. Three-foot long vertical connectors separate the lower platform from the circular rail (see Figure 4.4).

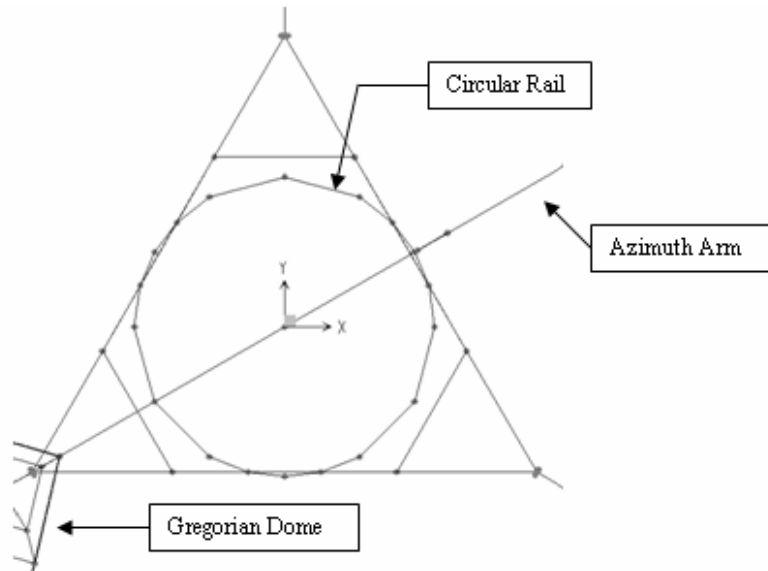


Figure 4.3. Plan view of platform in Model C

The Azimuth Arm is modeled with one single-plane truss and is connected to the rail at two points. Vertical connectors (8 ft long) separate the arm from the circular rail (see Figure 4.4).

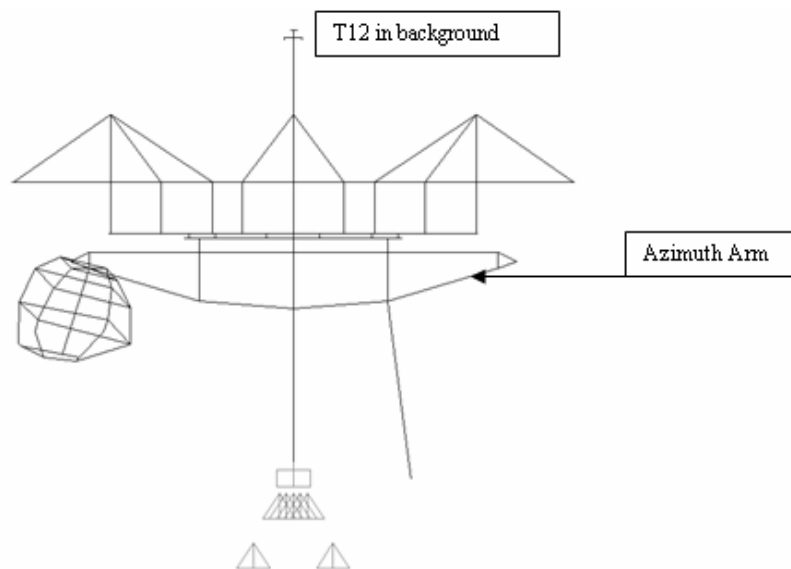


Figure 4.4. Elevation view of platform in Model C looking towards tower T12

The Gregorian dome is constructed in the SAP2000 model with a tri-dimensional frame as shown in Figure 3.5. The mass, however, is concentrated in the beam running through the centerline. The Gregorian Dome is at the 20° position in the Azimuth Arm. This represents the extreme position of the dome.

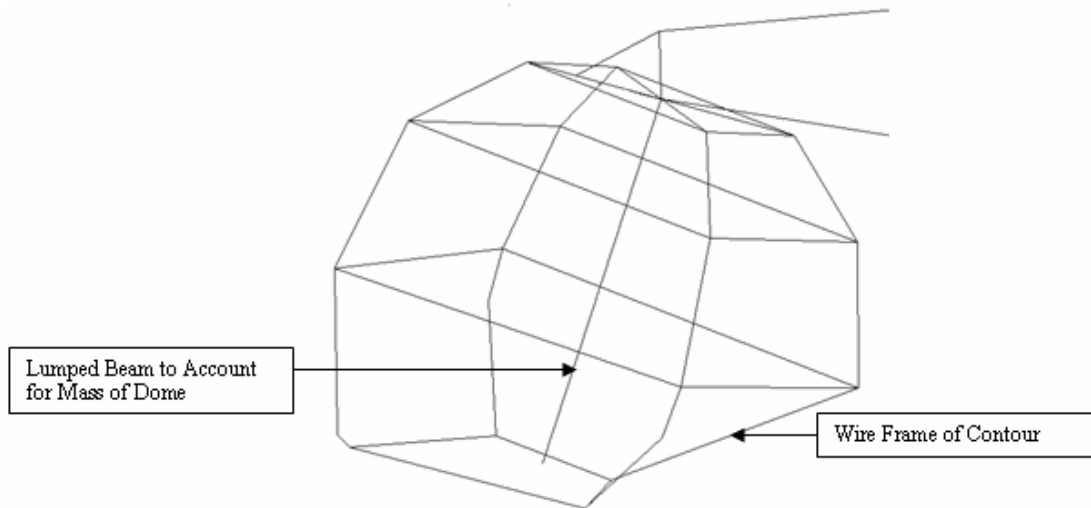


Figure 4.5. Gregorian Dome

The line feed antenna is modeled with two frame elements as shown in Figure 4.6. The short element represents the carriage house assembly while the long element represents the antenna itself. The line feed antenna is conservatively located at the stow position.

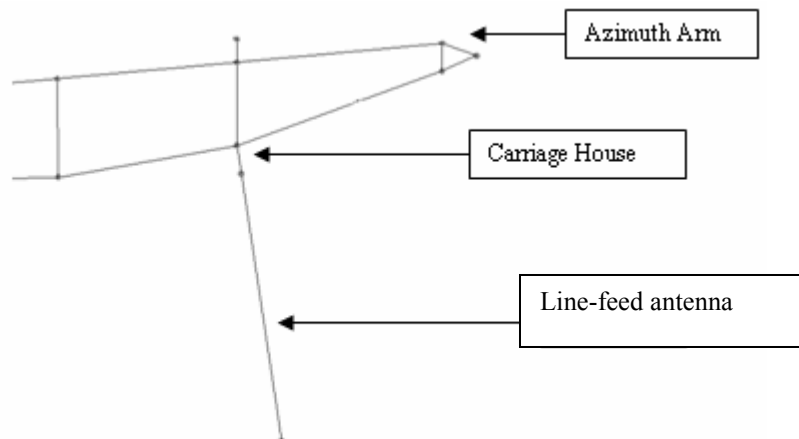


Figure 4.6. Line-feed antenna

4.2 Weight Distribution in Platform

The original weight of the platform is as follows:

- Total Suspended Weight of the platform (pre Gregorian) = 1150 kip
- Triangular platform weight (pre Gregorian) = 520 kip

Additional weight added on occasion of the Gregorian upgrade are given in Table 4.1.

Table 4.1. Additional suspended weight added in Gregorian upgrade

Part	Weight [kip]	Source
Platform Reinforcements and New Tiedown Weights	118 kip	Drawings (General II)
Azimuth Arm Track for Gregorian	78.3 kip	Drawings (General II)
Azimuth Arm Reinforcements	155.5 kip	Drawings (General II)
Gregorian Dome Weight	170 kip	Drawings (General II)
Carriage House 1 and Line Feed Antenna Weight	36 kip	Ing. Felipe Soberal
Removal of Original Tiedown Cables	-50 kip	Drawings (General II)

Weight Calculations:

Triangular Platform Weight

$$520 \text{ kip} + 118 \text{ kip} - 50 \text{ kip} = \underline{\underline{588 \text{ kip}}}$$

(Pre-Gregorian) (Platform Reinforcement) (Old tiedowns)

Azimuth Arm Weight

$$(1150 \text{ kip} - 520 \text{ kip}) + 78.3 \text{ kip} + 155.5 \text{ kip} - 36 \text{ kip} = \underline{\underline{827.8 \text{ kip}}}$$

(Pre-Gregorian) (Track) (Reinforcement) (Line Antenna)

CHECK Total Suspended Weight (must equal 1620 kip)

$$588 \text{ kip} + 827.8 \text{ kip} + 170 \text{ kip} + 36 \text{ kip} = \underline{\underline{1621.3 \text{ kip}}}$$

(Triangular Platform) (Azimuth Arm) (Gregorian Dome) (Line Antenna)

Calculation of Specific Weights and Mass Densities

To assure rigid body response, all the platform components have been modeled as members with a 5 ft x 5 ft solid cross section with the elastic modulus of steel. The weight density and mass density of the components is varied to assure the correct weight of the structure. The tiedown booms, the circular rail and other 'minor' members have been assigned a specific weight equal to approximately zero. The others are as follows:

Triangular Platform Specific Weight and Mass Density

The weight will be assigned to only the two triangular structures.

$$\text{Length of each side of the triangle} = 216 \text{ ft}$$

$$L_{\text{total}} = 216 \text{ ft/side} * 3 \text{ sides/triangle} * 2 \text{ triangles} = 1,296 \text{ ft}$$

$$\text{Volume} = \text{Length} * \text{Area} = 1296 \text{ ft} * 5 \text{ ft} * 5 \text{ ft} = 32,400 \text{ ft}^3$$

$$\text{Weight} = 588 \text{ kip} = 588,000 \text{ lb}$$

$$\text{Specific Weight} = \gamma = \text{Weight} / \text{Volume} = 588,000 \text{ lb} / 32,400 \text{ ft}^3 = \underline{\underline{18.15 \text{ lb/ft}^3}}$$

$$\text{Mass Density} = \gamma / g = 18.15 \text{ lb/ft}^3 / 32.2 \text{ ft/s}^2 = \underline{\underline{0.564 \text{ lb.s}^2/\text{ft/ft}^3}}$$

Azimuth Arm Specific Weight and Mass Density

$$L_{\text{total}} = 726.74 \text{ ft (Sum of the lengths of all the truss members in the arm)}$$

$$\text{Volume} = \text{Length} * \text{Area} = 726.74 \text{ ft} * 5 \text{ ft} * 5 \text{ ft} = 18,168.5 \text{ ft}^3$$

$$\text{Weight} = 827 \text{ kip} = 827,000 \text{ lb}$$

$$\text{Specific Weight} = \gamma = \text{Weight} / \text{Volume} = 827,000 \text{ lb} / 18,168.5 \text{ ft}^3 = \underline{\underline{45.52 \text{ lb/ft}^3}}$$

$$\text{Mass Density} = \gamma / g = 45.46 \text{ lb/ft}^3 / 32.2 \text{ ft/s}^2 = \underline{\underline{1.414 \text{ lb.s}^2/\text{ft/ft}^3}}$$

Gregorian Dome Specific Weight and Mass Density

$$L_{\text{total}} = 54 \text{ ft (Length of the lumped beam at dome's centerline)}$$

$$\text{Volume} = \text{Length} * \text{Area} = 54 \text{ ft} * 5 \text{ ft} * 5 \text{ ft} = 1350 \text{ ft}^3$$

$$\text{Weight} = 170 \text{ kip} = 170,000 \text{ lb}$$

$$\text{Specific Weight} = \gamma = \text{Weight} / \text{Volume} = 170,000 \text{ lb} / 1350 \text{ ft}^3 = \underline{\underline{125.9 \text{ lb/ft}^3}}$$

$$\text{Mass Density} = \gamma / g = 125.9 \text{ lb/ft}^3 / 32.2 \text{ ft/s}^2 = \underline{\underline{3.911 \text{ lb.s}^2/\text{ft/ft}^3}}$$

Line Feed Antenna Specific Weight and Mass Density

Carriage House 1

$$L_{\text{total}} = 10 \text{ ft}$$

$$\text{Volume} = \text{Length} * \text{Area} = 10 \text{ ft} * 5 \text{ ft} * 5 \text{ ft} = 250 \text{ ft}^3$$

Weight = 18 kip = 18,000 lb (It is assumed that half of the 36 kip weight corresponds to the carriage house)

$$\text{Specific Weight} = \gamma = \text{Weight} / \text{Volume} = 18,000 \text{ lb} / 250 \text{ ft}^3 = \underline{\underline{72.0 \text{ lb/ft}^3}}$$

$$\text{Mass Density} = \gamma / g = 72.0 \text{ lb/ft}^3 / 32.2 \text{ ft/s}^2 = \underline{\underline{2.236 \text{ lb.s}^2/\text{ft/ft}^3}}$$

Antenna

$$L_{\text{total}} = 96 \text{ ft}$$

$$\text{Volume} = \text{Length} * \text{Area} = 96 \text{ ft} * 5 \text{ ft} * 5 \text{ ft} = 2,400 \text{ ft}^3$$

Weight = 18 kip = 18,000 lb (It is assumed that half of the 36 kip weight corresponds to the antenna itself)

$$\text{Specific Weight} = \gamma = \text{Weight} / \text{Volume} = 18,000 \text{ lb} / 2,400 \text{ ft}^3 = \underline{\underline{7.5 \text{ lb/ft}^3}}$$

$$\text{Mass Density} = \gamma / g = 7.5 \text{ lb/ft}^3 / 32.2 \text{ ft/s}^2 = \underline{\underline{0.233 \text{ lb.s}^2/\text{ft/ft}^3}}$$

4.3 Maintaining the Platform Level

The extreme location of the Gregorian dome tends to tilt the platform towards tower T8. The only way to maintain the platform leveled (an operational constraint) is by tightening the T4 and T12 tiedowns. The T8 tiedowns will go almost slack. The objective of this iteration is to achieve a level state for the platform. Simultaneously, the sum of the tensions in all the tiedowns should equal 144 kip, the value specified in the drawings. Assume that the tension in the T8 tiedowns is reduced to 4 kip each (4 kip * 2 cables = 8 kip total) which is nearly zero, as expected. Let the T4 and T12 tiedowns resist the difference (144 kip – 8 kip = 136 kip) which is calculated at 136 kip / 4 tiedown cables = 34 kip per tiedown cable (for the T4 and T12 tiedowns).

It will be assumed that the preload in all the cables (except tiedowns) is the same as for the previous model (Model B). The reason is that variations in the orientation of the

azimuth arm and angle of the Gregorian dome are performed routinely in the operation of the radio telescope, without additional preloading of backstays and platform supporting cables. The preload state is given by the temperatures in Table 4.2.

Table 4.2. Invariant preload temperatures in Model C

TEMP MAIN [F]	0
TEMP AUX [F]	-235
TEMP GUYMAIN T12 [F]	-505
TEMP GUYAUX T12 [F]	-540
TEMP GUYMAIN T8 [F]	-465
TEMP GUYAUX T8 [F]	-487.5
TEMP GUYMAIN T4 [F]	-515
TEMP GUYAUX T4 [F]	-520

4.3.1 Results with Original Weight Distribution

The iteration chart with the results to achieve the equilibrium state under dead load is shown in Table 4.3. Only the tiedown temperatures are varied. The 34 kip target for the tension in the tiedowns was not met. The corrective action to achieve the 34 kip target will be addressed in Section 4.3.2.

Table 4.3. Iteration chart for tiedown preload

	STAGE 2C TE 1	STAGE 2C TE 2	STAGE 2C TE 3	STAGE 2C TE 4	STAGE 2C TE 5	STAGE 2C TE 6
INPUT						
Temp T8 Tiedown [deg F]	-3700	-3600	-3500	-3550	-3600	-3750
Temp T4 and T12 Tiedowns [deg F]	-4000	-3900	-3800	-3850	-3800	-3600
OUTPUT						
MAX Uz displacement at platform corners [ft]	-12.6	-12.3	Unstable	-12.2	-12.1	-11.6
MIN Uz displacement at platform corners [ft]	-12.6	-12.3	Unstable	-12.2	-12.3	-12.6
Tension T8 tiedown [kip] (4 kip target)	11	7	Unstable	4	5	6
Tension T4 and T12 tiedowns [kip] (34 kip target)	71	66	Unstable	64	63	57

Note case TE 5 was the best iteration step. Any additional reduction in thermal strains of T4 and T12 to try to achieve the 34 kip target tilts the platform towards T8. Observing the last column (Case TE 6) it can be seen that one end of the platform descended one foot further than the other. Note also that the higher tensions (higher than the 34 kip target) in the T4 and T12 tiedowns are causing the platform to descend one foot more than expected in all the iteration steps. In Model B the platform descent was 11.0 ft while in this case it is an average of 12.2 ft.

Possible Explanation for Higher than Predicted Tiedown Tension

It seems that the assumption of concentrating the Gregorian mass in a single element on its centerline, needs to be improved to achieve the proper balanced equilibrium state of the platform due to dead load. A significant portion of the Gregorian's mass is concentrated on the inboard side of the dome (the side nearest to the platform's centerline), where the instrumentation and its supporting structure is located. The outboard side of the dome is lined only with the secondary reflector.

Proposed approach: Weight Redistribution

To achieve a leveled platform with the expected tiedown tensions, some of the weight of the Gregorian dome will be redistributed to the line feed antenna which acts as a counterbalance to the dome. Other approaches to achieve a balanced platform could have been used; for example, the assumed length of the lumped beam, to account for the mass of the dome, could have been shortened to decrease the moment arm, or the elements of the dome could have been assigned weight to achieve the redistribution within the platform. It makes practically no difference (for this particular case) which approach is used since the only objective is to achieve a balanced platform (a constraint of the structure) to determine the overall effect on the system. If required, iterations will be performed on the magnitude of the mass redistribution such that the tension in the T4 and T12 tiedowns reaches the desired tension of 34 kip per cable while maintaining the platform level. The tension in the T8 tiedowns should be approximately 4 kips per cable to maintain the 144 kip constraint (sum of tensions in all tiedowns equals 144 kip). Before proceeding with this approach, the results (temperatures, displacements, tensions) for Model C, case TE 5 are recorded to be used as a comparison.

Displacement and Tension Results – Original Weight Distribution

The displacements and tensions obtained at the iteration step TE 5 are shown in Table 4.4. The results obtained for the uniform platform case (Model B) are also included for comparison.

Table 4.4. Displacement and tensions of Model C – original weight distribution

INPUT	MODEL B	MODEL C (Orig. Wt. Dist.) Case TE 5	% DIFF Model B vs Model C
TEMP MAIN [F]	0	0	0.0%
TEMP AUX [F]	-235	-235	0.0%
TEMP GUYMAIN T12 [F]	-505	-505	0.0%
TEMP GUYAUX T12 [F]	-540	-540	0.0%
TEMP GUYMAIN T8 [F]	-465	-465	0.0%
TEMP GUYAUX T8 [F]	-487.5	-487.5	0.0%
TEMP GUYMAIN T4 [F]	-515	-515	0.0%
TEMP GUYAUX T4 [F]	-520	-520	0.0%
TEMP T8 TIEDOWN [F]	-3300	-3600	9.1%
TEMP T4 and T12 TIEDOWNS [F]	-3300	-3800	15.2%
INITIAL Z OFFSET [ft]	10.872	10.872	0.0%
OUTPUT			
PLATFORM UZ [ft]	-11.0	-12.2	10.9%
UX T12 TOWER [in]	-0.00021	-0.03225	N/A
UY T12 TOWER [in]	0.01054	-1.07394	N/A
UX T8 TOWER [in]	-0.06977	0.70401	N/A
UY T8 TOWER [in]	-0.04129	0.40936	N/A
UX T4 TOWER [in]	0.0438	-1.06064	N/A
UY T4 TOWER [in]	-0.02948	0.57425	N/A
TENSION MAIN [kip] 480 k	496	530	6.9%
TENSION AUX [kip] 602 k	608	628	3.3%
TENSION GUYMAIN T12 [kip] 514 k	498	523	5.0%
TENSION GUYAUX T12 [kip] 727 k	665	694	4.4%
TENSION GUYMAIN T8 [kip] 503 k	456	481	5.5%
TENSION GUYAUX T8 [kip] 662 k	599	626	4.5%
TENSION GUYMAIN T4 [kip] 543 k	509	533	4.7%
TENSION GUYAUX T4 [kip] 728 k	640	667	4.2%
TENSION TIEDOWN T12 [kip] 24 k	24.1	4.9	N/A
TENSION TIEDOWN T8 [kip] 24 k	24.1	62.7	N/A
TENSION TIEDOWN T4 [kip] 24 k	24.1	62.7	N/A

Note from Table 4.4 that the towers are displaced close to an inch at the top. The excess tension in the tiedowns is flexing all the towers inwards (towards the platform) as shown in Figure 4.7. Also note from the table that the tension in all the cables has increased by approximately 5%, as a result of the increased preload in the tiedowns.



Figure 4.7. Deformed shape of towers (2000x mag.) – original weight distribution (cables not shown for clarity)

‘Major’ (M_{33}) bending moments in the towers – original weight distribution

The ‘major’ (M_{33}) bending moments in the towers are shown in Table 4.5. These moments are due to the towers flexing towards the platform as shown in Figure 3.7. Similar results for the uniform platform case (Model B) are also included for comparison.

Table 4.5. ‘Major’ M_{33} bending moments – original weight distribution

	MODEL B	MODEL C (Orig. Wt. Dist.) Case TE 5	% DIFF Model B vs Model C
M33 at TOP of Tower T12 [kip-ft]	2698	2673	-0.9%
M33 at BASE of Tower T12 [kip-ft]	-3501	-9870	181.9%
M33 at TOP of Tower T8 [kip-ft]	1616	1536	-5.0%
M33 at BASE of Tower T8 [kip-ft]	-2386	-8164	242.2%
M33 at TOP of Tower T4 [kip-ft]	2800	2759	-1.5%
M33 at BASE of Tower T4 [kip-ft]	-3389	-10762	217.6%

Note the moments at the top of the towers are essentially unchanged. This is expected, as there is basically no relief mechanism for the unbalanced moment of the auxiliary saddle. At the base of the towers the moments increased by a factor of approximately 2.5.

4.3.2 Redistribution of Weight

The objective of this section is to redistribute some of the weight of the Gregorian dome to the line antenna to achieve the expected tensions in the tiedown cables (4 kip in the T8 tiedowns and 34 kips in the T4 and T12 tiedowns). This is being performed as a correction to the shortcomings of the dome idealization. This approach assures that the correct balance will be achieved while maintaining constant the total mass of the platform. The mass of the Gregorian will be redistributed to the longer element of the line antenna to gain the maximum advantage. As mentioned previously, other approaches to achieve a balanced platform could have been used; for example, the assumed length of the lumped beam, to account for the mass of the dome, could have been shortened to decrease the moment arm, or the elements of the dome could have been assigned weight to achieve the redistribution within the platform. It makes practically no difference (for this particular case) which approach is used since the platform is assumed rigid, i.e., the only objective is to achieve a balanced platform (a constraint of the structure) to determine the overall effect on the system. It would make a difference in the case of a future research project to determine the response of the individual components of the platform to seismic loading. In that case, the mass and location of each individual component would have to be included in a detailed, non-rigid model of the platform.

Assumption 1: Redistribute 50 kip from the Gregorian to the Line Antenna

The 50 kip estimate was determined as follows. The results of Table 4.4 show the T4 and T12 tiedown tensions at 63 kip. The difference with respect to the target tension is approximately 25 kip. Using half of the difference and multiplying by the four tiedown cables of T4 and T12 gives $25 \text{ kip} / 2 * 4 \text{ cables} = 50 \text{ kip}$. Only half of the weight difference is used as the other half is counterbalanced.

The new properties are calculated in the last column of Table 4.6. The original properties are also included for comparison.

Table 4.6. Calculation of new properties - 50 kip weight redistribution

	Model C (Original Wt. Dist.)	Model C (50 kip Redist.)
PROPERTIES		
Weight Transfer (Relative to Zero) [kip]	0	50
GREGORIAN Weight [kip]	170	120
GREGORIAN Specific Weight [lb/ft ³]	125.9	88.9
GREGORIAN Mass Density [lb.s ² /ft ³]	3.911	2.761
Line ANTENNA Weight (long elem) [kip]	18	68
Line ANTENNA Specific Weight [lb/ft ³]	7.5	28.3
Line ANTENNA Mass Density [lb.s ² /ft ³]	0.233	0.880

The iterations to achieve the equilibrium state due to dead load are shown in Table 4.7. Note that almost perfect convergence is achieved in the fourth iteration. The tiedown tensions as well as the platform descent have achieved the targets.

Table 4.7. Iteration chart for 50 kip weight redistribution

	MODEL C TE 1	MODEL C TE 2	MODEL C TE 3	MODEL C TE 4
INPUT				
Temp T8 Tiedown [deg F]	-3750	-3350	-3250	-3230
Temp T4 and T12 Tiedowns [deg F]	-3600	-3300	-3320	-3340
OUTPUT				
MAX Uz Platform [ft]	-12.1	-10.9	-10.9	-11.0
MIN Uz Platform [ft]	-12.1	-11.3	-11.0	-11.0
Tension T8 tiedown [kip] (4 kip target)	22.3	7.1	4.5	4.1
Tension T4 and T12 tiedowns [kip] (34 kip target)	54	33.9	33.7	34.1

Displacement and Tension Results – 50 kip Weight Redistribution

The complete displacement and tension magnitudes for Model C with the weight redistribution are shown in Table 4.8. The results for the uniform platform case (Model B) are also included for comparison.

Table 4.8. Displacements and tensions – 50 kip weight redistribution

INPUT	Model B (Unif. Plat. Case TE 5)	Model C (50 kip Wt. Redist.) Case TE 4	% DIFF Model B vs Model C
TEMP MAIN [F]	0	0	0.0%
TEMP AUX [F]	-235	-235	0.0%
TEMP GUYMAIN T12 [F]	-505	-505	0.0%
TEMP GUYAUX T12 [F]	-540	-540	0.0%
TEMP GUYMAIN T8 [F]	-465	-465	0.0%
TEMP GUYAUX T8 [F]	-487.5	-487.5	0.0%
TEMP GUYMAIN T4 [F]	-515	-515	0.0%
TEMP GUYAUX T4 [F]	-520	-520	0.0%
TEMP T8 TIEDOWN [F]	-3300	-3230	-2.1%
TEMP T4 and T12 TIEDOWNS [F]	-3300	-3340	1.2%
INITIAL Z OFFSET [ft]	10.872	10.872	0.0%
OUTPUT			
PLATFORM UZ [ft]	-11.0	-11.00	0.0%
UX T12 TOWER [in]	-0.00021	-0.00993	N/A
UY T12 TOWER [in]	0.01054	-0.0066	N/A
UX T8 TOWER [in]	-0.06977	-0.06443	N/A
UY T8 TOWER [in]	-0.04129	-0.03819	N/A
UX T4 TOWER [in]	0.0438	0.03474	N/A
UY T4 TOWER [in]	-0.02948	-0.03549	N/A
TENSION MAIN [kip] 480 k	496	497	0.2%
TENSION AUX [kip] 602 k	608	608	0.0%
TENSION GUYMAIN T12 [kip] 514 k	498	498	0.0%
TENSION GUYAUX T12 [kip] 727 k	665	665	0.0%
TENSION GUYMAIN T8 [kip] 503 k	456	457	0.2%
TENSION GUYAUX T8 [kip] 662 k	599	599	0.0%
TENSION GUYMAIN T4 [kip] 543 k	509	508	-0.2%
TENSION GUYAUX T4 [kip] 728 k	640	640	0.0%
TENSION TIEDOWN T12 [kip] 24 k	24.1	4.1	N/A
TENSION TIEDOWN T8 [kip] 24 k	24.1	34.1	N/A
TENSION TIEDOWN T4 [kip] 24 k	24.1	34.1	N/A

Note in Table 4.8 that the displacements at the top of the towers have returned to approximately zero. Also, the tensions in all the cables have returned to the same magnitudes as for Model B (uniform platform). **These results show that any shift in the position of the Gregorian dome or the line antenna is effectively counterbalanced by the tiedown cables as long as the platform is level.** The deformed shape for the structure with the weight redistribution is shown in Figure 4.8.



Figure 4.8. Deformed shape of Model C – 50 kip weight redistribution

‘Major’ (M_{33}) bending moments in the towers – 50 kip Weight Redistribution

The ‘major’ (M_{33}) bending moments in the towers are shown in Table 4.9. Note that there are only negligible variations in bending moments as compared to the uniform platform case (Model B). The bending moments in the towers are independent of the model as long as the platform is leveled and the tiedown tensions add up to the same magnitude (144 kip in this case).

Table 4.9. Comparison of M_{33} bending moments – Model B vs Model C redistributed

	MODEL B	MODEL C (50 kip Wt. Redist.)	% DIFF Model B vs Model C
M33 at TOP of Tower T12 [kip-ft]	2698	2703	0.2%
M33 at BASE of Tower T12 [kip-ft]	-3501	-3531	0.9%
M33 at TOP of Tower T8 [kip-ft]	1616	1603	-0.8%
M33 at BASE of Tower T8 [kip-ft]	-2386	-2403	0.7%
M33 at TOP of Tower T4 [kip-ft]	2800	2805	0.2%
M33 at BASE of Tower T4 [kip-ft]	-3389	-3423	1.0%

4.4 Conclusions

In Chapters 2, 3 and 4 we described the three models A, B, and C, and the results of the procedure required to achieve the equilibrium state due to dead loads. The use of the three models allowed for a gradual immersion into the problem of achieving the equilibrium state due to dead loads. Numerous tests were performed which validate the results of the models.

Now, having achieved the deformed equilibrium state due to dead load, the investigation can proceed to determine the dynamic properties and the seismic response of the Arecibo Observatory structures. The dynamic properties are obtained in Chapter 5. Initial studies into the seismic response of the structure are performed in Chapter 6, while the final studies on the seismic response are documented in Chapter 7.

CHAPTER 5

Dynamic Properties

5.1 Introductory Concepts

Natural response, also referred to as free vibration, is the response of a structure when disturbed from its static equilibrium position by an initial displacement or velocity and then allowed to vibrate without any external excitation. Typically, the continuous system is discretized into a model with multiple degrees of freedom. The dynamic properties of the model are represented by its mode shapes and natural frequencies (each mode shape has one natural frequency at which it vibrates). This approach, called modal analysis, is used in the thesis. Mathematically, the natural frequencies correspond to the eigenvalues while mode shapes correspond to the eigenvectors that satisfy the set of linear homogeneous differential equations that define the system. The central concept of modal analysis is orthogonality of modes which decouples the governing differential equations. As a result, instead of solving a system of N simultaneous differential equations, the problem is transformed into one of solving N independent single-degree-of-freedom differential equations - a much simpler problem. The mode shapes are useful in developing an understanding of the behavior of the structure. This chapter focuses on this aspect. In addition, modal analysis can be used as the basis for calculating the forced response of the system by superimposing the contribution of each mode (modal superposition) to determine the total forced response of the structure. Time-history modal analysis is used in Chapters 6 and 7 of this thesis to determine the seismic response of the structure. Modal analysis is well documented in all textbooks of structural dynamics and mechanical vibrations.

This chapter documents the modal results for the three models. In addition, several sensitivity studies and comparisons are performed to obtain a good understanding for the natural response of the structure.

To properly run the modal analysis option in SAP2000 the “Stiffness at End of Nonlinear Case” alternative must be chosen (See Figure 5.1). By choosing this option, the

program will include the geometric stiffness terms calculated in the nonlinear p-delta analysis.

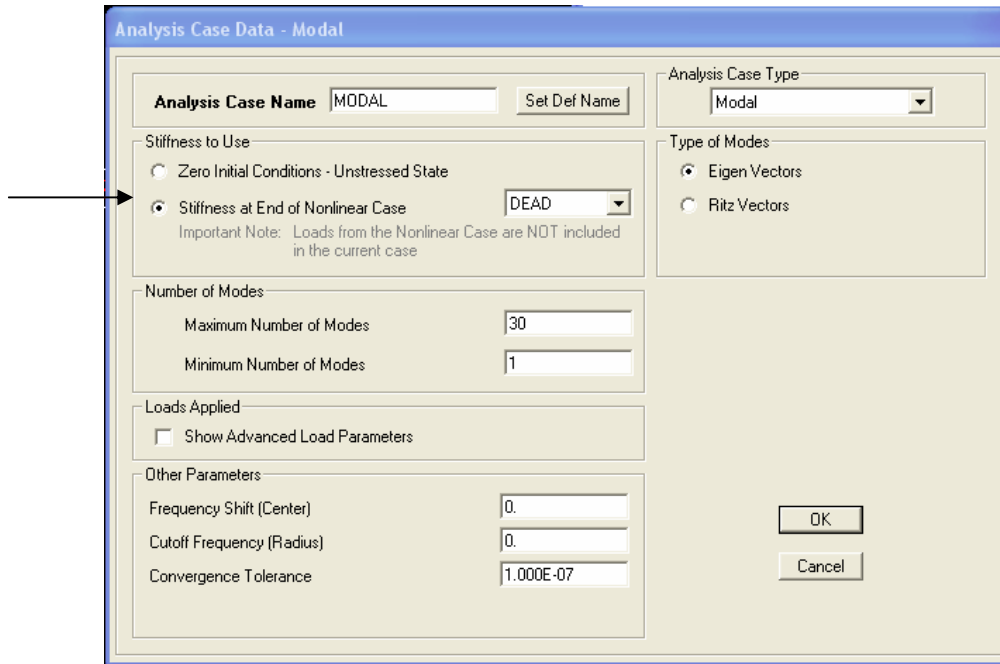


Figure 5.1. Typical SAP2000 Version 9 modal analysis case form

5.2 Modal Analysis of Model A (Uniform Platform, No Tiedowns)

The results of the modal analysis case were observed graphically using the deformed geometry option as well as the animation feature of SAP2000. The animation feature is especially useful since the dynamic characteristics of the natural response can be clearly observed. In this document, however, only a snap shot of the mode shape can be transferred to a figure. Nevertheless, a static figure still conveys the essence of the response.

5.2.1 Results

The mode shapes fall into three different types; these are, platform modes, tower modes, and independent cable modes. In addition there are interaction modes between them. Examples of the first type are included in Figures 5.2 through 5.5. The interaction modes are the most difficult to discern. These are caused by different modes which are activated at similar natural frequencies and combine to form an interaction mode. In this thesis the natural periods of the structure will be used to identify and describe the modes rather than the

natural frequencies. They are directly related as one is the reciprocal of the other when frequency is measured in Hz. The natural period is the time required for the mode to complete one full cycle.

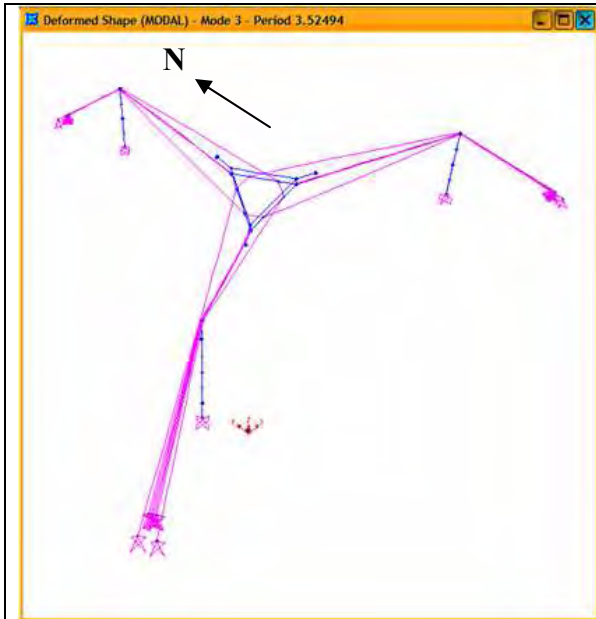


Figure 5.2. Example of platform mode (rotation about North-South axis)

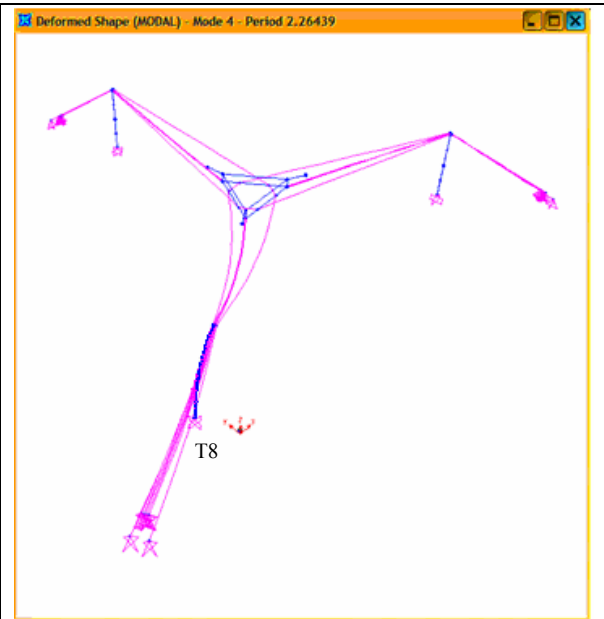


Figure 5.3. Example of tower mode (1st flexural mode of tower T8)

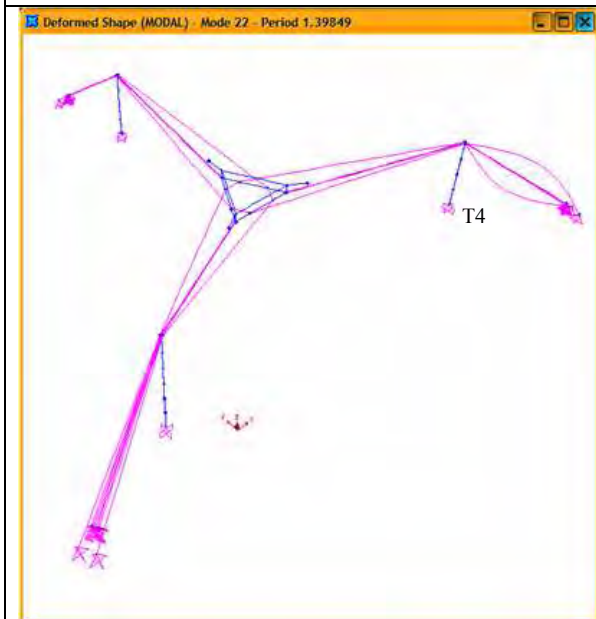


Figure 5.4. Example of independent cable mode (fundamental mode of auxiliary backstays in tower T4)

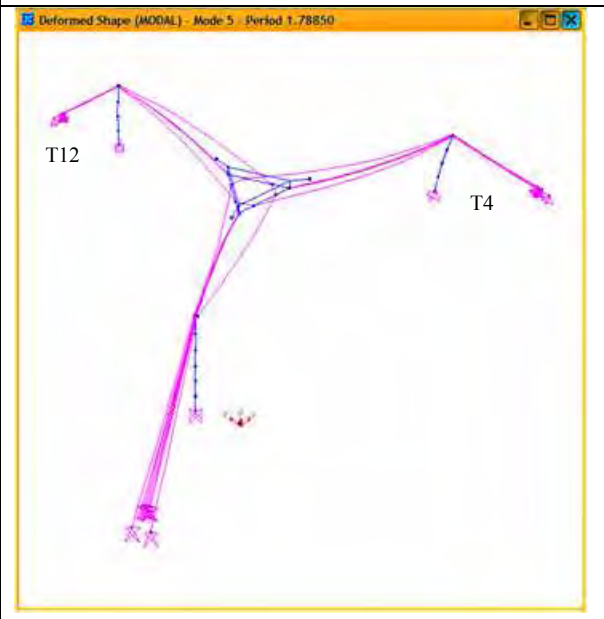


Figure 5.5. Example of interaction mode (tower T4 and T12 in fundamental mode while platform rotates around vertical axis)

The results of the modal analysis are included in Table 5.1 under the column “CASE TEMP15”. Several modes were selected and identified with capital letters in the first column of the table. Two additional cases (TEMP 4 and NO TEMP) were included in the table to determine the sensitivity of the natural periods to the variations in thermal strains. All the cases correspond to iterations carried out in Chapter 2 of the thesis (Table 2.18). The three cases shown are:

1. Case TEMP 4 (Maximum backstay thermal strain - towers flex radially outward)
2. Case TEMP 15 (Balanced backstay thermal strain - Towers achieve straightness)
3. Case NO TEMP (Zero backstay thermal strains - Towers flex radially inward).

Table 5.1. Comparison of modes and natural periods for three thermal strain cases

ID	MODE DESCRIPTION	CASE TEMP 4		CASE TEMP15		CASE NO TEMP		Max % Difference
		Mode Number	Period [sec]	Mode Number	Period [sec]	Mode Number	Period [sec]	
A	Platform vertical displacement	1	4.681	1	4.683	1	4.707	0.55
B	Platform rotation about East-West Axis	2	3.539	2	3.529	2	3.432	-2.83
C	Platform rotation about North-South Axis	3	3.534	3	3.525	3	3.429	-3.06
D	1st Mode Tower T8	4	2.264	4	2.264	4	2.283	0.83
E	1st Mode Towers T4 and T12 - In phase (Platform rotates about vertical axis)	5	1.787	5	1.788	17	1.781	-0.39
F	1st Mode Towers T4 and T12 - Out of phase	6	1.717	6	1.722	18	1.703	-1.12
G	2nd Mode Tower T8	68	1.101	68	1.100	88	1.099	-0.18
H	2nd Mode Towers T4 and T12 - In phase	101	0.749	101	0.752	105	0.753	0.53
I	2nd Mode Towers T4 and T12 - Out of phase (Cradle motion of platform)	102	0.733	102	0.733	116	0.732	-0.14
J	3rd Mode Tower T8	103	0.698	107	0.698	117	0.707	1.27
K	3rd Mode Tower T4	182	0.457	186	0.451	217	0.444	-2.93
L	3rd Mode Tower T12	187	0.447	188	0.447	218	0.444	-0.68
M	4th Mode Tower T8	183	0.450	187	0.450	212	0.451	0.22
N	4th Mode Tower T4	301	0.327	301	0.327	313	0.330	0.91
O	4th Mode Tower T12	304	0.322	302	0.322	326	0.322	0.00
P	5th Mode Tower T8	315	0.304	315	0.305	375	0.304	0.00
Q	1st Mode Auxiliary Cables	11	1.504	11	1.529	9	2.004	24.95
R	1st Mode Main Cables	32	1.291	35	1.284	44	1.220	-5.82
S	1st Mode T12 Auxiliary Backstays	60	1.144	61	1.181	35	1.409	18.81
T	1st Mode T8 Auxiliary Backstays	64	1.109	65	1.151	40	1.340	17.24
U	1st Mode T4 Auxiliary Backstays	22	1.334	22	1.398	19	1.672	20.22
V	1st Mode T12 Main Backstays	69	1.089	69	1.109	65	1.208	9.85
W	1st Mode T8 Main Backstays	79	1.072	79	1.065	79	1.143	6.21
X	1st Mode T4 Main Backstays	26	1.293	26	1.300	25	1.470	12.04

Note that the platform modes and the tower modes are essentially independent of the variations in thermal strains. Only the independent cable modes show sensitivity as their natural periods are directly dependent on the tension in the cable.

5.2.2 Validation of Independent Cable Modes

In this section the fundamental natural periods of the cables are compared against an empirical formula. This check only applies to independent cable modes, that is, for modes in which there is no interaction between the cables and the platform or towers. Essentially, independent cable modes behave as those for a single cable pinned at both ends.

Ren (2005) provides empirical formulas to fast estimate the cable tension if the cable fundamental frequency is known. The equations may be rearranged to solve for the natural period as a function of tension in the cable. For cables in a high state of tension the following equation is recommended:

$$T = 4 m L^2 f^2 \quad , \text{ where, using any consistent set of units,}$$

T = Tension in the cable

m = mass per unit length of the cable

L = Length of the cable

f = fundamental frequency of the cable in Hertz

The equation may be rearranged to calculate the fundamental period, as follows,

$$\text{Fundamental Period} = 1/f = \sqrt{\frac{4mL^2}{T}}$$

The fundamental periods of the cables have the shape of a half-sine wave. A typical fundamental cable mode is displayed in Figure 5.4, which shows both auxiliary backstays of tower T4 in their fundamental mode. Both backstays participate since they are identical and have the same tension. Note that practically no other structural component is in motion, i.e., there is no interaction between components for this particular mode.

The results of the comparison between the periods from the computer model and the empirical equation are shown in Table 5.2. The tension values are reported from the SAP2000 model results. The periods calculated with the empirical formula are in excellent agreement (less than 0.5% difference) thus validating the SAP2000 results.

Table 5.2. Comparison of SAP2000 periods against analytical equation (Ren 2005)

Cable Description	Mass per Unit Length m [lb-s ² /ft ²]	Tension [lb]	Length [ft]	Calculated Period [sec]	SAP2000 Period [sec]	% Difference	Mode Number
T8 Auxiliary (AUX)	0.675	365000	724.5	1.970	1.965	-0.3	11
T4 Auxiliary Backstays (GUYAUX)	0.838	463000	609.93	1.641	1.641	0.0	20
T4 Main Backstays (GUYMAIN)	0.675	405000	560.06	1.446	1.444	-0.1	27
T12 Main (MAIN)	0.574	554000	588	1.197	1.197	0.0	52

5.2.3 Validation of Tower Modes

The objective of this section is to verify the reasonableness of the natural periods of the towers by performing two comparisons of the results; the first comparison is to equation 30-8 of the 1997 Uniform Building Code ($T = 0.03 \cdot \text{height}^{0.75}$); the second comparison is to an independent finite element model of just tower T8.

The comparison versus the code equation is included in Table 5.3. This is an ‘order of magnitude’ type of verification and shows that results are reasonable.

Table 5.3. Comparison of tower periods vs. UBC-97 equation 30-8

Tower ID	Height [ft]	Fundamental Period (UBC-97 Equation 30-8) [sec]	Fundamental Period (SAP2000) [sec]	Percent Difference
T8	365	2.5	2.27	10%
T4 and T12	265	2.0	1.6	25%

The next validation check compares the tower periods of the full model to an isolated model of Tower 8 also using SAP2000. The single-tower model was fixed at the base. In addition, two roller supports were placed on top of the tower. One of the roller constraints simulates the restraint offered in the direction of the cables. The other roller constraint prevents vertical displacement to simulate the restraint offered by the vertical component of the cables. The comparison is presented in Table 5.4.

Table 5.4. Comparison of tower T8 periods against a single-tower model

Single-Tower Mode Number	Single-Tower Model Period of T8 [sec]	Full Model Mode Number	Full Model Period of T8 [sec]	Percent Difference
1	2.05	4	2.27	9.7%
2	0.98	88	1.1	11%
3	0.64	117	0.70	8.6%
4	0.35	212	0.45	22%
5	0.28	327	0.31	9.7%

Note from Table 5.4 that the periods of the full model are all higher than the respective periods of the single-tower model. This tendency makes sense because geometric stiffness effects were included in Model A while the single-tower model did not include them. Therefore, the compressive forces in Model A increase the flexibility of the towers so that the periods increase. The percent difference also seems reasonable. It is approximately 10% for all cases except for the 4th mode, which shows a 22% difference. This outlier seems to be due to interaction between tower T4 with the 5th mode of the main backstay cable bundle. The interaction reduces the restraint in the cable direction so the tower becomes more flexible at the top (and the period increases). It can be concluded that the modal results are reasonable.

5.2.4 Sensitivity Study: Effect of Service Cables

This section investigates the effect of the presence of the service cables in the overall natural periods of the structure. Figure 5.6 shows the simplified model described in Section 2.7.5.

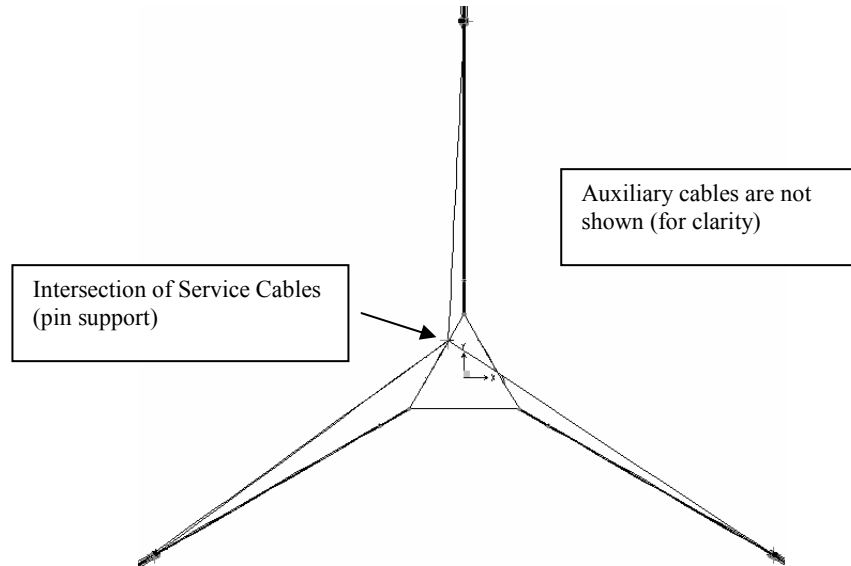


Figure 5.6. Plan view of simplified model with service cables

A comparison of the mode shapes and natural periods of the models of the structure without and with service cables is shown in Table 5.5. There is essentially no difference between the two cases. As expected, the service cables are shown to be effectively decoupled from the platform.

Table 5.5. Comparison of natural periods with and without service cables

MODE SHAPES AND PERIODS	PERIOD [sec] (NO Service Cables)	PERIOD [sec] (WITH pinned Service Cables)	Percent Difference [%]
[A] Platform vertical displacement	4.693	4.632	-1.3%
[B] Platform rotation about East-West axis	3.869	3.872	0.1%
[C] Platform rotation about North-South axis	3.864	3.867	0.1%
[D] 1st Mode Tower T8	2.259	2.258	0.0%
[E] 1st Mode Towers T4 and T12 (in phase)	1.772	1.765	-0.4%
[F] 1st Mode Towers T4 and T12 (out of phase)	1.711	1.707	-0.2%

5.3 Modal Analysis of Model B (Uniform Platform, With Tiedowns)

5.3.1 Results

The results, including those of Model A are included in Table 5.6.

Table 5.6. Modal results of Model B and comparison with Model A

ID	Mode Description	Model A (No Tiedowns)		Model B (With Tiedowns)		% DIFF
		Mode Number	Period [sec]	Mode Number	Period [sec]	
A	Platform Vertical Displacement	1	4.683	14	2.146	-54.2%
B	Platform Rotation about East-West Axis	2	3.529	17	1.628	-53.9%
C	Platform Rotation about North-South Axis	3	3.525	18	1.587	-55.0%
D	1st Mode Tower T8	4	2.264	13	2.260	-0.2%
E	1st Mode Towers T4 and T12 - In Phase (Platform rotates about vertical axis)	5	1.788	15	1.764	-1.3%
F	1st Mode Towers T4 and T12 - Out of Phase	6	1.722	16	1.723	0.1%
G	2nd Mode Tower T8	68	1.100	82	1.148	4.4%
H	2nd Mode Towers T4 and T12 - In Phase	101	0.752	137	0.739	-1.7%
I	2nd Mode Towers T4 and T12 - Out of Phase (Cradle Motion of Platform)	102	0.733	138	0.714	-2.6%
J	3rd Mode Tower T8	107	0.698	139	0.695	-0.4%
K	3rd Mode Tower T4	186	0.451	258	0.448	-0.7%
L	3rd Mode Tower T12	188	0.447	260	0.444	-0.7%
M	4th Mode Tower T8	187	0.450	259	0.447	-0.7%
N	4th Mode Tower T4	301	0.327	385	0.326	-0.3%
O	4th Mode Tower T12	302	0.322	410	0.321	-0.3%
P	5th Mode Tower T8	315	0.305	423	0.303	-0.7%
Q	1st Mode Auxiliary Cables	11	1.529	20	1.517	-0.8%
R	1st Mode Main Cables	35	1.284	57	1.283	-0.1%
S	1st Mode T12 Auxiliary Backstays	61	1.181	83	1.146	-3.0%
T	1st Mode T8 Auxiliary Backstays	65	1.151	87	1.127	-2.1%
U	1st Mode T4 Auxiliary Backstays	22	1.398	32	1.381	-1.2%
V	1st Mode T12 Main Backstays	69	1.109	91	1.089	-1.8%
W	1st Mode T8 Main Backstays	79	1.065	101	1.057	-0.8%
X	1st Mode T4 Main Backstays	26	1.300	48	1.29	-0.8%
Y	1st Mode Tiedowns	N/A	N/A	1	2.633	N/A

The natural periods of Model B are essentially identical to the results of Model A, except for the large (> 50%) difference in the periods of the platform modes. This result was expected and is due to the stiffening effects of the tiedown cables. The shapes of the modes themselves, however, are basically identical in the two models, including the platform mode shapes: the difference is only in the magnitude of the periods.

The presence of the tiedown cables introduces several additional independent cable modes. The first few calculated modes are all independent tiedown cable modes all similar to the shape shown in Figure 5.7. As a result the corresponding modes of Model B have a higher mode-number than those of model A.



Figure 5.7. First lateral independent cable mode of tiedowns

Eight interaction modes are shown in Figures 5.8 through 5.15. These are followed by Figures 5.16 through 5.31 which show the modes A through P described in Table 5.6.

Some Interaction Modes – Sheet 1 of 2



Figure 5.8. Mode 19. Strong rotation of platform about the vertical axis – Strong movement of main and auxiliary cables - Towers and backstays remain quiet.



Figure 5.9. Mode 29. Very similar to Mode 19 (Figure 5.8) but with a weaker rotation of the platform.



Figure 5.10. Mode 30. Weak rotation about North-South axis. Very similar to mode C but weaker. Main and Auxiliary cables displacing vertically and out of phase with each other.

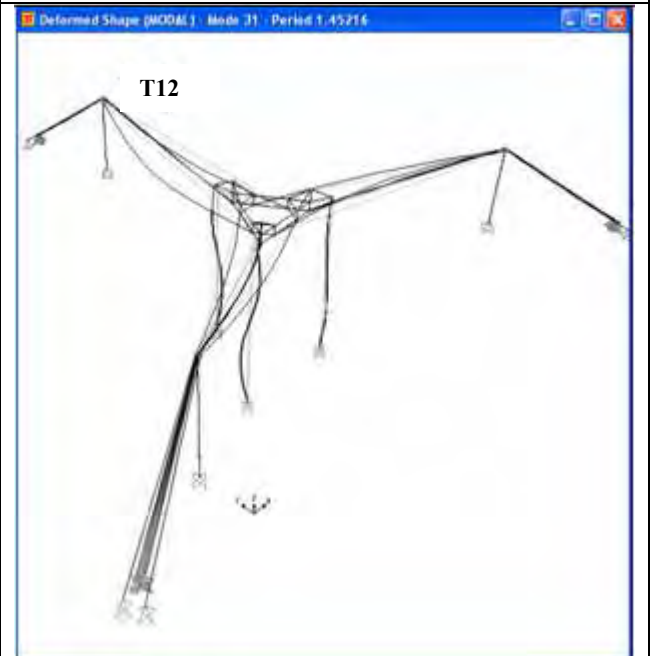


Figure 5.11. Mode 31. Very similar to Mode 19 (Figure 5.8) but with participation of Tower T12.

Some Interaction Modes – Sheet 2 of 2



Figure 5.12. Mode 80. Very similar to mode F (1st mode of towers T12 and T4 out of phase) but with weaker participation of the towers.



Figure 5.13. Mode 81. Very similar to mode E (1st mode of towers T12 and T4 in phase) but with weaker participation of the towers.



Figure 5.14. Mode 111. Very strong interaction mode. Creates a 1st mode type tower deflection (cantilever) in T8 but radially (same direction as cables). The radial direction is typical of even-numbered modes of the towers.

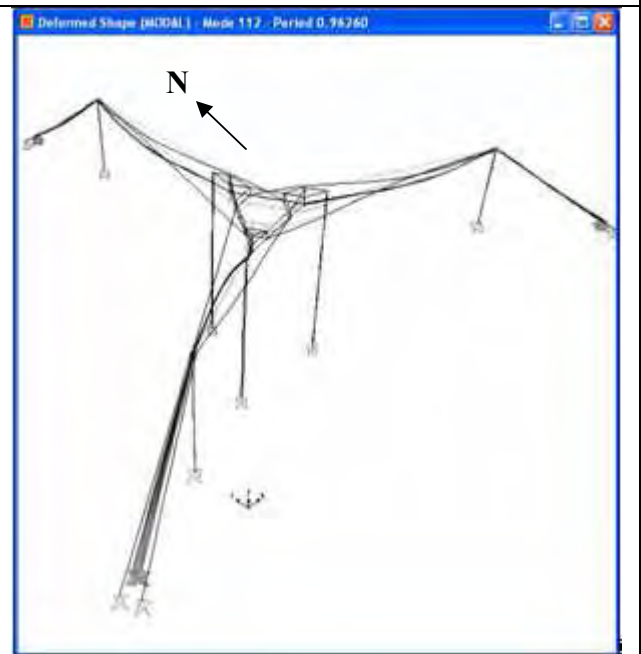


Figure 5.15. Mode 112. Equal to mode 111 (shown in Figure 5.14) except that platform rotation is about a North-South axis.



Figure 5.16. Table 5.6 id. A. Mode 14. Platform Vertical Displacement

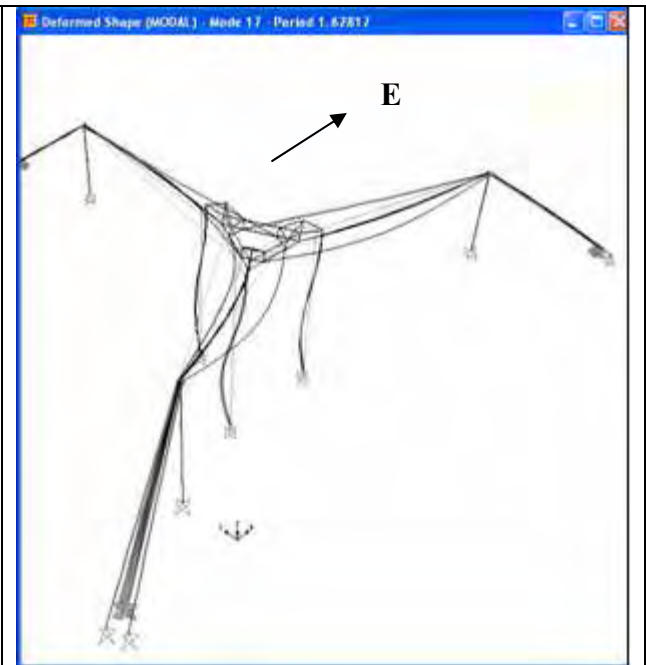


Figure 5.17. Table 5.6 id. B. Mode 17. Platform Rotation about East-West Axis.

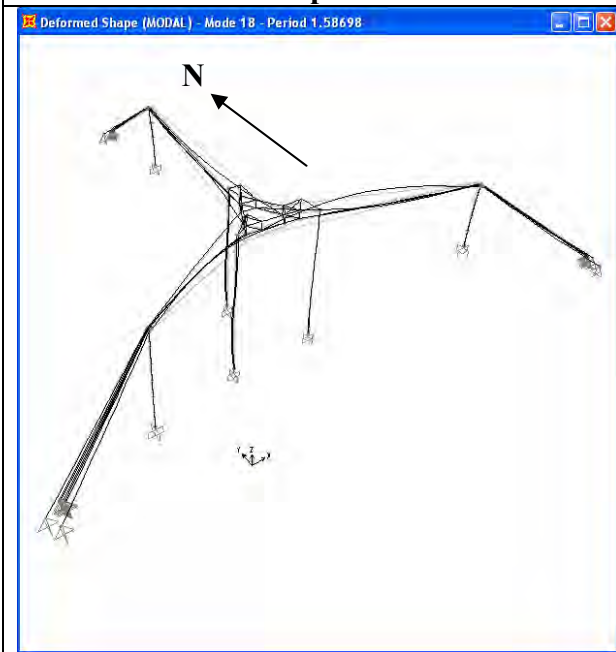


Figure 5.18. Table 5.6 id. C. Mode 18. Platform Rotation about North-South Axis.



Figure 5.19. Table 5.6 id. D. Mode 13. 1st Mode of Tower T8. This is a cantilever-type mode in the direction perpendicular to cable. Note that odd-numbered modes of towers are always normal to cables.



Figure 5.20. Table 5.6 id. E. Mode 15. 1st mode of Towers T4 and T12 – In Phase. Platform rotates about vertical axis.



Figure 5.21. Table 5.6 id. F. Mode 16. 1st mode of Towers T4 and T12 – Out of Phase. Note that since towers T4 and T12 are identical, their periods coincide.

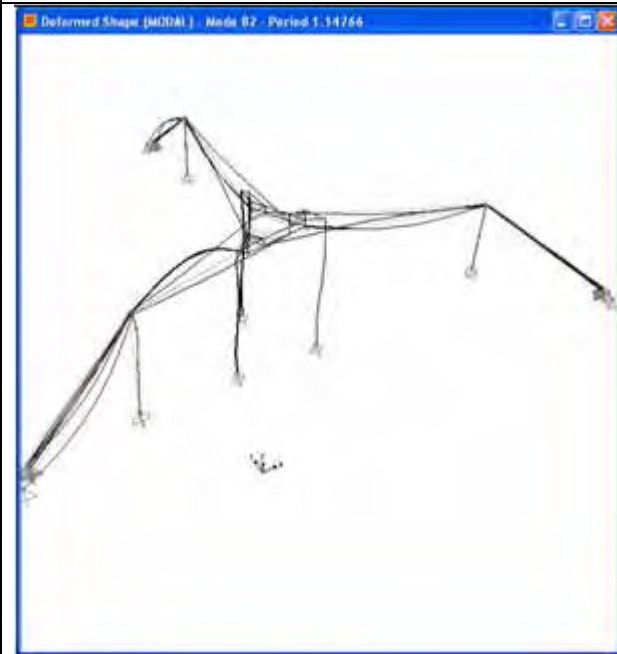


Figure 5.22. Table 5.6 id. G. Mode 82. 2nd mode of Tower T8. Note the similarity to the deformed shape of Figure 2.23. Note that even-numbered tower modes are always in the same direction as the cables.



Figure 5.23. Table 5.6 id. H. Mode 137. 2nd mode of towers T4 and T12 – In Phase.

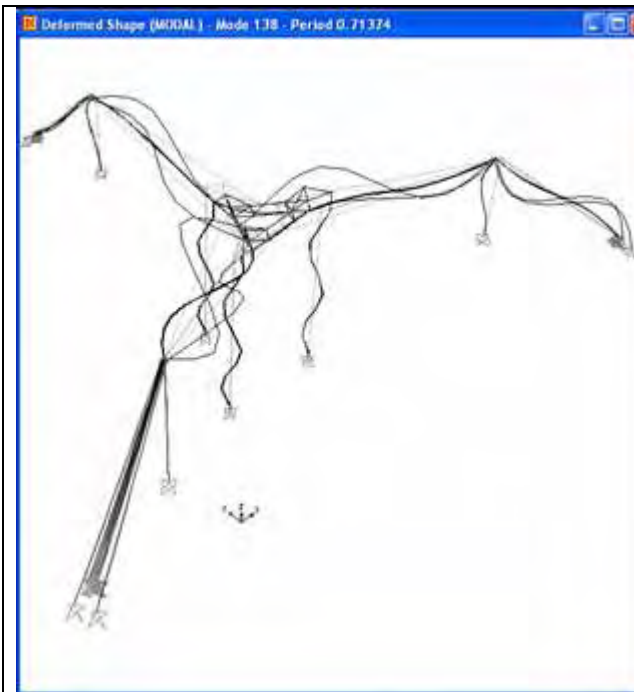


Figure 5.24. Table 5.6 id. I. Mode 138. 2nd mode of towers T4 and T12 – Out of Phase. Cradle Motion of Platform.

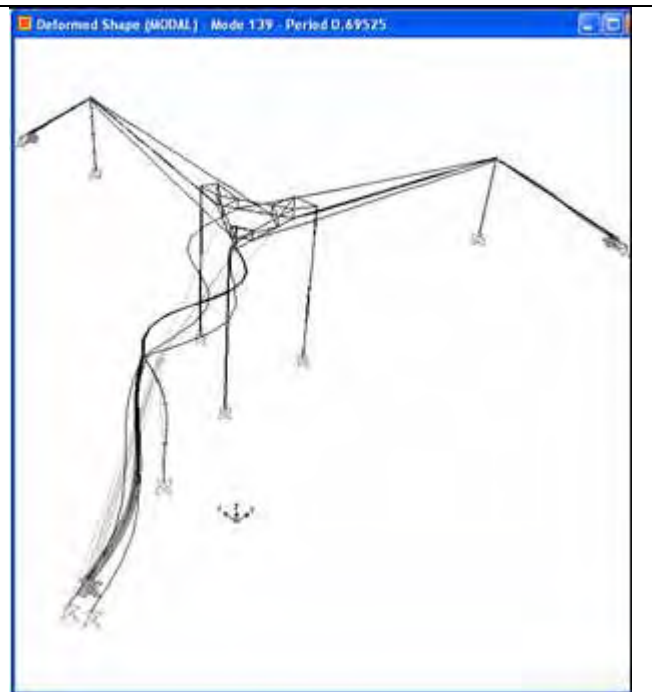


Figure 5.25. Table 5.6 id. J. Mode 139. 3rd mode of tower T8. Note that there is no interaction with the platform in this mode.



Figure 5.26. Table 5.6 id. K. Mode 258. 3rd mode of tower T4. Note that there is no interaction with the platform.



Figure 5.27. Table 5.6 id. L. Mode 260. 3rd mode of tower T12. Note that there is no interaction with the platform.



Figure 5.28. Table 5.6 id. M. Mode 259. 4th mode of tower T8. The period is almost identical to the 3rd modes of T4 and T12(id K, L) but they do not interact.



Figure 5.29. Table 5.6 id. N. Mode 385. 4th mode tower T4.



Figure 5.30. Table 5.6 id. O. Mode 410. 4th mode of tower T12. There is interaction with tower T4.



Figure 5.31. Table 5.6 id. P. Mode 423. 5th mode of tower T8.

5.3.2 Sensitivity Study: Modal Analysis Using $I_{cracked}$ for Towers – Model B

If during a seismic event the towers are flexed beyond the modulus of rupture (in tension) they will crack and the moment of inertia will be reduced. In this section a modal analysis is performed assuming that all the sections of all the towers have cracked. This sensitivity study will provide an understanding for the behavior of the towers at their most flexible state.

It will be assumed that the cruciform shaped cross section is modeled as a rectangle, as shown in Figure 5.32. In addition, it will be considered that the compression reinforcement does not contribute to the moment of inertia. Only the tension reinforcement is considered. It can be shown that the difference is less than 3%. The elastic modulus of concrete will be based on a strength of $f'c = 3,000$ psi (specified in the drawings). All these assumptions are conservative. The results are shown in Table 5.7 where 'h' is the depth of the section, and 'd' is the effective depth of the section measured to the centroid of the reinforcement. The remaining parameters used in Table 5.7 are defined in the next page.

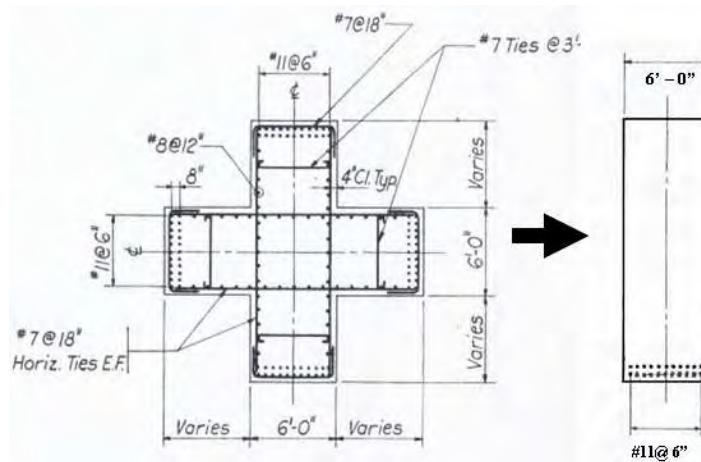


Figure 5.32. Idealization of cross section to determine $I_{cracked}$

Table 5.7. Calculations for $I_{cracked}$

SECTION	h [in]	d [in]	A_s [in ²]	B [1/in]	kd [in]	I_{cr} [ft ⁴]
TSEC1	108	97	17.16	0.466	18.37	53.2
TSEC2	156	145	17.16	0.466	22.89	124.9
TSEC3	216	205	34.32	0.233	37.87	478.9
TSEC4	288	277	34.32	0.233	44.65	907.2
TSEC5	360	349	34.32	0.233	50.60	1476.3
TSEC6	432	421	34.32	0.233	55.96	2187.8

Table 5.7 is based on the following information.

Elastic Modulus of Concrete: “Ec”

$$E_c = 57\sqrt{f'_c} = 57\sqrt{3000} = 3,122 \text{ ksi}$$

Elastic Modulus of Steel: “Es”

$$E_s = 29,000 \text{ ksi}$$

Ratio of Elastic Moduli: “n”

$$n = E_s/E_c = 29,000 \text{ ksi} / 3122 \text{ ksi} = 9.28 \approx 9 \text{ (Round off to nearest integer as recommended)}$$

Steel Area: “As”

Note that the steel area in the upper two tower segments is reduced by one half.

Parameter: “B”

$$B = b/(n \cdot A_s) \text{ where } b = 6 \text{ ft (constant width of the rectangular section)}$$

Distance to Neutral Axis of Section: “kd”

$$kd = \frac{\sqrt{2dB + 1} - 1}{B}$$

Cracked Moment of Inertia: “I_{cr}”

$$I_{cr} = b \cdot (kd)^3 / 3 + n \cdot A_s \cdot (d - kd)^2$$

A comparison of the cracked and the gross moments of inertia is shown in Table 5.8. Note that, in average, the moments of inertia are reduced to approximately 10% of their gross value, i.e., by one order of magnitude. Consequently, the flexural stiffness of the towers will also decrease by one order of magnitude. The tower periods should therefore increase by a factor of approximately $\sqrt{10} = 3.16$.

Table 5.8. Comparison of ‘cracked’ and ‘gross’ moments of inertia

SECTION	I _{cr} [ft ⁴]	I _{gross} [ft ⁴]	I _{cr} / I _{gross} [%]	Notes
TSEC1	53.2	419	12.7%	T4, T8 and T12
TSEC2	124.9	1225	10.2%	T4, T8 and T12
TSEC3	478.9	3132	15.3%	T4, T8 and T12
TSEC4	907.2	7236	12.5%	T4, T8 and T12
TSEC5	1476.3	13932	10.6%	T8 Only
TSEC6	2187.8	23868	9.2%	T8 Only

Equilibrium State Due to Dead Load Only – Model B Cracked

Table 5.9 compares the equilibrium states due to dead load for the ‘gross’ and ‘cracked’ towers. The preload temperatures that were input to the models are included in the first nine rows of the table and are exactly the same in both cases. The initial ‘z’ offset of the platform is also the same input for both cases. With respect to the output, the descent of the platform due to dead loads (‘platform UZ’) is exactly the same in both cases (11.0 ft). The displacements at the top of the towers (“UX T12 TOWER [in]”, etc) are all nearly equal to zero, which meets the criterion of verticality of the towers. Note the percentage error is not included as it is not appropriate for this comparison because the differences between the displacements are so close to zero, that the large resulting percentage errors would confuse rather than clarify. The displacement itself represents the error since it is the amount by which the top of the towers deviate from the zero-displacement target. The tensions in the cables are almost identical (less than 0.5% difference). Since there is practically no demand on the flexural capacity of the towers in this state (dead load only), all the results are nearly identical. The towers are simply providing an axial support for the cables.

Table 5.9. Comparison of equilibrium state between I_{gross} and $I_{cracked}$ – Model B

INPUT	Model B I_GROSS (With Tiedowns)	Model B I_CRACK (With Tiedowns)	% DIFF I_gross vs I_crack
TEMP MAIN [F]	0	0	0.0%
TEMP AUX [F]	-235	-235	0.0%
TEMP GUYMAIN T12 [F]	-505	-505	0.0%
TEMP GUYAUX T12 [F]	-540	-540	0.0%
TEMP GUYMAIN T8 [F]	-465	-465	0.0%
TEMP GUYAUX T8 [F]	-487.5	-487.5	0.0%
TEMP GUYMAIN T4 [F]	-515	-515	0.0%
TEMP GUYAUX T4 [F]	-520	-520	0.0%
TEMP TIEDOWNS [F]	-3300	-3300	0.0%
INITIAL Z OFFSET [ft]	10.872	10.872	0.0%
OUTPUT			
PLATFORM UZ [ft]	-11.0	-11.0	0.0%
UX T12 TOWER [in]	-0.00021	-0.00202	N/A
UY T12 TOWER [in]	0.01054	-0.10799	N/A
UX T8 TOWER [in]	-0.06977	-0.0014	N/A
UY T8 TOWER [in]	-0.04129	-0.00816	N/A
UX T4 TOWER [in]	0.0438	-0.06767	N/A
UY T4 TOWER [in]	-0.02948	0.00166	N/A
TENSION MAIN [kip] 480 k	496	497	0.2%
TENSION AUX [kip] 602 k	608	606	-0.3%
TENSION GUYMAIN T12 [kip] 514 k	498	497	-0.2%
TENSION GUYAUX T12 [kip] 727 k	665	667	0.3%
TENSION GUYMAIN T8 [kip] 503 k	456	456	0.0%
TENSION GUYAUX T8 [kip] 662 k	599	601	0.3%
TENSION GUYMAIN T4 [kip] 543 k	509	508	-0.2%
TENSION GUYAUX T4 [kip] 728 k	640	642	0.3%
TENSION TIEDOWN T12 [kip] 24 k	24.1	24.1	0.0%
TENSION TIEDOWN T8 [kip] 24 k	24.1	24.1	0.0%
TENSION TIEDOWN T4 [kip] 24 k	24.1	24.1	0.0%

Modal Analysis Results – $I_{cracked}$ – Model B

The results of the modal analysis using Model B with the reduced moments of inertia are shown in Table 5.10. The original results (using gross moment of inertia) are also included.

Table 5.10. Modal analysis results – $I_{cracked}$ – Model B

ID	Mode Description	I_{gross} (With Tiedowns)		$I_{cracked}$ (With Tiedowns)		% DIFF
		Mode Number	Period [sec]	Mode Number	Period [sec]	
A	Platform Vertical Displacement	14	2.146	18	2.177	1.4%
B	Platform Rotation about East-West Axis	17	1.628	22	1.624	-0.2%
C	Platform Rotation about North-South Axis	18	1.587	23	1.587	0.0%
D	1st Mode Tower T8	13	2.260	1	6.486	187.0%
E	1st Mode Towers T4 and T12 - In Phase (Platform rotates about vertical axis)	15	1.764	2	4.969	181.7%
F	1st Mode Towers T4 and T12 - Out of Phase	16	1.723	3	4.642	169.4%
G	2nd Mode Tower T8	82	1.148	4	3.603	213.9%
H	2nd Mode Towers T4 and T12 - In Phase	137	0.739	20	2.018	173.1%
I	2nd Mode Towers T4 and T12 - Out of Phase (Cradle Motion of Platform)	138	0.714	19	2.083	191.7%
J	3rd Mode Tower T8	139	0.695	17	2.305	231.7%
K	3rd Mode Tower T4	258	0.448	21	1.636	265.2%
L	3rd Mode Tower T12	260	0.444	21	1.636	268.5%
M	4th Mode Tower T8	259	0.447	88	1.147	156.6%
N	4th Mode Tower T4	385	0.326	149	0.675	107.1%
O	4th Mode Tower T12	410	0.321	149	0.675	110.3%
P	5th Mode Tower T8	423	0.303	119	0.895	195.4%
Q	1st Mode Auxiliary Cables	20	1.517	26	1.519	0.1%
R	1st Mode Main Cables	57	1.283	63	1.28	-0.2%
S	1st Mode T12 Auxiliary Backstays	83	1.146	89	1.145	-0.1%
T	1st Mode T8 Auxiliary Backstays	87	1.127	93	1.125	-0.2%
U	1st Mode T4 Auxiliary Backstays	32	1.381	38	1.38	-0.1%
V	1st Mode T12 Main Backstays	91	1.089	97	1.090	0.1%
W	1st Mode T8 Main Backstays	101	1.057	106	1.066	0.9%
X	1st Mode T4 Main Backstays	48	1.29	54	1.293	0.2%
Y	1st Mode Tiedowns	1	2.633	5	2.634	0.0%

Discussion of Modal Results – $I_{cracked}$

1. The first three modes (platform modes A, B, C) in Table 5.10 do not show a significant change with the reduction in tower stiffness. This result indicates that the vertical and rotational modes of the platform (modes A, B, C) are modes decoupled

from the towers and the backstays. It seems as if the towers were replaced by a fixed support, then modes A, B, C should still exist and have approximately the same natural periods. These platform modes seem to depend exclusively on the mass of the platform and the tension in the main, auxiliary, and tiedown cables. As long as there is some type of support (towers) that has sufficient rigidity to keep the platform suspended, these modes should appear and remain invariant.

2. As expected, all the natural periods of the towers increase significantly (modes D through P in Table 5.10) due to the increased flexibility. Note that the fundamental mode increases approximately by the predicted factor of 3.16. For example, the predicted fundamental period for tower T8 (mode D) due to cracked properties is $2.260 \times 3.16 = 7.1$ sec which compares reasonably well with the 6.5 sec period calculated by SAP (9% difference). The factor of 3.16 is calculated based on the

relationship $T = 2\pi\sqrt{\frac{m}{k}}$ where “T” represents the fundamental period, “m” represents mass and “k” the stiffness of the system (a concrete tower in this case). If the stiffness decreases by a factor of ten, the period is modified to $T_{\text{new}} = 2\pi\sqrt{\frac{m}{k/10}} = 2\pi\sqrt{\frac{10m}{k}} = (\sqrt{10})2\pi\sqrt{\frac{m}{k}} = 3.16T$.

3. The independent cable modes (Q through Y in Table 5.10) are essentially unchanged (less than 1.0% difference) since the tensions in the cables (and length) remain unchanged.
4. This sensitivity study assumes that all tower segments have cracked from the onset of the seismic excitation. A fully nonlinear time-history analysis (i.e., one that accounts for material nonlinearities) would be required to modify the stiffness of the tower as each segment cracks during a seismic event. This is beyond the scope of this study.

5.3.3 Sensitivity Study: Modal Analysis Using $I_{\text{effective}}$ for Towers

The previous study provided the dynamic properties of a model with a lower-bound stiffness, by assuming that the three towers have a cracked moment of inertia along their entire lengths. In reality, however, I_{cracked} applies only at the locations of the cracks. Those zones which have not cracked are still governed by I_{gross} . In this section, a more realistic value for the reduced moment of inertia is calculated per section 9.5.2.3 of the ACI 318-02 Reinforced Concrete Code. The code defines an effective moment of inertia, $I_{\text{effective}}$, which provides an intermediate value between I_{cracked} and I_{gross} that is supposed to be more representative of the overall moment of inertia of the towers after cracking. The code equation for $I_{\text{effective}}$ is:

$$I_{\text{effective}} = \left(\frac{M_{cr}}{M_a} \right)^3 I_{\text{gross}} + \left[1 - \left(\frac{M_{cr}}{M_a} \right)^3 \right] I_{\text{cracked}} \leq I_{\text{gross}}, \text{ where,}$$

- $M_{cr} = \frac{f_r I_{\text{gross}}}{y_t}$ (cracking moment, [in-lb])
- $f_r = 7.5\sqrt{f'_c} = 7.5\sqrt{3000} = 410.8$ psi (rupture modulus for normal weight concrete)
- y_t = distance from centroidal axis of gross section, neglecting reinforcement, to extreme fiber in tension, [in]
- M_a = maximum service moment in member, [in-lb]. These values represent the moment at first yield as it will be shown in Chapter 8.

As shown in Table 5.11, the difference between $I_{\text{eff}}/I_{\text{gross}}$ and $I_{\text{cr}}/I_{\text{gross}}$ (last column of the table), is minimal (3.3% maximum difference). Therefore, it is deemed unnecessary to perform an additional modal analysis with the effective moment of inertia.

Table 5.11. Calculation of $I_{\text{effective}}$ and comparison with I_{cracked}

SECTION	lcr [ft^4]	I_gross [ft^4]	I_gross [in^4]	h [ft]	yt [in]	Mcr [kip-in]	Ma [kip-in]	I_eff [ft^4]	% Diff lcr vs. I_eff	I_eff / I_gross [%]	I_cr / I_gross [%]	Difference Between Ratios
TSEC1	53.2	419	8.69E+06	9	54	6.61E+04	2.33E+05	61.5	13.5%	14.7%	12.7%	2.0%
TSEC2	124.9	1225	2.54E+07	13	78	1.34E+05	4.01E+05	165.6	24.6%	13.5%	10.2%	3.3%
TSEC3	478.9	3132	6.49E+07	18	108	2.47E+05	8.29E+05	549.1	12.8%	17.5%	15.3%	2.2%
TSEC4	907.2	7236	1.50E+08	24	144	4.28E+05	1.42E+06	1082.0	16.2%	15.0%	12.5%	2.4%
TSEC5	1476.3	13932	2.89E+08	30	180	6.59E+05	2.14E+06	1838.9	19.7%	13.2%	10.6%	2.6%
TSEC6	2187.8	23868	4.95E+08	36	216	9.41E+05	3.22E+06	2730.2	19.9%	11.4%	9.2%	2.3%

5.3.4 Sensitivity Study: Isolation of Platform Modes

This study was motivated by the sensitivity study using cracked tower properties (section 5.3.2). Although the flexibility of the towers increased by a factor of 10, the platform periods remained essentially unchanged (1% difference). This result indicates that, as long as there is some type of axial support (towers) that has sufficient rigidity to keep the platform suspended, the platform modes should appear and remain relatively invariant.

This sensitivity study will address the hypothetical case of isolating the platform from the towers and backstays by assigning pinned restraints at the tower saddles, as shown in Figure 5.33. All other input parameters remain unchanged. The results will help to clarify and identify the different types of platform modes of the Arecibo Observatory, especially with respect to uncovering platform modes which could be hidden by interactions with the towers.

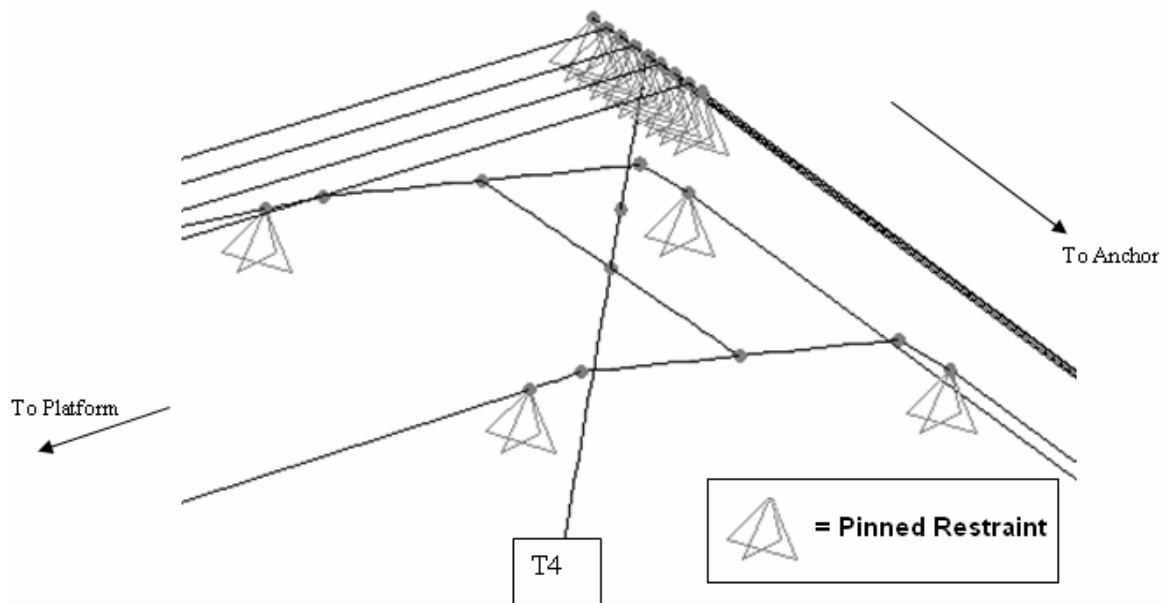


Figure 5.33. Pinned restraints at saddles to isolate the platform modes

Equilibrium State due to Dead Load – Isolation of Platform Modes

Table 5.12 compares the equilibrium states due to dead load for Model B and for the “pinned-saddles” model. The preload temperatures that were input to the models are included in the first nine rows of the table. Note that in the “pinned-saddles” model, the backstay temperatures do not apply since the platform has been isolated from the towers (and their respective backstays). The initial ‘z’ offset of the platform is also the same input for both cases. With respect to the output, the descent of the platform due to dead loads (‘platform UZ’) is exactly the same in both cases (11.0 ft). The displacements at the top of the towers for the “pinned-saddles” model are all equal to exactly zero due to the pinned restraint. Note the percentage error for the tower displacements is not included as it is not appropriate for this comparison. The tensions developed in the main and auxiliary cables are essentially identical. These results show that the “pinned-saddles” model is responding appropriately and that results are reliable.

Table 5.12. Equilibrium displacements and cable tensions: isolation of platform modes

INPUT	MODEL B (With Tiedowns)	<u>PINNED SADDLES</u> MODEL B (With Tiedowns)	% DIFF	
TEMP MAIN [F]	0	0	0.0%	
TEMP AUX [F]	-235	-235	0.0%	
TEMP GUYMAIN T12 [F]	-505	N/A	N/A	
TEMP GUYAUX T12 [F]	-540	N/A	N/A	
TEMP GUYMAIN T8 [F]	-465	N/A	N/A	
TEMP GUYAUX T8 [F]	-487.5	N/A	N/A	
TEMP GUYMAIN T4 [F]	-515	N/A	N/A	
TEMP GUYAUX T4 [F]	-520	N/A	N/A	
TEMP TIEDOWNS [F]	-3300	-3300	0.0%	
INITIAL Z OFFSET [ft]	10.872	10.872	0.0%	
OUTPUT				
PLATFORM UZ [ft]	-11.0	-11.0	0.0%	
UX T12 TOWER [in]	-0.00021	0	N/A	
UY T12 TOWER [in]	0.01054	0	N/A	
UX T8 TOWER [in]	-0.06977	0	N/A	
UY T8 TOWER [in]	-0.04129	0	N/A	
UX T4 TOWER [in]	0.0438	0	N/A	
UY T4 TOWER [in]	-0.02948	0	N/A	
TENSION MAIN [kip]	480 k	496	496	0.0%
TENSION AUX [kip]	602 k	608	609	0.2%

Modal Analysis Comparison – Isolation of Platform Modes

The results of the modal analysis for modes A, B, C and three cable modes are shown in Table 5.13. The original results are also included. The results are almost equal as expected which confirms the very low sensitivity of the modes A, B, C with respect to variations in the tower properties.

Table 5.13. Modal analysis comparison – isolation of platform modes

ID	Mode Description	MODEL B (With Tiedowns)		PINNED SADDLES MODEL B (With Tiedowns)		% DIFF
		Mode Number	Period [sec]	Mode Number	Period [sec]	
A	Platform Vertical Displacement	14	2.146	13	2.022	-5.8%
B	Platform Rotation about East-West Axis	17	1.628	15	1.532	-5.9%
C	Platform Rotation about North-South Axis	18	1.587	16	1.532	-3.5%
Q	1st Mode Auxiliary Cables	20	1.517	26	1.516	-0.1%
R	1st Mode Main Cables	57	1.283	63	1.271	-0.9%
Y	1st Mode Tiedowns	1	2.633	1	2.637	0.2%

Additional Modal Results - Isolation of Platform Modes

The results of the finite element analysis of the “pinned-saddles” model, reveal additional information. In addition to modes B and C (rotations about the horizontal axes), the platform also rotates about a vertical axis as shown in Figure 5.34.

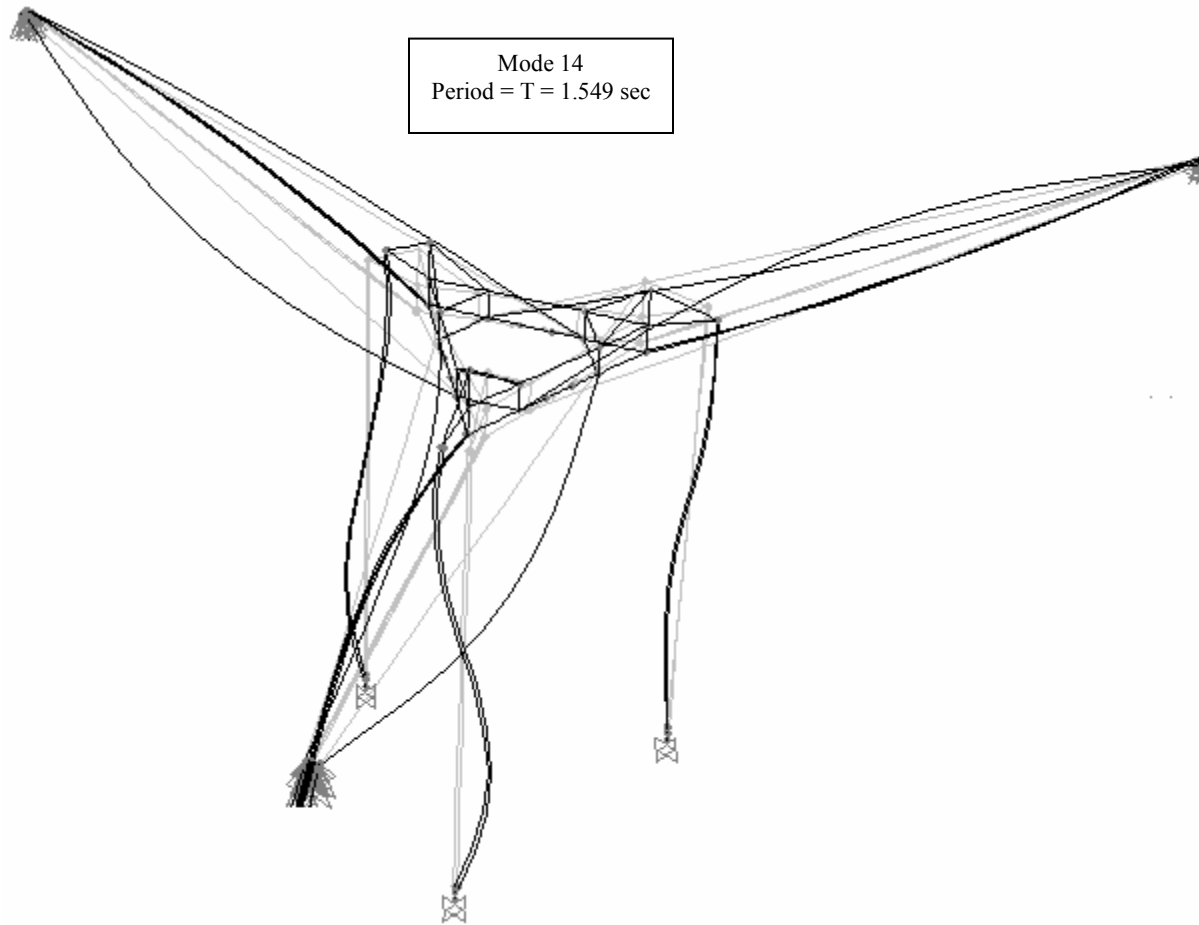


Figure 5.34. Platform rotation about vertical axis – isolation of platform modes

This mode was originally missed as a platform mode and was not included in Table 5.10 nor in previous similar tables. It was confounded in the interaction with the 1st mode of towers T4 and T12 (in-phase – see Figure 5.20) which also creates rotation of the platform about a vertical axis. This mode is first mentioned in Figure 5.8 as an interaction mode.

All the platform rotation modes (rotation about E-W axis, rotation about N-S axis, and rotation about vertical axis) reappear as the different cables in the system and their modal shape take turns governing the response of the system. This response has been summarized in Table 5.14. The modal shapes are all similar to previous figures so additional ones are not included.

Table 5.14. Activation of platform modes by cable type

Governing Condition	Period of Platform Rotation About E-W Axis [sec]	Period of Platform Rotation About N-S Axis [sec]	Period of Platform Rotation About Vertical Axis [sec]
1st Mode Auxiliary Cables *	Mode 15, 1.532 sec Mode 28, 1.404 sec	Mode 16, 1.532 sec Mode 27, 1.403 sec	Mode 14, 1.549 sec Mode 25, 1.499 sec
1st Mode Main Cables	Mode 76, 1.214 sec	Mode 77, 1.214 sec	Mode 78, 1.211 sec
2nd Mode Auxiliary Cables	Mode 133, 0.754 sec	Mode 134, 0.754 sec	Not Observed
2nd Mode Main Cables	Mode 183, 0.630 sec	Mode 184, 0.630 sec	Mode 182, 0.631 sec

* Two auxiliary cable modes (in 1st mode) activated the platform rotations.

In addition, a ‘cradle’ type vibration mode was identified as shown in Figures 5.35 and 5.36 (modes 119 and 120, respectively). These modes seem to be governed by the interaction of the second mode of both the main and the auxiliary cables. Note that the tiedowns are vibrating in their third mode shape. The ‘cradle’ modes were originally confounded with mode “I” (shown in Figure 5.24) due to interaction effects with the towers.

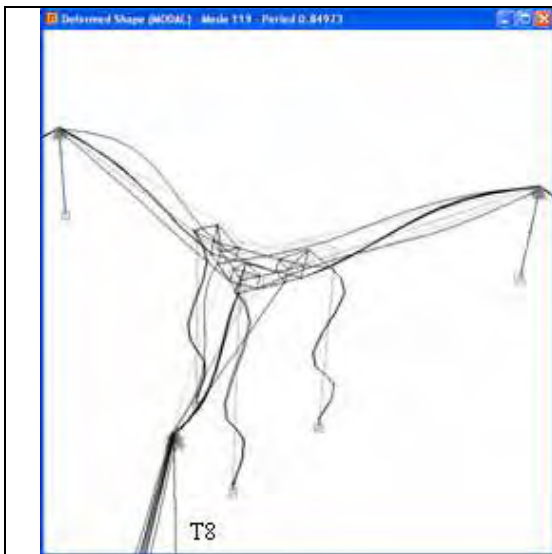


Figure 5.35. ‘Cradle’ type vibration mode. Motion towards T8. Isolation of platform modes

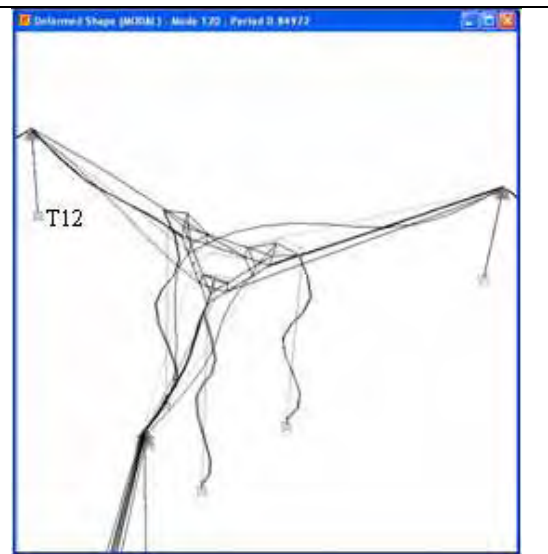


Figure 5.36. ‘Cradle’ type vibration mode. Motion towards T12. Isolation of platform modes

5.3.5 Sensitivity Study: Effect of Bridge and Service Cables

The effect of service cables was briefly studied in Section 5.2.5. In that case the three service cables were pinned at their intersection just above the platform. In this study the bridge and the cable-car cable are explicitly modeled. The necessary dimensions and cable tensions were obtained from drawings supplied by the offices of the Arecibo Observatory. The additions to the model are shown in Figure 5.37.

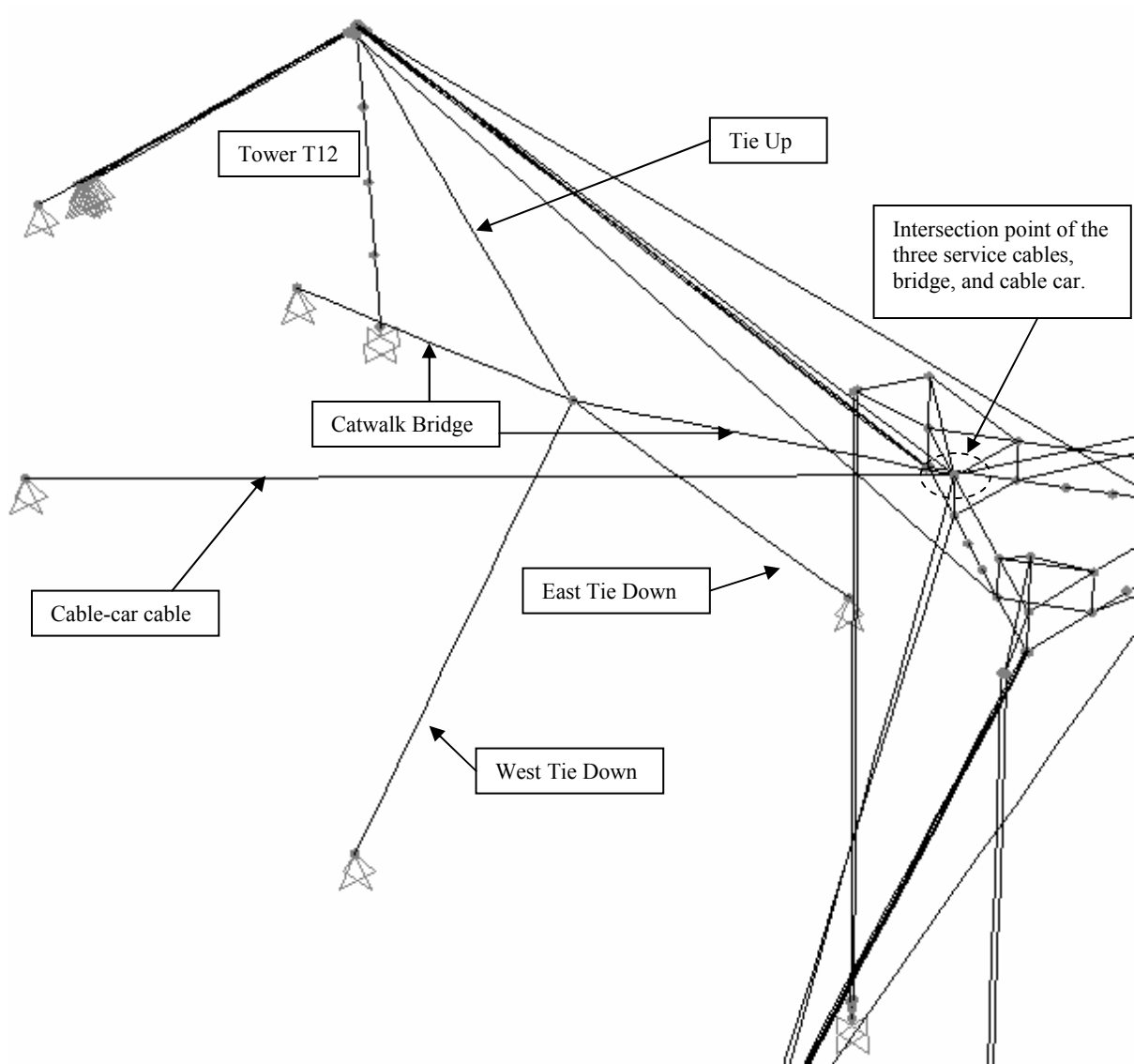


Figure 5.37. Model B including bridge, cable-car cable, and three service cables

The service cables were attached at the top of each tower by adding an additional frame element. Also, as shown in Figure 5.38, an additional joint and frame element were incorporated in tower T12 to include the attachment point for the tie-up cable which supports the catwalk bridge at approximately midspan (see Figure 5.37). The new joint is located 15 inches below the auxiliary saddle. All these modifications are shown in Figure 5.38.

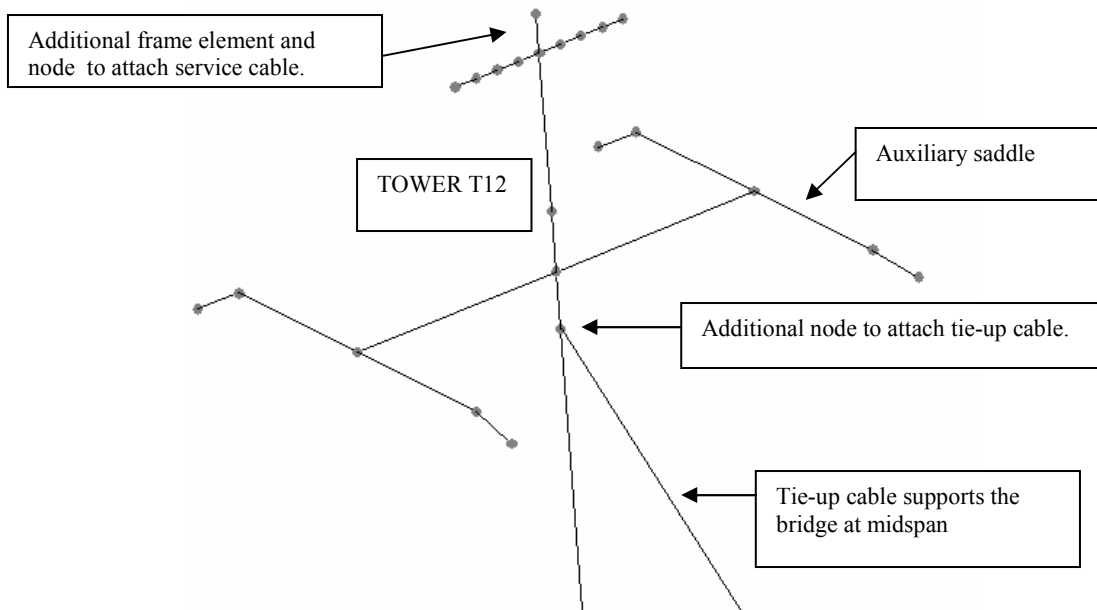


Figure 5.38. Detail at top of tower T12 to include service and tie-up cable (most cables not shown for clarity)

The tensions in each cable are included in Table 5.15.

Table 5.15. Tension values in the cables

Cable	Tension [kip]
Catwalk Bridge (Tower T12 side)	$80 \times 2 = 160$
Catwalk Bridge (Platform side)	$114 \times 2 = 228$
Tie up to T12	69
West Tie Down	30
East Tie Down	6
T12 Service Cable	224
T8 Service Cable	395
T4 Service Cable	345
Cable-Car Cable	15

Material Properties

Except for the 2-inch diameter bridge cables, the material properties used for the cables are assigned the name [STEELCABLE] and are defined as follows:

Cable specific weight = $\gamma = 490 \text{ lb/ft}^3$ [default value for steel]

Cable mass density = (cable unit weight)/g [default value]

E = 24E6 psi [wire “strand” cable]

Poisson’s ratio = 0.3

A second cable material [STEELCAB2] is defined for the pair of 2-inch bridge cables. A single cable of twice the effective area of the 2-inch diameter cables will be used. The mass of the entire catwalk bridge (including the mass of the cables) will be included in this equivalent cable. This approach (lumping the bridge mass on one cable) is deemed reasonable as the desired objective is to observe the influence of the bridge on the overall structure rather than observing in detail the bridge itself. As specified in the drawings, the weight of the catwalk bridge is 170 lb/ft. It is necessary to calculate an equivalent specific weight and mass density for the material that includes the weight of the bridge.

Let:

γ_{eq} = equivalent specific weight [lb/ft³] to be solved for, and

w = weight per unit length specified in drawings [lb/in] = 170 lb/ft * 1 ft/12 in = 14.16 lb/in

Since $w = \left(\frac{\gamma_{eq}}{12^3} \right) (A_{eff})$, rearrange to get $\gamma_{eq} = \frac{12^3 w}{A_{eff}}$ where the effective area of a single equivalent cable is

$$A_{eff} = 2 \frac{0.77 \pi D_{no\ min\ al}^2}{4} = 2 \frac{0.77 \pi 2^2}{4} = 4.84 \text{ in}^2$$

Substituting, the equivalent specific weight is

$$\gamma_{eq} = \frac{12^3 (14.16)}{4.84} = \underline{5055 \text{ lb/ft}^3}$$

And the equivalent mass density is

$$\rho_{eq} = \gamma_{eq}/g = 5055 \text{ lb/ft}^3 / 32.2 \text{ ft/s}^2 = \underline{157 \text{ lb.s}^2/\text{ft}^4}$$

Table 5.16 summarizes the section properties of all the cables. Once the materials are defined, the only section-property input required to SAP2000 is the effective area. The weight per unit length is shown in the table for reference since SAP2000 automatically calculates it using the specific weight assigned as a material property of the cables.

Table 5.16. Section properties of cables

Section Name used in SAP2000	Nominal Diameter [in]	Effective Area [in²]	Weight per Unit Length [lb/in]	Material
CATWLK	2.0	2.42	14.16	STEELCAB2
CATTYUP	2.125	2.73	0.77	STEELCAB
CATTYDN	1.875	2.13	0.60	STEELCAB
T12SERV	1.875	2.13	0.60	STEELCAB
T8SERV	3.25	6.38	1.81	STEELCAB
T4SERV	3.0	5.44	1.54	STEELCAB
CARCAB	1.875	2.13	0.60	STEELCAB

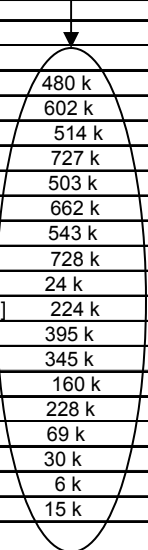
Equilibrium State Under Dead Load Only – Includes Catwalk Bridge

Five iterations were carried out using the non-linear p-delta analysis option of SAP2000 to achieve the equilibrium state under dead-load only. The results are shown in Table 5.17. As it was the case in the first sensitivity study using service cables (see Section 5.2.4), the towers displacements at the top do not converge to zero due to the off-radial component of tension in the service cables. The initial z-offsets for the tie-up and for the intersection of the service cables were changed in the fourth iteration and reasonable convergence was achieved.

Table 5.17. Iterations on Model B with bridge to achieve equilibrium under dead load

INPUT	Model B w. Serv.Cab w. Catwalk w. CableCar TEMP1	Model B w. Serv.Cab w. Catwalk w. CableCar TEMP2	Model B w. Serv.Cab w. Catwalk w. CableCar TEMP3	Model B w. Serv.Cab w. Catwalk w. CableCar TEMP4	Model B w. Serv.Cab w. Catwalk w. CableCar TEMP5
TEMP MAIN [F]	0	0	0	0	0
TEMP AUX [F]	-240	-240	-240	-240	-240
TEMP GUYMAIN T12 [F]	-520	-520	-535	-535	-535
TEMP GUYAUX T12 [F]	-590	-590	-605	-605	-605
TEMP GUYMAIN T8 [F]	-495	-495	-510	-510	-510
TEMP GUYAUX T8 [F]	-530	-530	-545	-545	-545
TEMP GUYMAIN T4 [F]	-520	-520	-535	-535	-535
TEMP GUYAUX T4 [F]	-580	-580	-595	-595	-595
TEMP TIEDOWNS [F]	-3300	-3400	-3420	-3390	-3380
TEMP SERV CABL T12 [F]	-660	-600	-620	-620	-650
TEMP SERV CABL T8 [F]	-425	-300	-320	-320	-320
TEMP SERV CABL T4 [F]	-420	-270	-260	-260	-220
TEMP CATWK (T12) [F]	-1000	-500	-800	-800	-700
TEMP CATWK (Plat) [F]	-500	-300	-200	-200	-200
TEMP CAT TyUp [F]	-500	-500	-400	-400	-350
TEMP CAT TyDn W [F]	-300	-400	-450	-450	-450
TEMP CAT TyDn E [F]	-300	-200	-450	-450	-450
TEMP CarCable [F]	-500	-400	-375	-375	-325
Platform INITIAL Z OFFSET [ft]	11.0	11.0	11.0	11.0	11.0
Y-plat INITIAL Z OFFSET [ft]	12.0	12.0	12.0	4.0	4.0
Y-MidSpan INITIAL Z OFFSET [ft]	5.0	5.0	5.0	1.0	1.0
OUTPUT					
PLATFORM UZ [ft]	-10.8	-11.4	-11.4	-11.3	-11.3
Y-Plat UZ [ft]	-5.4	-3.9	-4.1	-2.9	-2.2
Y-MidSpan UZ [ft]	-0.8	-0.7	-1.3	-1.2	-1.2
UX T12 TOWER [in]	-0.8132	-1.0966	-0.8899	-0.859	-0.8752
UY T12 TOWER [in]	-0.0394	-0.93831	-0.4063	-0.1955	-0.2087
UX T8 TOWER [in]	-0.9344	-0.5954	-0.8419	-0.8852	-0.9113
UY T8 TOWER [in]	3.1538	2.1009	2.1505	2.1563	1.9866
UX T4 TOWER [in]	-0.7980	-0.7764	-0.5306	-0.5171	-0.3974
UY T4 TOWER [in]	2.1174	1.5283	1.4506	1.4766	1.3265
TENSION MAIN [kip]	480 k	476	494	501	499
TENSION AUX [kip]	602 k	582	608	613	612
TENSION GUYMAIN T12 [kip]	514 k	514	535	536	533
TENSION GUYAUX T12 [kip]	727 k	730	754	759	753
TENSION GUYMAIN T8 [kip]	503 k	510	504	511	507
TENSION GUYAUX T8 [kip]	662 k	683	667	679	675
TENSION GUYMAIN T4 [kip]	543 k	549	543	552	549
TENSION GUYAUX T4 [kip]	728 k	756	745	758	754
TENSION TIEDOWNS [kip]	24 k	10.8	21.9	25.4	24.5
TENSION SERV CAB T12 [kip]	224 k	245	213	216	189
TENSION SERV CAB T8 [kip]	395 k	522	356	382	385
TENSION SERV CAB T4 [kip]	345 k	513	350	369	378
TENSION CATWK (T12) [kip]	160 k	265	163	123	144
TENSION CATWK (Plat) [kip]	228 k	328	46	206	231
TENSION CAT TyUp [kip]	69 k	63	133	90	96
TENSION CAT TyDn W [kip]	30 k	27	48	29	36
TENSION CAT TyDn E [kip]	6 k	12	14	8	13
TENSION CarCable [kip]	15 k	34	37	18	27

Target Tensions



Modal Analysis Results – Model B with Catwalk Bridge

The results of the modal analysis (in terms of natural periods) are shown in Table 5.18. The original results (without bridge and service cables) are also included. It can be observed that the results are almost identical. This was expected since the catwalk bridge assembly is decoupled from the platform. It is independently supported by the three service cables. In addition, the mass of the catwalk bridge is much smaller (by a factor of 14) than the platform mass so it plays a minor role in the dynamic response of the observatory. The results of this sensitivity study show that the catwalk bridge assembly may be safely neglected in determining the dynamic response. An additional sensitivity study that includes seismic loading will be performed in Chapter 6 to confirm that the tower bending moments are also insensitive to the presence of the bridge in the model.

Table 5.18. Modal results for Model B including catwalk bridge

MODE SHAPES AND PERIODS	ORIGINAL MODEL B Period [sec] (NO Service Cables)	MODEL B w. Service Cables w. Catwalk Bridge w. Cable-car Period [sec]	Percent Difference [%]
[A] Platform vertical displacement	2.146	2.122	-1.1%
[B] Platform rotation about East-West axis	1.628	1.618	-0.6%
[C] Platform rotation about North-South axis	1.587	1.582	-0.3%
[D] 1st Mode Tower T8	2.260	2.268	0.4%
[E] 1st Mode Towers T4 and T12 (in phase)	1.764	1.753	-0.6%
[F] 1st Mode Towers T4 and T12 (out of phase)	1.723	1.717	-0.3%

5.3.6 Conclusions on Modal Analysis of Model B (Uniform Platform with Tiedowns)

1. There are three different types of modes in the system. These are:
 - a. **PLATFORM MODES.** Five different modes exist as follows:
 - i. Vertical motion (up and down)
 - ii. Rotation about an E-W centroidal axis (Figure 5.39)
 - iii. Rotation about a N-S centroidal axis (Figure 5.39)
 - iv. Rotation about a vertical centroidal axis (Figure 5.39)
 - v. “Cradle” motion. This mode is similar to the rotation about the N-S or E-W centroidal axis, except that rotation takes place about an offset axes (Figure 5.40) so the resulting rotations are shallower.

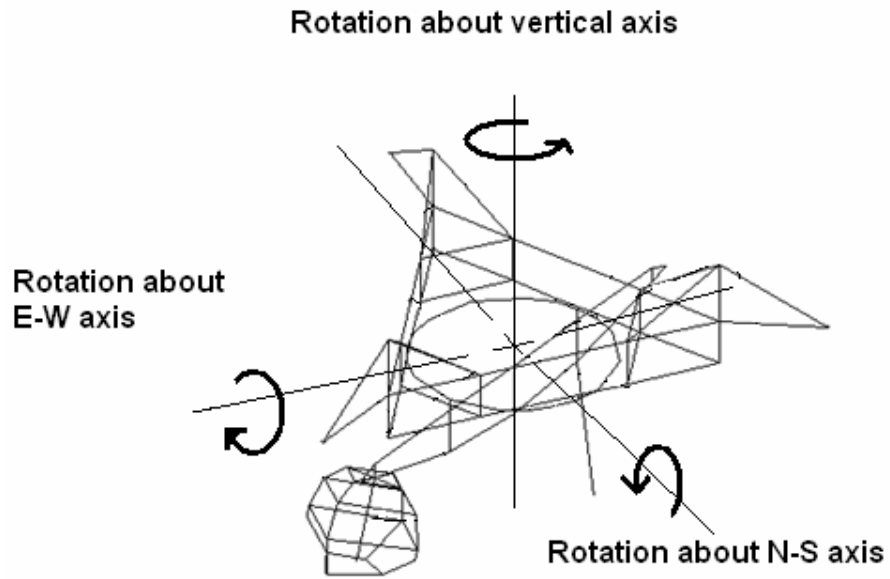


Figure 5.39. Schematic of platform rotation modes about the centroidal axes

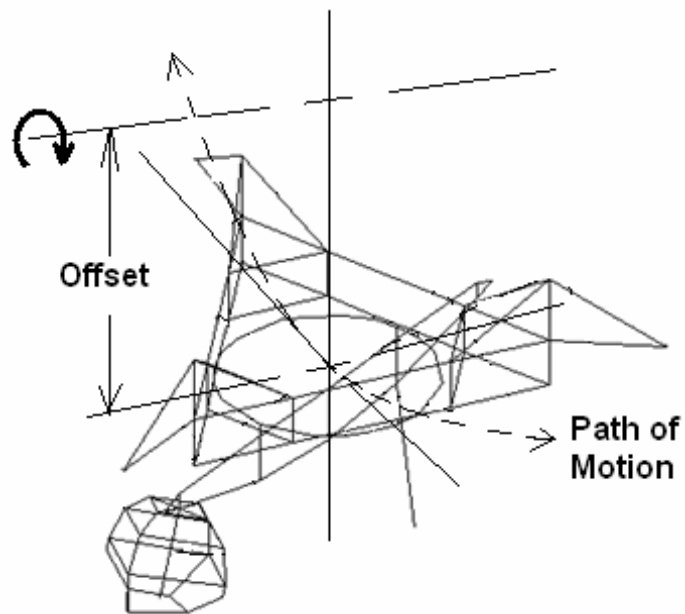


Figure 5.40. Schematic of platform "cradle" mode

b. **TOWER MODES.** The towers are the most massive members in the system and they exhibit flexural as well as axial modes. The odd-numbered flexural modes act perpendicular to the cables while the even-numbered modes are in the same direction as the cables. The first four modes of tower T8 are shown in Figure 5.41. Axial modes occur at very low periods (0.1 sec or lower). The axial modes consist of vertical stretching and contraction.

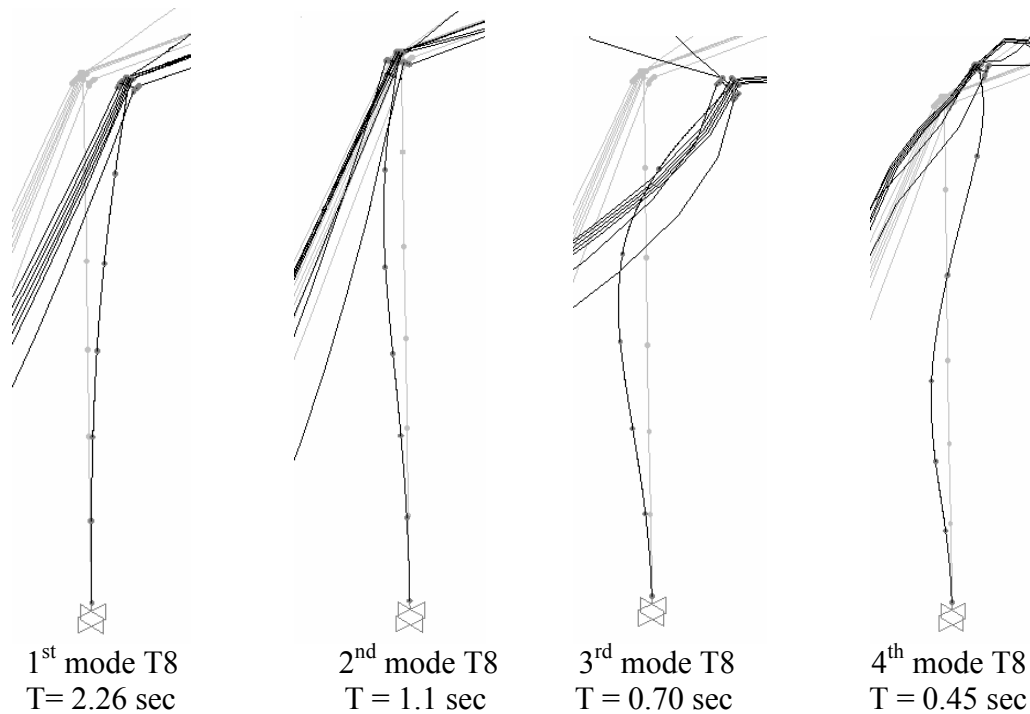


Figure 5.41. First four flexural modes of tower T8

c. **CABLE MODES.** These are the most numerous modes in the system. The platform and towers are so massive that, except for interaction modes, most cable modes are basically independent cable modes, that is, in most modes the cables tend to vibrate as if they were rigidly supported at their ends.

2. Very numerous interaction modes are observed. Interactions take place as the periods of the three different types of modes converge. One of the strongest interaction

modes seems to be the convergence of the first modes of the towers, especially T4 and T12, with the platform rotation modes.

3. When it is considered that the concrete of the towers is cracked (by reducing the moment of inertia), the flexibility of the towers is increased by a factor of ten. This results in an increase in the fundamental period of the towers by a factor of approximately 3.16 ($\approx \sqrt{10}$).
4. The effect of the presence of the catwalk bridge, the service cables and the cable-car cable is negligible in the overall natural response of the observatory. This is due to the fact that these are light-mass systems decoupled from the platform. They may be safely neglected from the analysis. Nevertheless, a follow-up sensitivity study will be carried out with applied seismic loading to confirm that there is no significant impact in the bending moments of the towers.

5.4 Modal Analysis of Model C (Distributed Platform, With Tiedowns)

Chapter 4 contains the details of this model, including the 50 kip redistribution of weight performed to balance the platform.

5.4.1 Comparison of Results: Calculated mass vs. 50 kip redistribution

A modal analysis of the models with calculated mass and with the 50 kip weight redistribution was performed in SAP2000. The natural periods of both models are shown in Table 5.19. As it can be observed, there is less than 3% difference between the two cases which may be considered small. Therefore, the 50-kip redistributed case will be used from this point onward.

Table 5.19. Comparison of modal results: calculated mass vs. 50 kip redistribution

ID	Mode Description	Model C Calculated Mass		Model C 50 kip Redistribution		% DIFF
		Mode Number	Period [sec]	Mode Number	Period [sec]	
A	Platform Vertical Displacement	10	2.181	22	2.141	1.9%
B	Platform Rotation about East-West Axis	31	1.506	31	1.53	-1.6%
C	Platform Rotation about North-South Axis	18	1.618	30	1.578	2.5%
D	1st Mode Tower T8	9	2.263	9	2.264	0.0%
E	1st Mode Towers T4 and T12 - In Phase (Platform rotates about vertical axis)	15	1.797	23	1.768	1.6%
F	1st Mode Towers T4 and T12 - Out of Phase	16	1.713	24	1.716	-0.2%

5.4.2 Comparison of Results: Models A, B, and C

The natural periods of the modal analysis for the three models A, B and C are shown in Table 5.20. The periods of the platform modes (mode id's. A, B, C) are ~50% lower for models B and C than for Model A due to the tiedowns which add stiffness to the platform.

The tower modes, on the other hand, are essentially equal from one model to another. The largest difference is in the 2nd mode of tower T8 (mode id. G) which shows a 5.5% difference. This mode generates platform rotation about a N-S axis, which is dependent on the presence of tiedown cables, as well as dependent on the weight distribution in the platform. In model C, the rotation is of the 'cradle' type discussed previously.

The periods of the independent cable modes are essentially equal in all models except for the tiedown cables. The tiedowns exhibit a different response in Model C due to the Gregorian dome unbalance in the platform. The T8 tiedown is almost slack so its period is very high. On the other hand the T4 and T12 tiedowns are much tighter to counterbalance the weight of the Gregorian dome so their periods are lower.

Table 5.20. Comparison of natural periods: Models A, B, C

ID	Mode Description	Model A (No Tiedowns)		Model B (With Tiedowns)		Model C (With Tiedowns)		Max % Diff.
		Mode Number	Period [sec]	Mode Number	Period [sec]	Mode Number	Period [sec]	
A	Platform Vertical Displacement	1	4.683	14	2.146	22	2.141	-54.3%
B	Platform Rotation about East-West Axis	2	3.529	17	1.628	31	1.530	-56.6%
C	Platform Rotation about North-South Axis	3	3.525	18	1.587	30	1.578	-55.2%
D	1st Mode Tower T8	4	2.264	13	2.260	9	2.264	0.2%
E	1st Mode Towers T4 and T12 - In Phase (Platform rotates about vertical axis)	5	1.788	15	1.764	23	1.768	-1.3%
F	1st Mode Towers T4 and T12 - Out of Phase	6	1.722	16	1.723	24	1.716	-0.4%
G	2nd Mode Tower T8	68	1.100	82	1.148	116	1.085	-5.5%
H	2nd Mode Towers T4 and T12 - In Phase	101	0.752	137	0.739	153	0.747	-1.7%
I	2nd Mode Towers T4 and T12 - Out of Phase (Cradle Motion of Platform)	102	0.733	138	0.714	162	0.727	-2.6%
J	3rd Mode Tower T8	107	0.698	139	0.695	163	0.695	-0.4%
K	3rd Mode Tower T4	186	0.451	258	0.448	264	0.448	-0.7%
L	3rd Mode Tower T12	188	0.447	260	0.444	265	0.444	-0.7%
M	4th Mode Tower T8	187	0.450	259	0.447	263	0.448	-0.7%
N	4th Mode Tower T4	301	0.327	385	0.326	378	0.327	-0.3%
O	4th Mode Tower T12	302	0.322	410	0.321	403	0.321	-0.3%
P	5th Mode Tower T8	315	0.305	423	0.303	424	0.303	-0.7%
Q	1st Mode Auxiliary Cables	11	1.529	20	1.517	32	1.519	-0.8%
R	1st Mode Main Cables	35	1.284	57	1.283	62	1.284	-0.1%
S	1st Mode T12 Auxiliary Backstays	61	1.181	83	1.146	91	1.146	-3.0%
T	1st Mode T8 Auxiliary Backstays	65	1.151	87	1.127	95	1.126	-2.2%
U	1st Mode T4 Auxiliary Backstays	22	1.398	32	1.381	45	1.380	-1.3%
V	1st Mode T12 Main Backstays	69	1.109	91	1.089	107	1.090	-1.8%
W	1st Mode T8 Main Backstays	79	1.065	101	1.057	118	1.057	-0.8%
X	1st Mode T4 Main Backstays	26	1.300	48	1.29	53	1.291	-0.8%
Y	1st Mode Tiedowns T8	N/A	N/A	1	2.633	1	6.575	60.0%
Z	1st Mode Tiedowns T4 & T12	N/A	N/A	1	2.633	10	2.21	-19.1%

5.4.3 Comparison of Several Modal Participating Mass Ratios – Models B and C

The mode-animation feature provided by SAP2000 suggests that platform mode B (rotation about E-W centroidal axis) is stronger in Model B than in Model C. This observation may be quantitatively verified by analyzing the participation_{mass} ratios of the modes. These quantities provide a measure of how important a mode is for computing the response to an acceleration load. The modal participating mass ratio (PMR) for mode “j” in the x-direction is defined as:

$$PMR_j^x = \frac{(\gamma_j^x)^2}{M_x},$$

where γ_j^x is the modal participation factor for mode “j” in the x-direction, and M_x is the sum of nodal (physical) masses in the x-direction:

$$\gamma_j^x = \{\phi_j\}^T [M] \{r_x\},$$

where $\{\phi_j\}^T$ is the transposed j^{th} mode, $[M]$ is the mass matrix, and $\{r_x\}$ is the vector of influence coefficients in the x-direction.

The definitions of PMR_j^x and γ_j^x assume that the modes are normalized with respect to the mass matrix $[M]$. Similar definitions of the participating mass ratio and participating factors apply for the other directions.

The cumulative sums of the participating mass ratios provide a simple measure to determine if the number of modes included in a modal time-history analysis for ground acceleration loading have achieved a given level of accuracy. Due to the very many independent cable modes with low participating mass ratios present in the response, a total of 1500 modes are required to achieve a cumulative of sum of 99% for all the degrees of freedom in the models of the Arecibo Observatory.

The modal participating mass ratios calculated by SAP2000 for the first few modes are shown in Table 5.21, for Model B, and in Table 5.22, for Model C.

Table 5.21. Modal participating mass ratios – Model B

TABLE: Modal Participating Mass Ratios UNIFORM PLATFORM CASE									
OutputCase	StepType	StepNum	Period	UX	UY	UZ	RX	RY	RZ
Text	Text	Unitless	Sec	Unitless	Unitless	Unitless	Unitless	Unitless	Unitless
MODAL	Mode A	14	2.14577	2.55E-05	7.25E-06	0.0702	5.94E-06	3.2E-05	1.52E-05
MODAL	Mode B	17	1.628166	0.0114	0.0283	2.13E-05	0.0312	0.012	0.0016
MODAL	Mode C	18	1.586981	0.0167	0.0137	1.22E-05	0.0146	0.0167	7.61E-06
MODAL	Mode D	13	2.260474	0.0463	0.1377	2.69E-06	0.1346	0.0437	0.2024
MODAL	Mode E	15	1.763827	0.0016	0.0781	5.21E-07	0.0807	0.0016	0.1245
MODAL	Mode F	16	1.723275	0.1742	0.021	1.36E-05	0.0217	0.1742	0.0071

Table 5.22. Modal participating mass ratios – Model C

TABLE: Modal Participating Mass Ratios - DISTRIBUTED PLATFORM CASE: 50 KIP REDIST.									
OutputCase	StepType	StepNum	Period	UX	UY	UZ	RX	RY	RZ
Text	Text	Unitless	Sec	Unitless	Unitless	Unitless	Unitless	Unitless	Unitless
MODAL	Mode A	22	2.141391	2.53E-05	1.93E-06	0.0698	1.51E-07	6.47E-05	1.17E-05
MODAL	Mode B	31	1.530441	0.0026	0.0028	2.42E-06	0.0031	0.0026	0.000445
MODAL	Mode C	30	1.577617	0.0013	1.21E-06	0.000319	8.99E-05	0.000469	0.000225
MODAL	Mode D	9	2.263751	0.044	0.1308	2.27E-06	0.128	0.0416	0.1989
MODAL	Mode E	23	1.767835	0.000988	0.0527	1.17E-06	0.0544	0.000974	0.1148
MODAL	Mode F	24	1.716103	0.1356	0.0243	3.77E-05	0.0255	0.1364	0.0046

The following observations can be made from the information presented in Tables 5.21 and 5.22:

For mode A (vertical displacement of the platform) the only important mass ratio is UZ which is to be expected since the platform is displacing vertically. Both tables indicate essentially the same results (0.07).

For mode B (platform rotation about an E-W axis) the tables show that all the degrees of freedom, except Uz, participate strongly; however, for Model C, which includes the dome, the participating mass ratios are all one order of magnitude (factor of 10) lower. This is the mode that motivated the comparison. The observation made during the mode animation is confirmed: this mode is not as strong in Model C, which includes the dome.

In mode C (platform rotation about N-S axis) the situation is reversed for the degrees of freedom in the z-direction, i.e., UZ (displacement) and RZ (rotations). For Model C the participating mass ratios of the degrees of freedom in the z-direction are one order of magnitude higher on account of the dome location at the end of the azimuth arm.

For the tower modes D, E, and F, the participating mass ratios show some differences but they are essentially equal to each other. It is in the platform rotational modes that there are significant differences (by factor of 10).

5.4.4 Ranking of Modal Participating Mass Ratios – Model C

A partial ranking of the 1500 modes of Model C, based on the magnitude of their modal participation mass ratios, is shown in Tables 5.23 and 5.24. Table 5.23 corresponds to the three displacement degrees of freedom (DOF) while Table 5.24 corresponds to the three rotational DOF. Only the strongest ten modes are shown for each DOF. Table 5.25 gives a description for all the modes listed in Tables 5.23 and 5.24.

Table 5.23. Ranking of participation mass ratios for displacement DOF – Model C

UX			UY			UZ		
Mode Number	Period [sec]	Modal Mass Ratio [unitless]	Mode Number	Period [sec]	Modal Mass Ratio [unitless]	Mode Number	Period [sec]	Modal Mass Ratio [unitless]
24	1.716	0.1356	9	2.264	0.1308	849	0.105	0.3245
43	1.434	0.0964	44	1.414	0.0974	872	0.076	0.1281
9	2.264	0.044	162	0.727	0.0936	870	0.078	0.0908
265	0.444	0.0401	163	0.695	0.0671	22	2.141	0.0698
153	0.747	0.0394	23	1.768	0.0527	912	0.047	0.0678
44	1.414	0.0385	424	0.303	0.0362	879	0.073	0.0287
503	0.258	0.0368	264	0.448	0.0273	873	0.076	0.0282
116	1.085	0.0317	761	0.180	0.0263	859	0.080	0.0249
85	1.229	0.0295	24	1.716	0.0243	970	0.029	0.0245
163	0.695	0.0223	790	0.169	0.0226	956	0.033	0.0242

Table 5.24. Ranking of participation mass ratios for rotational DOF – Model C

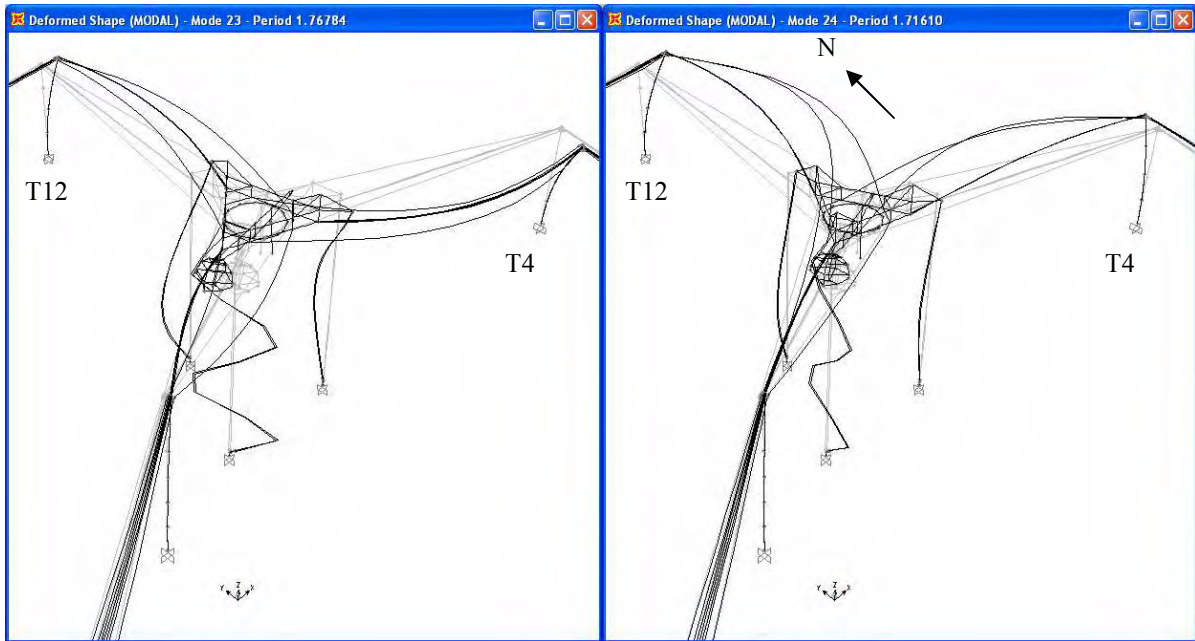
RX			RY			RZ		
Mode Number	Period [sec]	Modal Mass Ratio [unitless]	Mode Number	Period [sec]	Modal Mass Ratio [unitless]	Mode Number	Period [sec]	Modal Mass Ratio [unitless]
9	2.264	0.128	24	1.716	0.1364	9	2.264	0.1989
162	0.727	0.0948	43	1.434	0.0859	23	1.768	0.1148
44	1.414	0.0931	849	0.105	0.0728	163	0.695	0.0938
23	1.768	0.0544	9	2.264	0.0416	424	0.303	0.0512
163	0.695	0.0526	153	0.747	0.0381	265	0.444	0.0401
873	0.076	0.0416	44	1.414	0.0345	42	1.466	0.0351
424	0.303	0.026	265	0.444	0.0339	790	0.169	0.0322
24	1.716	0.0255	503	0.258	0.0277	846	0.108	0.0254
849	0.105	0.0252	116	1.085	0.0273	264	0.448	0.0235
761	0.180	0.0237	85	1.229	0.0267	29	1.586	0.0216

Table 5.25. Description of modes in Tables 5.23 and 5.24

Mode #	Description
9	1st mode tower T8
22	Platform Vertical Displacement
23	1st mode T4 and T12 in-phase; platform rotating about vertical axis. STRONG INTERACTION MODE
24	1st mode T4 and T12 out-of-phase; platform rotating about N-S axis. STRONG INTERACTION MODE
29	Platform rotating about vertical axis; similar to mode 23. Strong interaction.
42	Platform rotating about vertical axis; similar to mode 29 but interaction is not very strong.
43	Complex interaction mode. Towers T8 and T4 are in a mix between a cantilever 1st mode, but acting in the direction of the cables and the 2nd mode. T12 is in 1st mode. Strong E-W cradling of platform while rotating about its vertical axis. STRONG INTERACTION MODE
44	Complex interaction mode similar to mode 43 except towers T4 and T12 switch the type of response. Strong N-S cradling of platform while rotating about its vertical axis. STRONG INTERACTION MODE
85	Complex interaction mode. Tower T8 is in 2nd mode while the platform is rotating strongly about its N-S axis. The Gregorian dome is bobbing up and down. Towers T4 and T12 are in 1st mode.
116	2nd mode of tower T8. Some interaction with other towers and platform.
153	2nd mode of towers T4 and T12. In-phase. E-W cradling of platform. STRONG INTERACTION MODE
162	2nd mode of towers T4 and T12. Out-of-phase. N-S cradling action of platform. STRONG INTERACTION MODE
163	3rd mode of tower T8. No interactions.
264	3rd mode of tower T4. Some interaction with 4th mode of tower T8.
265	3rd mode of tower T12. Minimal interaction with 4th mode of tower T8.
424	5th mode of tower T8. No interactions.
503	6th mode of tower T8. No interactions.
761	4th mode of tower T12. Some interaction with tower T4 and platform rotation about E-W axis.
790	7th mode of tower T8. No interactions.
846	9th mode of tower T8. No interactions.
849	1st Axial mode of tower T8. No interactions.
859	1st Axial mode of tower T4 coupled with its 6th flexural mode. Platform rotation about N-S axis.
870	1st Axial mode of tower T12 coupled with its 6th flexural mode. Platform rotation about N-S axis.
872	Very similar to mode 870.
873	Very similar to mode 872.
879	Very similar to mode 873.
912	2nd Axial mode of tower T8
956	2nd Axial mode of tower T4 coupled with a high flexural mode
970	3rd Axial mode of tower T8 coupled with a high flexural mode

The strongest interaction modes listed in Table 5.25 are divided into three groups. The first group comprises modes 23, 24 with periods of ~ 1.7 sec; the second group comprises modes 43 and 44 with periods of ~ 1.4 sec; and the third group is comprised of modes 153 and 162 with periods of ~ 0.7 sec. Below 0.7 seconds the interactions are not very strong.

The first group (modes 23 and 24 with a period of ~ 1.7 sec) involves the tendency of the platform to rotate while interacting with the first flexural mode of the two shortest towers, T4 and T12. In the case of mode 23, the platform rotates about a vertical axis while T4 and T12 flex in phase with each other. In the case of mode 24, the platform rotates about a N-S axis while towers T4 and T12 flex out of phase with each other. These two modes are shown in Figure 5.42.



(a) Towers T4 and T12 in-phase

(b) Towers T4 and T12 out-of-phase

Figure 5.42. Strong interaction modes. Towers T4 and T12 in-phase and out-of-phase

The second and third groups involve the tendency of the platform to cradle while interacting with the towers. In all cases of strong interactions, the identical towers, T4 and T12, play a very important role. Interactions would have probably been stronger if all three towers had been identical to each other. T8 is 100 ft taller than T4 and T12.

CHAPTER 6

Initial Studies on Seismic Response

6.1 Introduction

Emphasis in this chapter is placed on testing the limitations of the model and analysis types offered by SAP2000 to perform seismic time-history analyses. The final studies on the seismic response of the structure are included in Chapter 7. In this chapter a total of six earthquake records are input to the model of the structural system, four of which are very strong. The following objectives are sought:

1. To generate an initial understanding of the dynamic response of the structure under strong seismic motion.
2. To validate the results of the model to assure reliability of results.
3. To determine if Ernst's linearized cable model holds for the expected tension variations during the shaking motion.
4. To determine if linear modal time history analyses are acceptable by comparing their results versus a fully geometrically nonlinear direct-integration analysis that includes the consideration of large displacements.
5. To generate a broader catalogue of dynamic responses by using several acceleration records from different earthquakes.
6. To observe the response of the structure assuming the towers have cracked.

6.2 Uniform Building Code – 1997 (UBC-97) Basis

The UBC-97 is the currently valid building code in Puerto Rico and, for this reason, it is used as the basis for guiding the seismic analysis. UBC-97 locates the site of the Arecibo Observatory in Seismic Zone 3. The limestone of the Karst landscape in which the Observatory is located is best described by UBC-97 soil type S_b . The code describes it as "Rock" with a shear wave velocity between 2,500 ft/s – 5,000 ft/s. Soil type S_a is not appropriate as it best describes the harder rock found in the eastern United States.

For seismic zone 3 and soil profile type S_b , the UBC-97 elastic design spectrum, shown in Figure 6.1, can be constructed based on the following information:

- $C_a = 0.3$ (Equivalent to the Peak Ground Acceleration (PGA) in g's)
- $C_v = 0.3$
- $T_s = C_v / (2.5 * C_a) = 0.3 / (2.5 * 0.3) = 0.4 \text{ sec}$
- $T_0 = 0.2 * T_s = 0.2 * 0.4 = 0.08 \text{ sec}$

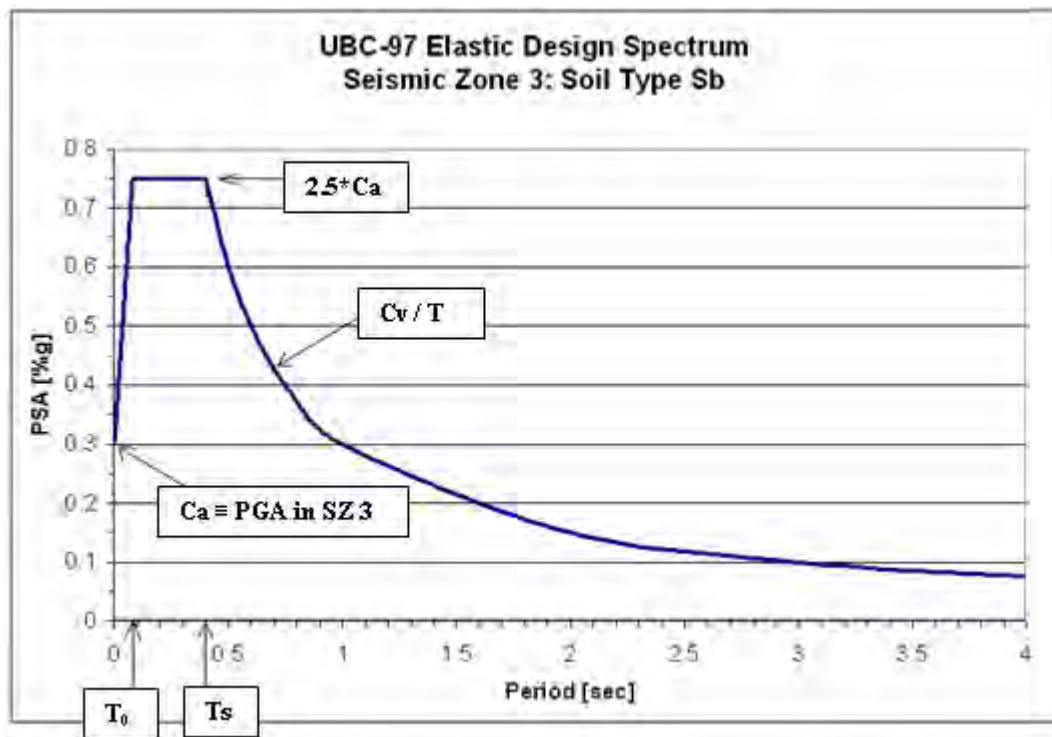


Figure 6.1. UBC-1997 Elastic Design Spectrum

6.3 The 1989 Loma Prieta Earthquake

The Loma Prieta, California earthquake of October 18, 1989 was the first one chosen for the initial study due to its predominant long-period spectral peak at approximately 1.2 seconds. It represents a very severe initial test to the long-period tower structures. Response spectra from the three components of the Gilroy #2 acceleration records are superimposed over the UBC-97 spectrum in Figs. 6.2 - 6.4.

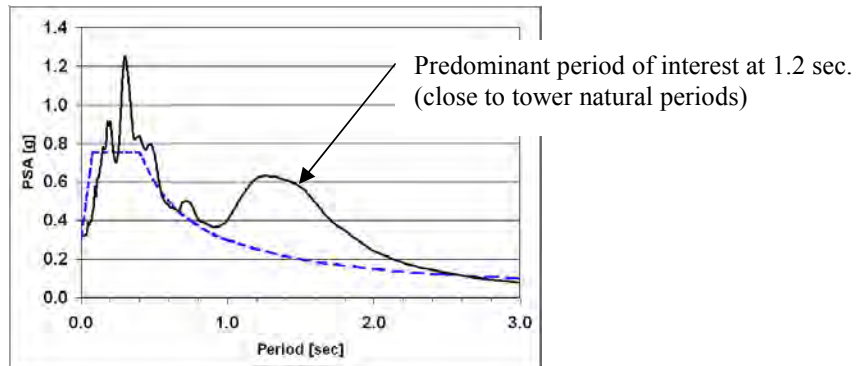


Figure 6.2. U1 (EW) Loma Prieta spectrum for 5% damping ratio vs UBC-97 spectrum

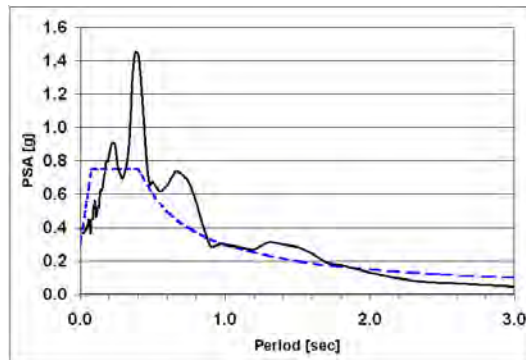


Figure 6.3. U2 (NS) Loma Prieta spectrum for 5% damping ratio vs UBC-97 spectrum

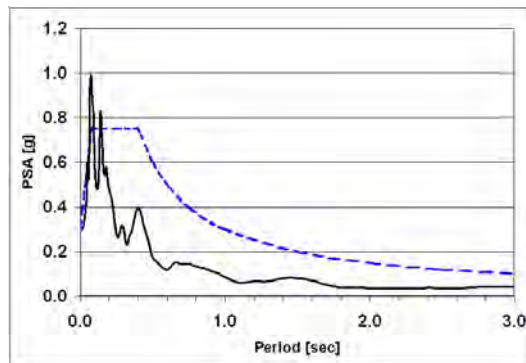


Figure 6.4. U3 (Up) Loma Prieta spectrum for 5% damping ratio vs UBC-97 spectrum

6.4 Other Earthquakes Chosen for Initial Set

The records chosen for the initial study are summarized in Table 6.1. Note that none are from Puerto Rico since there is not enough data of strong earthquake records in the island (this issue is addressed further in Chapter 7). The records were obtained from the Pacific Earthquake Engineering Research (PEER) database of the University of California at Berkeley. These may be obtained by searching the website <http://peer.berkeley.edu/smcat/search.html>. The database provides three orthogonal records per earthquake, which correspond to the North-South, East-West, and Up-Down directions. The search criterion was constrained to any earthquake with at least one PGA record between 0.3 and 0.33. The accelerograms retrieved were scaled to the 0.3 PGA target required by the UBC 97 for seismic zone 3 (see last column of Table 6.1 for factor used in SAP2000 model).

Table 6.1. Initial earthquake records and factor used in SAP models

Case	Magnitude (Richter)	Distance to Fault Rupture [km]	Number of Points [adim]	Delta T [sec]	Duration [sec]	PGA [%g]	g [in/s ²]	Factor (SAP) [in/s ²]
U1LomaPrieta	6.9	12.7	7990	0.005	39.95	0.322	386.4	360.0
U2LomaPrieta	6.9	12.7	7990	0.005	39.95	0.367	386.4	315.9
U3LomaPrieta	6.9	12.7	7990	0.005	39.95	0.294	386.4	262.9
U1EICentro	7.0	8.3	4000	0.01	40	0.215	386.4	539.2
U2EICentro	7.0	8.3	4000	0.01	40	0.313	386.4	370.4
U3EICentro	7.0	8.3	4000	0.01	40	0.205	386.4	377.0
U1ChiChi	7.6	33.0	18000	0.005	90	0.301	386.4	385.1
U2ChiChi	7.6	33.0	18000	0.005	90	0.413	386.4	280.7
U3ChiChi	7.6	33.0	18000	0.005	90	0.27	386.4	286.2
U1Kocaeli	7.4	12.7	5437	0.005	27.185	0.358	386.4	323.8
U2Kocaeli	7.4	12.7	5437	0.005	27.185	0.312	386.4	371.5
U3Kocaeli	7.4	12.7	5437	0.005	27.185	0.229	386.4	337.5
U1SanFernando	6.6	24.9	3000	0.01	30	0.268	386.4	432.5
U2SanFernando	6.6	24.9	3000	0.01	30	0.324	386.4	357.8
U3SanFernando	6.6	24.9	3000	0.01	30	0.171	386.4	451.9
U1Coalinga	5.0	12.7	7999	0.005	39.995	0.343	386.4	338.0
U2Coalinga	5.0	12.7	7999	0.005	39.995	0.313	386.4	370.4
U3Coalinga	5.0	12.7	7999	0.005	39.995	0.082	386.4	942.4

Notes:

1. U1 = East-West, U2 = North-South, U3 = Up and Down
2. Equation used to calculate U1 and U2 Factor: $\text{Factor} = 0.3 * \text{g} / \text{PGA}$
3. Equation used to calculate U3 Factor: $\text{Factor} = 2/3 * (0.3 * \text{g} / \text{PGA})$
4. Duration is required when defining the analysis cases

The May 19, 1940 El Centro, California earthquake has been used extensively in earthquake engineering studies. The 23.9 sec strong motion duration of this earthquake is very significant and could be damaging to the Observatory. The September 20, 1999 Chi Chi, Taiwan and the August 17, 1999 Kocaeli, Turkey earthquakes were chosen because they are of high magnitude – 7.6 and 7.4 moment magnitude, respectively – and could also be damaging to the Observatory. In summary, the Loma Prieta, El Centro, Chi Chi and Kocaeli earthquake records should place the Observatory in a very high state of stress.

The February 9, 1971 San Fernando, California earthquake is of a slightly lesser magnitude (6.6 moment magnitude).

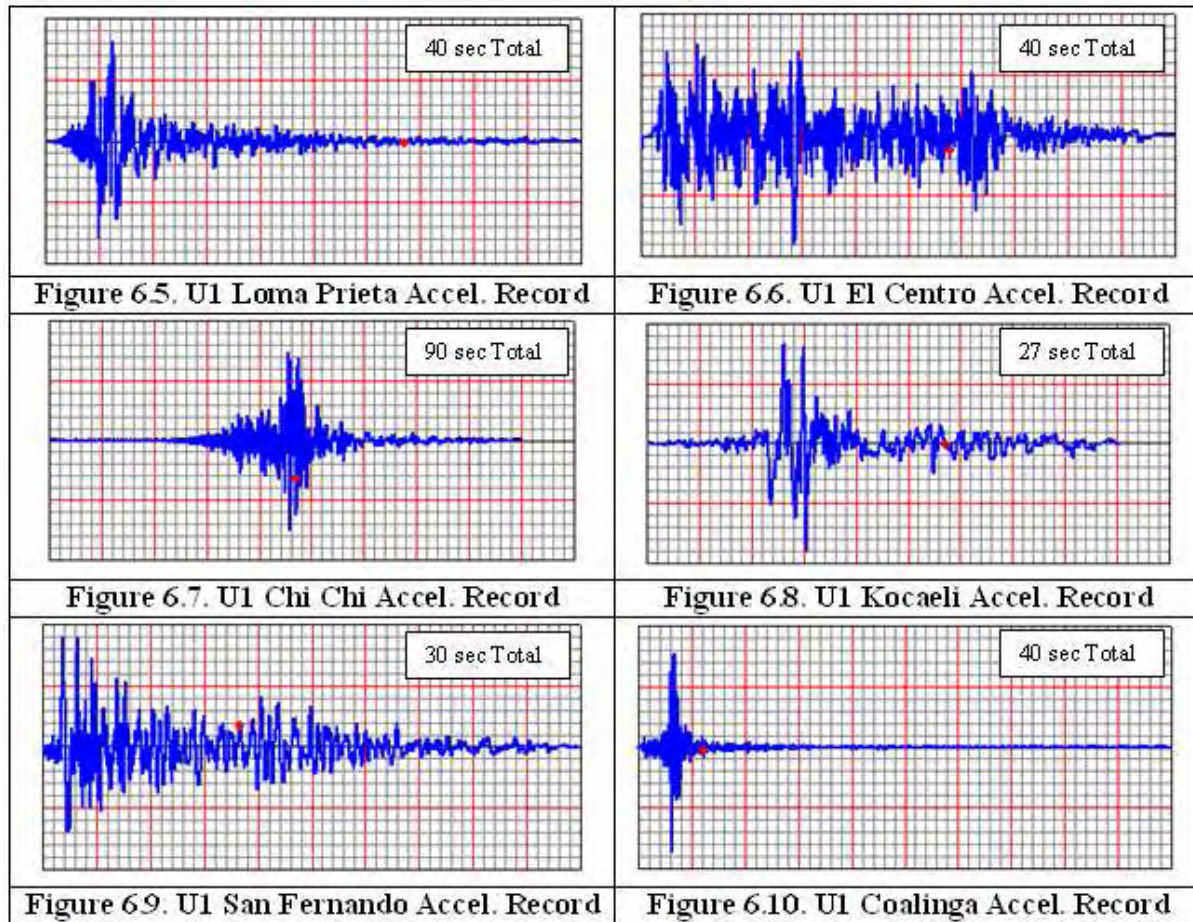
The May 9, 1983 Coalinga, California earthquake with a moment magnitude of 5.0 and a very short duration should be the least severe of the set.

The stations where these earthquake were recorded are included in Table 6.2.

Table 6.2. Stations where initial set of earthquakes were recorded

Earthquake	Date	Station Name
Loma Prieta, California	October 18, 1989	Gilroy Array #2
El Centro, California (Imperial Valley)	May 19, 1940	El Centro Array #9
Chi Chi, Taiwan	September 20, 1999	TCU047
Kocaeli, Turkey	August 17, 1999	Duzce
San Fernando, California	February 9, 1971	24278 Castaic – Old Ridge Route
Coalinga, California	May 9, 1983	46T06 Oil Fields – Skunk Hollow

The U1 (EW) unscaled acceleration records of the six earthquakes are shown in Figures 6.5 through 6.10. These were obtained directly from the SAP2000 function files.



6.5 Modal Time-History Linear Analysis – Loma Prieta Earthquake – Model A

A modal time-history linear analysis with a constant damping ratio of 5% (all modes) is performed on Model A for the Loma Prieta earthquake. The results of this analysis are used to perform many of the required validation studies. The following five cases are run:

1. Record in the U1 direction only (East-West)
2. Record in the U2 direction only (North-South)
3. Record in the U3 direction only (Up and Down)
4. Simultaneous records in the U1 and U2 directions
5. Simultaneous records in the U1, U2, and U3 directions.

The analyses are based on 1500 modes which represent a dynamic modal load participation factor of 99% (cumulative). Note that most of these modes are independent cable modes which do not have strong participation; however, they have the effect of dispersing the stronger tower and platform modes so a very large number (1500) must be considered. The results of the modal time-history analysis for the Loma Prieta earthquake are shown in Table 6.3. The maximum and minimum values are shown.

Table 6.3. Loma Prieta earthquake results – Model A (No Ties, Unif. Plat)

Label	Description	U1 (E-W) Only		U2 (N-S) Only		U3 (U-D) Only		U1 and U2		U1, U2, and U3	
		MAX	MIN	MAX	MIN	MAX	MIN	MAX	MIN	MAX	MIN
UX Displacement											
J27	Top of tower T12 [in]	15.8	-19.2	0.9	-0.9	0.005	-0.005	15.9	-19.2	15.9	-19.2
J36	Top of tower T8 [in]	7.0	-6.7	5.6	-3.3	0.2	-0.2	7.6	-7.7	7.8	-7.6
J43	Top of tower T4 [in]	6.7	-9.5	3.0	-3.5	0.2	-0.2	9.1	-11.0	8.9	-11.1
UY Displacement											
J27	Top of tower T12 [in]	0.9	-1.0	4.0	-2.6	0.2	-0.2	4.4	-3.4	4.2	-3.6
J36	Top of tower T8 [in]	8.7	-8.1	6.3	-6.7	0.1	-0.1	6.2	-7.1	6.3	-7.5
J43	Top of tower T4 [in]	8.0	-7.5	5.5	-6.4	0.1	-0.1	11.1	-12.6	11.1	-12.6
UZ Displacement											
J99	Platform corner T12 [in]	1.4	-1.3	6.0	-6.5	2.7	-3.1	6.4	-7.5	7.5	-10.1
J104	Platform corner T8 [in]	12.1	-12.7	3.1	-3.1	2.7	-3.1	14.8	-15.8	14.1	-16.1
J111	Platform corner T4 [in]	12.1	-11.1	3.1	-2.9	2.7	-3.1	9.1	-9.4	9.1	-10.2
M33 Moment											
F4 R 1	Top of tower T12 [kip-ft]	286	-315	1326	-1982	46	-61	1368	-2011	1365	-2023
F11 R 1	Top of tower T8 [kip-ft]	2519	-2018	803	-921	13	-17	3210	-2939	3206	-2941
F16 R 1	Top of tower T4 [kip-ft]	1675	-1261	900	-662	91	-65	1150	-1340	1131	-1360
M22 Moment											
F1 R 0	Base of tower T12 [kip-ft]	19040	-21260	116700	-85560	1690	-1861	123900	-91520	123000	-91710
F6 R 0	Base of tower T8 [kip-ft]	320900	-292000	77250	-74930	2323	-1903	360900	-343600	361500	-344900
F13 R 0	Base of tower T4 [kip-ft]	107500	-114200	41570	-53250	2058	-2266	75230	-104700	74050	-106400
M22 Moment											
F1 R 0	Base of tower T12 [kip-ft]	164400	-117900	7883	-7541	41	-42	164700	-117900	164700	-117900
F6 R 0	Base of tower T8 [kip-ft]	91960	-102900	151100	-119400	29	-26	105600	-150900	105600	-150800
F13 R 0	Base of tower T4 [kip-ft]	58280	-81770	77910	-84910	23	-20	132400	-166700	132400	-166700
ΔTENSION											
F271 R 0.5	Main Cable T12 [kip]	19.3	-21.8	84.2	-82.3	7.4	-6.3	96.4	-96.6	103	-90.2
F275 R 0.5	Main Cable T8 [kip]	141.9	-151.4	29.0	-34.1	7.3	-6.5	171	-180	177	-175
F280 R 0.5	Main Cable T4 [kip]	105.1	-143.1	39.9	-40.2	7.5	-6.4	90.8	-114	92.7	-109
ΔTENSION											
F282 R 0.5	Auxiliary Cable T12 [kip]	31.4	-28.6	49.8	-88.9	4.7	-4	64.9	-111	65.6	-106
F284 R 0.5	Auxiliary Cable T8 [kip]	107.6	-87.9	37.0	-44.9	4.9	-4.1	122	-118	132	-114
F287 R 0.5	Auxiliary Cable T4 [kip]	101.1	-127.8	35.2	-38.2	5.1	-4.4	80.6	-104	78.9	-108
ΔTENSION											
F251 R 0.5	Main Backstay T12 [kip]	21.3	-20.5	58.0	-87.5	5.5	-5.0	75.9	-95.8	80.1	-91.8
F256 R 0.5	Main Backstay T8 [kip]	171.8	-165.8	44.0	-45.7	5.5	-5.0	216	-211	220	-207
F261 R 0.5	Main Backstay T4 [kip]	132.2	-117.6	35.1	-25.5	5.4	-4.9	107	-88.3	111	-87.5
ΔTENSION											
F264 R 0.5	Auxiliary Backstay T12 [kip]	48.4	-38.8	66.5	-101	6.2	-5.7	105	-118	108	-113
F267 R 0.5	Auxiliary Backstay T8 [kip]	200.8	-198.5	51.7	-50.1	6.1	-5.5	249	-249	254	-244
F269 R 0.5	Auxiliary Backstay T4 [kip]	152.0	-132.8	43.6	-31.6	6.2	-5.6	120	-110	125	-110

Figure 6.11 shows an exaggerated deformed shape (50x mag.) of the structure 5.1 sec into the earthquake. At this time the structure experiences the highest bending moment $M_{33} = -365,000$ kip-ft in tower T8. Note that tower T8 is deformed in the second mode shape while towers T4 and T12 are in a first mode deformation pattern. These modes have periods close to the predominant 1.2-second peak of the Loma Prieta earthquake response spectrum. Note that the platform is exhibiting rotation about the N-S Axis.

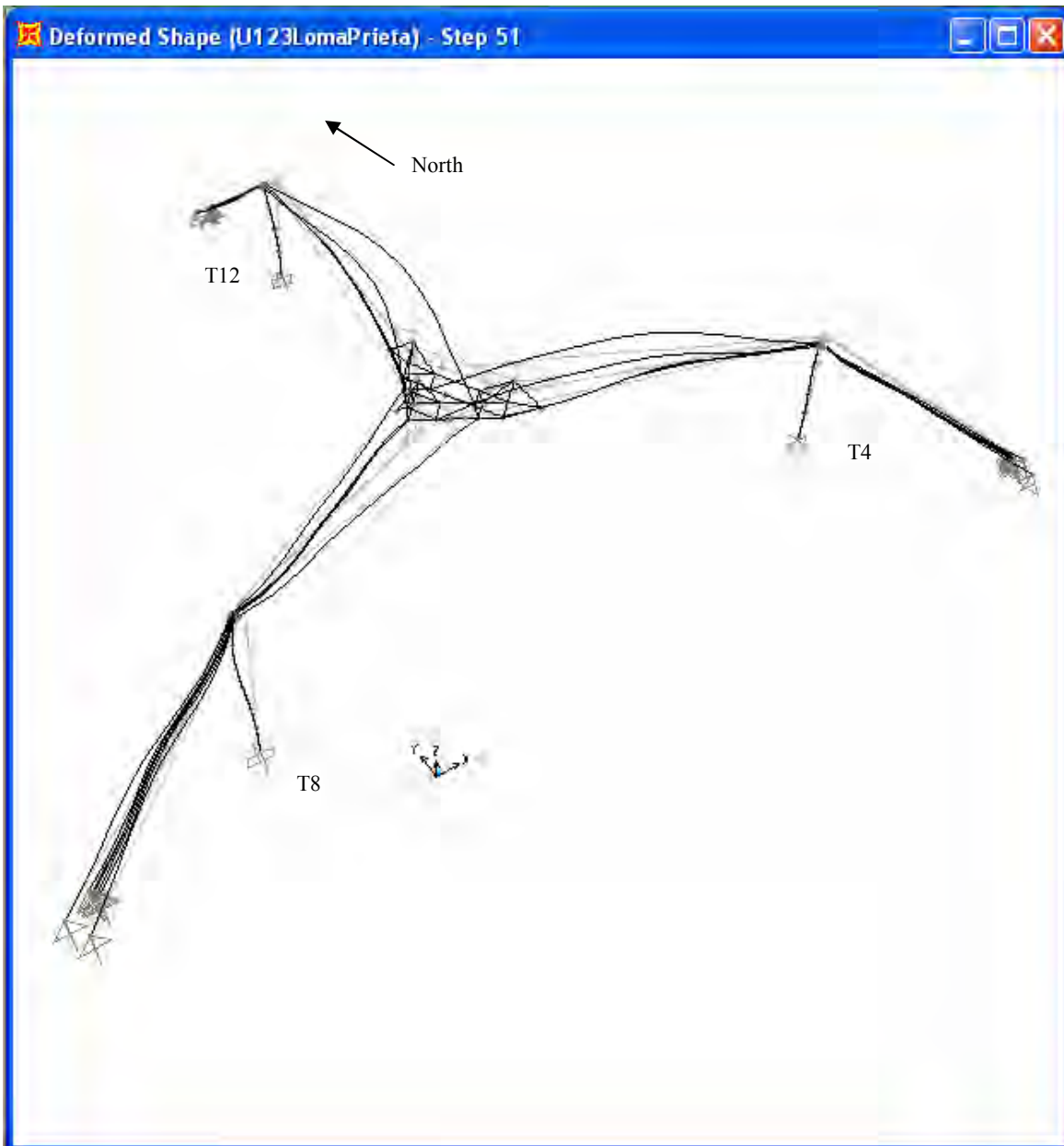


Figure 6.11. Deformed shape (50x mag.) of structure 5.1 sec into Loma Prieta

6.6 Discussion of the Loma Prieta Earthquake Results (Table 6.3) – Model A

1. The response in the $U1 = U_x$ direction at the top of tower T12 is shown in Figure 6.12. According to Table 6.3 the displacements at the top of tower T12 are almost 20 inches which is very significant. Tower T12 is the easiest to interpret as the x and y directions coincide, respectively, with the tangential and radial directions of the model. The radial direction coincides with the orientation of the main platform cables and backstays. Note from Table 6.3 that there are U_x displacements of 19.2 inches on tower T12 for all cases containing the U1 record.

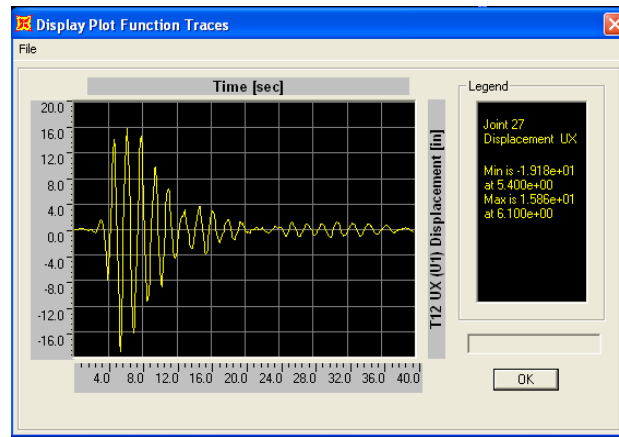


Figure 6.12. Tangential displacements [inch] (perpendicular to cables) at Tower T12. All components of Loma Prieta earthquake included – No Tiedowns

2. The platform corners undergo vertical displacements on the order of 16 inches. The displacement in the global-z direction at the platform corner pointing at Tower T8 is shown in Figure 6.13.

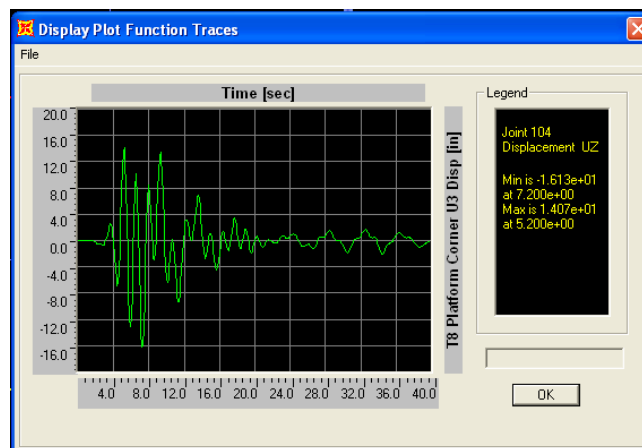
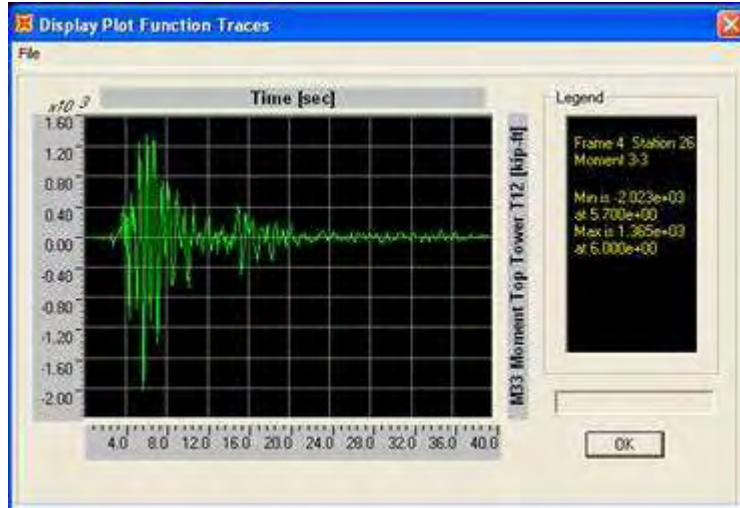


Figure 6.13. U3 Displacement [in] at platform corner pointing at Tower T8. All components of Loma Prieta earthquake included – No Tiedowns

- The M_{33} bending moment at the top of tower T12 displayed in Figure 6.14 is on the order of 2000 kip-ft, the same magnitude as the unbalanced moment in the auxiliary saddle (see section 2.7). The total M_{33} moment at the top of tower T12 is therefore, by superposition, of the order of 4000 kip-ft.



**Figure 6.14. M_{33} Moment [kip-ft] at TOP of Tower T12.
All components of Loma Prieta earthquake included – No Tiedowns**

- The maximum M_{33} bending moment (parallel to cables) at the base of tower T8, whose time variation is shown in Figure 6.15, is on the order of 360,000 kip-ft.

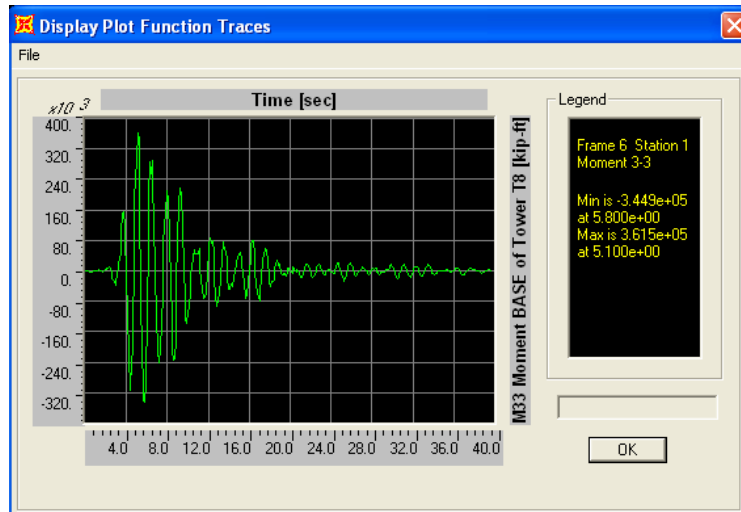


**Figure 6.15. M_{33} Moment [kip-ft] at BASE of Tower T8.
All components of Loma Prieta earthquake included – No Tiedowns**

- The M_{22} bending moments (perpendicular to cables) at the base of the towers are also very high; in fact, they are higher than M_{33} in the case of Tower T4. The M_{22} time history at the base of tower T4 is shown in Figure 6.16.

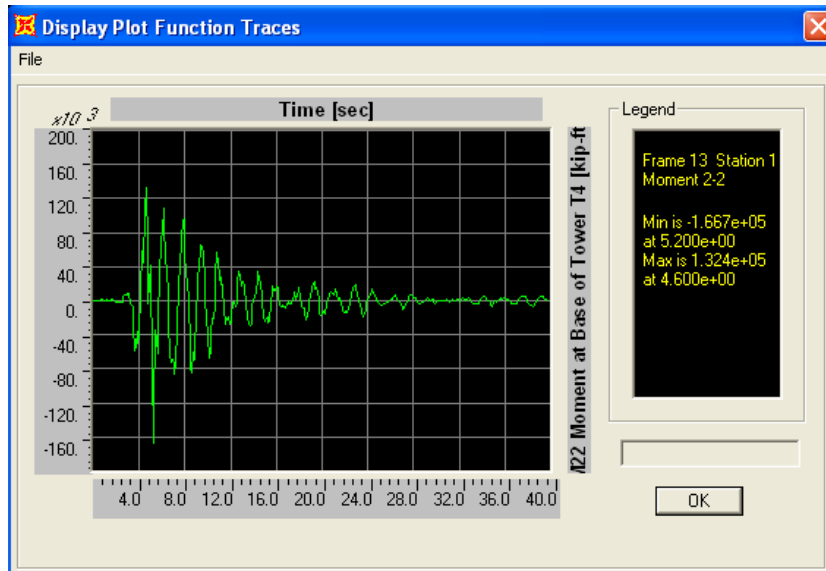


**Figure 6.16. M_{22} moment [kip-ft] at BASE of Tower T4.
All components of Loma Prieta earthquake included – No Tiedowns**

- The trend of the five cases shown in Table 6.3 is consistent with the data input. For example, the results of the single $U_1=U_x$ input case show highest displacements and moments in the 'x' direction while for the single input in the $U_2=U_y$ direction the highest displacements are in the 'y' direction. Tower T12 is the most appropriate for a comparison as the U_1 direction is equivalent to the 'x' direction and the U_2 direction is equivalent to the 'y' direction.
- Note that the isolated case "U3 (Up and Down) Only" has a very small effect on the structure in all respects. Of special note is the fact that the up and down movement of the platform has a very small effect on changing the tensions in the cables. The vertical component of acceleration is usually of concern only very near the ruptured fault. Even if this was the case the Arecibo Observatory shows a very small response to this input.

8. Since the “U3 (Up and Down) Only” input has a very small effect on the structure, the “U1 and U2” results are almost equal to the “U1, U2, and U3” case.
9. The cables show a relatively large variation in tension. For example, the main cables of Tower T8 show a maximum variation of $\Delta T = 177$ kip from the initial state as shown in Table 6.3. As a result, the Ernst’s linearized-modulus assumption must be checked to determine if it still holds under this level of variation.
10. As shown in Figure 6.17, the cables assume negative values according to this type of analysis. This is one of the limitations of the modal time-history linear analysis. Although the modes are calculated after the non-linear P-delta analysis, the modal time-history analysis starts from a zero stress initial condition, i.e., the initial tension in the cables is reset to zero at the start of the time-history modal analysis. Rather than decreasing tension from its high state, the cables start from zero and go into compression. This inconsistency is bypassed when a non-linear direct-integration time-history analysis is run, which uses the deformed equilibrium state due to dead load at the end of the P-delta analysis as its initial condition. Rather than going into compression, the tension level drops from a high tensile value to a lower one. The penalty for using this type of analysis is the computational time: it takes approximately 14 hours to run each single case on a 2.8 GHz desktop computer with 384 MB of RAM. In addition, achieving convergence of the solution is not a trivial issue. This case is addressed in the next section (validations).

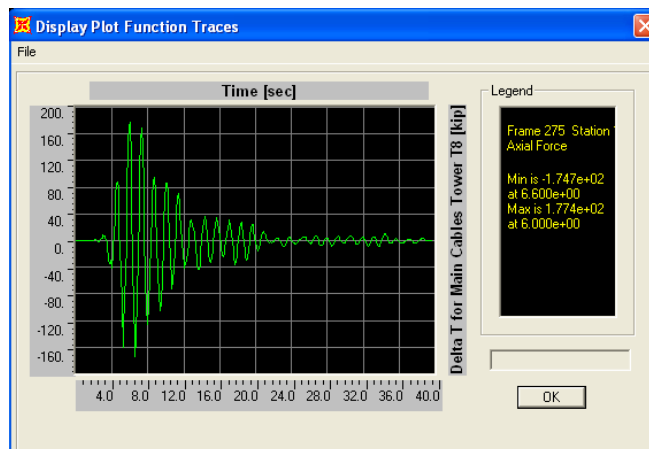


Figure 6.17. ΔT Tensions [kip] in main cables of Tower T8. All components of Loma Prieta earthquake included – No Tiedowns

6.7 Validation Studies – Loma Prieta Earthquake – Model A

The following issues require validation before continuing to investigate additional earthquake records and the more complex Model B and Model C:

1. Are the magnitudes of the very large bending moments, on the order of 360,000 kip-ft at the base of tower T8, and 160,000 kip-ft at the base of towers T4&T12, reasonable? Calculate the Overturning Moment of the isolated towers based on UBC-1997. Compare results. They should be reasonably similar.
2. What is the performance of the towers alone? To answer this question the time history cases with a model that isolates the towers (cables and platform deleted from model) will be run. This model should better represent the Overturning Moment calculation based on UBC-97. It will also provide a sense for the strength of the coupling effect between towers and platform.
3. Main cable tensions show a reduction of 177 kip. Is it still acceptable to assume that the cables remain in the linear regime or will geometric nonlinearities be required to model the cable response? The equation for Ernst's equivalent modulus will be examined to determine a reasonable linearized range for ΔT .
4. The linear time-history analysis shows cables going into compression because all stresses in the model, including initial cable tensions, are reset to zero in SAP2000 for modal time-history analysis. In reality, cable tensions are most likely reduced from a high tension state to a lower one so the cables never actually lose the tension, i.e., they never go into compression. Is the compression shown by the linear analysis compromising the accuracy of the results? To shed light on this issue, a non-linear direct-integration time-history analysis including P-delta effects and large displacements will be performed. This is the most complex option offered by SAP2000 that includes geometric nonlinearities. The results will be compared with the linear case.

6.7.1 Overturning Moment of Tower T8 per UBC-97

Section 1630 of the UBC-97 code specifies the procedure to determine the minimum design lateral forces and related effects such as the overturning moment. The first item to determine is the weight of the tower which is given in Table 6.4.

Table 6.4. Weight calculation for tower T8

Section	Area [ft ²]	h [ft]	Volume [ft ³]	Weight [kip]
TSEC1	72	60	4320	648
TSEC2	120	61	7320	1098
TSEC3	180	61	10980	1647
TSEC4	252	61	15372	2305.8
TSEC5	324	61	19764	2964.6
TSEC6	396	61	24156	3623.4
TOTAL	N/A	N/A	N/A	12286.8

According to section 1630.2.1 of the UBC-97 code, the total design base shear must be calculated with the following expression:

$$V = \frac{C_v IW}{RT}, \text{ where}$$

$C_v = 0.3$ (seismic coefficient for zone 3, soil profile S_b)

$I = 1$ (importance factor. Use $I = 1$ as a nominal case to consider elastic regime)

$W = 12286.8$ kip (total weight of tower)

$R = 1$ (response modification factor. Use $R = 1$ for elastic response)

$T = 2.26$ sec (fundamental period of tower T8)

Substituting the values and solving for the base shear,

$$V = 1631 \text{ kip}$$

The vertical distribution of lateral force over the height of the tower is calculated from section 1630.5 of the UBC-97 code. Long-period structures ($T > 0.7$ sec) must carry an additional concentrated lateral force at the top given by the following expression:

$$F_t = 0.07TV \leq 0.25V, \text{ where}$$

$T = 2.26$ sec (fundamental period of tower T8)

$V = 1631$ kip (design base shear for tower T8)

Substituting the values and solving for the concentrated force at the top,

$$F_t = 258 \text{ kip } (\leq 408 \text{ kip ok})$$

The lateral force " F_x " applied at each "story" (each ~60 ft segment is considered a story) of the tower must be calculated with the following expression from section 1630.5 of the UBC-97 code:

$$F_x = \frac{(V - F_t)w_x h_x}{\sum_{i=1}^n w_i h_i}, \text{ where}$$

$V = 1631$ kip (design base shear force for tower T8)

$F_t = 258$ kip (concentrated force at the top)

w_x, w_i = portion of the weight applied to level 'x' or 'i', respectively

h_x, h_i = height in feet above the base to level 'x' or 'i', respectively

n = the uppermost level

The calculations are summarized in Table 6.5. Note the portion of the weight applied at each level (w_x, w_i) is calculated by adding one-half of the weight of the story directly below and one-half of the weight of the story directly above the level being considered.

Table 6.5. Lateral force at each level of tower T8 per UBC-97

At Top of Section	"Story" Weight "wx" [kip]	Height from Base "hx" [ft]	wx*hx [kip-ft]	Lateral Force "Fx" [kip]	Fx*hx [kip-ft]
TSEC1	324	365	118260	101.3	36959
TSEC2	873	305	266265	228.0	69536
TSEC3	1373	244	334890	286.7	69966
TSEC4	1976	183	361681	309.7	56672
TSEC5	2635	122	321494	275.3	33584
TSEC6	3294	61	200934	172.0	10495
			1603525 SUM		277212 SUM

Finally, the calculation of the overturning moment is calculated per section 1630.8 of the UBC-97 code using the following expression:

$$M_{OT} = \sum_{x=1}^n F_x h_x + F_t h_n, \text{ where}$$

$F_x h_x$ is given in the last column of Table 6.5 for each tower segment

$F_t = 258$ kip (concentrated force at the top of tower T8)

$h_n = 365$ ft (moment arm for concentrated force at the top)

Substituting the values and solving for the overturning moment,

$$M_{OT} = 371,391 \text{ kip-ft}$$

In conclusion, this result validates the 361,500 kip-ft M_{33} maximum moment calculated with the finite element model.

6.7.2 Overturning Moment of Towers T4 and T12 per UBC-97

Towers T4 and T12 are identical. Section 1630 of the UBC-97 code specifies the procedure to determine the minimum design lateral forces and related effects such as the overturning moment. The first item to determine is the weight of the tower which is given in Table 6.4.

Table 6.6. Weight calculation for tower T4 and T12

Section	Area [ft ²]	h [ft]	Volume [ft ³]	Weight [kip]
TSEC1	72	62.5	4500	675
TSEC2	120	62.5	7500	1125
TSEC3	180	62.5	11250	1687.5
TSEC4	252	62.5	15750	2362.5
TOTAL	N/A	N/A	N/A	5850

According to section 1630.2.1 of the UBC-97 code, the total design base shear must be calculated with the following expression:

$$V = \frac{C_v IW}{RT}, \text{ where}$$

$C_v = 0.3$ (seismic coefficient for zone 3, soil profile S_b)

$I = 1$ (importance factor. Use $I = 1$ as a nominal case to consider elastic regime)

$W = 5850$ kip (total weight of each tower)

$R = 1$ (response modification factor. Use $R = 1$ for elastic response)

$T = 1.79$ sec (fundamental period of tower T4 or T12)

Substituting the values and solving for the base shear,

$$V = 980 \text{ kip}$$

The vertical distribution of lateral force over the height of the tower is calculated from section 1630.5 of the UBC-97 code. Long-period structures ($T > 0.7$ sec) must carry an additional concentrated lateral force at the top given by the following expression:

$$F_t = 0.07TV \leq 0.25V, \text{ where}$$

$T = 1.79$ sec (fundamental period of tower T4 or T12)

$V = 980$ kip (design base shear for tower T4 or T12)

Substituting the values and solving for the concentrated force at the top,

$$F_t = 123 \text{ kip } (\leq 245 \text{ kip ok})$$

The lateral force " F_x " applied at each "story" (each 62.5 ft segment is considered a story) of the tower must be calculated with the following expression from section 1630.5 of the UBC-97 code:

$$F_x = \frac{(V - F_t)w_x h_x}{\sum_{i=1}^n w_i h_i}, \text{ where}$$

$V = 980$ kip (design base shear force for tower T4 or T12)

$F_t = 123$ kip (concentrated force at the top of tower T4 or T12)

w_x, w_i = portion of the weight applied to level 'x' or 'i', respectively

h_x, h_i = height in feet above the base to level 'x' or 'i', respectively

n = the uppermost level

The calculations are summarized in Table 6.7. Note the portion of the weight applied at each level (w_x, w_i) is calculated by adding one-half of the weight of the story directly below and one-half of the weight of the story directly above the level being considered.

Table 6.7. Lateral force at each level of tower T4 and T12 per UBC-97

At Top of Section	"Story" Weight "wx" [kip]	Height from Base "hx" [ft]	wx*hx [kip-ft]	Lateral Force "Fx" [kip]	Fx*hx [kip-ft]
TSEC1	338	250.0	84375	130.2	32544.3
TSEC2	900	187.5	168750	260.4	48816.46
TSEC3	1406	125.0	175781	271.2	33900.32
TSEC4	2025	62.5	126563	195.3	12204.11
			555469 SUM		127465 SUM

Finally, the calculation of the overturning moment is calculated per section 1630.8 of the UBC-97 code using the following expression:

$$M_{OT} = \sum_{x=1}^n F_x h_x + F_t h_n, \text{ where}$$

$F_x h_x$ is given in the last column of Table 6.7 for each tower segment

$F_t = 123$ kip (concentrated force at the top)

$h_n = 250$ ft (moment arm for concentrated force at the top)

Substituting the values and solving for the overturning moment,

$$M_{OT} = 158,178 \text{ kip-ft}$$

In conclusion, this result validates the 166,700 kip-ft M_{33} maximum moment calculated with the finite element model.

6.7.3 Sensitivity Study: Isolation of Towers

All the cables and the platform were deleted from the model to isolate the performance of the towers. The results are shown in Table 6.8.

Table 6.8. Modal time-history results - Isolated Towers (no cables nor platform)

Label	Description	Isolated Towers Scaled Loma Prieta (No Cables)		MODEL A Scaled Loma Prieta (With Cables)		% DIFF MAX	% DIFF MIN
		U1, U2, and U3		U1, U2, and U3			
		MAX	MIN	MAX	MIN		
	UX Displacement						
J27	Top of tower T12 [in]	21.0	-23.4	15.9	-19.2	32%	22%
J36	Top of tower T8 [in]	16.7	-18.2	7.8	-7.6	114%	139%
J43	Top of tower T4 [in]	21	-23.4	8.9	-11.1	136%	111%
	UY Displacement						
J27	Top of tower T12 [in]	9.8	-9.6	4.2	-3.6	133%	167%
J36	Top of tower T8 [in]	8.6	-10.7	6.3	-7.5	37%	43%
J43	Top of tower T4 [in]	9.8	-9.6	11.1	-12.6	-12%	-24%
	M33 Moment						
F4 R 1	Top of tower T12 [kip-ft]	15.4	-13.2	1365	-2023	N/A	N/A
F11 R 1	Top of tower T8 [kip-ft]	21.0	-19.2	3206	-2941	N/A	N/A
F16 R 1	Top of tower T4 [kip-ft]	20.0	-14.9	1131	-1360	N/A	N/A
	M22 Moment						
F1 R 0	Base of tower T12 [kip-ft]	104400	-127200	123000	-91710	-15%	39%
F6 R 0	Base of tower T8 [kip-ft]	213200	-217300	361500	-344900	-41%	-37%
F13 R 0	Base of tower T4 [kip-ft]	127800	-115400	74050	-106400	73%	8%
	M22 Moment						
F1 R 0	Base of tower T12 [kip-ft]	205500	-184100	164700	-117900	25%	56%
F6 R 0	Base of tower T8 [kip-ft]	118900	-168200	105600	-150800	13%	12%
F13 R 0	Base of tower T4 [kip-ft]	164500	-213000	132400	-166700	24%	28%

Without cables, the displacements at the top of the towers are not restrained and show higher magnitudes in both the x and y directions. In addition, without cables the M_{33} moments at the top of the towers drop to almost zero since they are essentially cantilever beams. These results were expected.

With respect to the M_{22} moments at the base of the towers, the isolated case shows higher bending moments across the board. On the other hand, the M_{33} moments at the base show mixed results. At the base of tower T8, M_{33} is significantly higher in the case with cables, thus showing a high degree of interaction with the cables and the platform. These results show that the interaction between the towers and the platform is actually beneficial for the structure except for tower T8 where the M_{33} bending moment is 42% higher due to the interaction.

It is interesting to note that, based on the scaled record of the Loma Prieta earthquake, the UBC-97 overturning moment calculations are closer to the model with cables. The UBC-

97 calculations overestimate the maximum bending moment at the base of tower T8 by only 2.7% while underestimating the maximum bending moment at the base of tower T12 by only 5.4%. On the other hand, in the case of the isolated towers, which is a better representation of the code assumptions, the UBC-97 overestimates the bending moment at the base of tower T8 by 42% and underestimates the bending moment by 26% at the base of towers T4 and T12. Nevertheless, this validation study has shown that all the calculations are within the same order of magnitude.

6.7.4 Examination of Ernst's Linearized Assumption in Cables

A typical linearized approach to account for the sag effect of inclined cables is to consider an equivalent straight chord member with an equivalent modulus of elasticity, E_{eq} , given by Ernst's tangent modulus equation (Ren 1999a):

$$E_{eq} = \frac{E}{1 + \frac{(wL)^2 AE}{12T^3}}, \text{ where, for any consistent set of units,}$$

E = Cable Apparent Modulus of Elasticity (24E6 psi for wire 'strand')

w = weight per unit length = (Specific weight) * (Effective Area)

L = horizontal projected length of the cable

A = Effective area of the cable

T = Tension in the cable

Note that as T increases the value of E_{eq} asymptotically approaches E . Ernst's modulus was calculated in Section 2.1.6 and it was shown that $E_{eq} \approx E$, i.e., the asymptotic value had been reached due to the very high tensions in the cable.

The objective of this section is to determine if the reduction in cable tension during a seismic event invalidates the linearized approach. In other words, it is desired to establish whether the reduction in E_{eq} is so large as to merit a secant modulus approach or a fully non-linear analysis approach to take into account updated values of E_{eq} . This problem is approached by plotting Ernst's modulus and determining an acceptable range for which the linearized tangent modulus is acceptable. The main cables, those that span between the platform corners and the towers, are used for the analysis.

Figure 6.18 plots Ernst's modulus using the "main" cable parameters and shows the asymptotic behavior of E_{eq} . Note that an arbitrary 10% reduction in the equivalent modulus, which is an acceptable variation for a linearized analysis, is located slightly above the "knee" of the curve. At this point $E_{eq} = 21,600$ ksi and the tension in the cable is 220 kip. This represents a $\Delta T = -260$ kip (54.1% reduction).

Per Table 6.3, tension in the "main" cables is reduced by as much as $\Delta T = -175$ kip from the original state of 480 kip. This represents a 36% reduction in the tension state of the cable which falls within the range of acceptable values in Fig. 6.18. Therefore, even with a reduction as high as 175 kip, the remaining 305 kip tension in the cables is still high enough to consider that the cables respond within the acceptable linearized range. The modulus is actually reduced to $E_{eq} = 22,951$ ksi which represents only a 4.4% reduction.

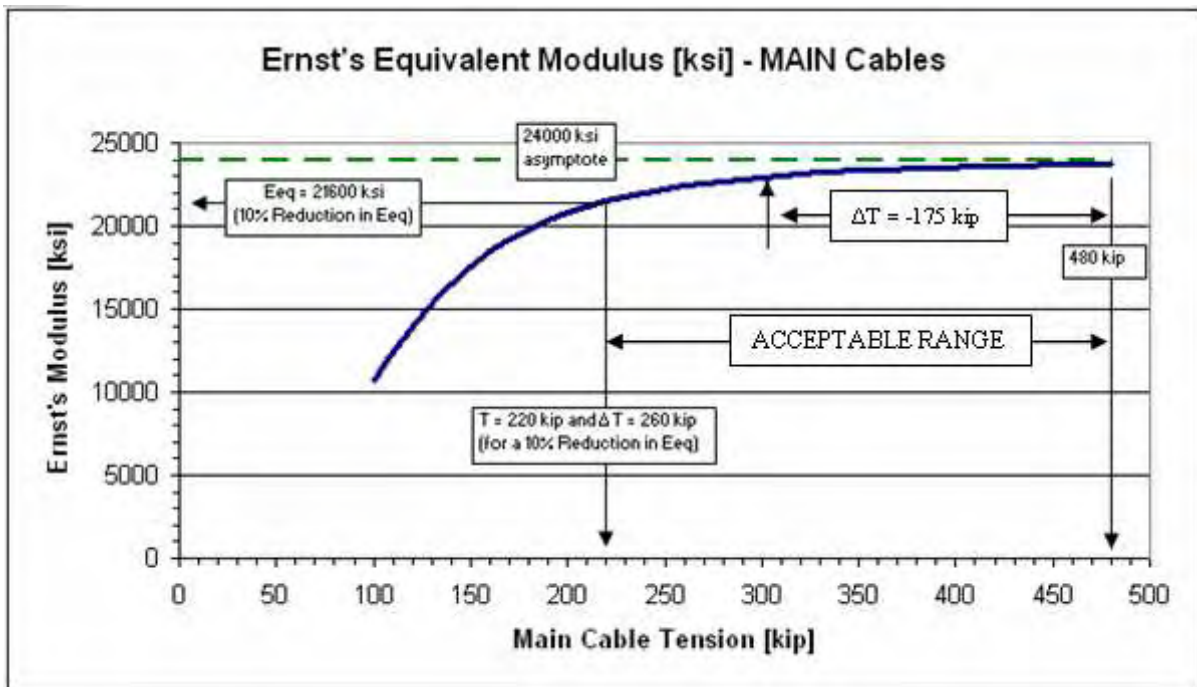


Figure 6.18. Asymptotic behavior of Ernst's equivalent modulus for main cables

The auxiliary backstay of tower T8 shows the highest reduction at $\Delta T = -254$ kip. In this case, the cable starts with an initial tension of 662 kip. It can be shown that all the cables behave similarly to Figure 6.18 and that all variations fall within the acceptable range; therefore the linearized approach to take into account cable sag is validated.

6.8 Consideration of Large Displacements

The literature survey documented in Chapter 1 showed that similarly large and tightly tensioned structures, such as suspension and cable-stayed bridges, did not require consideration of large displacements to obtain accurate results (Ren 1999b, Fleming 1979, Fleming 1980, Nazmy 1990). This was determined by comparing the calculations using large displacements versus the calculations for a linear case that ignored them. In all bridge cases reported in the literature, the results were very similar thus proving that consideration of large displacements is unnecessary. This is a significant finding since consideration of large displacements using the non-linear direct-integration option in SAP2000 requires approximately 14 hours of computing time per single analysis case on a desktop computer running at 2.8GHz with 384 MB of RAM. While in large displacement mode, the program updates the coordinates of each node as the model deforms. In addition, achieving convergence is a very demanding endeavor. On occasions, the solution may converge for the first few seconds into the earthquake and then crash, i.e., this is often an unstable process.

While Chang (2001) cites Fleming (1980) as a basis to ignore large displacements of a long-span cable-stayed bridge, this thesis will make the comparison to test if the Arecibo Observatory structure responds in the same linear manner as a cable-stayed bridge. A case using large displacements will be compared to a linear case that ignores large displacements. The comparison will be performed for both the static case (used to reach the deformed equilibrium state due to dead loads) and a dynamic case. Model B, which includes tiedowns and a uniform platform, will be used for the study. This model is more representative of the structure than Model A (no tiedown cables). It is also not as unstable as Model C in which the tension in the T8 vertical tiedown is nearly zero.

6.8.1 Static P-delta Analysis with Large Displacement Option (Dead Load)

This analysis is the prerequisite case used to reach the deformed equilibrium state due to dead loads. It is necessary to consider any additional cases such as modal analysis or a time-history analysis. The comparison of results is shown in Table 6.9. Note the input temperatures given in the first nine rows of the table (used to apply preload to the cables) are exactly the same in both cases. The initial platform offset in the vertical ('z') direction is

also the same in both cases. The descent of the platform due to dead loads ('platform UZ') shows a difference of only 2.8% which may be considered negligible.

Table 6.9. Comparison with static “large displacements” case (DEAD analysis case)

INPUT	MODEL B P-DELTA	MODEL B P-DELTA WITH LARGE DISPLACEMENTS	% ERROR
TEMP MAIN [F]	0	0	0 (same input)
TEMP AUX [F]	-235	-235	0 (same input)
TEMP GUYMAIN T12 [F]	-505	-505	0 (same input)
TEMP GUYAUX T12 [F]	-540	-540	0 (same input)
TEMP GUYMAIN T8 [F]	-465	-465	0 (same input)
TEMP GUYAUX T8 [F]	-487.5	-487.5	0 (same input)
TEMP GUYMAIN T4 [F]	-515	-515	0 (same input)
TEMP GUYAUX T4 [F]	-520	-520	0 (same input)
TEMP TIEDOWNS [F]	-3300	-3300	0 (same input)
INITIAL Z OFFSET [ft]	10.872	10.872	0 (same input)
OUTPUT			
PLATFORM UZ [ft]	-11.0	-10.7	-2.8%
UX T12 TOWER [in]	-0.00021	-0.0014	N/A
UY T12 TOWER [in]	0.01054	-0.18904	N/A
UX T8 TOWER [in]	-0.06977	0.06235	N/A
UY T8 TOWER [in]	-0.04129	0.03515	N/A
UX T4 TOWER [in]	0.0438	-0.13736	N/A
UY T4 TOWER [in]	-0.02948	0.07695	N/A
TENSION MAIN [kip] 480 k	496	504	1.6%
TENSION AUX [kip] 602 k	608	615	1.1%
TENSION GUYMAIN T12 [kip] 514 k	498	504	1.2%
TENSION GUYAUX T12 [kip] 727 k	665	672	1.0%
TENSION GUYMAIN T8 [kip] 503 k	456	462	1.3%
TENSION GUYAUX T8 [kip] 662 k	599	605	1.0%
TENSION GUYMAIN T4 [kip] 543 k	509	514	1.0%
TENSION GUYAUX T4 [kip] 728 k	640	647	1.1%
TENSION TIEDOWN T12 [kip] 24 k	24.1	39.5	39.0%
TENSION TIEDOWN T8 [kip] 24 k	24.1	39.5	39.0%
TENSION TIEDOWN T4 [kip] 24 k	24.1	39.5	39.0%
MODE SHAPES AND PERIODS			
[A] Platform vertical displacement	2.146	2.104	-2.0%
[B] Platform rotation about East-West axis	1.628	1.654	1.6%
[C] Platform rotation about North-South axis	1.587	1.61	1.4%
[D] 1st Mode Tower T8	2.260	2.262	0.1%
[E] 1st Mode Towers T4 and T12 (in phase)	1.764	1.768	0.2%
[F] 1st Mode Towers T4 and T12 (out of phase)	1.723	1.728	0.3%
[Q] 1st Mode Auxiliary Cables	1.517	1.504	-0.9%
[R] 1st Mode Main Cables	1.283	1.268	-1.2%

The displacements at the top of the towers (“UX T12 TOWER [in]”, etc) are all nearly equal to zero, which meets the criterion of verticality of the towers. Note that the percentage error is not included as it is not appropriate for this comparison. The differences between the displacements are so close to zero that the large resulting percentage errors

would confuse rather than clarify. The displacement itself represents the error since it is the amount by which the top of the towers deviate from the zero-displacement target. Tensions in the main, auxiliary and guy cables are all very similar as well. The largest percentage error in tensions for these is only 1.6% which may be considered negligible.

Only the tiedown cables show a significant difference (39%). The large difference is a consequence of the model itself which requires the vertical tiedown cables to be specified nearly 11 feet longer than their actual length, in order to attach them to the platform (achieve compatibility) in the undeformed state. This requires much more shrinkage of the tiedowns (compared to the other cables) to achieve the correct preload while the platform descends ~ 11 feet under its own weight to reach its correct elevation . The very large shrinkage requirement is evidenced by the large temperature (3300° F per Table 6.9) required to create the necessary compressive thermal strain. The vertical tiedown cables are the only structural component for which the large-displacement option shows an effect. Note that since the towers are meeting the verticality criterion and the platform has descended to its expected elevation with the given input, the only change to the model would be to iterate on the tiedown temperatures to achieve the correct tension of 24 kip per cable. This would require lowering the specified temperature slightly from its current value of -3300° F until the correct tiedown tension is achieved. The effect of this change on the rest of the structure would be negligible. Therefore, the only difference between the large-displacement model and the linear model would be the input temperature of the tiedown cables. The output would be nearly identical with maximum differences on the order of 3%, as shown in Table 6.9, which are considered negligible. It can be concluded that accounting for large displacements is unnecessary to achieve the deformed equilibrium state due to dead loads.

6.8.2 Large-Displacement Non-Linear Direct-Integration Case – Loma Prieta

This is the most complex dynamic analysis option that SAP2000 offers. Convergence is very highly dependent on the number of elements, the time-step size, the number of iterations allowed, and the integration parameters. In the Loma Prieta case, the solution was repeatedly made to converge only for the first 4.8 seconds and then it crashed (with the Coalinga earthquake, considered in the next section, SAP2000 was able to complete the run). Nevertheless, the results indicate a very similar response between analyses types; therefore, linear modal time-history are acceptable and large displacement consideration is unnecessary. This finding reinforces the conclusions of the literature survey. The comparisons are shown in the next eight figures.

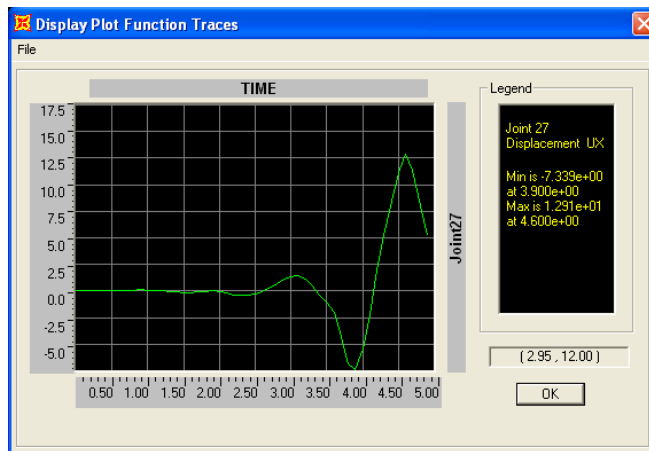


Figure 6.19. Nonlinear with large displacements – Ux disp. at top of T12 [in]. All components of Loma Prieta earthquake included – (Model B)

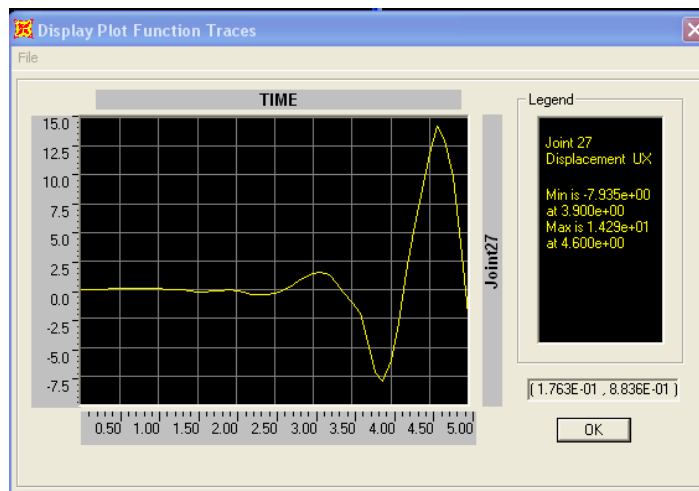


Figure 6.20. Linear modal analysis – Ux disp. at top of T12 [in]. All components of Loma Prieta earthquake included – (Model B)

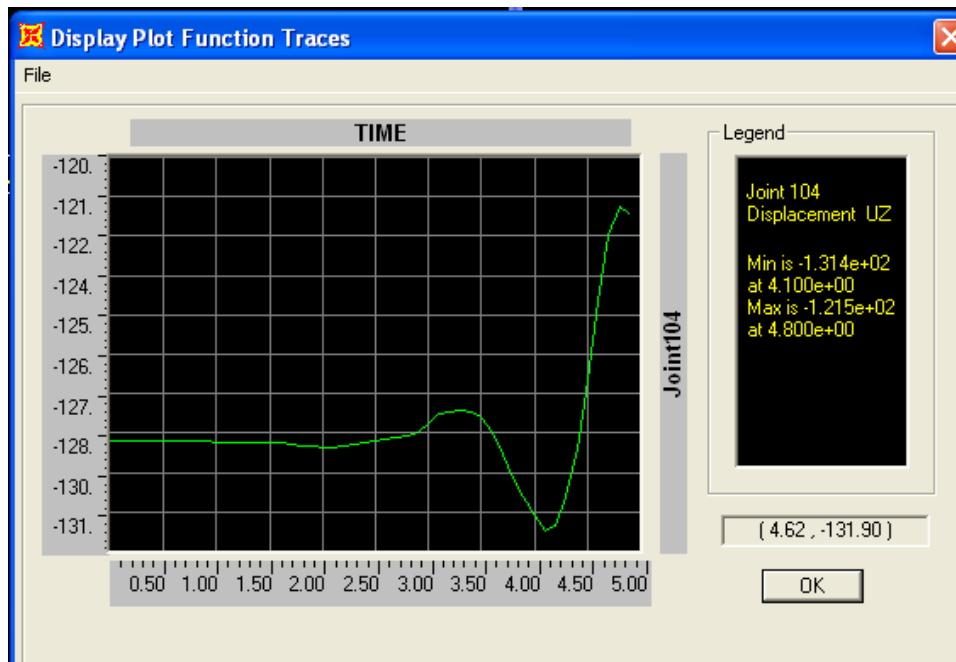


Figure 6.21. Nonlinear with large displacements – z displacement at platform. All components of Loma Prieta earthquake included – (Model B). (Note the 128 inch descent of the platform remains in the analysis)

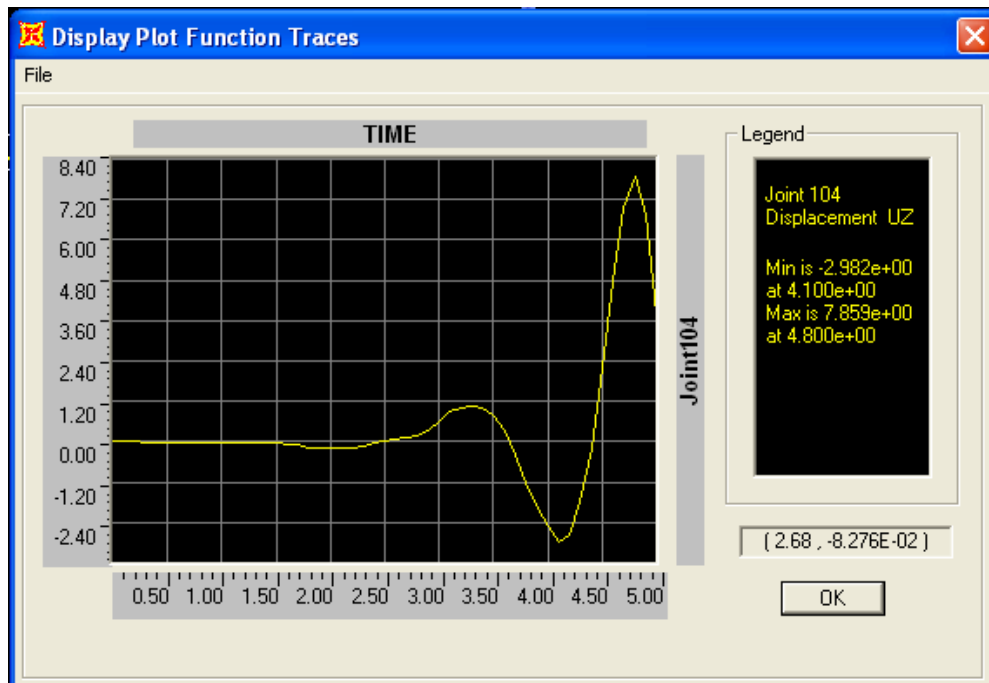


Figure 6.22. Linear modal analysis – z displacement at platform. All components of Loma Prieta earthquake included – (Model B)

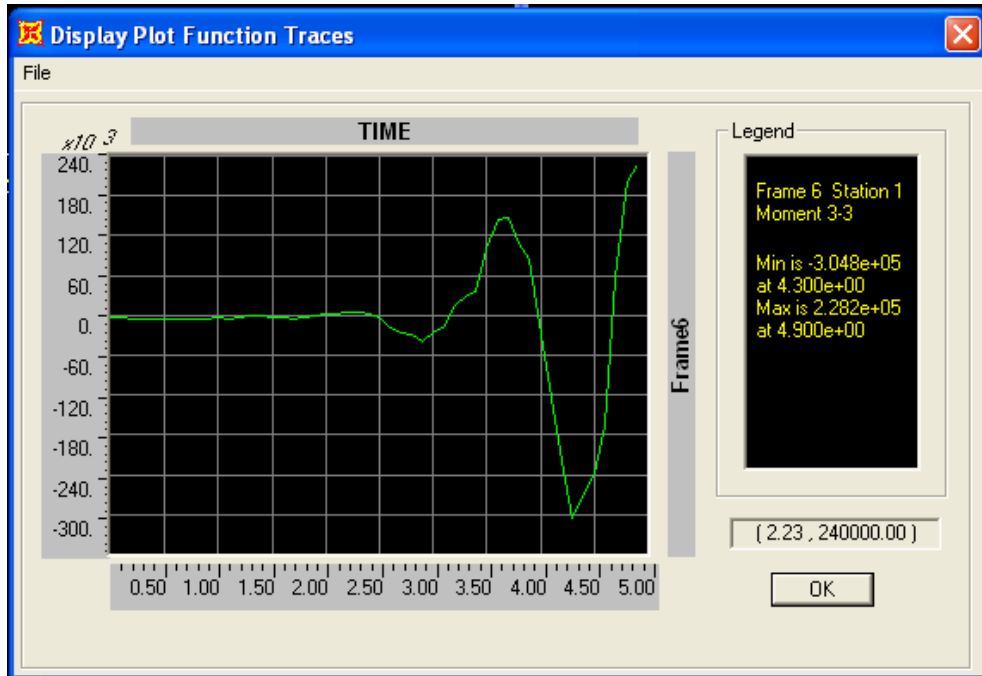


Figure 6.23. Nonlinear with large displacements – M_{33} [kip-ft] at base of T8. All components of Loma Prieta earthquake included – (Model B)

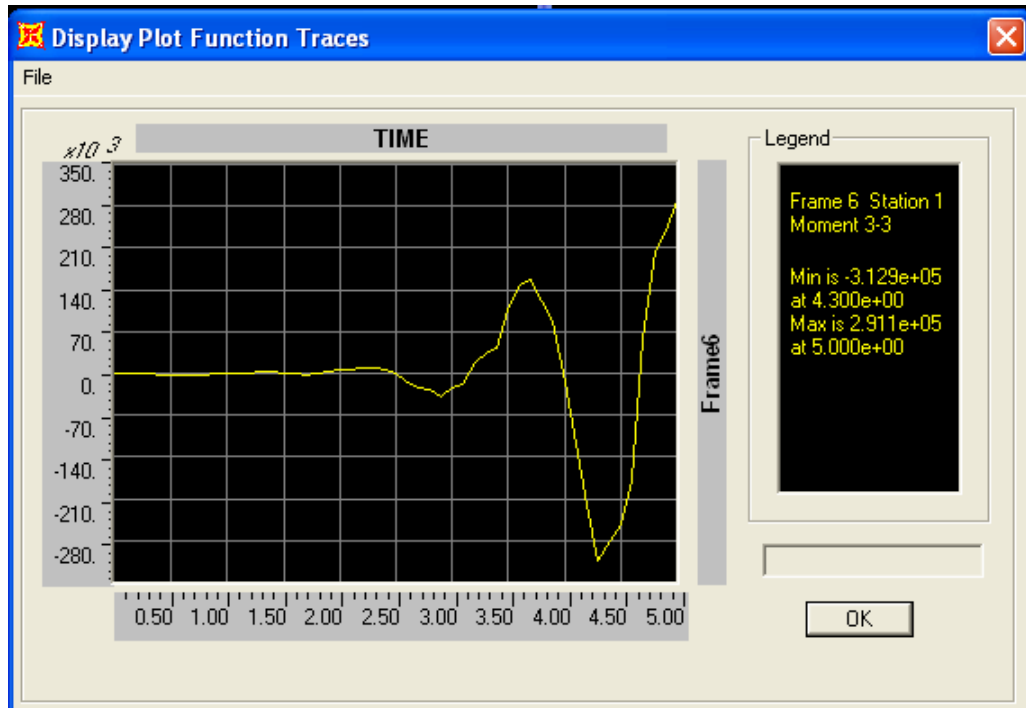


Figure 6.24. Linear modal analysis – M_{33} [kip-ft] at base of T8. All components of Loma Prieta earthquake included – (Model B)

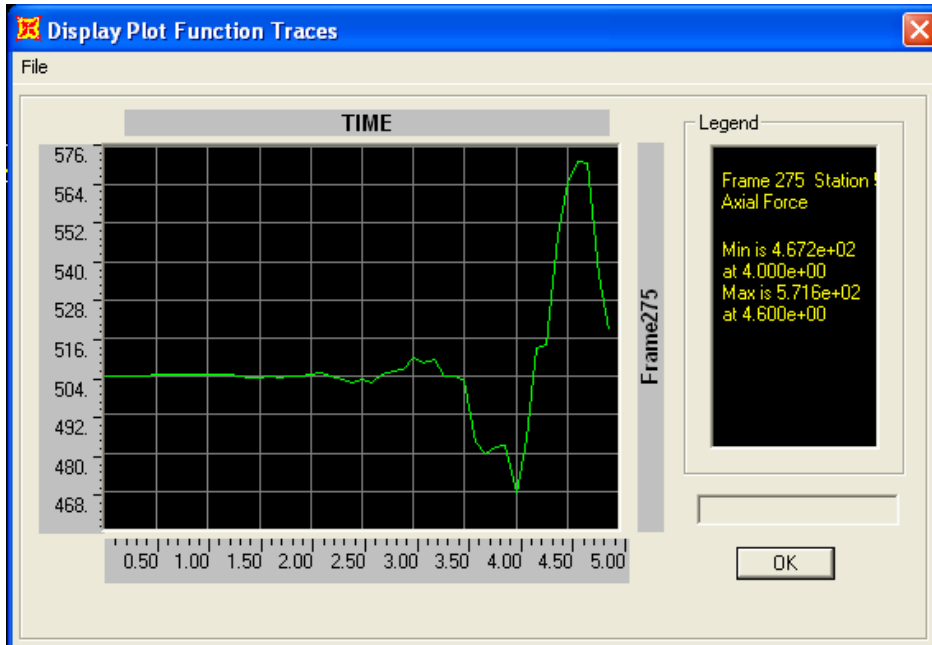


Figure 6.25. Nonlinear with large displacements – Tension T8 Main Cable [kip]. All components of Loma Prieta earthquake included – (Model B). (Note the initial tension of 504 kip remains in the analysis)

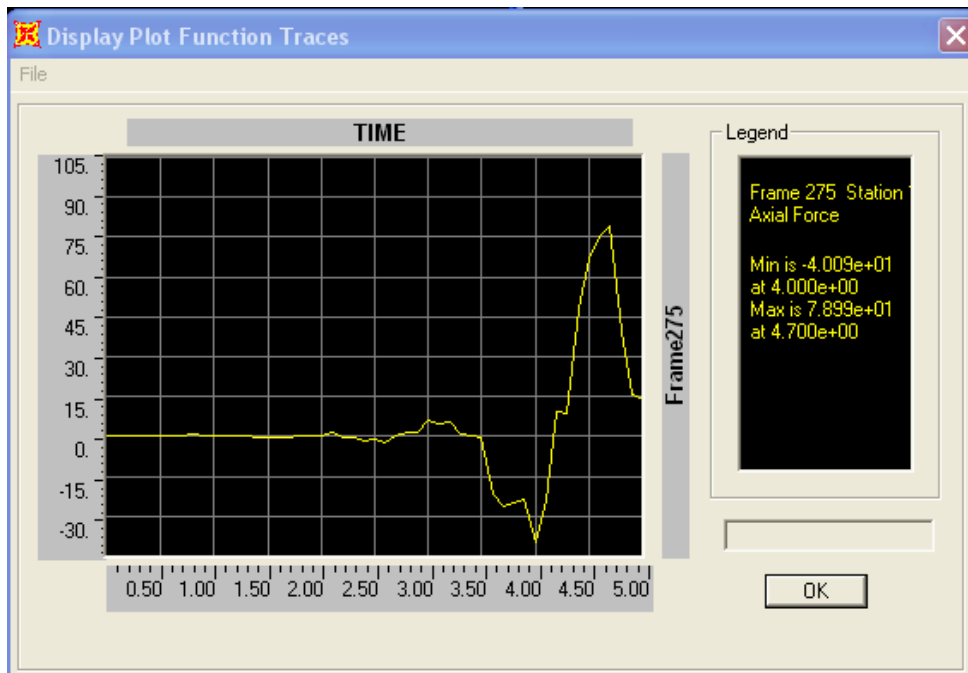


Figure 6.26. Linear modal analysis – Tension T8 Main Cable [kip]. All components of Loma Prieta earthquake included – (Model B)

6.8.3 Large-displacement Non-Linear Direct-Integration Case – Coalinga

Convergence throughout the entire record was achieved with the Coalinga record which is a less severe earthquake than Loma Prieta. The elapsed time to run the single analysis was approximately 14 hours on a desktop computer running at 2.8GHz with 384 MB of RAM. The bending moment variation throughout the earthquake at the base of tower T8 is essentially equal, as shown in Figure 6.27 (large displacement) and Figure 6.28 (linear).

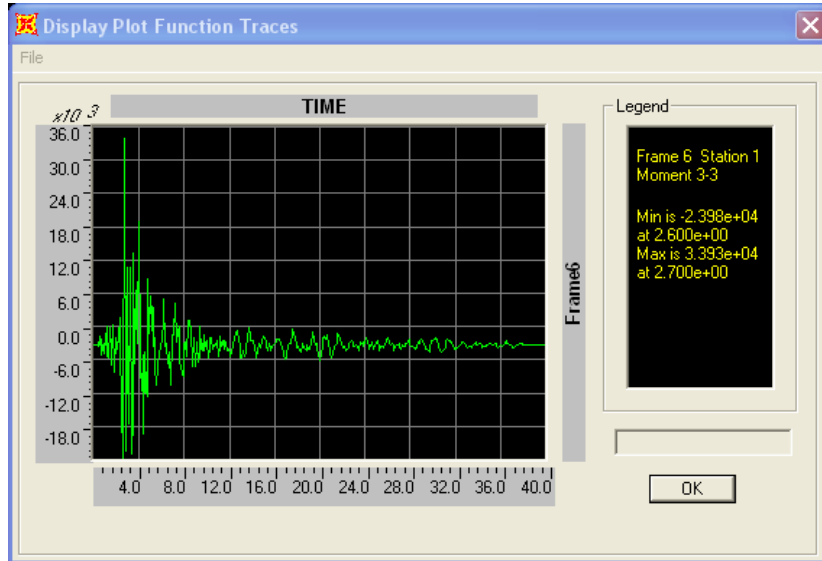


Figure 6.27. Nonlinear with large displacements – M_{33} [kip-ft] at base of T8. All components of Coalinga earthquake included – (Model B)

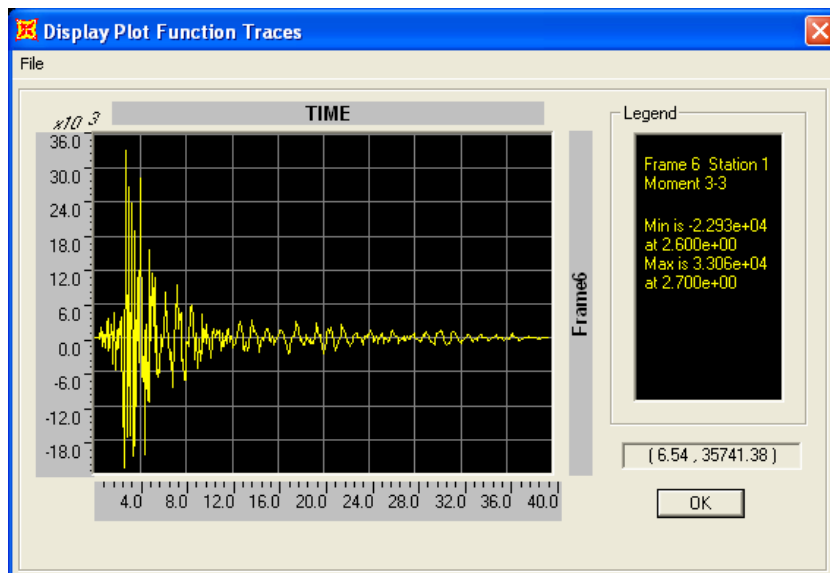


Figure 6.28. Linear modal analysis – M_{33} [kip-ft] at base of T8. All components of Loma Prieta earthquake included – (Model B)

Table 6.10 includes a comparison between the two cases. An additional “Delta” column (difference between MAX and MIN) has been added to facilitate the comparison since the Non-linear large-displacement case does not reset stresses to zero. Although the results are not identical, it can be concluded that the linear modal time-history analysis provides excellent results. Accounting for large displacements is therefore unnecessary. This finding verifies the conclusions reported in the literature survey and shows that the Arecibo Observatory behaves like a cable-stayed bridge in this respect.

Table 6.10. Comparison of non-linear large displacements vs linear modal results

Label	Description	Linear Modal Time-History			NonLinear Large Disp Time-History		
		COALINGA			COALINGA		
		MAX	MIN	Delta	MAX	MIN	Delta
	UX Displacement						
J27	Top of tower T12 [in]	0.5	-0.7	1.2	0.4	-0.7	1.1
J36	Top of tower T8 [in]	0.7	-0.7	1.4	0.7	-0.5	1.2
J43	Top of tower T4 [in]	0.4	-0.4	0.8	0.2	-0.6	0.8
	UY Displacement						
J27	Top of tower T12 [in]	0.4	-0.5	0.9	0.14	-0.6	0.74
J36	Top of tower T8 [in]	0.8	-0.8	1.6	0.7	-0.7	1.4
J43	Top of tower T4 [in]	0.5	-0.6	1.1	0.5	-0.45	0.95
	UZ Displacement						
J99	Platform corner T12 [in]	0.3	-0.3	0.6	-128.4	-128.9	0.5
J104	Platform corner T8 [in]	0.4	-0.3	0.7	-128.4	-129.0	0.6
J111	Platform corner T4 [in]	0.4	-0.4	0.8	-128.3	-129.0	0.7
	M33 Moment						
F4 R 1	Top of tower T12 [kip-ft]	208	-172	380	2884	2451	433
F11 R 1	Top of tower T8 [kip-ft]	467	-280	747	1993	1354	639
F16 R 1	Top of tower T4 [kip-ft]	336	-220	556	3085	2500	585
F1 R 0	Base of tower T12 [kip-ft]	11080	-18070	29150	5445	-23610	29055
F6 R 0	Base of tower T8 [kip-ft]	33060	-22930	55990	33930	-23980	57910
F13 R 0	Base of tower T4 [kip-ft]	22010	-14800	36810	17570	-15470	33040
	M22 Moment						
F1 R 0	Base of tower T12 [kip-ft]	14800	-12740	27540	14730	-13380	28110
F6 R 0	Base of tower T8 [kip-ft]	54500	-39920	94420	54670	-27320	81990
F13 R 0	Base of tower T4 [kip-ft]	19330	-15150	34480	15030	-15430	30460
	ΔTENSION						
F271 R 0.5	Main Cable T12 [kip]	12	-8	20	514	498	16
F275 R 0.5	Main Cable T8 [kip]	8	-11	19	510	494	16
F280 R 0.5	Main Cable T4 [kip]	11	-12	23	515	494	21
F282 R 0.5	Auxiliary Cable T12 [kip]	10	-8	18	624	608	16
F284 R 0.5	Auxiliary Cable T8 [kip]	6	-9	15	622	607	15
F287 R 0.5	Auxiliary Cable T4 [kip]	11	-10	21	626	607	19
F251 R 0.5	Main Backstay T12 [kip]	10	-9	19	514	497	17
F256 R 0.5	Main Backstay T8 [kip]	12	-9	21	474	455	19
F261 R 0.5	Main Backstay T4 [kip]	10	-9	19	523	506	17
F264 R 0.5	Auxiliary Backstay T12 [kip]	10	-10	20	682	663	19
F267 R 0.5	Auxiliary Backstay T8 [kip]	12	-10	22	617	597	20
F269 R 0.5	Auxiliary Backstay T4 [kip]	13	-11	24	658	638	20
F289 R 0.5	Tiedown T12 TENSION [kip]	2	-2	4	42	38	4
F291 R 0.5	Tiedown T8 TENSION [kip]	3	-3	6	42	38	4
F292 R 0.5	Tiedown T4 TENSION [kip]	3	-3	6	42	37	5

6.9 Results for the Six Earthquake Records (Model A: No Tiedowns, Uniform Platform)

The results for the six earthquakes are shown in Tables 6.11 and 6.12. Only the results corresponding to the combined three orthogonal earthquake records are included.

Table 6.11. Results for Loma Prieta, El Centro and Chi Chi earthquakes – Model A

		MODEL A					
		Loma Prieta		El Centro		Chi Chi, Taiwan	
		U1, U2, and U3		U1, U2, and U3		U1, U2, and U3	
Label	Description	MAX	MIN	MAX	MIN	MAX	MIN
	UX Displacement						
J27	Top of tower T12 [in]	15.9	-19.2	9.4	-10.2	8.7	-7.4
J36	Top of tower T8 [in]	7.8	-7.6	15.1	-14.1	9.4	-8.3
J43	Top of tower T4 [in]	8.9	-11.1	6.0	-5.6	3.4	-5.6
	UY Displacement						
J27	Top of tower T12 [in]	4.2	-3.6	3.1	-2.8	2.6	-2.8
J36	Top of tower T8 [in]	6.3	-7.5	20.8	-25.2	6.6	-8.7
J43	Top of tower T4 [in]	11.1	-12.6	6.4	-7.1	4.4	-5.6
	UZ Displacement						
J99	Platform corner T12 [in]	7.5	-10.1	6.7	-6.3	6.9	-8.3
J104	Platform corner T8 [in]	14.1	-16.1	14.0	-10.3	12.2	-16.3
J111	Platform corner T4 [in]	9.1	-10.2	11.6	-15.9	10.6	-8.9
	M33 Moment						
F4 R 1	Top of tower T12 [kip-ft]	1365	-2023	1248	-1410	1549	1448
F11 R 1	Top of tower T8 [kip-ft]	3206	-2941	1870	-2359	2229	-1819
F16 R 1	Top of tower T4 [kip-ft]	1131	-1360	1652	-1721	1693	-1622
F1 R 0	Base of tower T12 [kip-ft]	123000	-91710	85070	-108100	87520	-90520
F6 R 0	Base of tower T8 [kip-ft]	361500	-344900	272700	-223700	180200	-197900
F13 R 0	Base of tower T4 [kip-ft]	74050	-106400	103200	-106700	95960	-116100
	M22 Moment						
F1 R 0	Base of tower T12 [kip-ft]	164700	-117900	119800	-108000	70170	-68690
F6 R 0	Base of tower T8 [kip-ft]	105600	-150800	326500	-264700	152400	-202500
F13 R 0	Base of tower T4 [kip-ft]	132400	-166700	85280	-71940	62320	-73150
	ΔTENSION						
F271 R 0.5	Main Cable T12 [kip]	103	-90.2	77	-93	67	-61
F275 R 0.5	Main Cable T8 [kip]	177	-175	112	-112	112	-72
F280 R 0.5	Main Cable T4 [kip]	92.7	-109	102	-83	102	-91
F282 R 0.5	Auxiliary Cable T12 [kip]	65.6	-106	85	-103	64	-65
F284 R 0.5	Auxiliary Cable T8 [kip]	132	-114	79	-84	104	-77
F287 R 0.5	Auxiliary Cable T4 [kip]	78.9	-108	78	-101	115	-82
F251 R 0.5	Main Backstay T12 [kip]	80.1	-91.8	61	-67	63	-57
F256 R 0.5	Main Backstay T8 [kip]	220	-207	131	-141	97	-104
F261 R 0.5	Main Backstay T4 [kip]	111	-87.5	58	-68	74	-52
F264 R 0.5	Auxiliary Backstay T12 [kip]	108	-113	72	-84	71	-63
F267 R 0.5	Auxiliary Backstay T8 [kip]	254	-244	166	-162	115	-102
F269 R 0.5	Auxiliary Backstay T4 [kip]	125	-110	67	-74	85	-59

Table 6.12. Results for Kocaeli, San Fernando and Coalinga earthquakes – Model A

		MODEL A					
		Kocaeli, Turkey		San Fernando		Coalinga	
		U1, U2, and U3		U1, U2, and U3		U1, U2, and U3	
Label	Description	MAX	MIN	MAX	MIN	MAX	MIN
UX Displacement							
J27	Top of tower T12 [in]	16.1	-16.7	4.9	-6.5	0.5	-0.7
J36	Top of tower T8 [in]	12.8	-9.4	2.8	-2.9	0.7	-0.7
J43	Top of tower T4 [in]	8.0	-8.2	2.1	-4.0	0.4	-0.4
UY Displacement							
J27	Top of tower T12 [in]	2.8	-3.0	1.5	-1.8	0.4	-0.5
J36	Top of tower T8 [in]	17.0	-11.9	2.0	-2.2	0.8	-0.8
J43	Top of tower T4 [in]	12.7	-14.6	4.4	-4.4	0.5	-0.6
UZ Displacement							
J99	Platform corner T12 [in]	34.5	-29.3	2.3	-2.5	0.2	-0.2
J104	Platform corner T8 [in]	17.6	-18.4	3.7	-4.8	0.2	-0.3
J111	Platform corner T4 [in]	11.4	-10.7	2.3	-1.8	0.3	-0.2
M33 Moment							
F4 R 1	Top of tower T12 [kip-ft]	1721	-1475	1241	-904	205	-173
F11 R 1	Top of tower T8 [kip-ft]	2776	-2407	1587	-1696	468	-282
F16 R 1	Top of tower T4 [kip-ft]	11212	-1255	992	-1036	338	-228
M22 Moment							
F1 R 0	Base of tower T12 [kip-ft]	107700	-110600	61460	-44280	11190	-18080
F6 R 0	Base of tower T8 [kip-ft]	326400	-343300	141500	-197600	33090	-23050
F13 R 0	Base of tower T4 [kip-ft]	70390	-94470	71770	-63330	22040	-14780
M22 Moment							
F1 R 0	Base of tower T12 [kip-ft]	157400	-150500	53360	-70030	14800	-12730
F6 R 0	Base of tower T8 [kip-ft]	227700	-266700	67410	-64550	54500	-40020
F13 R 0	Base of tower T4 [kip-ft]	168000	-151000	62130	-42110	19340	-15150
ΔTENSION							
F271 R 0.5	Main Cable T12 [kip]	61	-109	37	-37	11	-8
F275 R 0.5	Main Cable T8 [kip]	153	-119	62	-60	8	-10
F280 R 0.5	Main Cable T4 [kip]	94	-132	46	-47	11	-12
M22 Moment							
F282 R 0.5	Auxiliary Cable T12 [kip]	93	-97	33	-32	10	-8
F284 R 0.5	Auxiliary Cable T8 [kip]	111	-123	51	-44	6	-9
F287 R 0.5	Auxiliary Cable T4 [kip]	100	-83	43	-30	10	-10
M22 Moment							
F251 R 0.5	Main Backstay T12 [kip]	67	-63	40	-34	10	-9
F256 R 0.5	Main Backstay T8 [kip]	180	-154	72	-71	13	-9
F261 R 0.5	Main Backstay T4 [kip]	88	-109	32	-28	10	-8
M22 Moment							
F264 R 0.5	Auxiliary Backstay T12 [kip]	93	-97	46	-35	10	-10
F267 R 0.5	Auxiliary Backstay T8 [kip]	187	-172	78	-83	13	-10
F269 R 0.5	Auxiliary Backstay T4 [kip]	117	-130	37	-35	13	-10

In general, the results are as expected. The Loma Prieta, El Centro, Chi Chi, and Kocaeli earthquakes are indeed the worst cases. San Fernando was of medium severity and, finally, Coalinga was the weakest. Also as expected, the Loma Prieta earthquake turned out to be the worst case for many of the response items investigated. Figure 6.11 shows a deformed shape of the structure 5.1 seconds into the Loma Prieta earthquake when the highest M_{33} bending moments at the base of tower T8 are recorded.

6.10 Results for the Six Earthquake Records (Model B: Tiedowns, Uniform Platform)

Similar results as those presented in Tables 6.11 and 6.12 are shown in Tables 6.13 and 6.14 but for Model B. Only the results corresponding to the combined three orthogonal earthquake records are included.

Table 6.13. Results for Loma Prieta, El Centro and Chi Chi earthquakes – Model B

Label	Description	MODEL B					
		Loma Prieta		El Centro		Chi Chi, Taiwan	
		U1, U2, and U3		U1, U2, and U3		U1, U2, and U3	
		MAX	MIN	MAX	MIN	MAX	MIN
	UX Displacement						
J27	Top of tower T12 [in]	15.5	-19.3	9.2	-10.8	8.8	-6.8
J36	Top of tower T8 [in]	4.8	-6.7	15.9	-12.6	8.9	-7.2
J43	Top of tower T4 [in]	8.3	-10.8	4.4	-4.7	3.6	-4.4
	UY Displacement						
J27	Top of tower T12 [in]	2.9	-2.8	2.3	-2.1	1.8	-2.2
J36	Top of tower T8 [in]	5.1	-5.5	23	-26.2	7.6	-9.2
J43	Top of tower T4 [in]	9.1	-12.9	6.6	-7.6	4.6	-6.8
	UZ Displacement						
J99	Platform corner T12 [in]	8.6	-7.3	6.6	-6.2	7.6	8.8
J104	Platform corner T8 [in]	16.8	-16.1	7.1	-7.1	9.2	-7.3
J111	Platform corner T4 [in]	9.7	-11.2	6.7	-7.4	9.1	-11.3
	M33 Moment						
F4 R 1	Top of tower T12 [kip-ft]	1406	-1739	1222	-1361	1458	-1296
F11 R 1	Top of tower T8 [kip-ft]	2993	-3023	1750	-1892	2909	-2269
F16 R 1	Top of tower T4 [kip-ft]	1057	-1171	1549	-1712	1704	-1744
F1 R 0	Base of tower T12 [kip-ft]	106200	-86560	76030	-107200	77670	-86080
F6 R 0	Base of tower T8 [kip-ft]	347000	-324200	291400	-263100	277500	-280900
F13 R 0	Base of tower T4 [kip-ft]	45280	-88110	103600	-118100	105200	-106900
	M22 Moment						
F1 R 0	Base of tower T12 [kip-ft]	162800	-117600	117700	-108100	78130	-72020
F6 R 0	Base of tower T8 [kip-ft]	105500	-150400	327300	-269200	153900	-203600
F13 R 0	Base of tower T4 [kip-ft]	133000	-164700	84440	-79990	61920	-73600
	ΔTENSION						
F271 R 0.5	Main Cable T12 [kip]	54	-91	73	-66	58	-73
F275 R 0.5	Main Cable T8 [kip]	115	101	57	-54	49	-37
F280 R 0.5	Main Cable T4 [kip]	65	-59	78	-72	73	-81
F282 R 0.5	Auxiliary Cable T12 [kip]	49	-88	80	-99	66	-69
F284 R 0.5	Auxiliary Cable T8 [kip]	158	-159	94	-91	64	-54
F287 R 0.5	Auxiliary Cable T4 [kip]	102	-90	63	-86	75	-67
F251 R 0.5	Main Backstay T12 [kip]	62	-63	45	-51	47	-41
F256 R 0.5	Main Backstay T8 [kip]	135	-129	75	-92	116	-95
F261 R 0.5	Main Backstay T4 [kip]	81	-53	56	-62	55	-68
F264 R 0.5	Auxiliary Backstay T12 [kip]	96	-80	45	-60	68	-40
F267 R 0.5	Auxiliary Backstay T8 [kip]	157	-153	122	-107	141	-118
F269 R 0.5	Auxiliary Backstay T4 [kip]	76	-46	62	-74	63	-79
F289 R 0.5	Tiedown T12 TENSION [kip]	66	-54	51	-46	53	-63
F291 R 0.5	Tiedown T8 TENSION [kip]	132	-126	55	-55	65	-57
F292 R 0.5	Tiedown T4 TENSION [kip]	73	-87	52	-59	66	-80

Table 6.14. Results for Kocaeli, San Fernando and Coalinga earthquakes – Model B

		MODEL B					
		Kocaeli, Turkey		San Fernando		Coalinga	
		U1, U2, and U3		U1, U2, and U3		U1, U2, and U3	
Label	Description	MAX	MIN	MAX	MIN	MAX	MIN
	UX Displacement						
J27	Top of tower T12 [in]	16.1	-16.9	4.9	-6.5	0.5	-0.7
J36	Top of tower T8 [in]	11.4	-8.9	2.6	-2.8	0.7	-0.7
J43	Top of tower T4 [in]	8.5	-9.1	2.4	-4.0	0.4	-0.4
	UY Displacement						
J27	Top of tower T12 [in]	3.0	-3.1	1.1	-1.4	0.4	-0.5
J36	Top of tower T8 [in]	18.0	-13.1	2.5	-1.7	0.8	-0.8
J43	Top of tower T4 [in]	11.1	-13.2	4.6	-4.4	0.5	-0.6
	UZ Displacement						
J99	Platform corner T12 [in]	9.6	-10.1	3.6	-3.7	0.3	-0.3
J104	Platform corner T8 [in]	15.0	-10.3	5.3	-5.0	0.4	-0.3
J111	Platform corner T4 [in]	11.3	-11.6	3.8	-3.2	0.4	-0.4
	M33 Moment						
F4 R 1	Top of tower T12 [kip-ft]	1364	-1579	1199	-826	208	-172
F11 R 1	Top of tower T8 [kip-ft]	2758	-2600	1613	-1672	467	-280
F16 R 1	Top of tower T4 [kip-ft]	869	-1525	940	-1000	336	-220
F1 R 0	Base of tower T12 [kip-ft]	97350	-104800	57020	-42880	11080	-18070
F6 R 0	Base of tower T8 [kip-ft]	314200	-321900	165500	-197900	33060	-22930
F13 R 0	Base of tower T4 [kip-ft]	77920	-77420	69700	-64060	22010	-14800
	M22 Moment						
F1 R 0	Base of tower T12 [kip-ft]	157400	-152800	53390	-69570	14800	-12740
F6 R 0	Base of tower T8 [kip-ft]	228000	-278400	67480	-64330	54500	-39920
F13 R 0	Base of tower T4 [kip-ft]	169100	-152700	61680	-42140	19330	-15150
	ΔTENSION						
F271 R 0.5	Main Cable T12 [kip]	67	-78	32	-28	12	-8
F275 R 0.5	Main Cable T8 [kip]	100	-97	39	-26	8	-11
F280 R 0.5	Main Cable T4 [kip]	75	-76	37	-38	11	-12
F282 R 0.5	Auxiliary Cable T12 [kip]	93	-72	25	-27	10	-8
F284 R 0.5	Auxiliary Cable T8 [kip]	166	-153	44	-49	6	-9
F287 R 0.5	Auxiliary Cable T4 [kip]	91	-104	36	-40	11	-10
F251 R 0.5	Main Backstay T12 [kip]	70	-66	32	-25	10	-9
F256 R 0.5	Main Backstay T8 [kip]	136	-136	64	-69	12	-9
F261 R 0.5	Main Backstay T4 [kip]	69	-65	32	-20	10	-9
F264 R 0.5	Auxiliary Backstay T12 [kip]	107	-100	36	-29	10	-10
F267 R 0.5	Auxiliary Backstay T8 [kip]	138	-152	75	-81	12	-10
F269 R 0.5	Auxiliary Backstay T4 [kip]	71	-80	34	-23	13	-11
F289 R 0.5	Tiedown T12 TENSION [kip]	70	-69	26	-26	2	-2
F291 R 0.5	Tiedown T8 TENSION [kip]	113	-78	41	-40	3	-3
F292 R 0.5	Tiedown T4 TENSION [kip]	80	-93	28	-25	3	-3

The results are very similar to Tables 6.11 and 6.12. In general, the addition of tiedowns did not modify significantly the state of stress in the towers nor the displacements. The M_{33} moment at the base of tower T8 for Loma Prieta was reduced 4% from 361,500 kip-ft to 347,000 kip-ft. For El Centro, however, an increase of 6% is seen at the same location from 272,700 kip-ft to 291,400 kip-ft. In general, the tiedowns are not influencing the results dramatically.

Figure 6.29 shows the deformed shape at 5.1 seconds into the Loma Prieta earthquake. Note that this shape is very similar to Figure 6.11 for Model A, i.e., the tiedowns have not modified significantly the results of the model. Note that tower T8 is in a second mode vibration pattern whereas towers T4 and T12 are mostly vibrating in their first mode. At this time the structure exhibits the highest bending moment $M_{33} = 347,000$ kip-ft at the base of tower T8.

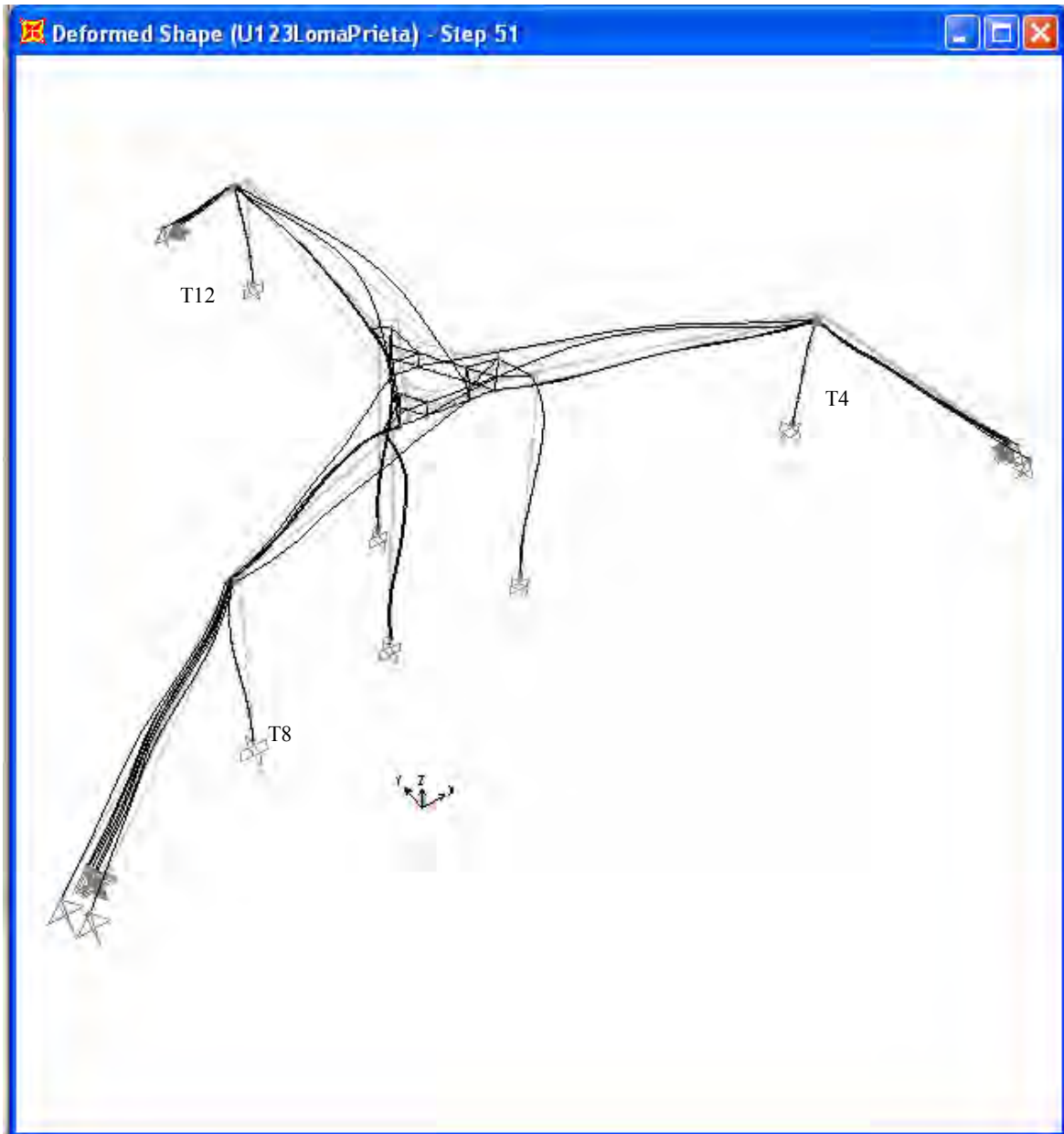


Figure 6.29. Deformed shape (50x mag.) of structure 5.1 sec into Loma Prieta. Model B (Tiedowns, Uniform Platform)

6.11 Results for the Six Earthquake Records (Model C: Tiedowns, Dome)

The next set of results corresponds to Model C which includes the Gregorian Dome. Tables 6.15 and 6.16 show the response quantities for the six earthquakes considered. Only the results corresponding to the combined three orthogonal earthquake records are included.

Table 6.15. Results for Loma Prieta, El Centro and Chi Chi earthquakes – Model C

Label	Description	MODEL C					
		Loma Prieta		El Centro		Chi Chi, Taiwan	
		U1, U2, and U3		U1, U2, and U3		U1, U2, and U3	
		MAX	MIN	MAX	MIN	MAX	MIN
	UX Displacement						
J27	Top of tower T12 [in]	15.8	-19.5	9.8	-10.8	8.6	-7.2
J36	Top of tower T8 [in]	6.8	-8.2	15.2	-14.0	8.3	-7.9
J43	Top of tower T4 [in]	10	-11.7	5.7	-4.8	3.4	-5.0
	UY Displacement						
J27	Top of tower T12 [in]	4.4	-4.2	3.4	-3.0	2.2	-2.9
J36	Top of tower T8 [in]	6.6	-6.3	22.1	-26.7	7.3	-9.5
J43	Top of tower T4 [in]	10.7	-12.4	6.0	-6.7	4.3	-5.9
	UZ Displacement						
J99	Platform corner T12 [in]	3.2	-2.9	2.3	-2.0	4.4	-3.0
J104	Platform corner T8 [in]	4.6	-4.5	2.6	-2.7	3.8	-4.1
J111	Platform corner T4 [in]	3.7	-2.9	1.7	-2.0	4.0	-3.2
	M33 Moment						
F4 R 1	Top of tower T12 [kip-ft]	1407	-1950	1206	-1445	1556	-1401
F11 R 1	Top of tower T8 [kip-ft]	2958	-2987	1720	-2157	2219	-2192
F16 R 1	Top of tower T4 [kip-ft]	1204	-1210	1570	-1671	1786	-1730
F1 R 0	Base of tower T12 [kip-ft]	119900	-95430	86310	-110900	83770	-92630
F6 R 0	Base of tower T8 [kip-ft]	341800	-309600	242600	-198700	225900	-237300
F13 R 0	Base of tower T4 [kip-ft]	58500	-100600	97060	-106600	95940	-120500
	M22 Moment						
F1 R 0	Base of tower T12 [kip-ft]	163800	-117900	120700	-110400	71630	-70110
F6 R 0	Base of tower T8 [kip-ft]	105600	-150100	330300	-271100	154500	-204600
F13 R 0	Base of tower T4 [kip-ft]	133200	-165600	85900	-72160	61410	-75740
	ΔTENSION						
F271 R 0.5	Main Cable T12 [kip]	86	-108	75	-84	60	-75
F275 R 0.5	Main Cable T8 [kip]	191	-186	104	-107	79	-79
F280 R 0.5	Main Cable T4 [kip]	88	-107	76	-82	94	-82
F282 R 0.5	Auxiliary Cable T12 [kip]	58	-102	84	-97	59	-82
F284 R 0.5	Auxiliary Cable T8 [kip]	173	-174	94	-89	89	-82
F287 R 0.5	Auxiliary Cable T4 [kip]	81	-113	78	-105	92	-87
F251 R 0.5	Main Backstay T12 [kip]	94	-96	64	-75	63	-50
F256 R 0.5	Main Backstay T8 [kip]	211	-182	107	-121	79	-92
F261 R 0.5	Main Backstay T4 [kip]	114	-89	57	-68	59	-48
F264 R 0.5	Auxiliary Backstay T12 [kip]	122	-116	67	-93	74	-49
F267 R 0.5	Auxiliary Backstay T8 [kip]	242	-210	146	-140	95	-87
F269 R 0.5	Auxiliary Backstay T4 [kip]	123	-87	65	-77	67	-55
F289 R 0.5	Tiedown T12 TENSION [kip]	22	-20	15	-13	23	-14
F291 R 0.5	Tiedown T8 TENSION [kip]	36	-34	18	-18	22	-23
F292 R 0.5	Tiedown T4 TENSION [kip]	26	-20	12	-12	21	-18

Table 6.16. Results for Kocaeli, San Fernando and Coalinga earthquakes – Model C

Label	Description	MODEL C					
		Kocaeli, Turkey		San Fernando		Coalinga	
		U1, U2, and U3		U1, U2, and U3		U1, U2, and U3	
		MAX	MIN	MAX	MIN	MAX	MIN
	UX Displacement						
J27	Top of tower T12 [in]	16.4	-17.3	5.0	-6.5	0.5	-0.7
J36	Top of tower T8 [in]	12.6	-9.9	2.7	-2.9	0.7	-0.7
J43	Top of tower T4 [in]	9.1	-9.0	2.1	-4.1	0.4	-0.5
	UY Displacement						
J27	Top of tower T12 [in]	2.6	-3.2	1.2	-2.0	0.4	-0.5
J36	Top of tower T8 [in]	17.1	-13.6	2.1	-2.2	0.8	-0.8
J43	Top of tower T4 [in]	13.0	-14.5	4.4	-4.4	0.5	-0.6
	UZ Displacement						
J99	Platform corner T12 [in]	4.7	-4.8	0.8	-0.8	0.1	-0.1
J104	Platform corner T8 [in]	5.7	-6.0	1.3	-1.4	0.1	-0.1
J111	Platform corner T4 [in]	4.7	-4.4	0.7	-0.8	0.1	-0.1
	M33 Moment						
F4 R 1	Top of tower T12 [kip-ft]	1477	-1669	1280	-917	210	-172
F11 R 1	Top of tower T8 [kip-ft]	2807	-2633	1633	-1670	462	-278
F16 R 1	Top of tower T4 [kip-ft]	1277	-1294	997	-1083	346	-231
F1 R 0	Base of tower T12 [kip-ft]	114100	-108200	57600	-43180	11060	-18120
F6 R 0	Base of tower T8 [kip-ft]	322900	-326200	141100	-195800	32860	-22930
F13 R 0	Base of tower T4 [kip-ft]	79050	-103700	76980	-64800	22190	-14810
	M22 Moment						
F1 R 0	Base of tower T12 [kip-ft]	158500	-155000	53430	-69680	14790	-12730
F6 R 0	Base of tower T8 [kip-ft]	225900	-271600	67470	-64480	54500	-39960
F13 R 0	Base of tower T4 [kip-ft]	169700	-152000	61760	-42160	19340	-15150
	ΔTENSION						
F271 R 0.5	Main Cable T12 [kip]	62	-92	34	-34	11	-8
F275 R 0.5	Main Cable T8 [kip]	146	-120	61	-52	8	-10
F280 R 0.5	Main Cable T4 [kip]	102	-121	38	-46	11	-11
F282 R 0.5	Auxiliary Cable T12 [kip]	88	-117	34	-33	10	-8
F284 R 0.5	Auxiliary Cable T8 [kip]	144	-119	56	-49	7	-9
F287 R 0.5	Auxiliary Cable T4 [kip]	99	-125	40	-45	10	-10
F251 R 0.5	Main Backstay T12 [kip]	72	-57	45	-28	10	-9
F256 R 0.5	Main Backstay T8 [kip]	173	-153	73	-71	13	-9
F261 R 0.5	Main Backstay T4 [kip]	85	-97	33	-27	10	-8
F264 R 0.5	Auxiliary Backstay T12 [kip]	100	-90	50	-36	10	-10
F267 R 0.5	Auxiliary Backstay T8 [kip]	179	-170	79	-83	13	-10
F269 R 0.5	Auxiliary Backstay T4 [kip]	115	-114	37	-34	13	-10
F289 R 0.5	Tiedown T12 TENSION [kip]	27	-29	5	-4	0.5	-0.4
F291 R 0.5	Tiedown T8 TENSION [kip]	35	37	8	-9	0.7	-0.5
F292 R 0.5	Tiedown T4 TENSION [kip]	28	-24	4	-5	0.5	-0.7

The results are also very similar to Tables 6.11 through 6.14 and 6.8. Interestingly, the M_{33} moment at the base of tower T8 for Loma Prieta was reduced an additional 1.5% compared to Model B. Model C was expected to predict the worst response; however, the results in terms of the tower bending moments are not showing much difference. Only the cables, except for the tiedowns, are more highly stressed in this model. Taking Loma Prieta as an example, the tension in the auxiliary backstays of tower T8 increased 10% compared to model A. The variation in the tiedown cable tensions is dramatically reduced in this model.

Figure 6.30 shows the deformed shape at 5.1 seconds into the Loma Prieta earthquake. At this time the structure exhibits the highest bending moment $M_{33} = 341,800$ kip-ft at the base of tower T8. Note that Fig. 6.30 is very similar to Figs. 6.28 and 6.29: tower T8 is deformed with the shape of the second mode while towers T4 and T12 are deformed mostly in first mode. In this case, however, the platform exhibits more of a ‘cradle’ motion rather than rotation about its centroidal axis. Therefore, the tight tiedown cables, which counterbalance the Gregorian dome, undergo smaller tension variations than if the platform corners were bobbing up and down due to rotation about its centroidal axis. Note that the T8 tiedown cable is vibrating in a higher mode than the other two tiedowns. This is due to the reduced stiffness of that cable (T8 tiedown) as it is almost slack.

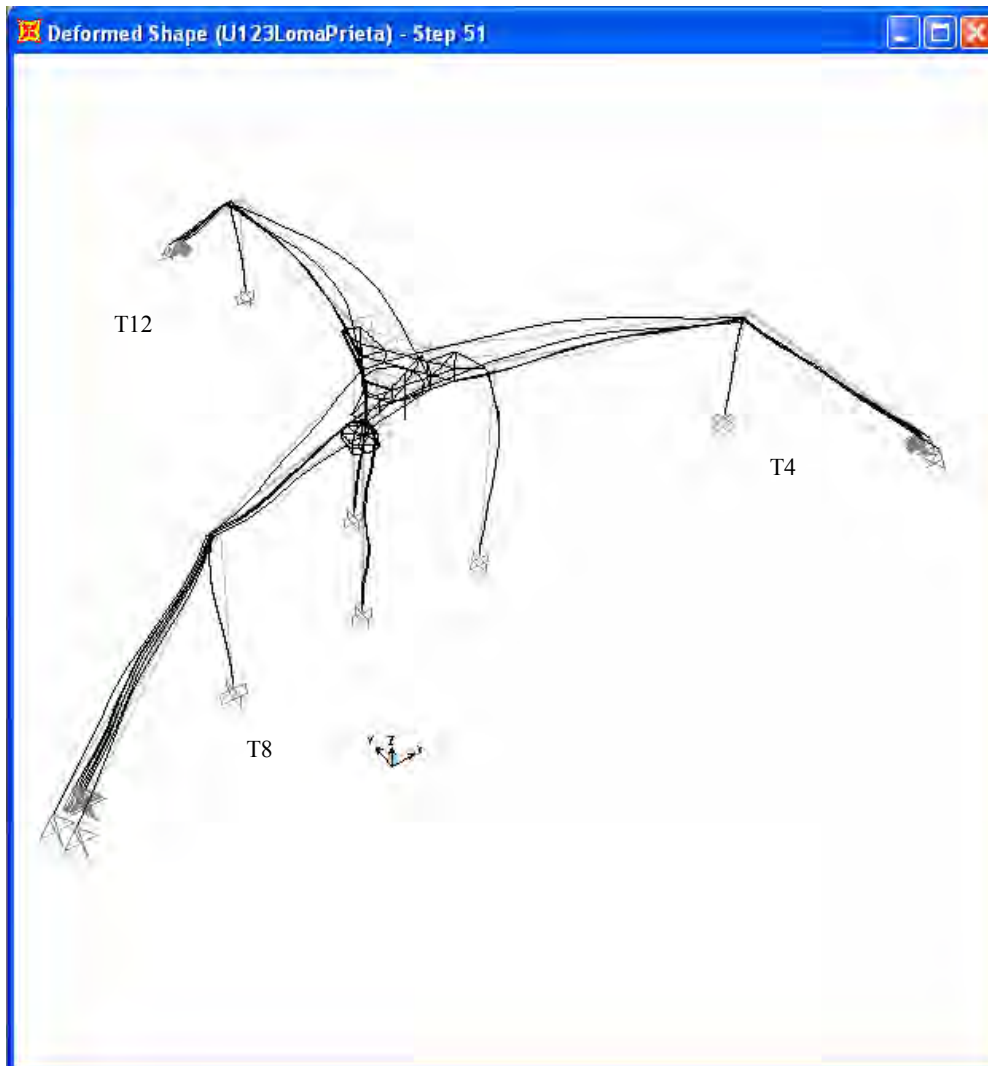


Figure 6.30. Deformed shape (50x mag.) of structure 5.1 sec into Loma Prieta Model C (Tiedowns, Dome)

6.12 Two Additional Sensitivity Studies with Model B

6.12.1 Sensitivity Study: Results Using Cracked Moment of Inertia for Towers

Table 6.17 shows the results of the seismic response of the structure using the cracked moment of inertia for the towers. The original (gross) area moments of inertia were reduced by approximately 90%. As expected there is a dramatic reduction in practically all categories of internal forces. Once the towers crack, they become more flexible and disallow the very large stress build-up predicted by the models using the gross moment of inertia.

Table 6.17. Seismic response using I_{cracked} – Model B

Label	Description	Model B I_CRACKED		Model B I_GROSS		% Diff (MAX)	% Diff (MIN)
		U123 Loma Prieta MAX	MIN	U123 Loma Prieta MAX	MIN		
	UX Displacement						
J27	Top of tower T12 [in]	19.0	-18.8	15.5	-19.3	22.6%	-2.6%
J36	Top of tower T8 [in]	3.8	-5.1	4.8	-6.7	-20.8%	-23.9%
J43	Top of tower T4 [in]	8.9	-7.0	8.3	-10.8	7.2%	-35.2%
	UY Displacement						
J27	Top of tower T12 [in]	1.9	-1.4	2.9	-2.8	-34.5%	-50.0%
J36	Top of tower T8 [in]	4.5	-6.4	5.1	-5.5	-11.8%	16.4%
J43	Top of tower T4 [in]	14.5	-13.9	9.1	-12.9	59.3%	7.8%
	UZ Displacement						
J99	Platform corner T12 [in]	3.5	-3.6	8.6	-7.3	-59.3%	-50.7%
J104	Platform corner T8 [in]	7.2	-6.2	16.8	-16.1	-57.1%	-61.5%
J111	Platform corner T4 [in]	3.8	-3.8	9.7	-11.2	-60.8%	-66.1%
	M33 Moment						
F4 R 1	Top of tower T12 [kip-ft]	619	1143	1406	-1739	-56.0%	-165.7%
F11 R 1	Top of tower T8 [kip-ft]	1439	-754	2993	-3023	-51.9%	-75.1%
F16 R 1	Top of tower T4 [kip-ft]	852	-737	1057	-1171	-19.4%	-37.1%
F1 R 0	Base of tower T12 [kip-ft]	42700	-37370	106200	-86560	-59.8%	-56.8%
F6 R 0	Base of tower T8 [kip-ft]	56740	-105500	347000	-324200	-83.6%	-67.5%
F13 R 0	Base of tower T4 [kip-ft]	44940	-41320	45280	-88110	-0.8%	-53.1%
	M22 Moment						
F1 R 0	Base of tower T12 [kip-ft]	51260	-57550	162800	-117600	-68.5%	-51.1%
F6 R 0	Base of tower T8 [kip-ft]	25940	-28590	105500	-150400	-75.4%	-81.0%
F13 R 0	Base of tower T4 [kip-ft]	45210	-39900	133000	-164700	-66.0%	-75.8%
	ΔTENSION						
F271 R 0.5	Main Cable T12 [kip]	33	-37	54	-91	-38.9%	-59.3%
F275 R 0.5	Main Cable T8 [kip]	60	-41	115	101	-47.8%	-140.6%
F280 R 0.5	Main Cable T4 [kip]	26	-21	65	-59	-60.0%	-64.4%
F282 R 0.5	Auxiliary Cable T12 [kip]	36	-48	49	-88	-26.5%	-45.5%
F284 R 0.5	Auxiliary Cable T8 [kip]	77	-64	158	-159	-51.3%	-59.7%
F287 R 0.5	Auxiliary Cable T4 [kip]	82	-70	102	-90	-19.6%	-22.2%
F251 R 0.5	Main Backstay T12 [kip]	24	-38	62	-63	-61.3%	-39.7%
F256 R 0.5	Main Backstay T8 [kip]	59	-57	135	-129	-56.3%	-55.8%
F261 R 0.5	Main Backstay T4 [kip]	38	-33	81	-53	-53.1%	-37.7%
F264 R 0.5	Auxiliary Backstay T12 [kip]	38	-48	96	-80	-60.4%	-40.0%
F267 R 0.5	Auxiliary Backstay T8 [kip]	86	-67	157	-153	-45.2%	-56.2%
F269 R 0.5	Auxiliary Backstay T4 [kip]	69	-67	76	-46	-9.2%	45.7%
F289 R 0.5	Tiedown T12 TENSION [kip]	25	-27	66	-54	-62.1%	-50.0%
F291 R 0.5	Tiedown T8 TENSION [kip]	54	-47	132	-126	-59.1%	-62.7%
F292 R 0.5	Tiedown T4 TENSION [kip]	29	-29	73	-87	-60.3%	-66.7%

Figure 6.31 shows the deformed shape at 5.6 seconds into the Loma Prieta earthquake. At this time (half a second later than when using I_{gross}) the structure exhibits the highest bending moment $M_{33} = -105,500$ kip-ft at the base of tower T8. Note that tower T8 is responding predominantly in its fourth mode of vibration while towers T4 and T12 are responding predominantly in their third mode of vibration.

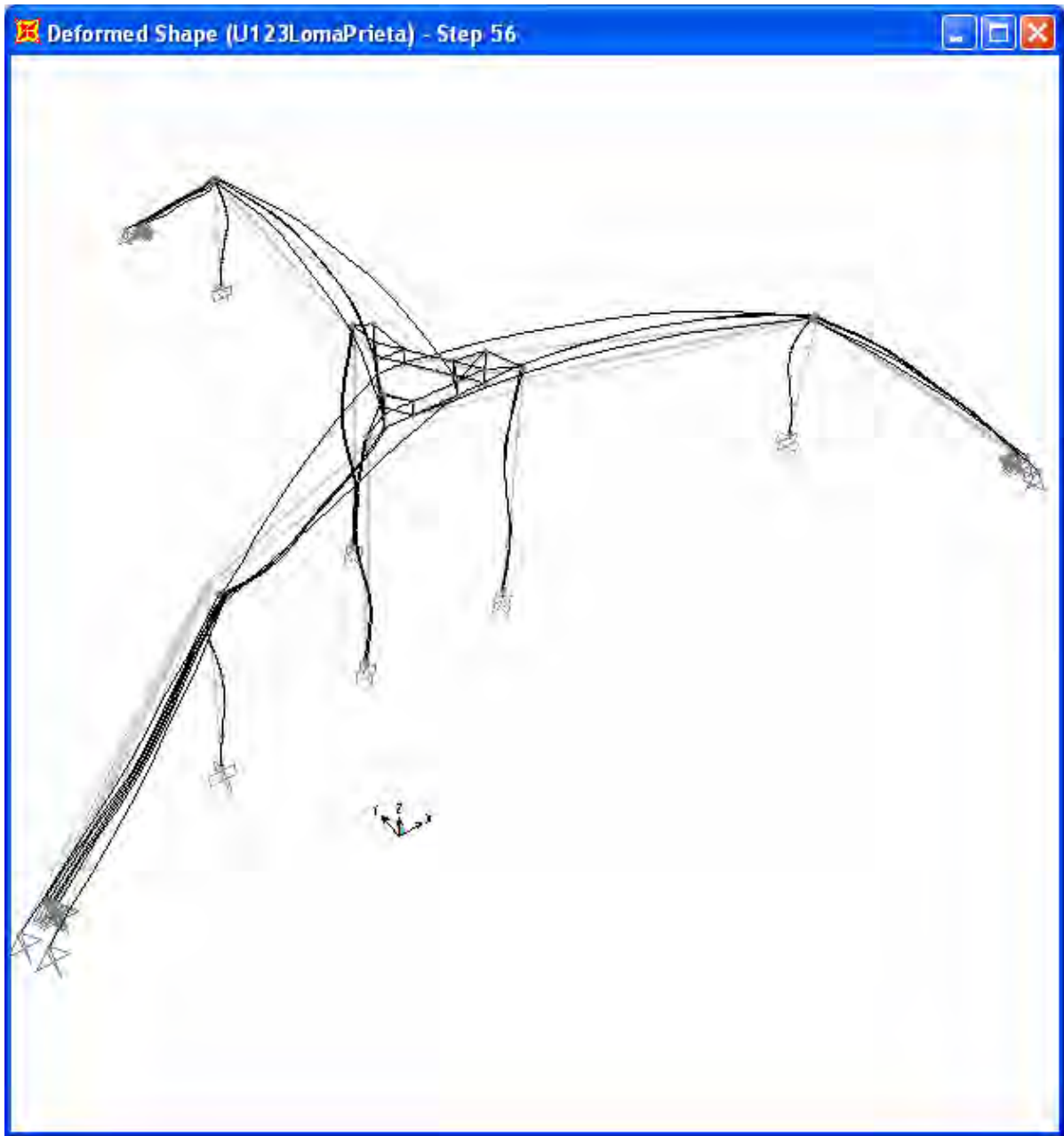


Figure 6.31. Deformed shape (50x mag.) using Icracked 5.6 sec into Loma Prieta Model B (Tiedowns, Uniform Platform)

The response at higher modes introduces curvatures, and therefore bending moments, in the midsections of the towers. Table 6.18 records the M_{33} bending moments at different levels of the towers.

Table 6.18. M_{33} moments at different levels in tower T8 – Model B – $I_{cracked}$

Elevation Level	Model B using $I_{cracked}$		
	Tower T12	Tower T8	Tower T4
	M_{33} [kip-ft]	M_{33} [kip-ft]	M_{33} [kip-ft]
Top of TSEC1	32	-181	757
Bottom of TSEC1	9688	-4764	6261
Bottom of TSEC2	-3599	460	2822
Bottom of TSEC3	-20644	19442	-12503
Bottom of TSEC4	2408	30762	-41316
Bottom of TSEC5	N/A	-7435	N/A
Bottom of TSEC6	N/A	-105524	N/A

6.12.2 Sensitivity Study: Response with Bridge and Service Cables

Table 6.19 shows the results of the seismic response of the structure including the bridge, service cable and cable-car cable. The record of the Loma Prieta ground motion was used as input. As expected, the results are essentially equal to the response of the original model (without bridge). The only significant difference is at the top of the towers where the moments are very low, and so, the differences are magnified.

Table 6.19. Seismic response including bridge, service cable and cable-car cable

Label	Description	Model B With Bridge		Model B Original		% Diff (MAX)	% Diff (MIN)
		U123 Loma Prieta	U123 Loma Prieta	U123 Loma Prieta	U123 Loma Prieta		
		MAX	MIN	MAX	MIN		
	UX Displacement						
J27	Top of tower T12 [in]	15.4	-19.2	15.5	-19.3	-0.6%	-0.5%
J36	Top of tower T8 [in]	4.8	-6.8	4.8	-6.7	0.0%	1.5%
J43	Top of tower T4 [in]	8.4	-10.9	8.3	-10.8	1.2%	0.9%
	UY Displacement						
J27	Top of tower T12 [in]	2.9	-2.8	2.9	-2.8	0.0%	0.0%
J36	Top of tower T8 [in]	5.1	-5.4	5.1	-5.5	0.0%	-1.8%
J43	Top of tower T4 [in]	9.2	-12.8	9.1	-12.9	1.1%	-0.8%
	UZ Displacement						
J99	Platform corner T12 [in]	8.7	-7.2	8.6	-7.3	1.2%	-1.4%
J104	Platform corner T8 [in]	16.7	-16.0	16.8	-16.1	-0.6%	-0.6%
J111	Platform corner T4 [in]	9.8	-11.2	9.7	-11.2	1.0%	0.0%
	M33 Moment						
F4 R 1	Top of tower T12 [kip-ft]	1996	-2334	1406	-1739	29.6%	25.5%
F11 R 1	Top of tower T8 kip-ft]	2963	-2970	2993	-3023	-1.0%	-1.8%
F16 R 1	Top of tower T4 [kip-ft]	920	-1035	1057	-1171	-13.0%	-11.6%
F1 R 0	Base of tower T12 [kip-ft]	105900	-86220	106200	-86560	-0.3%	-0.4%
F6 R 0	Base of tower T8 [kip-ft]	356200	-328100	347000	-324200	2.7%	1.2%
F13 R 0	Base of tower T4 [kip-ft]	44330	-86900	45280	-88110	-2.1%	-1.4%
	M22 Moment						
F1 R 0	Base of tower T12 [kip-ft]	162500	-117800	162800	-117600	-0.2%	0.2%
F6 R 0	Base of tower T8 [kip-ft]	102600	-146100	105500	-150400	-2.7%	-2.9%
F13 R 0	Base of tower T4 [kip-ft]	131500	-161300	133000	-164700	-1.1%	-2.1%
	ΔTENSION						
F271 R 0.5	Main Cable T12 [kip]	56	-91	54	-91	3.7%	0.0%
F275 R 0.5	Main Cable T8 [kip]	116	-103	115	-101	0.9%	2.0%
F280 R 0.5	Main Cable T4 [kip]	64	-57	65	-59	-1.5%	-3.4%
F282 R 0.5	Auxiliary Cable T12 [kip]	50	-88	49	-88	2.0%	0.0%
F284 R 0.5	Auxiliary Cable T8 [kip]	159	-156	158	-159	0.6%	-1.9%
F287 R 0.5	Auxiliary Cable T4 [kip]	101	-87	102	-90	-1.0%	-3.3%
F251 R 0.5	Main Backstay T12 [kip]	61	-63	62	-63	-1.6%	0.0%
F256 R 0.5	Main Backstay T8 [kip]	134	-132	135	-129	-0.7%	2.3%
F261 R 0.5	Main Backstay T4 [kip]	80	-52	81	-53	-1.2%	-1.9%
F264 R 0.5	Auxiliary Backstay T12 [kip]	89	-79	96	-80	-7.3%	-1.3%
F267 R 0.5	Auxiliary Backstay T8 [kip]	156	-155	157	-153	-0.6%	1.3%
F269 R 0.5	Auxiliary Backstay T4 [kip]	76	-45	76	-46	0.0%	-2.2%
F289 R 0.5	Tiedown T12 TENSION [kip]	68	-54	66	-54	3.0%	0.0%
F291 R 0.5	Tiedown T8 TENSION [kip]	132	-126	132	-126	0.0%	0.0%
F292 R 0.5	Tiedown T4 TENSION [kip]	75	-87	73	-87	2.7%	0.0%

Figure 6.32 shows the deformed shape at 5.1 seconds into the Loma Prieta earthquake. Note that it is essentially equal to Figure 6.29 for Model B, i.e., the bridge, service cables and the cable-car cable have not altered the results of the model. This deformed-geometry plot confirms the results of Table 6.19, namely that the addition of the bridge, service cables and cable-car cable may be safely neglected from the analysis.



Figure 6.32. Deformed shape (50x mag.) of the structure 5.1 sec into Loma Prieta. Model B with bridge, service cables, and cable-car cable

CHAPTER 7

Final Studies on Seismic Response

This chapter presents the selection of the maximum-credible earthquake records used in the investigation and the response of the structure to these seismic events.

7.1 Seismic Hazard of the Arecibo Observatory Site

This section addresses the seismic hazard of the Arecibo Observatory site based on previous research results. Irizarry (1999) recommends design spectra for Mayagüez, Ponce and San Juan based on worldwide strong motion records. A chapter in the work of Llop (2002) describes the development of a site-specific spectrum for two dams very near the Arecibo Observatory, using the same procedure as Irizarry (1999). The work of Dames & Moore (1999) provides a probabilistic assessment of the seismic hazard in Puerto Rico's major cities including Arecibo. Figure 7.1 shows the location of the Arecibo Observatory with respect to other relevant sites in Puerto Rico.



Figure 7.1. Location of Arecibo Observatory with respect to other sites in Puerto Rico

7.1.1 Overview of Plate Tectonics

Puerto Rico is located in the northeast corner of the Caribbean plate. The Caribbean plate, nearly rectangular in shape, spans the Caribbean Sea from Central America on the west

to the Lesser Antilles on the east. The northern border passes just below Cuba but includes Jamaica, Hispaniola and Puerto Rico. The southern border is defined by the coast of South America. The North American plate moves west relative to the Caribbean plate which creates a predominantly left-lateral strike-slip plate boundary zone to the north of the Caribbean plate.

Jansma (2002) indicates that the northeast corner of the Caribbean plate is not clearly defined; instead, it is a ~ 250-km wide diffuse boundary zone - its northern limit defined by the Puerto Rico Trench while the southern limit is defined by the Muertos Trough. The diffuse zone includes Hispaniola, Puerto Rico and the Virgin Islands. Three proposed microplates lie within this diffuse boundary zone, the easternmost of which is the Puerto Rico-Northern Virgin Islands (PRVI) microplate (Figure 7.2).

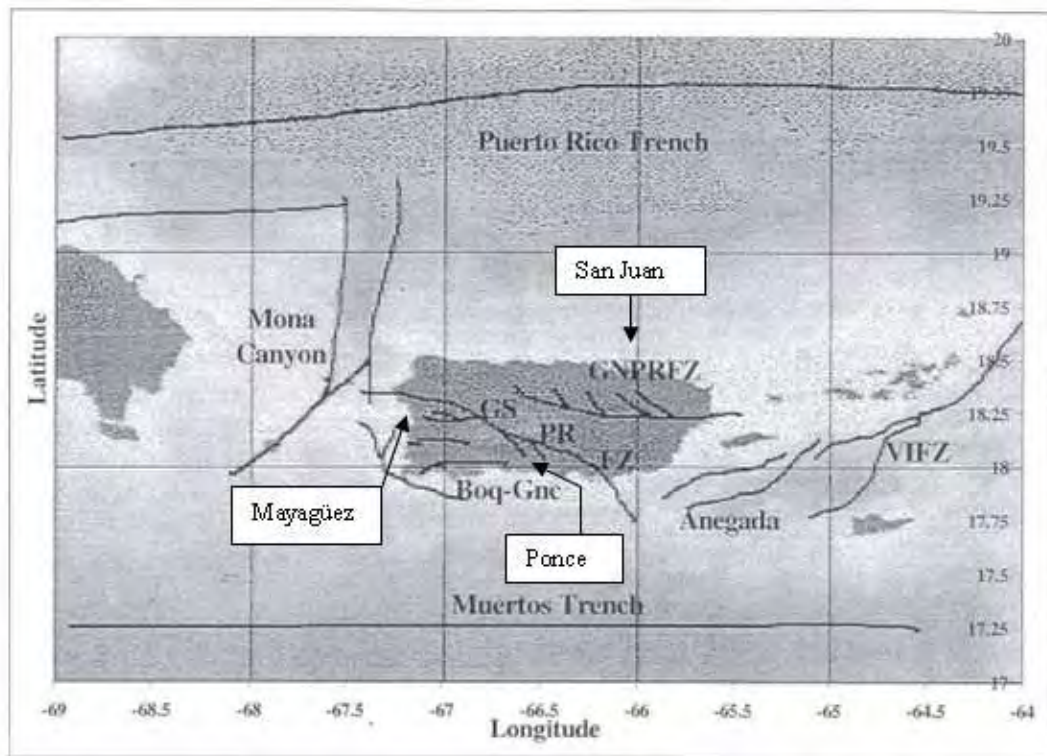


Figure 7.2. The Puerto Rico Virgin Islands (PRVI) microplate (taken from Irizarry 1999)

Figure 7.1 shows that the PRVI microplate is bounded by the Puerto Rico Trench on the north, the Muertos Trough on the south, the Mona Canyon on the west and the Anegada Trough on the east. In addition, Puerto Rico is traversed by two northwest-southeast striking

fault zones; the Great Northern Puerto Rico fault zone (GNPRFZ) and the Great Southern Puerto Rico fault zone (GSPRFZ) which represent large areas of weaknesses within PRVI along which intra-block motion may be localized. Irizarry (1999) considers a distinct Boquerón-Guánica (Boq-Gnc) fault zone (separate from GSPRFZ) for the southwest of Puerto Rico whose northern boundary is approximately defined by a straight line between Mayagüez and Ponce.

Jansma (2002) indicates that the prevailing scientific opinion is that the PRVI microplate remains rigid and deformations occur primarily on the boundaries. However, Jansma (2002) also identifies the presence of high levels of onshore (intra-island) seismicity recorded by the Puerto Rico Seismic Network, especially in the southwest of the island in the Lajas valley (Boq-Gnc fault zone). This high-level of seismic activity indicates an earthquake potential for intra-island faults that challenges the rigid-PRVI-plate hypothesis. Irizarry (1999) points out that an exhaustive examination in 1991 by the seismologist E. Asencio of the distribution of 268 tremors recorded during a one-year period in western Puerto Rico suggests shallow geologically active structures within Puerto Rico. Irizarry (1999) also cites a study conducted in 1991 by Moya and McCann which concluded that faults within the Mayagüez area are possible sources of strong shallow earthquakes. A further examination of the Puerto Rico Seismic Network records by Irizarry (1999) concludes that the areas of Ponce and Mayagüez are exposed to a shallow-earthquake hazard while San Juan is not.

7.1.2 Historical Records of Earthquakes in Puerto Rico

Three major earthquakes are known to have significantly affected Puerto Rico in the past 220 years, all of which have occurred offshore in the boundaries of the PRVI microplate. The first occurred along the Puerto Rico Trench on May 2, 1787 ($M \approx 8.0$) which caused damage on essentially the entire northern shore of Puerto Rico. The second originated in the Anegada Trough on November 17, 1867 ($M_s \approx 7.3$) which caused damage on the eastern shore of the island, including a tsunami that ran inland almost 140 meters in the low parts of the coast of Yabucoa. The third triggered in the Mona Canyon on October 11, 1918 ($M_s \approx 7.3$) and caused damage, as well as 116 deaths, in the entire west coast of the island, including a tsunami. There are no acceleration records from any of these earthquakes.

According to Irizarry (1999), the Puerto Rico Strong Motion Program has recently recorded a total of eight acceleration records in Puerto Rico from five tremors with a maximum coda magnitude of 4.5. Since 1999, and up to April, 2006, the Puerto Rico Strong Motion Program has recorded an additional 47 records, from 16 tremors with a maximum coda magnitude of 4.9. However, these local earthquakes are not strong enough to be used for seismic resistant design in Puerto Rico.

7.1.3 Selection of Maximum-Credible Earthquakes for the Arecibo Site

In the absence of strong motion records from the PRVI microplate, Irizarry (1999) examined worldwide strong motion records and recommended design earthquakes and design spectra for Puerto Rico's main cities of San Juan, Mayagüez and Ponce. The search parameters were earthquake magnitude, focal depth, epicentral distance, site's geology and fault-structure type. These were calibrated to the parameters of each city to obtain a suitable match. In general, the study concludes that Mayagüez and Ponce can be grouped together and are exposed to the same, and very high, seismic hazard while San Juan is exposed to a different and much lesser seismic hazard. The San Juan response spectrum envelope is shown in Figure 7.3 while the envelope for Mayagüez and Ponce is shown in Figure 7.4.

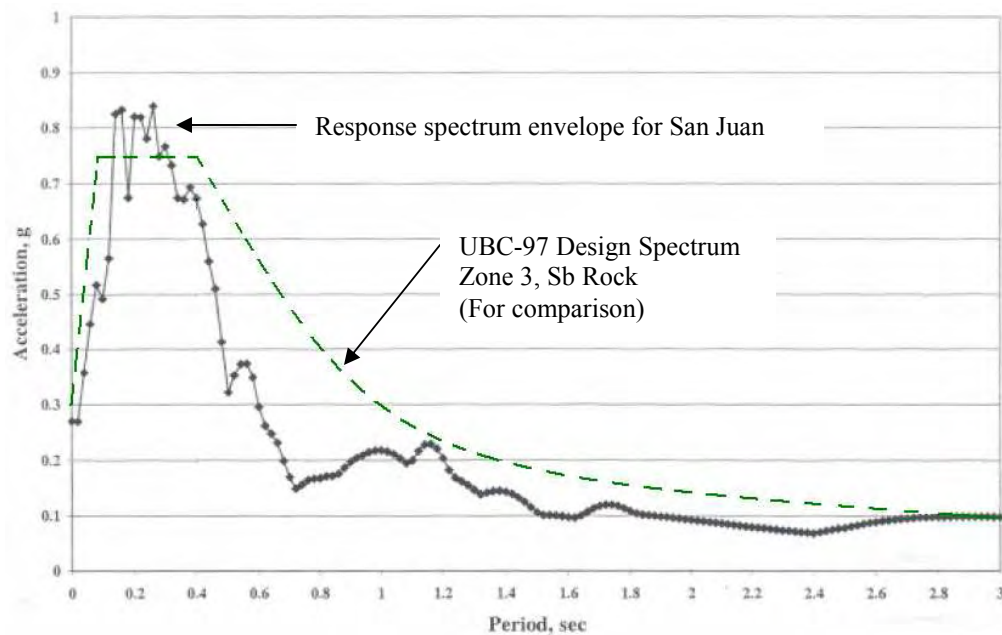


Figure 7.3. Response spectrum envelope for San Juan (from Irizarry 1999)

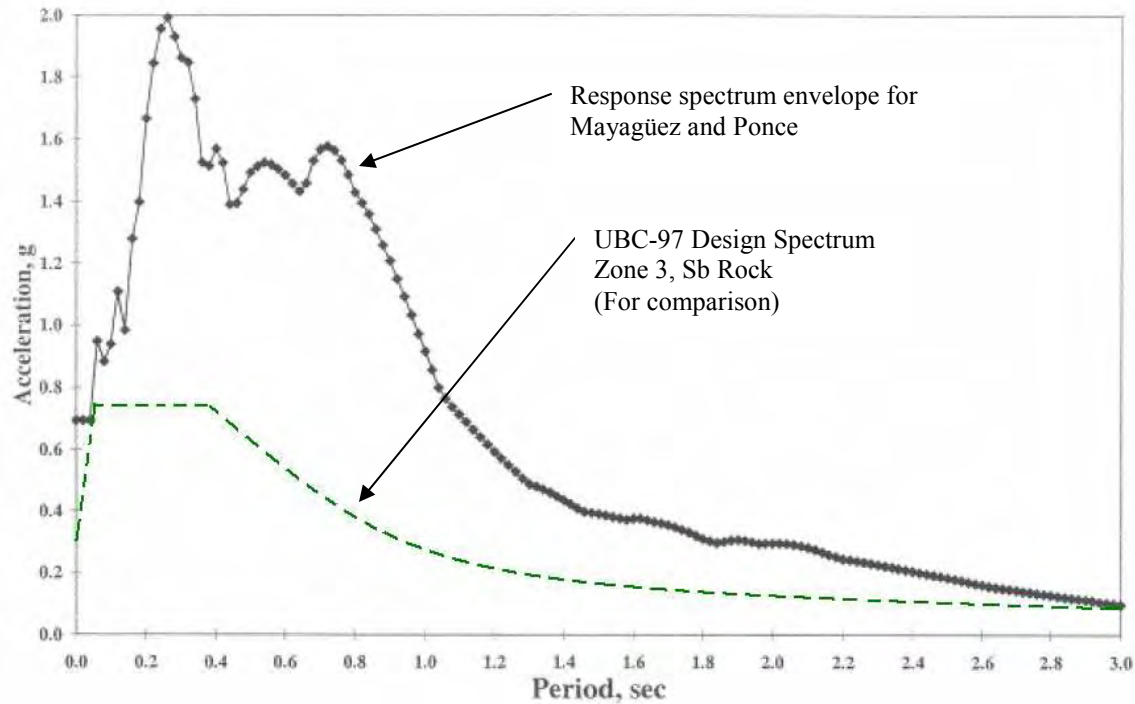


Figure 7.4. Response spectrum envelope for Mayagüez and Ponce (from Irizarry 1999)

Irizarry (1999) concludes the Mayagüez and Ponce envelope is governed almost entirely by the 1986 San Salvador earthquake ($M = 5.4$), CIG station (Geotechnical Research Center) EW record. Figure 7.5 displays the first 9 seconds of the San Salvador record and Figure 7.6 shows its ground response spectrum superimposed with the UBC-97 design spectrum. In order to compare these spectra, the San Salvador and all other spectra are calculated using a 5% damping ratio. San Salvador was deemed to represent a possible shallow earthquake generated at the Boquerón-Guánica intra-island fault. In addition to its shallowness (8 km), the CIG station record also includes near-fault effects since the epicentral distance was only 4 km (~ 9 km hypocentral). The near-fault effect explains the high PGA ($\sim 0.7g$) recorded for this relatively low-magnitude earthquake ($M = 5.4$). The other governing earthquake is the 1994 Northridge earthquake ($M = 6.7$), Castaic station EW record. The accelerogram of this particular Northridge earthquake and its response spectrum are displayed in Figures 7.7 and 7.8, respectively. Northridge provides a good normal-fault representation of an offshore earthquake in the Mona Canyon. The Castaic record is particularly interesting and powerful as it includes a strong directivity component (focalization of energy in the direction of fault rupture) of the Northridge earthquake.

Directivity towards the west coast of Puerto Rico is expected to play a role in the Mona Canyon normal fault, although Northridge-Castaic may be conservative. From figures 7.6 and 7.8, note that the response spectra of the San Salvador-CIG and Northridge-Castaic records are very much above the UBC-97 design spectrum.

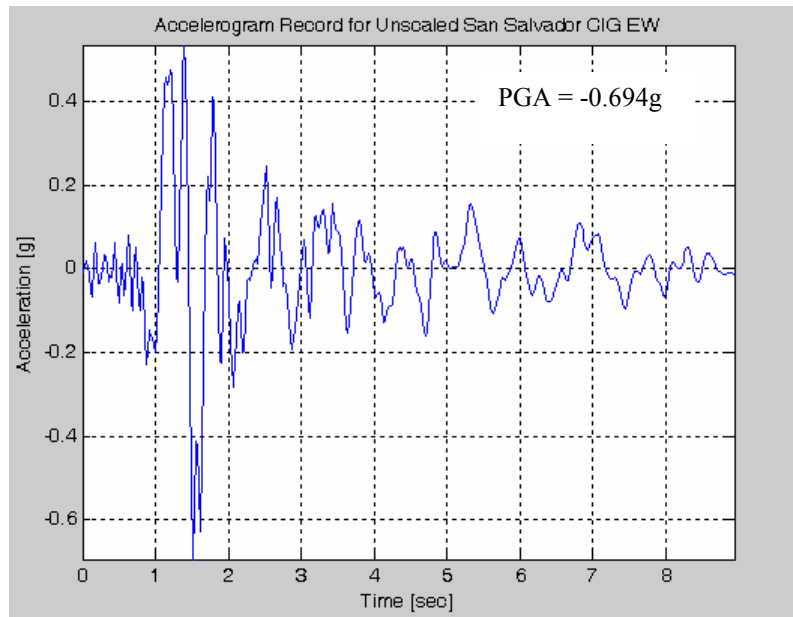


Figure 7.5. Accelerogram of the San Salvador-CIG EW record

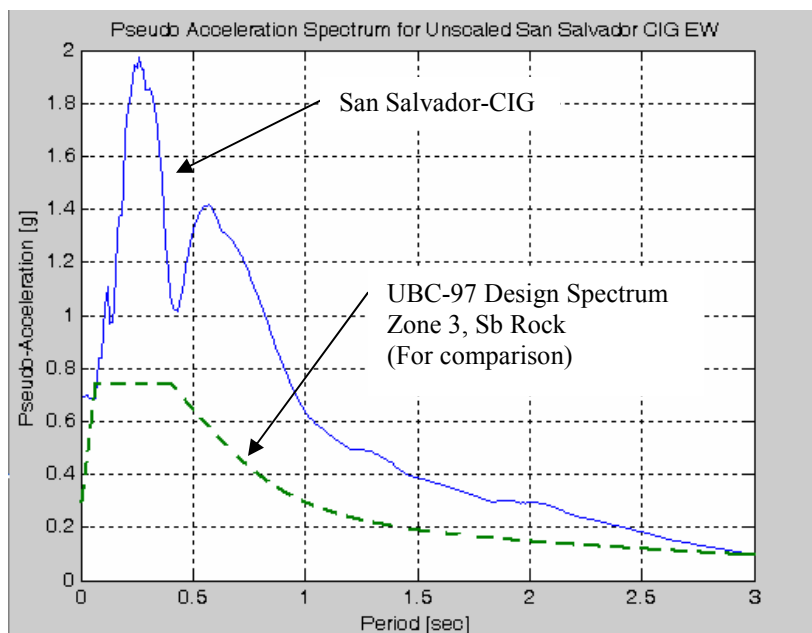


Figure 7.6. PSA spectrum of the San Salvador-CIG EW record

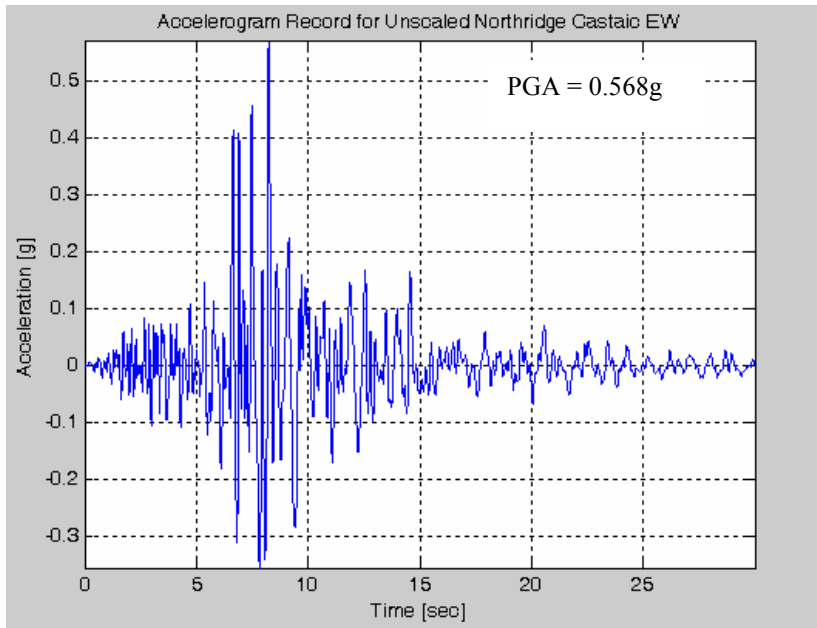


Figure 7.7. Accelerogram of the Northridge–Castaic EW record

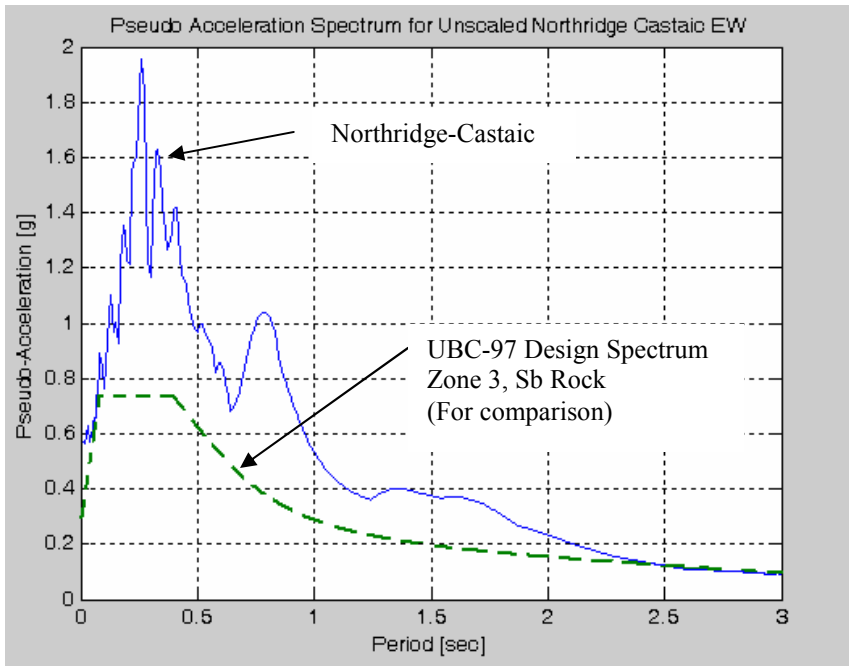


Figure 7.8. PSA spectrum of Northridge–Castaic EW record

For San Juan, Irizarry (1999) reported that the 1966 Parkfield earthquake ($M=6.1$), station097, usaca01.109 EW record provides a good representation of an earthquake generated in the GNPRFZ. The Parkfield accelerogram is shown in Figure 7.9 while Figure 7.10 displays its response spectrum along with the UBC-97 design spectrum. This Parkfield record governs the San Juan spectrum at short periods (compare to Fig. 7.3).

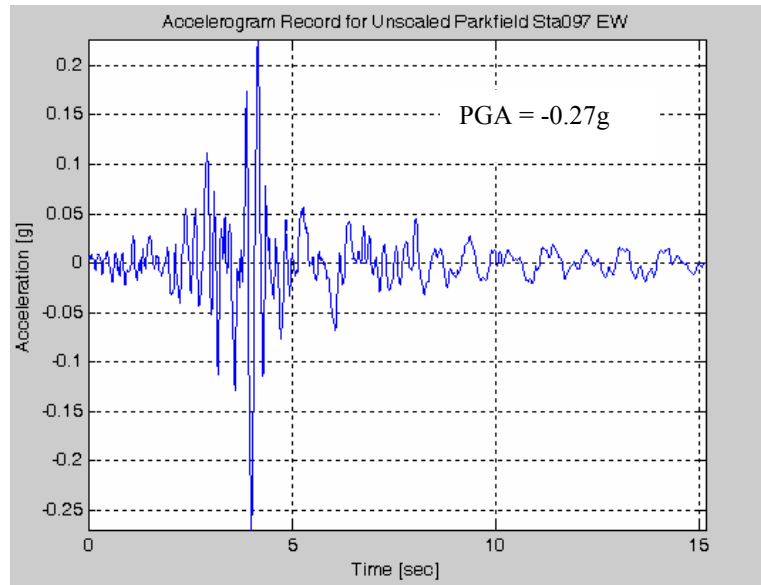


Figure 7.9. Accelerogram of the Parkfield–station097 usaca01.109 EW record

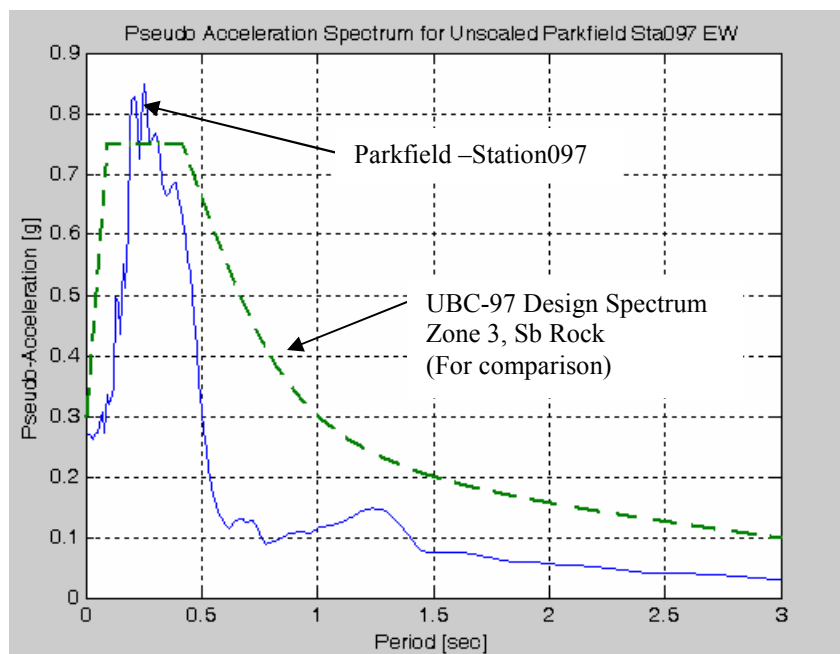


Figure 7.10. PSA spectrum of the Parkfield-station097usaca01.109 EW record

Llop (2002) undertook a study similar to Irizarry but to determine a site-specific spectrum for the Dos Bocas and Guajataca dams located very near the Arecibo Observatory (see Figure 7.1 for its location within Puerto Rico). The final response spectrum envelope is shown in Figure 7.11.

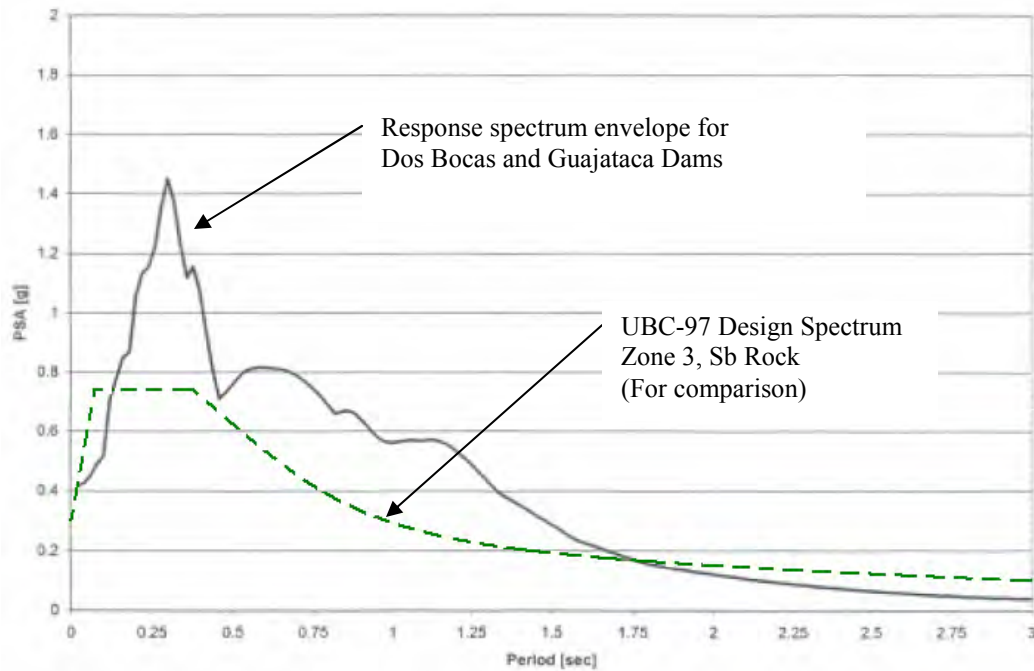


Figure 7.11. Response spectrum envelope for the Dos Bocas and Guajataca Dams (taken from Llop 2002)

A comparison between the three response spectrum envelopes (shown in Figures 7.3, 7.4, and 7.11) indicates that the envelope for the dams near the Observatory (Figure 7.11) falls in between the San Juan and the Mayagüez-Ponce envelopes. Llop (2002) initially considered the San Salvador-CIG EW record as a possibility for a shallow rupture in GNPRFZ but discards it as improbable based on seismic data in the vicinity of the dams and the low capacity of saturated rock. Northridge-Castaic was also considered initially and it was discarded as well. It may be argued that the Arecibo Observatory site is 25 miles further away from the Mona Canyon fault than Mayagüez, and so the Northridge-Castaic accelerogram would have undergone significant attenuation by the time it reached the Observatory.

The governing earthquake record selected for the site of the dams was the 1984 Morgan Hill (M=6.2) – Gilroy6 EW (usaca36.011) record. Figure 7.12 displays the original (unscaled) Morgan Hill accelerogram and Figure 7.13 its response spectrum along with the UBC-97 design spectrum for rock soil profile. It can be seen that the Morgan Hill record governs the intermediate periods (<1.8 sec) and part of the shorter ranges as well.

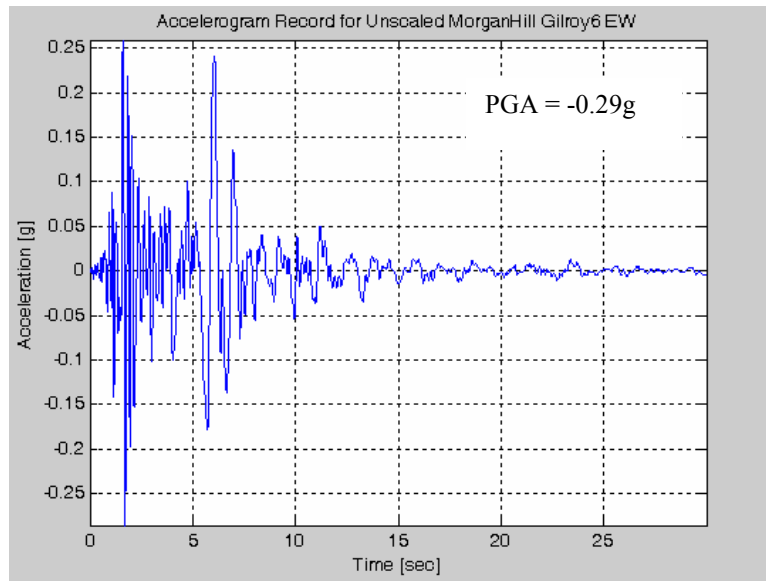


Figure 7.12. Accelerogram of the Morgan Hill – Gilroy6 ~EW record

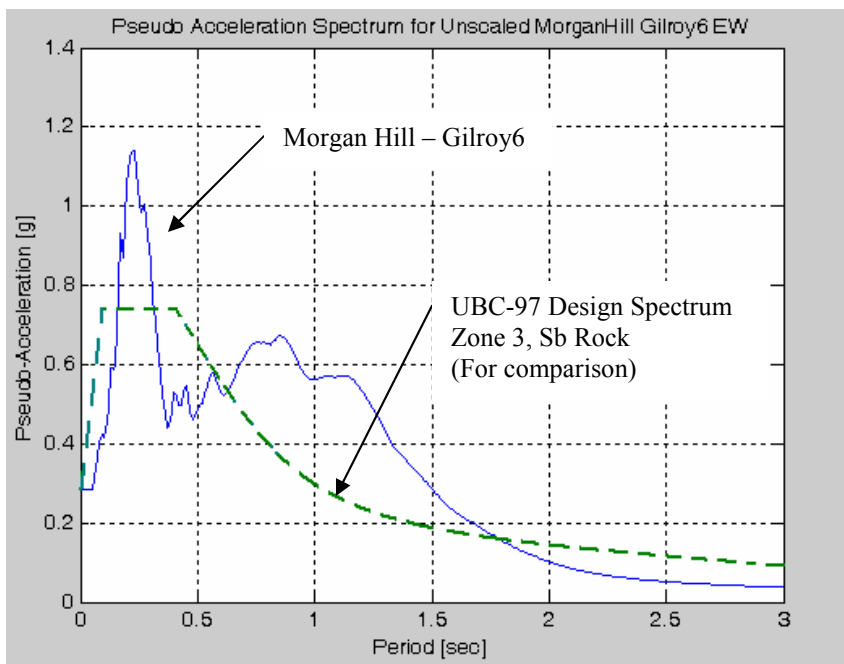


Figure 7.13. PSA spectrum of the Morgan Hill – Gilroy6 ~EW record

In addition to the investigations of Irizarry (1999) and Llop (2002), the company Dames & Moore (1999) prepared a probabilistic seismic hazard analysis for different cities of Puerto Rico. This study concludes that the cities of Arecibo and San Juan are exposed to the same seismic hazard. For an earthquake with a 475 year recurrence period, the recommended hazard is slightly below the design spectrum recommended by UBC-97. Note that a 475 year recurrence period earthquake is equivalent to one with a 10% probability of exceeding the value in 50 years. This is the criterion used by the UBC-97 code to specify the design spectrum. Dames & Moore (1999) also concludes that Mayagüez and Ponce are exposed to essentially the same seismic hazard which confirms the conclusion reached by Irizarry (1999).

Based on the UBC-97 code and on the Dames & Moore (1999) study, it seems prudent to discard the San Salvador–CIG and Northridge-Castaic as improbable earthquakes for the Arecibo Observatory. Nevertheless, the response to these very strong records will be considered so as to test the capacity limits of the structure. Although the San Salvador and Northridge earthquakes are not of very high magnitude, the near-fault effects of the first, and the directivity of the second, magnify their potential for destruction. A second cycle of runs will be carried out but this time all the components of the San Salvador and Northridge earthquake records will be scaled to meet a maximum PGA = 0.3g. The scaling factor will decrease the demands to the levels recommended by UBC-97 and Dames & Moore (1999). A third, and final cycle of runs will consider the 1966 Parkfield-station097 and the 1984 Morgan Hill-Gilroy6 records. The 1966 Parkfield record represents the San Juan response envelope determined by Irizarry (1999) while the 1984 Morgan Hill record represents the Dos Bocas/Guajataca-dams response envelope determined by Llop (2002). Note that the 1966 Parkfield record is slightly on the unconservative side (see Figure 7.10) by virtue of being below the UBC-97 design spectrum in most ranges of periods. On the other hand, the 1984 Morgan Hill earthquake is on the conservative side (see Figure 7.13) by virtue of being above the UBC-97 design spectrum in most ranges of periods, especially in the intermediate range of periods which will most likely excite the stronger modes of the structure.

7.1.4 SIMQKE Artificial Record Compatible with UBC-97 Design Spectrum

The use of artificial earthquake records compatible with a prescribed design spectrum represents another approach to perform transient seismic analysis. This study considers an artificial record compatible with the UBC-97 design spectrum for zone 3 and soil type Sb. The record (Figure 7.14) was generated by Vázquez (2003) using the computer program SIMQKE modified for Windows. The spectrum of this artificial earthquake, superimposed over the UBC-97 design spectrum, is shown in Figure 7.15.

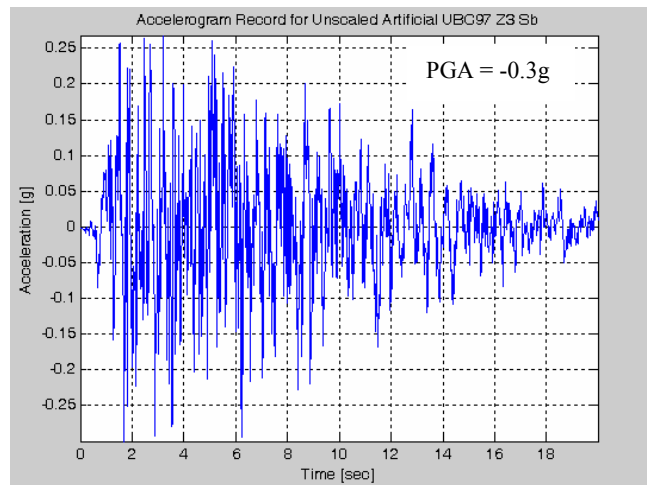


Figure 7.14. Accelerogram of the Artificial UBC-97 (Z3, “Sb”) compatible record

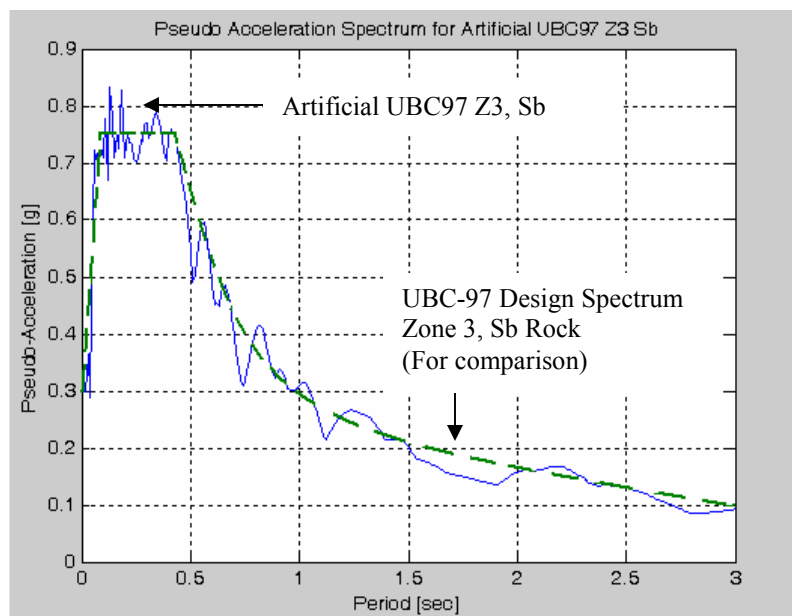


Figure 7.15. PSA spectrum of the Artificial UBC-97 (Z3, “Sb”) compatible record

In conclusion, the earthquakes shown in Table 7.1 will be used in the study. All three records (North-South, East-West, and Up-Down) of each station will be used in the simulation.

Table 7.1. Earthquakes selected for the Arecibo Observatory site

Run	Earthquake	Station	Mag.	Epic. Dist. [km]	Depth [km]	Comments
1	San Salvador (1986) UNSCALED PGA = 0.69g	CIG (Geotech.. Research Ctr.)	5.4	4.3	8	Improbable. (Mayagüez-Ponce envelope) Check if towers are capable of resisting. Shallow and near an Intra-Island Fault
1	Northridge (1994) UNSCALED PGA = 0.57g	Castaic	6.7	41	18	Improbable. (Mayagüez-Ponce envelope) Check if towers are capable of resisting. Mona Canyon Fault with strong directivity
1	Artificial (SIMQKE) INHERENTLY SCALED PGA = 0.3g	N/A	N/A	N/A	N/A	UBC-97 Design Spectrum Zone 3, Sb Rock Use as baseline to compare results with other quakes.
2	San Salvador (1986) SCALED TO 0.3g PGA (all the components with a PGA higher than 0.3g were scaled down to 0.3g)	CIG (Geotech.. Research Ctr.)	5.4	4.3	8	Observe results with a diminished PGA. Shallow and near an Intra-Island Fault. (Mayagüez-Ponce envelope) Only on Model C.
2	Northridge (1994) SCALED TO 0.3g PGA (all the components with a PGA higher than 0.3g were scaled down to 0.3g)	Castaic	6.7	41	18	Observe results with a diminished PGA. Mona Canyon Fault with strong directivity. (Mayagüez-Ponce envelope) Only on Model C.
3	Parkfield (1966) SCALED NS to 0.3g PGA PGA EW = 0.27g	097	6.1	27	6	Probable. (San Juan envelope) GNPRFZ Only on Model C.
3	Morgan Hill (1984) UNSCALED PGA = 0.29g	Gilroy #6	6.2	9.0	37	Probable. (Dos Bocas envelope) GNPRFZ – shallow Only on Model C.

The information for each earthquake record is shown in Table 7.2 along with the calculation of the factors used in SAP2000. The scaling factors at the right end of the table are the values entered into the program SAP2000. The values in the column identified as “Unscaled Factor” just represent the constants for conversion of the data to units of in/s/s. The “Scaled” column includes the conversion of units in addition to a reduction according to the fraction of 0.3g/PGA. The Artificial earthquake, by virtue of its compatibility with the UBC-97 design spectrum, is inherently calibrated to a PGA of 0.3g with a maximum spectral response approximately equal to 0.75g (see Figure 7.8).

Table 7.2. Accelerogram data for selected earthquakes

Case	Mag.	Depth [km]	Epi. Dist. [km]	No. of Pts. [adim]	Delta T [sec]	Duration [sec]	PGA [g]	Unscaled Factor (SAP) [in/s^2]	Scaled Factor (SAP) [in/s^2]	Notes
E-W San Salvador_CIG	5.4	8.0	4.0	453	0.02	9.04	0.69	0.394	0.17	2
N-S San Salvador_CIG	5.4	8.0	4.0	452	0.02	9.02	0.42	0.394	0.283	2
UP San Salvador_CIG	5.4	8.0	4.0	452	0.02	9.02	0.39	0.394	0.304	2, 6
E-W Northridge_Castaic	6.7	18.0	41.0	2000	0.02	40	0.22	386.4	386.4	1, 3
N-S Northridge_Castaic	6.7	18.0	41.0	2000	0.02	40	0.57	386.4	204.1	1, 3
UP Northridge_Castaic	6.7	18.0	41.0	2000	0.02	40	0.51	386.4	150.4	3, 5
E-W Artificial_UBC97	N/A	N/A	N/A	1000	0.02	20	0.3	386.4	N/A	3, 4
N-S Artificial_UBC97	N/A	N/A	N/A	1000	0.02	20	0.3	386.4	N/A	3, 4
UP Artificial_UBC97	N/A	N/A	N/A	1000	0.02	20	0.3	257.6	N/A	3, 4, 5
E-W Parkfield_Sta097	5.5	6	27	1608	0.02	32.14	0.27	N/A	0.0394	7
N-S Parkfield_Sta097	5.5	6	27	1608	0.02	32.14	0.35	N/A	0.0307	7
UP Parkfield_Sta097	5.5	6	27	1608	0.02	32.14	0.13	N/A	0.0394	7
E-W Morgan Hill_Gilroy6	6.2	37	9	3000	0.02	60	0.29	0.394	N/A	2
N-S Morgan Hill_Gilroy6	6.2	37	9	3000	0.02	60	0.28	0.394	N/A	2
UP Morgan Hill_Gilroy6	6.2	37	9	3000	0.02	60	0.42	0.394	N/A	2,8

Notes:

1. E-W and N-S records swapped for Northridge Castaic to correctly simulate directivity.
2. The original acceleration records are in units of cm/s/s.
3. The original acceleration records are in units of g.
4. There is only one record for the Artificial earthquake which is used in all three directions.
5. UP records for Northridge and Artificial scaled to 2/3*(0.3g) per code. No near-fault effects
6. UP record for San Salvador not scaled an additional 2/3 since it involves near-fault action
7. The original acceleration records are in units of cm/s/s/10 (Divide data by 10 to obtain cm/s/s)
8. UP record left unscaled as effects are minimal.

7.2 Seismic Response First Run– Unscaled San Salvador, Northridge and Artificial

7.2.1 Seismic Response First Run – Unscaled Results for Model A

The results for Model A are shown in Table 7.3. Recall that Model A does not include the dome nor tiedown cables. Note the responses for the unscaled San Salvador and for Northridge-Castaic accelerograms are similar to the scaled Loma Prieta results included in Chapter 6 with maximum moments on the order of 350,000 kip-ft at the base of tower T8. The response to the artificial earthquake is lower, as expected, based on its less-severe spectrum.

Table 7.3. Seismic response (unscaled) for Model A

Label	Description	Model A U123 San Salvador CIG Station		Model A U123 Northridge Castaic Station		Model A U123 Artificial SIMQKE Program	
		MAX	MIN	MAX	MIN	MAX	MIN
UX Displacement							
J27	Top of tower T12 [in]	16.8	-15.4	15.6	-12.2	7.8	-5.4
J36	Top of tower T8 [in]	19.1	-14.0	9.6	-9.0	4.6	-4.8
J43	Top of tower T4 [in]	8.6	-8.8	11.1	-9.7	5.7	-4.1
UY Displacement							
J27	Top of tower T12 [in]	7.0	-6.7	6.6	-4.2	3.2	-3.1
J36	Top of tower T8 [in]	23.4	-25.8	12.0	-17.2	5.8	-5.8
J43	Top of tower T4 [in]	13.8	-14.5	18.6	-15.1	8.8	-6.8
UZ Displacement							
J99	Platform corner T12 [in]	14.9	-9.7	9.4	-11.5	21	-19.3
J104	Platform corner T8 [in]	9.2	-11.1	14.0	-17.1	29.9	-36.2
J111	Platform corner T4 [in]	12.8	-16.0	9.6	-12.1	15.8	-16.7
M33 Moment							
F4 R 1	Top of tower T12 [kip-ft]	3986	-4723	2842	-3730	1057	-1287
F11 R 1	Top of tower T8 [kip-ft]	3175	-4415	3375	-3716	2746	-2021
F16 R 1	Top of tower T4 [kip-ft]	1207	-2310	2540	-2401	460	486
M22 Moment							
F1 R 0	Base of tower T12 [kip-ft]	257100	-251800	214800	-205900	82690	-66480
F6 R 0	Base of tower T8 [kip-ft]	347400	-308000	330200	-376700	273100	-223500
F13 R 0	Base of tower T4 [kip-ft]	109200	-101600	162000	-135500	39390	-38300
M22 Moment							
F1 R 0	Base of tower T12 [kip-ft]	126800	-175400	149800	-161900	95940	-87160
F6 R 0	Base of tower T8 [kip-ft]	343600	-333000	225400	-325100	80730	-91610
F13 R 0	Base of tower T4 [kip-ft]	124100	-145000	168600	-150300	117000	-123400
ATENSION							
F271 R 0.5	Main Cable T12 [kip]	134	-184	158	-92	73	-85
F275 R 0.5	Main Cable T8 [kip]	101	-124	153	-142	112	-89
F280 R 0.5	Main Cable T4 [kip]	123	124	124	-124	48	-51
Auxiliary Cables							
F282 R 0.5	Auxiliary Cable T12 [kip]	137	-145	131	-121	65	-74
F284 R 0.5	Auxiliary Cable T8 [kip]	114	-150	106	-114	106	-119
F287 R 0.5	Auxiliary Cable T4 [kip]	104	-101	101	-107	68	-89
Main Backstay							
F251 R 0.5	Main Backstay T12 [kip]	144	-147	94	-141	70	-70
F256 R 0.5	Main Backstay T8 [kip]	120	-176	197	-197	124	-104
F261 R 0.5	Main Backstay T4 [kip]	139	-108	99	-95	36	-42
Auxiliary Backstay							
F264 R 0.5	Auxiliary Backstay T12 [kip]	166	-199	112	-184	79	-90
F267 R 0.5	Auxiliary Backstay T8 [kip]	108	-187	238	-223	140	-126
F269 R 0.5	Auxiliary Backstay T4 [kip]	171	-130	108	-119	45	-45

A deformed geometry plot at the time of maximum moment during the Northridge-Castaic event is shown in Figure 7.16 (Step 135 represents $t = 13.5$ sec into the earthquake). The M_{33} bending moment time response at the base of tower T8 is shown in Figure 7.17.

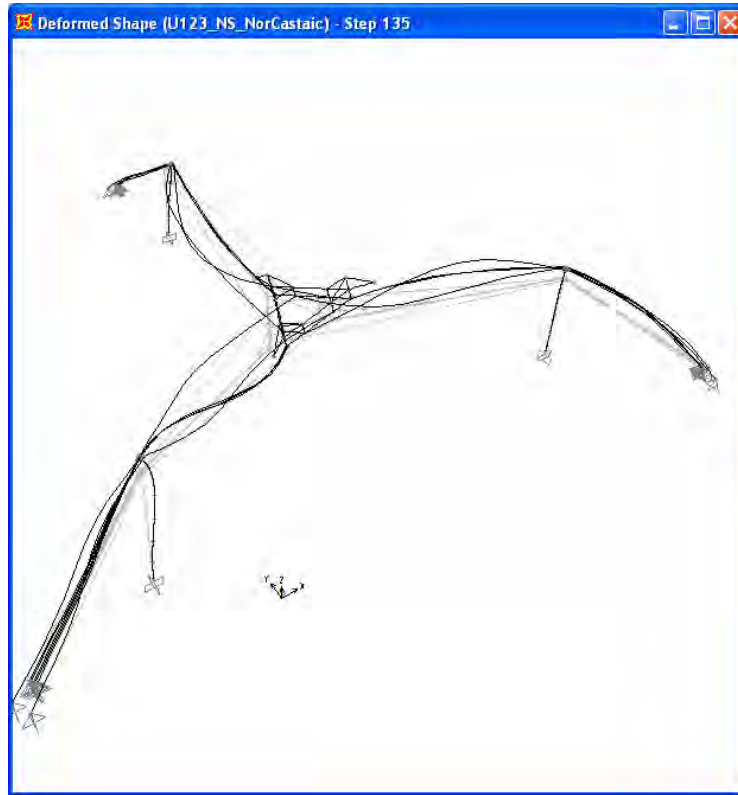


Figure 7.16 Deformed shape (50x mag.) 13.5 sec into unscaled Northridge-Castaic

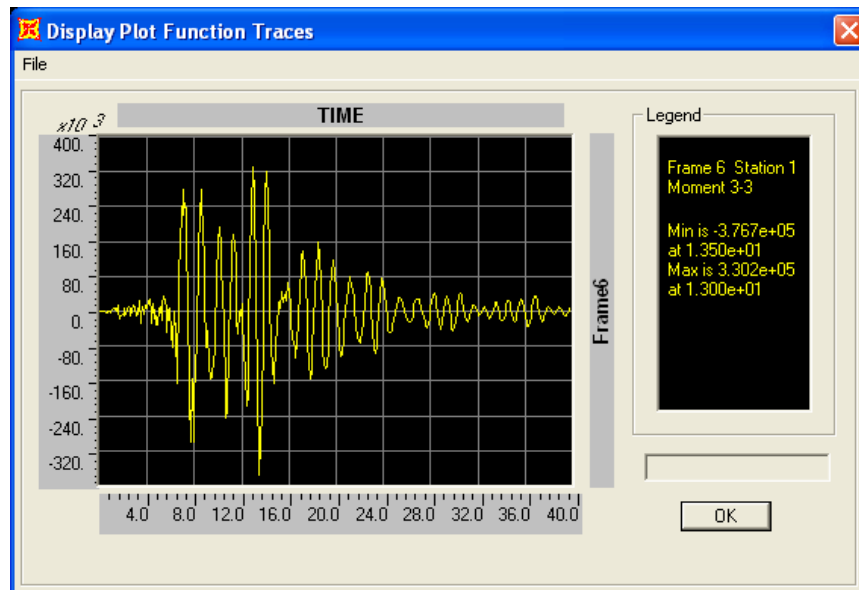


Figure 7.17. M_{33} [kip-ft] at the base of T8 for unscaled Northridge-Castaic – Model A

7.2.2 Seismic Response First Run – Unscaled Results for Model B

The results for Model B (uniform platform with tiedowns) for the unscaled earthquakes are shown in Table 7.4. Note that the values are very similar to those of Table 7.3 for Model A. This same trend, in which the response is essentially independent of the tiedown cables, was also observed with the earthquakes of Chapter 6.

Table 7.4. Seismic response (unscaled) for Model B

Label	Description	Model B U123 San Salvador CIG Station		Model B U123 Northridge Castaic Station		Model B U123 Artificial SIMQKE Program	
		MAX	MIN	MAX	MIN	MAX	MIN
	UX Displacement						
J27	Top of tower T12 [in]	17.0	-15.5	15.1	-12.4	7.9	-5.2
J36	Top of tower T8 [in]	18.1	-14.8	9.6	-9.7	3.6	-4.7
J43	Top of tower T4 [in]	6.7	-8.0	11.6	-11.5	6.1	-4.9
	UY Displacement						
J27	Top of tower T12 [in]	5.0	-6.4	4.8	-4.0	2.1	-1.8
J36	Top of tower T8 [in]	23.1	-26.6	11.0	-11.8	5.2	-6.0
J43	Top of tower T4 [in]	12.8	-13.4	17	-14.2	8.8	-7.3
	UZ Displacement						
J99	Platform corner T12 [in]	12.7	-10.7	12.6	-12	5.4	-6.5
J104	Platform corner T8 [in]	8.9	-8.6	11.7	-14.4	8.0	-8.0
J111	Platform corner T4 [in]	15.0	-11.6	9.2	-11.4	4.6	-5.7
	M33 Moment						
F4 R 1	Top of tower T12 [kip-ft]	4042	-4522	2700	-3423	983	-1082
F11 R 1	Top of tower T8 [kip-ft]	3066	-4484	2781	-3765	2088	-2036
F16 R 1	Top of tower T4 [kip-ft]	1255	-2368	2488	-2200	541	-447
F1 R 0	Base of tower T12 [kip-ft]	236500	-242900	183000	-177400	70020	-48900
F6 R 0	Base of tower T8 [kip-ft]	348500	-315100	311100	-305900	210900	-220700
F13 R 0	Base of tower T4 [kip-ft]	110200	-98670	126700	-127700	30300	-26110
	M22 Moment						
F1 R 0	Base of tower T12 [kip-ft]	127100	-174500	150000	-161100	96320	-85610
F6 R 0	Base of tower T8 [kip-ft]	343300	-343400	224800	-322200	82910	-90990
F13 R 0	Base of tower T4 [kip-ft]	128300	-145400	166000	-153900	116800	-123700
	ΔTENSION						
F271 R 0.5	Main Cable T12 [kip]	115	-156	124	-118	36	-56
F275 R 0.5	Main Cable T8 [kip]	77	-99	98	-99	66	-65
F280 R 0.5	Main Cable T4 [kip]	76	-92	111	-82	20	-26
F282 R 0.5	Auxiliary Cable T12 [kip]	183	-188	115	-153	51	-56
F284 R 0.5	Auxiliary Cable T8 [kip]	146	-131	143	-141	91	-90
F287 R 0.5	Auxiliary Cable T4 [kip]	101	-104	113	-86	38	-34
F251 R 0.5	Main Backstay T12 [kip]	136	-105	86	-103	41	-47
F256 R 0.5	Main Backstay T8 [kip]	98	-175	131	-145	93	-85
F261 R 0.5	Main Backstay T4 [kip]	88	-95	71	-63	19	-23
F264 R 0.5	Auxiliary Backstay T12 [kip]	157	-150	117	-138	53	-61
F267 R 0.5	Auxiliary Backstay T8 [kip]	97	-186	148	-187	110	-95
F269 R 0.5	Auxiliary Backstay T4 [kip]	113	-117	69	-72	21	-24
F289 R 0.5	Tiedown T12 TENSION [kip]	95	-85	100	-92	39	-40
F291 R 0.5	Tiedown T8 TENSION [kip]	73	-70	90	-111	54	-54
F292 R 0.5	Tiedown T4 TENSION [kip]	115	-88	67	-85	25	-32

A deformed geometry plot at the time of maximum moment during the unscaled San Salvador event is shown in Figure 7.18 (Step 15 represents $t = 1.5$ sec into the earthquake). The time variation of the M_{33} bending moment at the base of tower T8 is shown in Figure 7.19.



Figure 7.18. Deformed shape (50x mag.) 1.5 sec into unscaled San Salvador

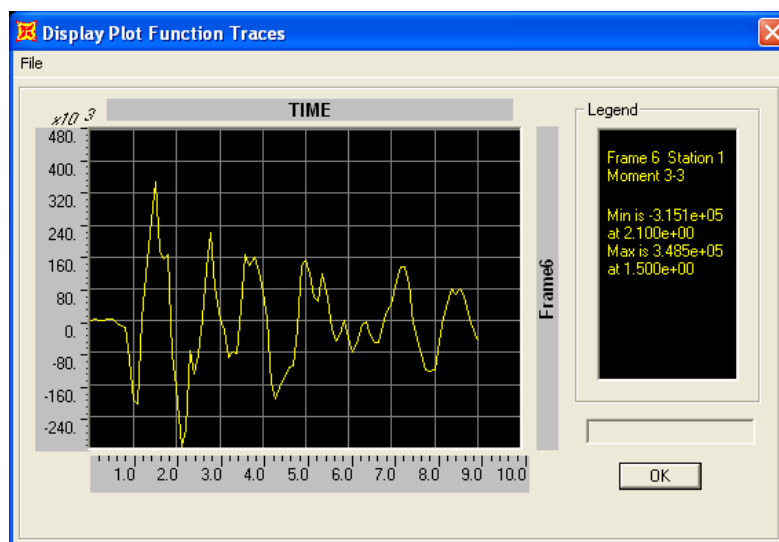


Figure 7.19. M_{33} [kip-ft] at the base of tower T8 for unscaled San Salvador – Model B

7.2.3 Seismic Response First Run – Unscaled Results for Model C

The results for Model C (which includes the dome) using the unscaled earthquakes are shown in Table 7.5. The results are similar to both Models A and B. The biggest difference in Model C is the smaller variation in tiedown tensions. This is due to the tendency of the platform to move in a “cradle” motion rather than the rotation about a longitudinal centroidal axis seen in Models A and B.

Table 7.5. Seismic response (unscaled) for Model C

Label	Description	Model C U123 San Salvador CIG Station		Model C U123 Northridge Castaic Station		Model C U123 Artificial SIMQKE Program	
		MAX	MIN	MAX	MIN	MAX	MIN
UX Displacement							
J27	Top of tower T12 [in]	17.1	-15.5	16.1	-12.4	7.9	-5.2
J36	Top of tower T8 [in]	19.4	-14.0	11.3	-8.5	4.7	-5.5
J43	Top of tower T4 [in]	8.0	-9.0	12.1	-10.2	6.2	-4.3
UY Displacement							
J27	Top of tower T12 [in]	6.5	-7.4	7.1	-3.9	3.0	-2.7
J36	Top of tower T8 [in]	23.4	-25.8	12.0	-13.5	5.1	-5.9
J43	Top of tower T4 [in]	14	-15.8	18.5	-15.8	8.8	-7.1
UZ Displacement							
J99	Platform corner T12 [in]	2.9	-2.9	3.3	-2.5	4.5	-4.7
J104	Platform corner T8 [in]	1.9	-1.8	4.4	-4.1	5.6	-5.8
J111	Platform corner T4 [in]	1.9	-2.3	2.5	-2.1	5.0	-5.0
M33 Moment							
F4 R 1	Top of tower T12 [kip-ft]	4144	-4825	2793	-3819	961	-1230
F11 R 1	Top of tower T8 [kip-ft]	3193	-4508	3131	-3816	2179	-1744
F16 R 1	Top of tower T4 [kip-ft]	1236	-2392	2579	-2628	514	-464
F1 R 0	Base of tower T12 [kip-ft]	253700	-256200	215400	-197600	88100	-67350
F6 R 0	Base of tower T8 [kip-ft]	347700	-307100	340800	-341500	227900	-218300
F13 R 0	Base of tower T4 [kip-ft]	108100	-99130	169500	-134300	35440	-36610
M22 Moment							
F1 R 0	Base of tower T12 [kip-ft]	129700	-175600	150300	-162200	96380	-85720
F6 R 0	Base of tower T8 [kip-ft]	343100	-349700	225100	-325000	80830	-91290
F13 R 0	Base of tower T4 [kip-ft]	138000	-146400	169900	-154700	117300	-124900
ΔTENSION							
F271 R 0.5	Main Cable T12 [kip]	113	-175	155	-93	60	-72
F275 R 0.5	Main Cable T8 [kip]	112	-136	151	-160	84	-80
F280 R 0.5	Main Cable T4 [kip]	111	-116	132	-117	26	-35
F282 R 0.5	Auxiliary Cable T12 [kip]	135	-217	150	-130	60	-62
F284 R 0.5	Auxiliary Cable T8 [kip]	145	-138	125	-133	82	-79
F287 R 0.5	Auxiliary Cable T4 [kip]	126	-127	146	-131	34	-35
F251 R 0.5	Main Backstay T12 [kip]	158	-138	85	-154	62	-67
F256 R 0.5	Main Backstay T8 [kip]	124	-174	177	-192	115	-108
F261 R 0.5	Main Backstay T4 [kip]	135	-115	102	-104	30	-28
F264 R 0.5	Auxiliary Backstay T12 [kip]	182	-187	115	-197	71	-84
F267 R 0.5	Auxiliary Backstay T8 [kip]	108	-184	216	-234	127	-121
F269 R 0.5	Auxiliary Backstay T4 [kip]	167	-139	107	-132	37	-27
F289 R 0.5	Tiedown T12 TENSION [kip]	18	-19.5	24.2	-20.2	23	-23
F291 R 0.5	Tiedown T8 TENSION [kip]	13.5	-13.5	33	-29.4	33	-31
F292 R 0.5	Tiedown T4 TENSION [kip]	12.2	-15.0	18.4	-14.4	27	-26

A plot of the fully deformed structure at the time of maximum moment during the unscaled San Salvador event is shown in Figure 7.20 (Step 15 represents $t = 1.5$ sec into the earthquake). The M_{33} bending moment (as a function of time) at the base of tower T8 is shown in Figure 7.21.

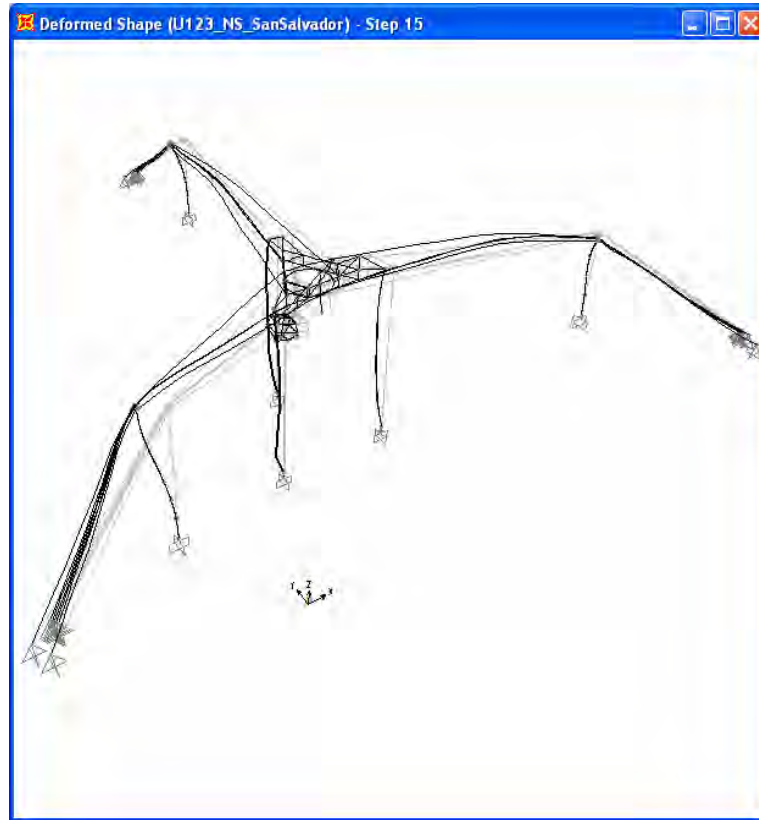


Figure 7.20. Deformed shape (50x mag.) 1.5 sec into unscaled San Salvador

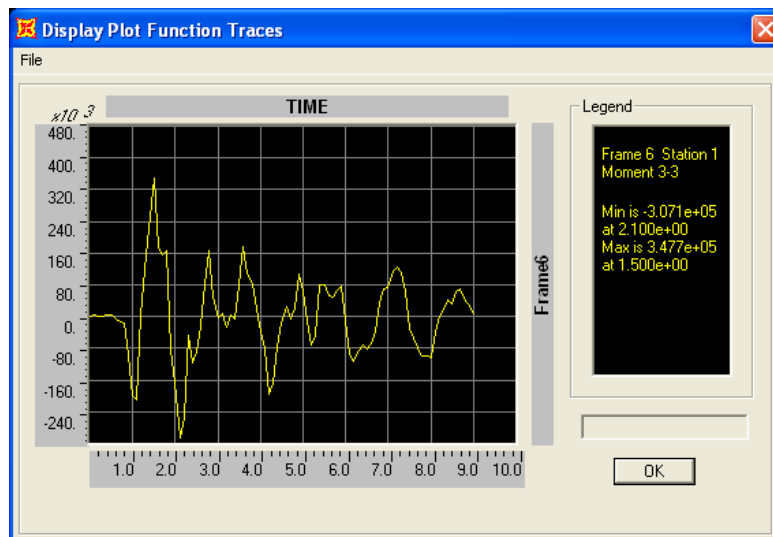


Figure 7.21. M_{33} [kip-ft] at the base of tower T8 for unscaled San Salvador – Model C

Figure 7.22 shows the deformed geometry of the Observatory structures at the time of maximum moment during the unscaled Northridge-Castaic event (Step 135 represents $t = 13.5$ sec into the earthquake). The M_{33} bending moment (as a function of time) at the base of tower T8 is shown in Figure 7.23.

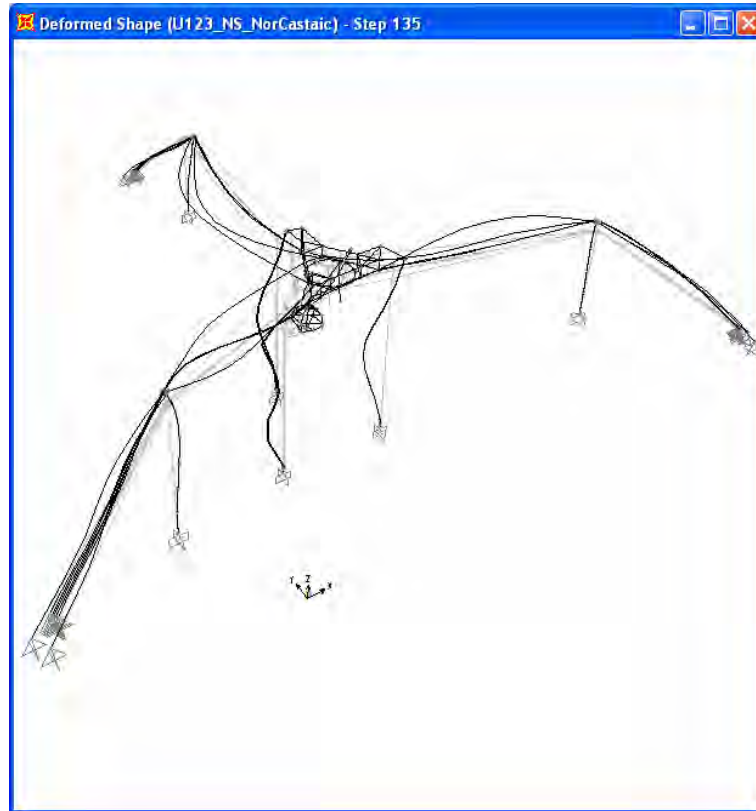


Figure 7.22. Deformed shape (50x mag.) 13.5 sec into unscaled Northridge-Castaic

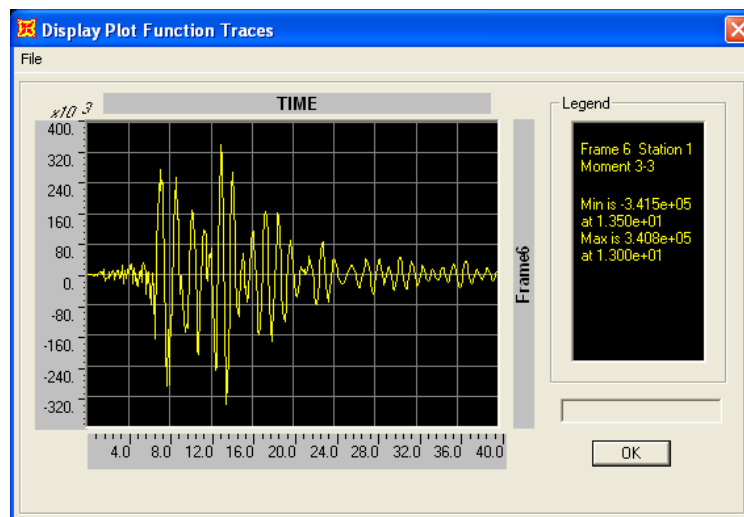


Figure 7.23. M_{33} [kip-ft] at base of T8 for unscaled Northridge-Castaic – Model C

A deformed geometry plot at the time of maximum moment during the Artificial SIMQKE event is shown in Figure 7.24 (Step 56 represents $t = 5.6$ sec into the earthquake). The Artificial earthquake, by virtue of its compatibility with the UBC-97 design spectrum, is inherently calibrated to a PGA of 0.3g. Figure 7.25 shows the variation in time of the M_{33} bending moment at the base of tower T8.

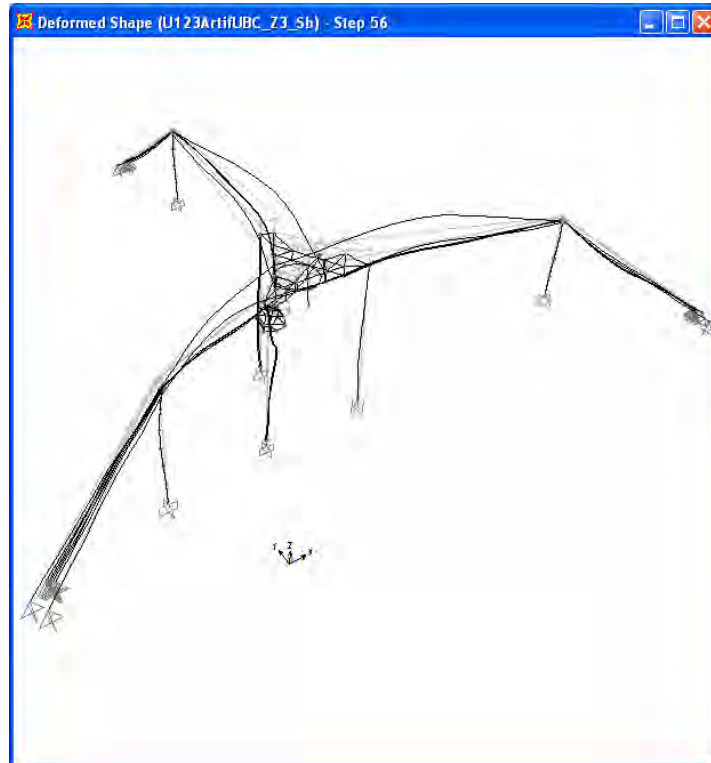


Figure 7.24. Deformed shape (75x mag.) of structure 5.6 sec into Artificial-SIMQKE

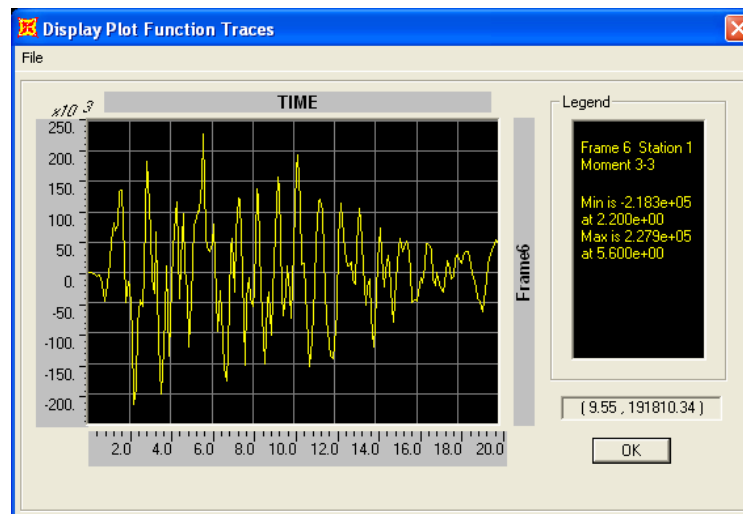


Figure 7.25. M_{33} [kip-ft] at the base of tower T8 for Artificial-SIMQKE – Model C

7.3 Additional First Run Results for Model C – Unscaled Earthquakes

The bending moments in the towers and the variations in the state of tension in the cables for the unscaled selected earthquakes are very similar in all three models A, B, and C. Model C, which best represents the real platform, will be used for a more focused investigation of the seismic response.

7.3.1 Maximum and Minimum Moments at All Tower Steps

Table 7.6 shows the maximum and minimum bending moments at all the steps in the 60 ft tower segments. In general, the moments increase as they approach the base.

Table 7.6. Maximum and minimum moments at all tower steps (unscaled earthquakes)

Label	Description	Model C U123 San Salvador CIG Station		Model C U123 Northridge Castaic Station		Model C U123 Artificial SIMQKE Program	
		MAX [kip-ft]	MIN [kip-ft]	MAX [kip-ft]	MIN [kip-ft]	MAX [kip-ft]	MIN [kip-ft]
TOWER T12 - M33							
F4-1	Base of TSEC1	42580	-49550	33930	-33220	13140	-11700
F3	Base of TSEC2	25270	-24080	31020	-34630	18340	-17770
F2	Base of TSEC3	122900	-107000	99130	-76510	38330	-29260
F1	Base of TSEC4	253700	-256200	215400	-197600	88100	-67350
TOWER T12 - M22							
F4-1	Base of TSEC1	20180	-25800	15320	-24520	16450	-14900
F3	Base of TSEC2	55810	-60790	44420	-55050	27220	-30260
F2	Base of TSEC3	73210	-85510	73030	-89850	31510	-43660
F1	Base of TSEC4	129700	-175600	150300	-162200	96380	-85720
TOWER T8 - M33							
F11-1	Base of TSEC1	26510	-58980	39830	-44540	23970	-19970
F10	Base of TSEC2	35500	-55160	41190	-43070	22800	-30560
F9	Base of TSEC3	65150	-55410	33840	-49120	38860	-37610
F8	Base of TSEC4	187100	-99000	141600	-116200	59520	-65210
F7	Base of TSEC5	243300	-145000	244800	-233000	133000	-106800
F6	Base of TSEC6	347700	-307100	340800	-341500	227000	-218300
TOWER T8 - M22							
F11-1	Base of TSEC1	39410	-25110	28580	-28930	5309	-4756
F10	Base of TSEC2	100200	-73220	58220	-68180	12580	-11600
F9	Base of TSEC3	141000	-111700	68080	-72130	23990	-20740
F8	Base of TSEC4	169800	-127300	80310	-86330	34190	-32890
F7	Base of TSEC5	213700	-201300	128400	-179400	51510	-54030
F6	Base of TSEC6	343100	-349700	225100	-325000	80830	-91290
TOWER T4 - M33							
F16-1	Base of TSEC1	18420	-20330	22850	-30110	4276	-4466
F15	Base of TSEC2	26000	-26880	18080	-23260	7189	-5728
F14	Base of TSEC3	48200	-49550	73640	-63450	16280	-14690
F13	Base of TSEC4	108100	-99130	169500	-134300	35440	-36610
TOWER T4 - M22							
F16-1	Base of TSEC1	31370	-21620	25180	-21910	20550	-21900
F15	Base of TSEC2	56410	-54110	58680	-54190	39690	-3674
F14	Base of TSEC3	71920	-78760	115200	-89250	57700	-43870
F13	Base of TSEC4	138000	-146400	169900	-154700	117300	-124900

7.3.2 Biaxial Bending State at All Tower Bases

The biaxial bending state at all tower bases is shown in Table 7.7. The table was generated by retrieving the time at which the maximum M_{33} moment (absolute value) occurred at each tower for each earthquake and then obtaining the corresponding M_{22} moment and seismic axial force at exactly the same time. The axial force due to dead loading is superimposed to the seismic axial force to obtain the total axial force reacting at the base of each tower. This approach assures that a combination of realistic values for bending moments and axial forces are used for a comparison with the section capacities in the next chapter.

Table 7.7. Biaxial bending state at all tower bases (unscaled earthquakes)

	Model C U123 San Salvador CIG Station	Model C U123 Northridge Castaic Station	Model C U123 Artificial SIMQKE Program
BASE of T12 (F1)			
Time at Max M33 [sec]	2.1	9.5	6.4
Max (or Min) M33 [kip-ft]	-256200	215400	88100
M22 [kip-ft]	-175600	12740	11550
Seismic Axial Force [kip]	-675	507	506
Dead Axial Force [kip]	-8785	-8785	-8785
Total Axial Force [kip]	-9460	-8278	-8279
BASE of T8 (F6)			
Time at Max M33 [sec]	1.5	13.5	5.6
Max (or Min) M33 [kip-ft]	347700	-341500	227900
M22 [kip-ft]	-100000	40810	31140
Seismic Axial Force [kip]	-3235	-583	-152
Dead Axial Force [kip]	-14530	-14530	-14530
Total Axial Force [kip]	-17765	-15113	-14682
BASE of T4 (F13)			
Time at Max M33 [sec]	1.9*	12.2	3.3*
Max (or Min) M33 [kip-ft]	146400*	169500	-124900*
M22 [kip-ft]	94904*	-66700	-9667*
Seismic Axial Force [kip]	-673	472	-1303
Dead Axial Force [kip]	-8785	-8785	-8785
Total Axial Force [kip]	-9458	-8313	-10088

* The values of M33 and M22 were swapped so as to obtain the more critical combination

7.4 Second Run Results for Model C – Scaled San Salvador and Northridge

This section presents the results of the scaled San Salvador-CIG and Northridge-Castaic earthquakes. The scale factor represents a reduction from the high PGA's in the original records (all components) down to 0.3g PGA. In this manner the records are tuned to the requirements of the UBC-97 and closer to Dames & Moore (1999). Only Model C has been chosen for this study as it is the model which best represents the real platform.

7.4.1 Maximum and Minimum Moments at All Tower Steps

Table 7.8 shows the maximum and minimum bending moments at all the steps in the 60 ft tower segments. The reduction is evident compared to Table 7.6.

Table 7.8. Maximum and minimum moments at all tower steps (scaled earthquakes)

Label	Description	Scaled to 0.3 PGA Model C U123 San Salvador CIG Station		Scaled to 0.3 PGA Model C U123 Northridge Castaic Station	
		MAX [kip-ft]	MIN [kip-ft]	MAX [kip-ft]	MIN [kip-ft]
	TOWER T12 - M33				
F4-1	Base of TSEC1	30940	-35360	32720	-31940
F3	Base of TSEC2	18340	-17770	31460	-34240
F2	Base of TSEC3	86080	-75850	95510	-70730
F1	Base of TSEC4	178300	-181700	210900	-188400
	TOWER T12 - M22				
F4-1	Base of TSEC1	8686	-11170	8075	-12970
F3	Base of TSEC2	24070	-26280	23420	-28410
F2	Base of TSEC3	31610	-37000	38540	-47140
F1	Base of TSEC4	56690	-76060	79300	-85320
	TOWER T8 - M33				
F11-1	Base of TSEC1	29130	-21290	25100	-27590
F10	Base of TSEC2	15160	-26890	22250	-27580
F9	Base of TSEC3	32170	-30730	22940	-29100
F8	Base of TSEC4	92390	-55780	84180	-67660
F7	Base of TSEC5	116400	-82340	143500	-128100
F6	Base of TSEC6	162400	-126900	202300	-203800
	TOWER T8 - M22				
F11-1	Base of TSEC1	29130	-21290	25100	-27590
F10	Base of TSEC2	74160	-59300	58510	-56250
F9	Base of TSEC3	102400	-83010	62390	-76560
F8	Base of TSEC4	108100	-90070	88640	-105200
F7	Base of TSEC5	157700	-149100	104500	-114300
F6	Base of TSEC6	250000	-264900	234000	-229200
	TOWER T4 - M33				
F16-1	Base of TSEC1	8288	-7318	15550	-15660
F15	Base of TSEC2	13030	-12310	12000	-14920
F14	Base of TSEC3	23110	-15470	49130	-32930
F13	Base of TSEC4	48270	-36630	107700	-85820
	TOWER T4 - M22				
F16-1	Base of TSEC1	19670	-14850	24330	-19780
F15	Base of TSEC2	36910	-36910	54770	-47140
F14	Base of TSEC3	54260	-52060	98650	-75300
F13	Base of TSEC4	96170	-92580	153800	-141800

7.4.2 Biaxial Bending State at All Tower Bases (scaled)

The biaxial bending moment state at all tower bases for the scaled earthquakes is shown in Table 7.9. The axial forces required to check the capacity of the columns are also included. The table was generated by searching for the time at which the maximum M_{33} moment (in absolute value) occurred at each tower for each earthquake and obtaining at exactly the same time the corresponding M_{22} moment and seismic axial force. The axial force due to dead loading is superimposed to the seismic axial force to obtain the total axial force reacting at the base of each tower. By using this approach, a combination of realistic values for bending moments and axial forces will be used in the next chapter to compare the seismic demand with the section capacities.

Table 7.9. Biaxial bending state at all tower bases (scaled earthquakes)

	Model C U123 San Salvador CIG Station Scaled to 0.3g	Model C U123 Northridge Castaic Station Scaled to 0.3g
BASE of T12 (F1)		
Time at Max M33 [sec]	2.1	9.5
Max (or Min) M33 [kip-ft]	-181700	210900
M22 [kip-ft]	-76061	5879
Seismic Axial Force [kip]	-470	462
Dead Axial Force [kip]	-8785	-8785
Total Axial Force [kip]	-9255	-8323
BASE of T8 (F6)		
Time at Max M33 [sec]	3.2*	9.9*
Max (or Min) M33 [kip-ft]	-264900*	234000*
M22 [kip-ft]	7793*	10444*
Seismic Axial Force [kip]	-719	-86
Dead Axial Force [kip]	-14530	-14530
Total Axial Force [kip]	-15249	-14616
BASE of T4 (F13)		
Time at Max M33 [sec]	2.9*	9.9*
Max (or Min) M33 [kip-ft]	96170*	153800*
M22 [kip-ft]	-9117*	27740*
Seismic Axial Force [kip]	-554	-54
Dead Axial Force [kip]	-8785	-8785
Total Axial Force [kip]	-9339	-8839

* The values of M33 and M22 were swapped so as to obtain the more critical combination

7.5 Third Run Results for Model C – Parkfield and Morgan Hill

The results obtained with the Parkfield and Morgan Hill earthquakes are presented in this section. These two records are closer to the UBC-97 design spectrum and have a higher probability of representing the actual seismic demand at the Arcibo site. The San Salvador-CIG and Northridge-Castaic are much more powerful records.

7.5.1 Maximum and Minimum Moments at All Tower Steps

Table 7.10 shows the maximum and minimum bending moments at all the steps in the tower segments. It can be seen that the Morgan Hill record, which is tuned to longer periods (and closer to the natural periods of the towers) than the Parkfield record, generates significantly higher bending moments at most locations.

Table 7.10. Maximum and minimum moments at all tower steps (Third Run)

Label	Description	Model C U123 Parkfield 097 Station		Model C U123 Morgan Hill Gilroy6 Station	
		MAX [kip-ft]	MIN [kip-ft]	MAX [kip-ft]	MIN [kip-ft]
	TOWER T12 - M33				
F4-1	Base of TSEC1	3715	-5044	10590	-10650
F3	Base of TSEC2	8205	-9164	5821	-5945
F2	Base of TSEC3	12170	-8471	19940	-20380
F1	Base of TSEC4	24370	-20140	54390	-62720
	TOWER T12 - M22				
F4-1	Base of TSEC1	8665	-12290	11700	-15510
F3	Base of TSEC2	10880	-20440	24300	-36730
F2	Base of TSEC3	15520	-26000	48270	-50010
F1	Base of TSEC4	33600	-56400	72410	-67150
	TOWER T8 - M33				
F11-1	Base of TSEC1	8559	-10100	30630	-32900
F10	Base of TSEC2	14870	-20270	38240	-33260
F9	Base of TSEC3	21370	-24870	24840	-28010
F8	Base of TSEC4	39040	-26120	90580	-92370
F7	Base of TSEC5	53340	-49610	165000	-175600
F6	Base of TSEC6	71000	-97100	233600	-275900
	TOWER T8 - M22				
F11-1	Base of TSEC1	8261	-6332	9261	-10030
F10	Base of TSEC2	8951	-10360	19460	-21860
F9	Base of TSEC3	8973	-14450	26530	-23620
F8	Base of TSEC4	22050	-22910	19840	-17770
F7	Base of TSEC5	22100	-18800	35470	-31160
F6	Base of TSEC6	53760	-32570	72680	-78960
	TOWER T4 - M33				
F16-1	Base of TSEC1	3969	-4052	16110	-18590
F15	Base of TSEC2	6692	-6632	11780	-14530
F14	Base of TSEC3	13080	-10400	45370	-40830
F13	Base of TSEC4	25230	-27780	103400	-93400
	TOWER T4 - M22				
F16-1	Base of TSEC1	14440	-10780	9128	-8614
F15	Base of TSEC2	19540	-17260	24650	-16490
F14	Base of TSEC3	25850	-14680	31340	-30710
F13	Base of TSEC4	52880	-48010	40110	-52620

7.5.2 Biaxial Bending State at All Tower Bases (Third Run)

The biaxial bending moments and axial forces at all tower bases for the Parkfield and Morgan Hill earthquakes are shown in Table 7.11. As in the previous cases, the table was created by obtaining the time at which the maximum M_{33} moment (in absolute value) occurred at each tower for each earthquake and then obtaining the corresponding M_{22} moment and seismic axial force at this time. The total axial force reacting at the base of each tower is obtained by superposition of the axial force due to dead loading and the seismic axial force.

Table 7.11. Biaxial bending state at all tower bases (Third Run)

	Model C U123 Parkfield 097 Station	Model C U123 Morgan Hill Gilroy6 Station
BASE of T12 (F1)		
Time at Max M33 [sec]	4.1*	6.6*
Max (or Min) M33 [kip-ft]	-56400*	72410*
M22 [kip-ft]	-14036	20283
Seismic Axial Force [kip]	-23	-98
Dead Axial Force [kip]	-8785	-8785
Total Axial Force [kip]	-8808	-8883
BASE of T8 (F6)		
Time at Max M33 [sec]	4.1	6.9
Max (or Min) M33 [kip-ft]	-97100	-275900
M22 [kip-ft]	53764	-56307
Seismic Axial Force [kip]	364	56
Dead Axial Force [kip]	-14530	-14530
Total Axial Force [kip]	-14166	-14474
BASE of T4 (F13)		
Time at Max M33 [sec]	4.1*	7.4
Max (or Min) M33 [kip-ft]	52880*	103400
M22 [kip-ft]	25225	-4007
Seismic Axial Force [kip]	-121	370
Dead Axial Force [kip]	-8785	-8785
Total Axial Force [kip]	-8906	-8415

* The values of M33 and M22 were swapped so as to obtain the more critical combination

7.6 Recommendation for Accelerometer Locations

The Puerto Rico Strong Motion program, based on the Civil Engineering Department of UPR-RUM, has plans to instrument the structures of the Arecibo Observatory. Therefore, it is relevant to produce some recommendations for locations of the accelerometers based on the numerous analysis performed on the course of the present research.

It is recommended that all accelerometers mounted at the observatory shall be of the triaxial type or, as an alternative, mount three, one-axis accelerometers to measure the three orthogonal components. All the strong motion records researched for this thesis invariably contained records for three orthogonal directions. The records from Puerto Rico would join the world-wide earthquake record database on equal terms. The direction of least importance for the Arecibo Observatory structures is the “up” direction. It was shown in Chapter 6 (see Table 6.3) that the towers and cable structures are practically insensitive to motion in the vertical (up and down) direction. At the very least, two orthogonal directions in the horizontal plane should be included.

Several interesting investigations could be performed with the data and each depends on the location of the accelerometers. Some of these research possibilities are presented below to provide a context upon which to base the recommendations.

1. Soil-structure interaction / Multiple support excitation

The hill on which tower T12 is founded provides the most accessible platform to conduct this investigation (Figure 1.1). An accelerometer should be placed on the foundation of the tower and another at approximately the same elevation approximately two hundred feet away near the access road to the pedestrian bridge. If, as expected, there is negligible soil-structure interaction then the two records should be nearly identical. This would validate the fixed-tower-base assumption used in this work. It will be very useful if accelerometers can be placed in this same manner on each tower. The recordings will permit to investigate the differences in accelerations at each support. Depending on the results, a new study considering full multiple support excitation may be of interest. To investigate the wave-passage effect (time lag), the accelerometers must keep a very precise time record.

2. Topographic amplification effect

Assuming that point 1 above is fulfilled for tower T12, an additional accelerometer should be placed at a convenient spot near the base of the same hill, for example, near the cable-car shed. If the topographic effect is negligible, the records from the base as well as from the top of the hill (the one located at a distance away from foundation) should be nearly identical. Otherwise, the record from the top of the hill should be in an amplified state as compared with the record from the base of the hill. In this thesis the topographic amplification effect was not taken into account.

3. Verification of the fundamental periods of towers

The ideal location to place an accelerometer to determine the fundamental period of each tower would be at the top of the towers, where the largest displacements take place. At least two towers should be instrumented since there are two distinct types. Tower T8 should be instrumented on account of being the tallest and either tower T4 or T12, which are identical, should also be instrumented.

4. Verification of the higher modes and natural periods of towers

The stepped nature of the towers creates large variations in stiffness which promote the activation of higher modes of vibrations during a seismic event. Accelerometers placed at each step of the towers would provide excellent data to plot and validate several of the higher flexural modes of the towers. The horizontal surface at each step is an ideal location as it facilitates installation. Negligible differences in the up-down records at each step would confirm the minimal response in the vertical (axial) direction predicted by the finite element models. Otherwise, biaxial instruments can be used to reduce the instrumentation costs.

5. Platform response

Accelerometers placed at each corner of the platform can help to shed light on the response of the platform and the records obtained could be used to validate the platform modes and interaction modes predicted by the finite element model.

CHAPTER 8

Failure Criteria

This chapter examines the capacity of the structure and compares it to the bending moments obtained from the analysis described in the previous chapter to determine if the Arecibo Observatory is capable of resisting the maximum credible earthquakes. As defined in Chapter 7, the “First Run” corresponds to the unscaled San Salvador-CIG and Northridge Castaic records (improbable records which are included to test the limits of the structure); the “Second Run” corresponds to the scaled (down to 0.3g PGA) San Salvador-CIG and Northridge Castaic records; and the “Third Run” corresponds to the more probable Parkfield-station097 and Morgan Hill-Gilroy#6 records. The results of the artificial record, compatible with the UBC-97 design spectrum, are included in the “First Run”.

8.1 Appropriateness of Reinforcement Development Length

Reinforced concrete depends on a strong bond between the concrete and the reinforcement bars to transfer loads between each other. McGregor (1996) indicates the following: “Because the actual bond stress varies along the length of a bar anchored in a zone of tension, the ACI code uses the concept of development length rather than bond stress. The development length, l_d , is the shortest length of bar in which the bar stress can increase from zero to the yield strength, f_y . If the distance from a point where the bar stress equals f_y to the end of the bar is less than the development length, the bar will pull out of the concrete”. A lap splice (overlap length equal to at least l_d) is a typical manner of achieving the required development length in two subsequent longitudinal bars. As shown in Figure 8.1, there is a 5 ft overlap length for #11 bar splices in an intermediate tower-step. The 5-ft overlap (development length) is typical for all the #11 bars in all the towers at all locations.

Figures 8.2 and 8.3 show typical sections of the towers. Figure 8.2 corresponds to the top two steps of all the towers. Figure 8.3 corresponds to all other steps. The main difference between the two sections is that the top two steps have only one layer of 11#11 bars.

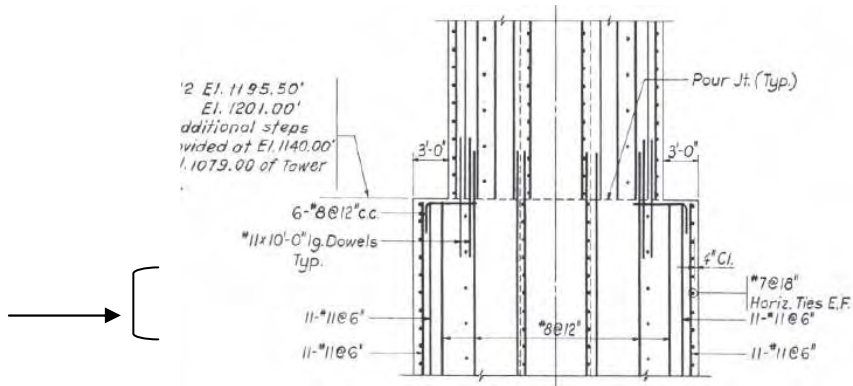
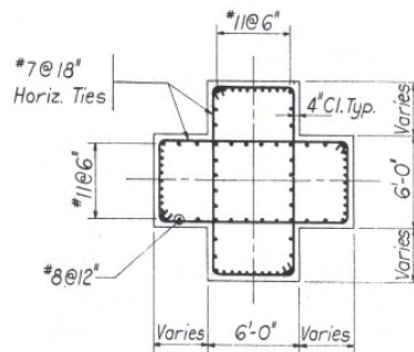
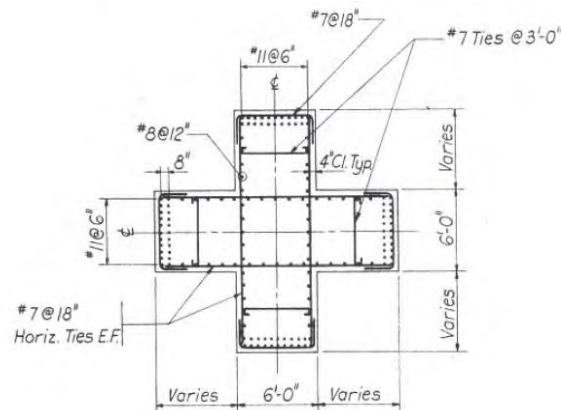


Figure 8.1. Lap splice at intermediate tower step



SECTION OF TOWER
 EL. 1258' TO EL. 1383' FOR TOWERS T4 & T12
 EL. 1262' TO EL. 1383' FOR TOWER T8

Figure 8.2. Cross section at the top two steps of all the towers



TYPICAL SECTION
 EL. 1133' TO EL. 1258' FOR TOWERS T4 & T12
 EL. 1018' TO EL. 1262' FOR TOWER T8

Figure 8.3. Cross section at all steps of the towers except the top two steps

ACI 318-02 Code Requirements for Development Length

Chapter 12 of ACI 318-02 covers development length and splices. Chapter 21, which covers special provisions for seismic design, does not apply if the failure criterion is taken as first yield of the steel bars. As stated in the scope of the ACI code,

21.2.1.1 – Chapter 21 contains special requirements for design and construction of reinforced concrete members of a structure for which the design forces, related to earthquake motions, have been determined on the basis of energy dissipation in the nonlinear range of response.

Equation 12.1 of the code, states the development length as:

$$l_d = \left[\frac{3}{40} \frac{f_y}{\sqrt{f'_c}} \frac{\alpha\beta\gamma\lambda}{\left(\frac{c + K_{tr}}{d_b} \right)} \right] d_b$$

where,

l_d = development length [in] (to be calculated)

f_y = 40,000 psi (Rebar yield strength ... “intermediate grade steel”)

f'_c = 3,000 psi (compressive strength of concrete)

α = 1.0 (Reinforcement Location Factor ... not horizontal)

β = 1.0 (Coating factor... not epoxy coated)

γ = 1.0 (Reinforcement size factor... for #7 and larger bars)

λ = 1.0 (Lightweight aggregate concrete factor... using normal weight concrete)

c = 3.0 in (spacing or cover dimension ... one-half the center-to-center spacing of bars)

d_b = 1.41 in (nominal diameter of #11 bar)

K_{tr} = transverse reinforcement index

$$K_{tr} = \frac{A_{tr} f_{yt}}{1500sn}$$

Where,

$A_{tr} = 4 * 0.6 \text{ in}^2 = 2.4 \text{ in}^2$ (transverse reinforcement cross-sectional area within spacing 's')

$f_{yt} = 40,000 \text{ psi}$ (yield strength of transverse reinforcement)

$s = 18 \text{ in}$ (maximum center-to-center spacing of transverse reinforcement within l_d)

$n = 22$ (number of bars spliced along the plane of splitting... worst case)

Substituting in the equation for K_{tr}

$$K_{tr} = \frac{(2.4)(40,000)}{(1500)(18)(22)} = 0.16$$

Substituting in the term within parenthesis in the equation for l_d

$$\left(\frac{c + K_{tr}}{d_b} \right) = \frac{3.0 + 0.16}{1.41} = 2.24 \leq 2.5 \text{ ok}$$

Note the advantage of providing good clear cover and comfortable bar spacing.

Substituting in the expression for l_d

$$l_d = \left[\frac{3}{40} \frac{40,000}{\sqrt{3,000}} \frac{(1)(1)(1)(1)}{2.24} \right] 1.41 = 34.5 \text{ inch}$$

In addition, the lap splice is "Class B" since the laps are not staggered, i.e., all laps occur at the step between different sections. Therefore, an additional factor of $1.3 * l_d$ must be applied, i.e.,

$$l_d = 1.3 (34.5) = 45 \text{ inch which is less than 60 inch}$$

Even using Equation 21-6 of the code (applying seismic provision of Chapter 21), and a factor of 3.5 according to 21.5.4.2(b), the required development length is 55 inches which is within the existing 60 inches.

Conclusion: The 5-ft length lap splice is appropriate in both the linear as well as nonlinear (plastic deformations) regime of the towers

8.2 Introduction to Elastic Failure Criterion for Towers

Two failure criteria are examined for the Arecibo Observatory towers. The first criterion, discussed in this section, requires that bending moments in the towers remain in the elastic regime. This stringent requirement is based on the required positional accuracy of the instrumentation housed in the suspended platform. Plastically deformed towers would result in misalignment of the instrumented platform and would defeat the scientific mission of the Arecibo Observatory. As a result, the towers shall be considered an integral component of the precise instrumentation systems used for astrophysical and ionospheric research, and are expected to respond elastically.

For the elastic failure criterion all strength reduction factors are set to 1.0 based on the stringent quality assurance observed during construction of the observatory, the excellent maintenance and conservation efforts during the past 45 years, and its excellent performance demonstrated during major hurricanes where no tower segment has even reached M_{cr} , the cracking moment of the reinforced concrete sections. In addition, the humid environment where it is located assures the concrete has cured well. All load amplification factors are also set to 1.0. The dead load is known with good accuracy and the applied seismic loads are very high. Therefore, the comparison between moment demands and moment capacity will be based on a nominal (unfactored) state.

The nominal Axial-Force/Bending-Moment interaction diagrams for the six tower sections are given in Figures 8.4 - 8.9. They were created using program XTRACT by Imbsen Software Systems Inc (Version 3.0.5 of January, 2006). These six graphs provide a sense for the nominal capacity of all the towers. They are not used directly in the investigation of the elastic failure criterion since they are based on ultimate moment capacity rather than first-yield moment capacity. Nevertheless, since $M_u \approx M_y$ it provides a good feel for the interaction between axial load and uniaxial bending moments even when the failure criterion is based on an elastic response. Note that section TSEC1 refers to the top step of all the towers, TSEC2 corresponds to the next step, etc. Towers T4 and T12 have only four steps so their base is described by TSEC4. Tower T8, on the other hand, has two additional steps so its base is described by TSEC6.

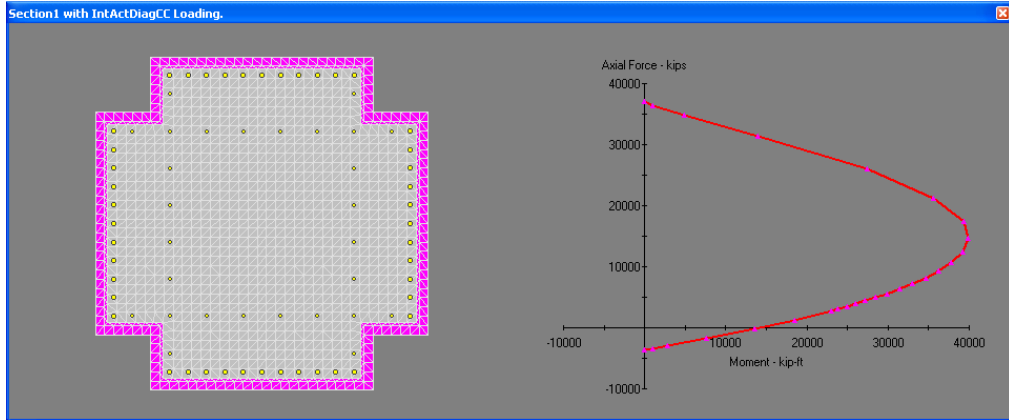


Figure 8.4. Nominal interaction diagram for TSEC1 (top step of tower)
 TSEC1 is 9 ft wide. The curve crosses the horizontal axis at approx. 13,600 kip-ft.

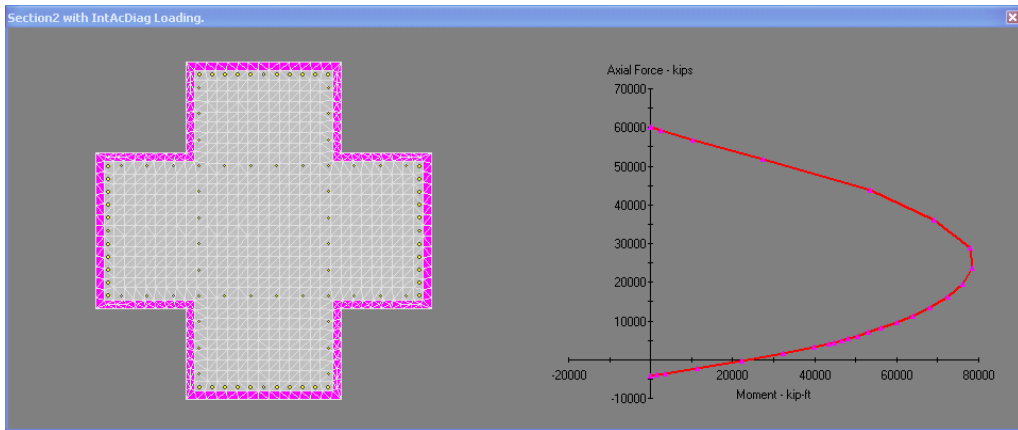


Figure 8.5. Nominal interaction diagram for TSEC2
 TSEC2 is 13 ft wide. The curve crosses the horizontal axis at approx. 22,300 kip-ft.

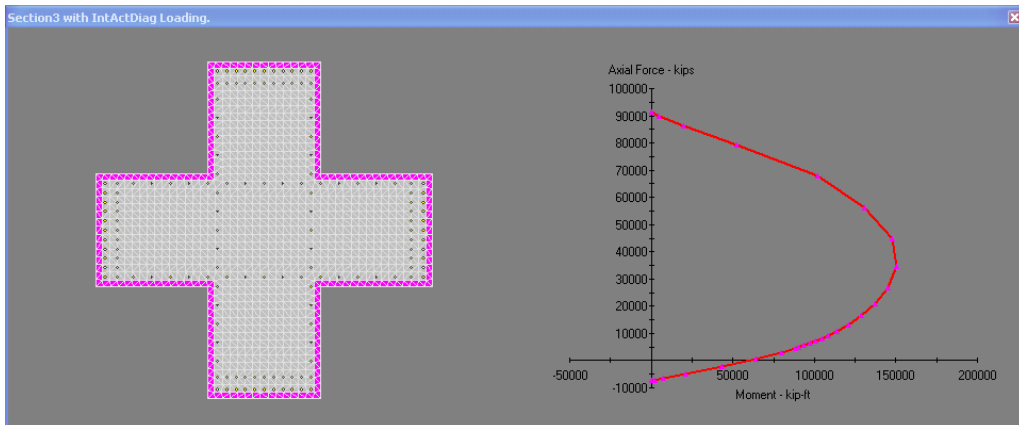


Figure 8.6. Nominal interaction diagram for TSEC3
 TSEC3 is 18 ft wide. The curve crosses the horizontal axis at approx. 60,000 kip-ft.

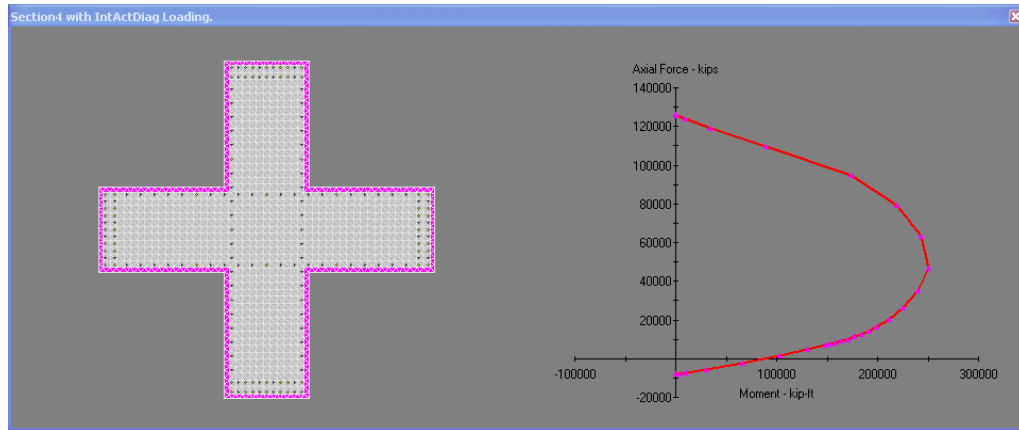


Figure 8.7. Nominal interaction diagram for TSEC4
TSEC4 is 24 ft wide. The curve crosses the horizontal axis at approx. 90,000 kip-ft.

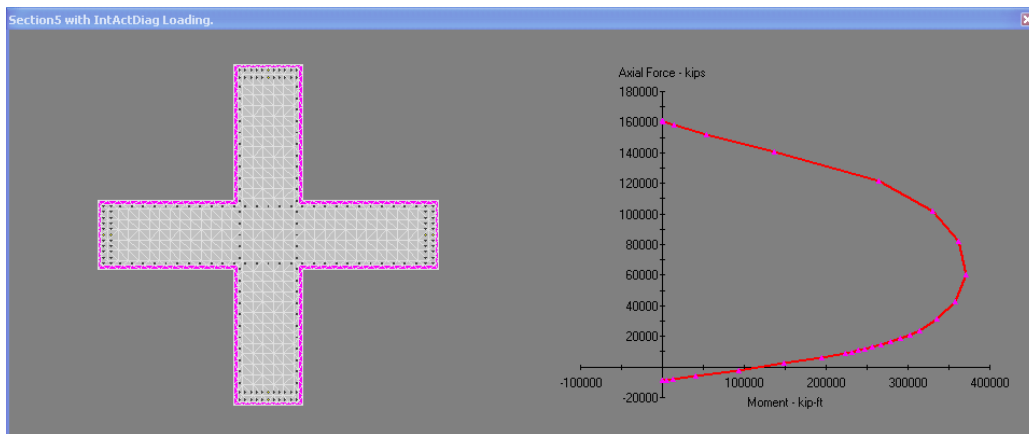


Figure 8.8. Nominal interaction diagram for TSEC5 (tower T8 only)
TSEC5 is 30 ft wide. The curve crosses the horizontal axis at approx. 120,000 kip-ft.

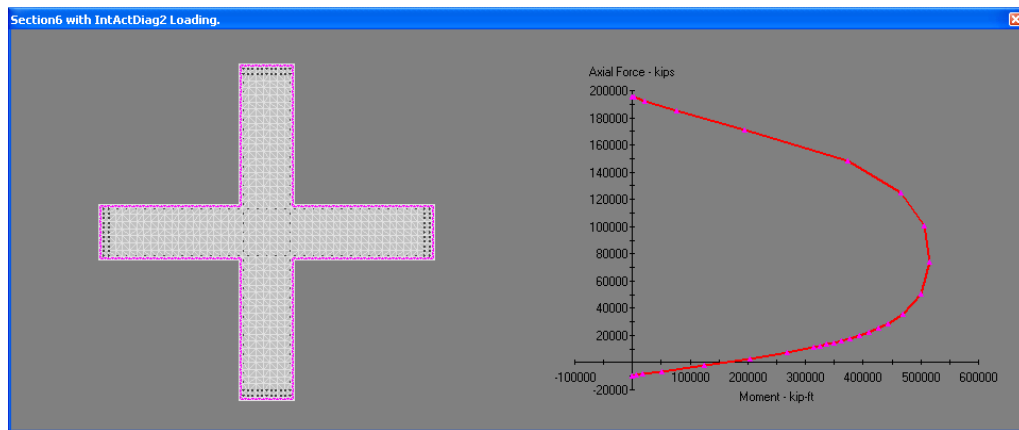


Figure 8.9. Nominal interaction diagram for TSEC6 (tower T8 only)
TSEC6 is 36 ft wide. The curve crosses the horizontal axis at approx. 160,000 kip-ft.

Figures 8.4 through 8.9 show that the towers have a significant ultimate moment capacity. The actual capacity at any arbitrary point in time during the earthquake is a function of the actual axial force in the towers. Given the axial force level in the vertical axis, a horizontal line is drawn from that point until it intersects the interaction curve. The moment capacity is determined by drawing a vertical line from the intersection and reading the value in the horizontal axis.

Interaction diagrams are obtained by performing multiple moment-curvature graphs at different levels of axial force and plotting the coordinates (Axial force, M_{ult}). A typical moment-curvature graph from XTRACT is shown in Figure 8.10.

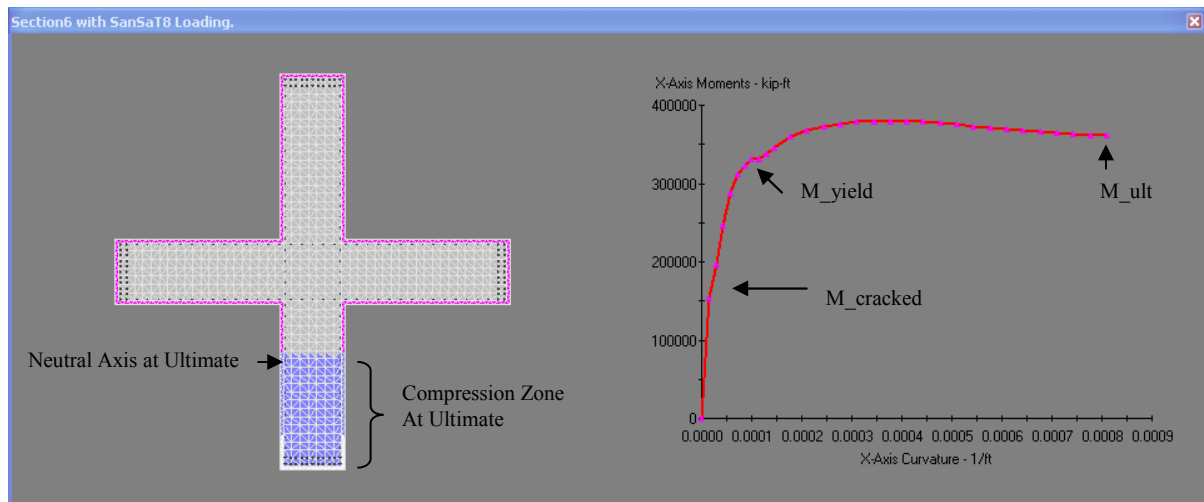


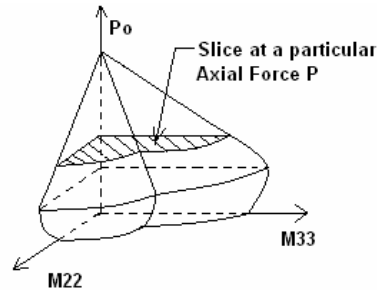
Figure 8.10. Moment-curvature graph (TSEC6). Axial Load = 17765 kip (San Salvador)

Figure 8.10 corresponds to the moment-curvature graph of section TSEC6 (base of tower T8). The axial force used is 17765 kip which corresponds to the time at which the maximum moment occurs in the San Salvador earthquake (see Table 7.7). The coordinates obtained from Fig. 8.10 (Axial Force = 17765 kip, $M_{ult} = \sim 360000$ kip-ft) are observed to be part of the TSEC6 interaction diagram of Figure 8.9.

In typical uniaxial design situations the axial force and the bending moment in the structural member are plotted as a point in a factored interaction diagram graph. If the point falls inside the interaction curve the section is deemed to have sufficient capacity. If the point falls outside the curve the section is too weak and must be strengthened. When there

are significant bending moments in both the x and y directions a biaxial interaction diagram is used. As shown in Table 7.7, this is the case of the Arecibo Observatory towers.

A schematic of a biaxial diagram is shown in Figure 8.11. Note that it is a spatial (3D) diagram. In a typical design situation a section is deemed to have sufficient capacity if the point represented by the coordinate (F_{axial} , M_{33} , M_{22}) resides inside the diagram.



(Only one octant of the biaxial interaction diagram is shown for clarity)

Figure 8.11. Schematic of a biaxial interaction diagram

An alternative to plotting in 3D is to take a horizontal slice of the biaxial diagram at the level of the applied axial force, as shown in Figure 8.11, and plotting the contour of the diagram at that level to create an “orbit” plot. The program XTRACT performs this step. A typical orbit plot is shown in Figure 8.12. It corresponds to an axial force level of 17765 kip, the same level as for Figure 8.10. Note the orbit is symmetrical since the section is symmetrical. In addition, note that the maximum moments are on the order of 360,000 kip-ft which corresponds to M_{ult} from the moment-curvature graph (Figure 8.10). In a typical design situation the section is deemed to have sufficient capacity if the coordinate (M_{33} , M_{22}) resides inside the orbit.

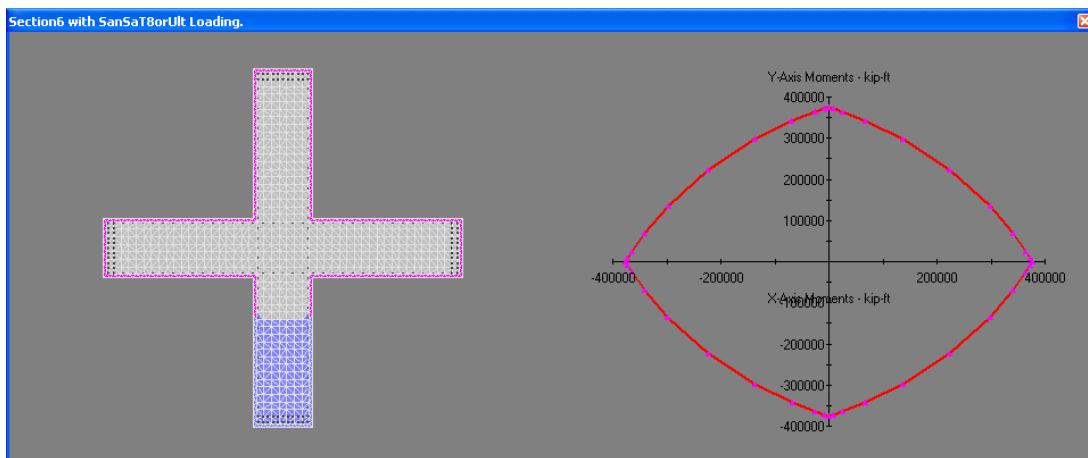


Figure 8.12. Orbit plot for biaxial bending – TSEC6 – Axial Load = 17765 kip

Figure 8.13 shows a sequence for section TSEC6 as the software XTRACT makes the calculation for the orbital plot at first yield of the section. Note that the neutral axis changes orientation as the software analyzes the section for different biaxial combinations.

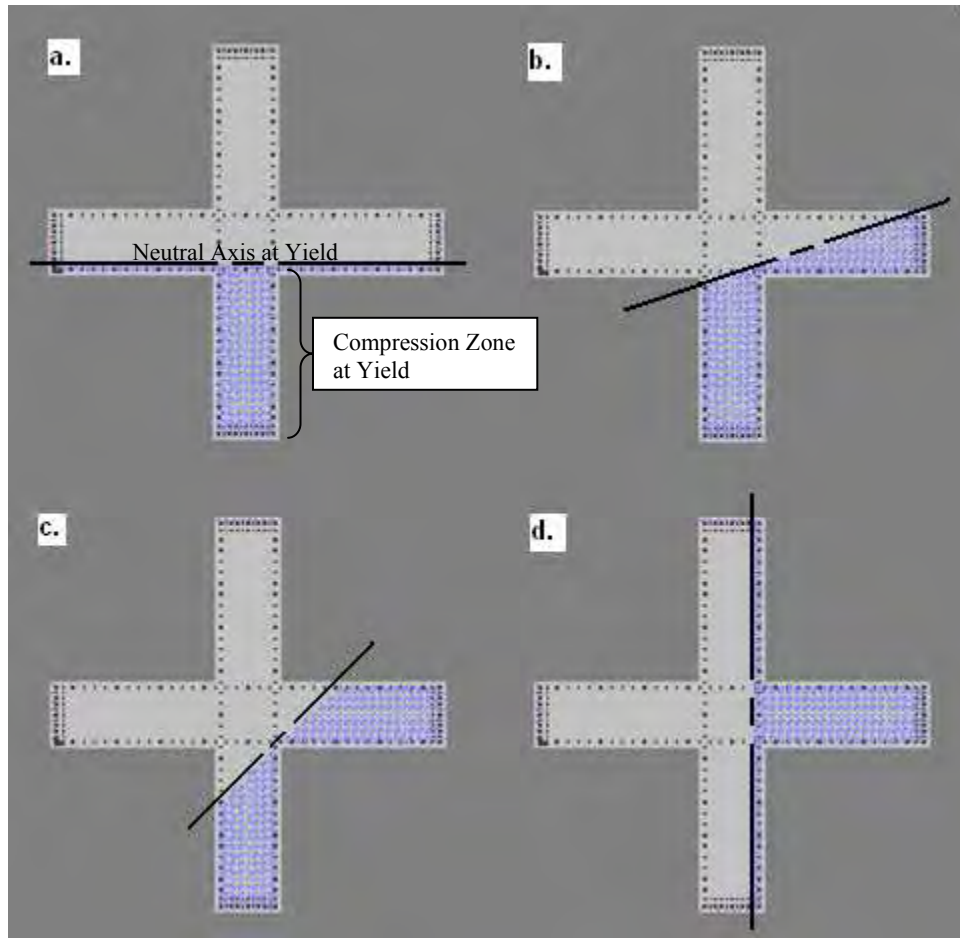


Figure 8.13. Sequence of biaxial combinations for orbit plot at first yield

8.3 First Run: Unscaled San Salvador, Northridge and Artificial Records

8.3.1 Elastic Criterion at the Bases of the Towers – First Run

Orbit plots are used in this study to determine if the biaxial bending capacity of the towers is sufficient for the applied bending moments. The orbit plots for the maximum stress state induced by the unscaled earthquakes are shown in Figures 8.14 through 8.22. The bases of the three towers (T12, T8 and T4) are examined for the three unscaled earthquakes. Note that nine different plots are necessary since the axial force is different for each case and the

“slice” in the biaxial diagram (see Figure 8.11) occurs at different heights. In all cases, the slice is taken at an axial load lower than that corresponding to the balanced reinforcement case (the point at which the maximum moment is generated), i.e., the towers were designed comfortably within the tension zone of the interaction diagram. The figures include the orbit plot at first yield as well as the orbit plot at ultimate. The data for the plots was obtained from XTRACT and plotted in Excel. This was done to combine both orbits in the same plot and to include the coordinates (F_{axial} , M_{33} , M_{22}) for each of the stress states in Table 7.7 (shown with a mark). The same scale was used in all plots to facilitate a comparison between the capacities of the three towers. Tower T8 has the largest capacity on account of having the largest base. The size of the bases of towers T4 and T12 are identical. The first three figures correspond to the unscaled San Salvador earthquake.

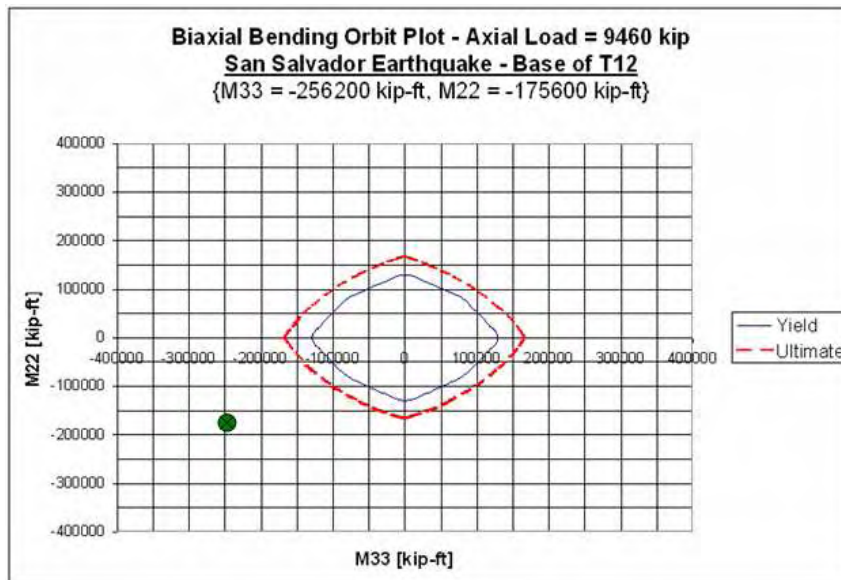


Figure 8.14. Orbit plot – unscaled San Salvador earthquake – Base of T12

This first orbit plot (Figure 8.14) shows that the base of tower T12 does not have sufficient capacity to resist within the elastic range the bending moment combination of the unscaled San Salvador earthquake. The stress state is represented by the circular dot which, in this case, resides outside the plot indicating insufficient capacity. Note the dot is very distant (factor of $\sim 2.5x$) from the yield orbit. The M_{33} - M_{22} moment combination is particularly damaging in this case since they are both very high. The bending moment M_{22} is 70% of the M_{33} value.

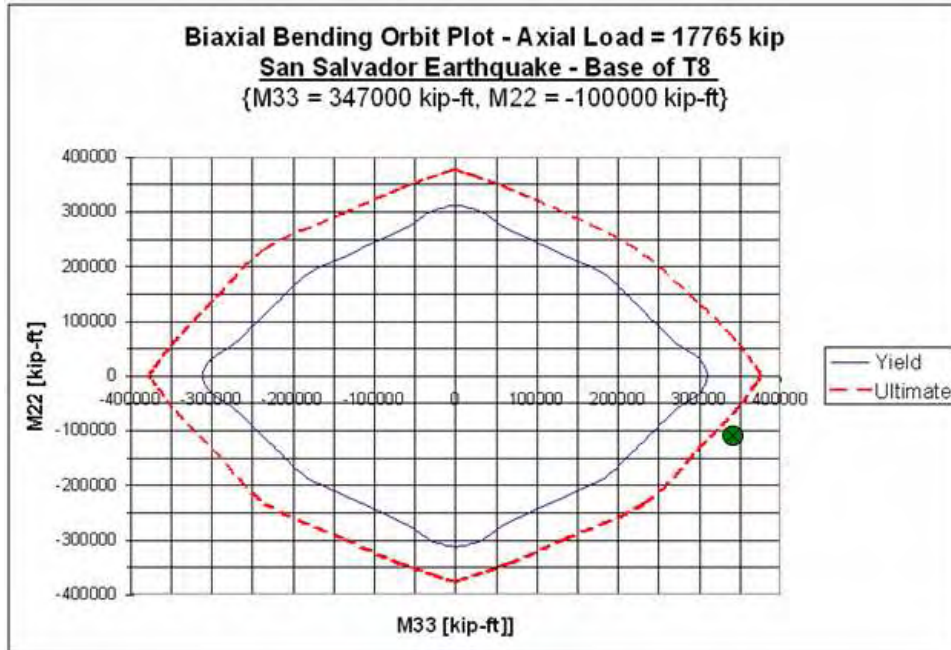


Figure 8.15. Orbit plot – unscaled San Salvador earthquake – Base of T8

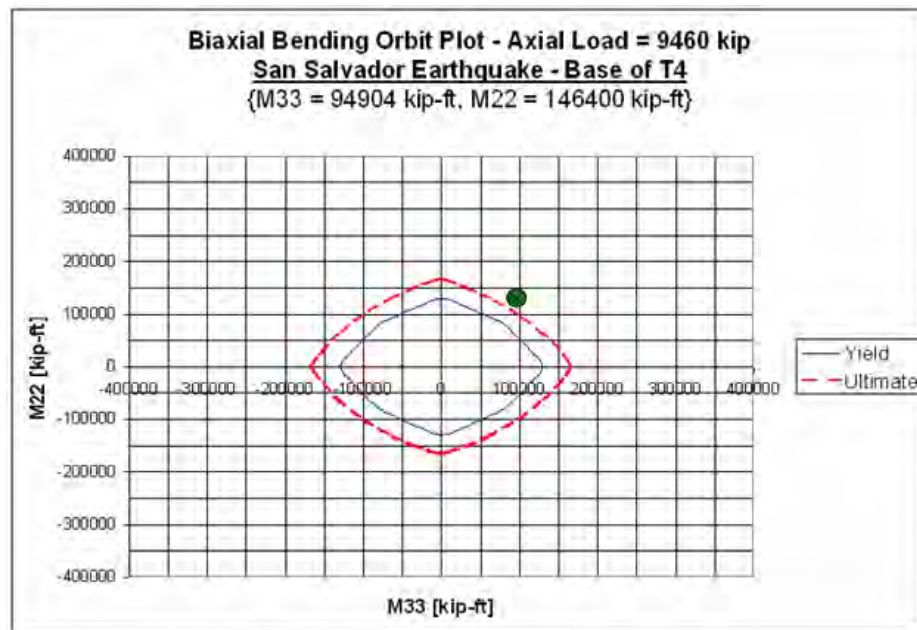


Figure 8.16. Orbit plot – unscaled San Salvador earthquake – Base of T4

At the base of both towers T8 (Figure 8.15) and T4 (Figure 8.16) the circular dot is just outside the ultimate orbit plot which also indicates insufficient capacity, albeit the situation is not as bad as in tower T12. In summary, all three tower bases would yield in an earthquake equal to the unscaled San Salvador-CIG record.

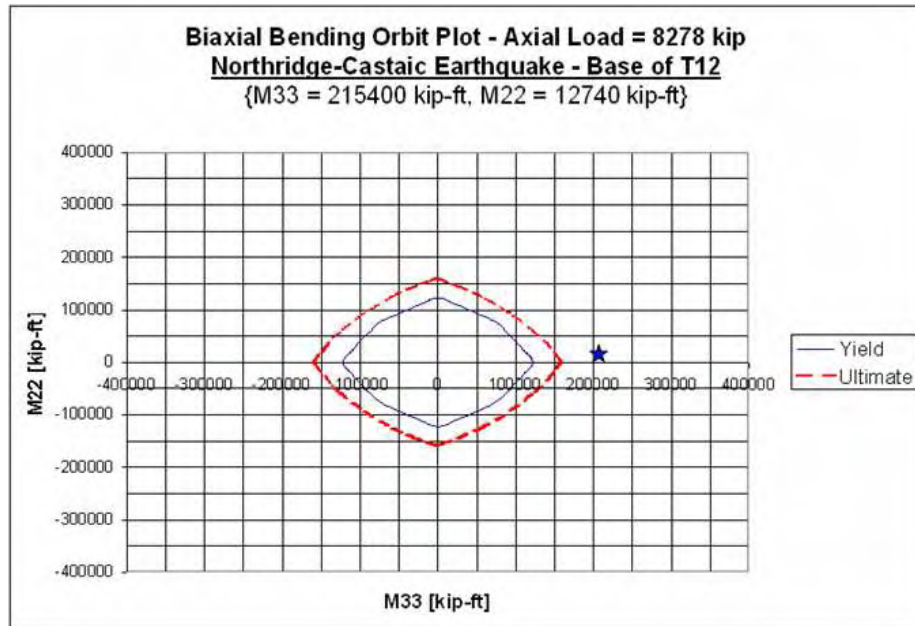


Figure 8.17. Orbit plot – unscaled Northridge-Castaic earthquake – Base of T12

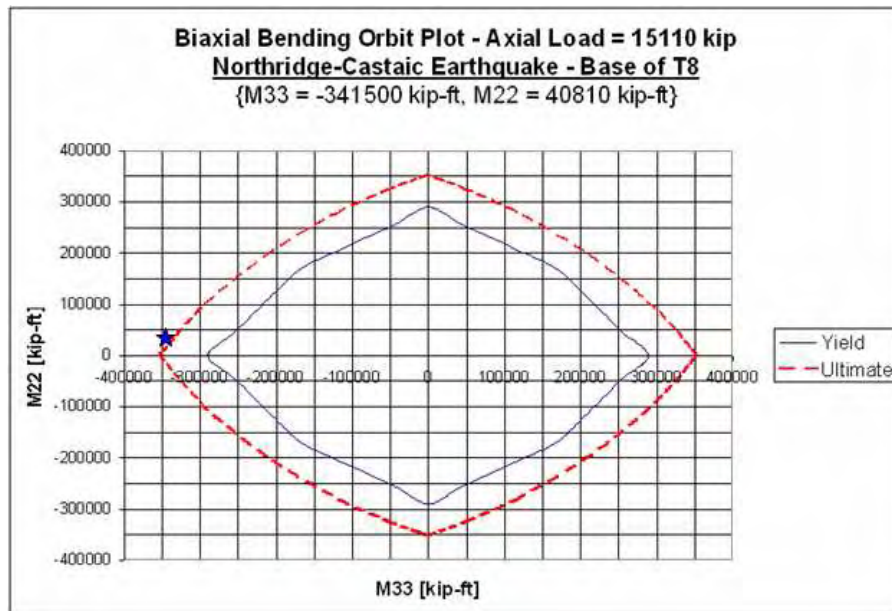


Figure 8.18. Orbit plot – unscaled Northridge-Castaic earthquake – Base of T8

Figures 8.17 and 8.18 display the orbit plots for the maximum stress state caused by the unscaled Northridge-Castaic earthquake record. Note that towers T12 and T8 are not capable of resisting the earthquake loading within the elastic regime. The same result is observed for Tower T4 in Figure 8.19.

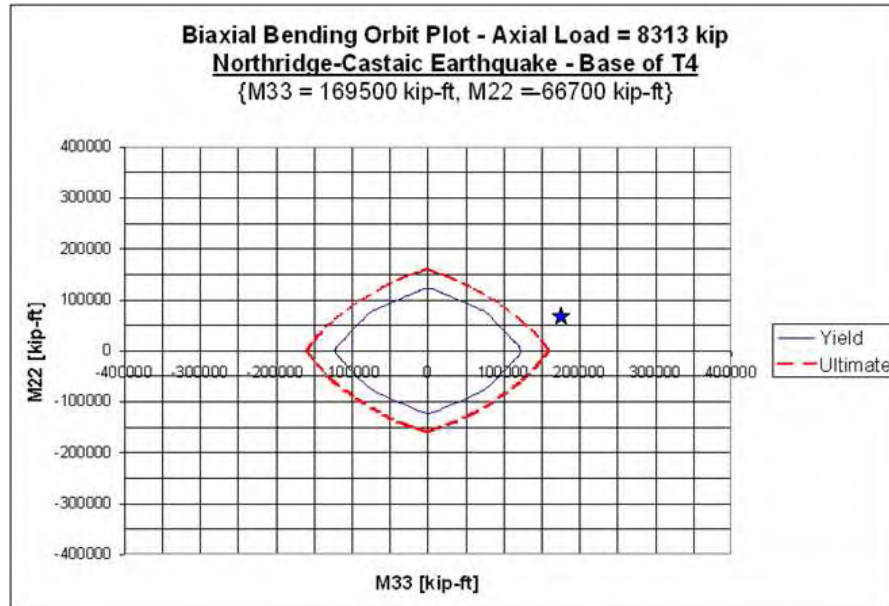


Figure 8.19. Orbit plot – unscaled Northridge-Castaic earthquake – Base of T4

As in the San Salvador case, none of the tower bases was capable of resisting within the elastic regime the Northridge-Castaic earthquake record.

The following three figures show the orbit plots corresponding to the artificial earthquake generated with the SIMQKE software. This earthquake is compatible with the UBC-97 spectrum for seismic zone 3 and S_b rock conditions.

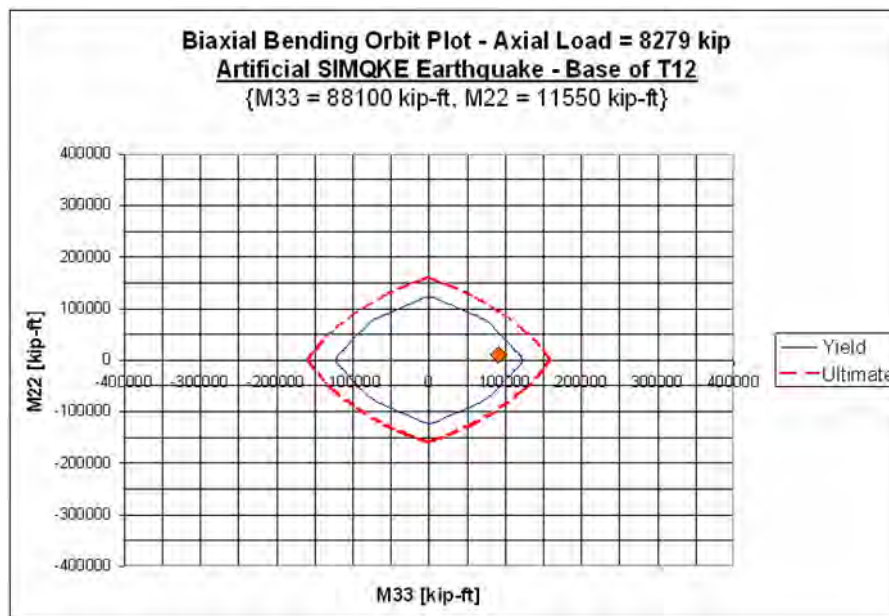


Figure 8.20. Orbit plot – unscaled Artificial earthquake – Base of T12

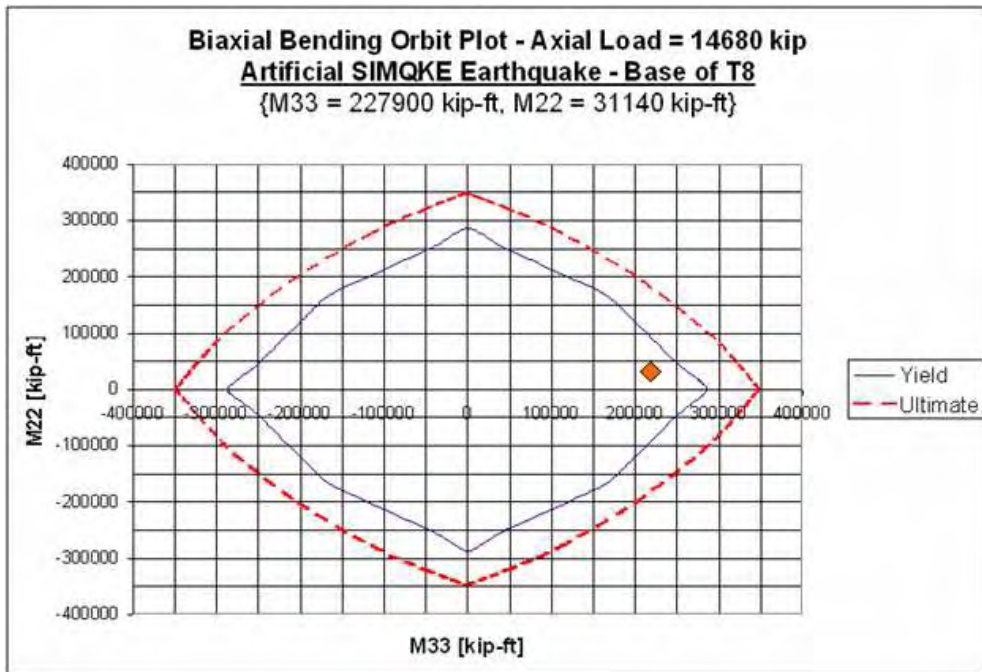


Figure 8.21. Orbit plot – unscaled Artificial earthquake – Base of T8

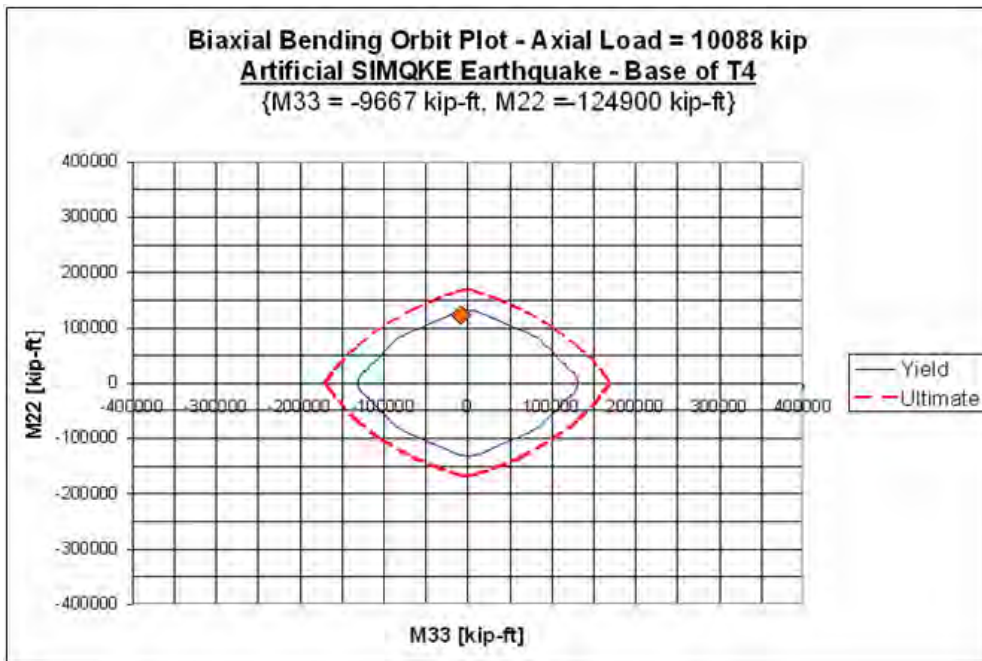


Figure 8.22. Orbit plot – unscaled Artificial earthquake – Base of T4

Unlike the unscaled San Salvador-CIG and Northridge-Castaic earthquakes, all three tower bases are capable of resisting the artificial earthquake loading generated by SIMQKE.

All the previous results are qualitatively summarized in Table 8.1. For the unscaled San Salvador earthquake, all three tower bases failed the elastic criterion. The failure in tower T12 was the worst in all nine cases examined. The result shows that the required capacity must be increased by a factor of approximately 2.5x to satisfy the elastic criterion. For the unscaled Northridge-Castaic earthquake, all three tower bases also failed the criterion. An increase in capacity on the order of 2x is required to maintain the elastic criterion. For the artificial SIMQKE earthquake, all tower bases passed the elastic criterion.

Table 8.1. Qualitative summary of elastic criterion test in tower bases (Unscaled Earthquakes)

Unscaled Earthquake and Tower Number	Pass (Elastic Criterion)	Fail (Elastic Criterion)
San Salvador-CIG, Base of T12		X
San Salvador-CIG, Base of T8		X
San Salvador-CIG, Base of T4		X
Northridge-Castaic, Base of T12		X
Northridge-Castaic, Base of T8		X
Northridge-Castaic, Base of T4		X
Artificial Earthquake-SIMQKE, Base of T12	X	
Artificial Earthquake-SIMQKE, Base of T8	X	
Artificial Earthquake-SIMQKE, Base of T4	X	

8.3.2 Elastic Criterion at All Tower Segments – First Run

Table 8.2 shows the capacities of all the tower segments at the cracked, yield and ultimate levels retrieved from XTRACT. M_{ult} has been provided for information only. The axial force level corresponds to the dead load case.

Table 8.2. Tower capacities in all segments

Section	Axial Force [kip]	$M_{cracked}$ [kip-ft]	M_{yield} [kip-ft]	M_{ult} [kip-ft]
TSEC1	3610	11040	20220	23660
TSEC2	4735	20830	35530	43140
TSEC3	6425	38890	73320	93250
TSEC4	8785	66230	125400	155200
TSEC5	10910	100400	191300	230000
TSEC6	14530	146000	285700	333300

Table 8.3 shows the maximum moments recorded at the bottom of each of the tower segments TSEC1, TSEC2, etc. These values were read from Table 7.6.

Table 8.3. Maximum moments recorded at the bottom of each tower segment (Unscaled earthquakes)

Section	Yield Capacity [kip-ft]	Unscaled San Salvador - CIG		Unscaled Northridge-Castaic		Unscaled Artificial-SIMQKE	
		M_{max} [kip-ft]	Yield Pass or Fail	M_{max} [kip-ft]	Yield Pass or Fail	M_{max} [kip-ft]	Yield Pass or Fail
TSEC1	20220	58980	Fail	44540	Fail	23970	Fail
TSEC2	35530	100200	Fail	68180	Fail	39690	Fail
TSEC3	73320	141000	Fail	115200	Fail	57700	Pass
TSEC4	125400	256200	Fail	215400	Fail	96380	Pass
TSEC5	191300	243300	Fail	244800	Fail	133000	Pass
TSEC6	285700	349700	Fail	-341500	Fail	227000	Pass

A comparison between Tables 8.2 and 8.3 (based on uniaxial bending) shows that the cracking moment ($M_{cracked}$) is always exceeded regardless of the earthquake. In addition the top two segments always reach yielding, regardless of the earthquake. Note that the top two segments only have a single layer of #11 reinforcement bars (see Figure 8.2) so M_{yield} is exceeded even for the weaker artificial earthquake. In the bottom four segments the yielding capacity is only satisfied by the artificial earthquake. This information has been summarized in the pass/fail columns of Table 8.3.

8.3.3 Likelihood of Tower Collapse – First Run

The previous section showed that the towers are not capable of resisting the unscaled San Salvador and Northridge earthquakes in the elastic regime. Permanent (plastic) deformations would take place if the towers were exposed to this type of seismic hazard. Furthermore, it was shown that the top two segments are the most vulnerable on account of the combination of high bending moments and the fact that there is only a single layer of 11#11 steel reinforcement bars. It was noted previously that these two seismic events are improbable for the observatory site; nevertheless, they represent an upper-bound case worth investigating. Conceding the fact that the towers would plastically deform, this section addresses the likelihood of tower collapse while subjected to the unscaled San Salvador-CIG and Northridge-Castaic earthquakes. The investigation is based on the R-factor of UBC-97. A nonlinear pushover analysis is beyond the scope of this thesis and it is suggested as future work as it represents a very interesting case with high-mode activation.

The seismic design provisions of UBC-97 prescribe lateral strengths which are lower - sometimes by as much as a factor of eight - than the lateral strength required to maintain elastic behavior during a major earthquake. The principal argument to sustain this level of strength reduction is that structures are allowed to respond nonlinearly during strong seismic events, which results in energy dissipation through hysteretic behavior. The extent of available energy dissipation capacity depends on the degree of detailing for ductile behavior. In addition to ductility, overstrength also plays a major role in sustaining the argument of lateral strength reduction. Overstrength has three components (El-Tawil 2002): design overstrength, material overstrength and system overstrength. When combined, the ductility and overstrength factors form the Response Modification Factor or R-factor.

UBC-97 specifies an R-factor = 2.2 for a cantilever structure. Although the towers of the Arecibo Observatory are not exactly cantilevered (the cables offer some restraint so R could be higher), a reduction in required strength by a factor of 2x provides a reasonable and conservative approximation to determine if the towers are in danger of collapse. UBC-97 analytical calculations for base shear and overturning moment were performed in Chapter 6 as part of the validation studies for the finite element model. The overturning moment calculation is based on a linear equation so the results may be scaled directly by the R-factor.

A similar reduction may be performed on the finite element results. The reduced values for the bases of the towers are summarized in Table 8.4. The maximum moment at the base was divided by an R-factor = 2.0. To estimate a biaxial component a value equal to 70% of the maximum moment was used. This was the highest percentage observed in Table 7.7. The UBC-97 code only requires 30% but the higher value is used as it has been previously recorded.

Table 8.4 Reduced bending moments (R=2) at the base of the towers

	San Salvador-CIG	Northridge-Castaic	Artificial-SIMQKE	Analytical UBC
BASE of T12 (F1)				
Max abs(M) [kip-ft]	128100	-107700	-48190	79100
0.7*Max abs(M) [kip-ft]	89670	75390	-33733	-55370
Dead Axial Force [kip]	-8785	-8785	-8785	-8785
BASE of T8 (F6)				
Max abs(M) [kip-ft]	174850	-170750	-113950	185700
0.7*Max abs(M) [kip-ft]	122395	119525	-79765	-129990
Dead Axial Force [kip]	-14530	-14530	-14530	-14530
BASE of T4 (F13)				
Max abs(M) [kip-ft]	73200	-84950	-62200	79100
0.7*Max abs(M) [kip-ft]	51240	59465	-43540	-55370
Dead Axial Force [kip]	-8785	-8785	-8785	-8785

The results are plotted in the next three biaxial orbit diagrams (one per quadrant). The axial force corresponds to the dead load case. Figure 8.23 shows the results at the base of tower T12. The points for the San Salvador-CIG and Northridge-Castaic barely fall inside the orbit but pass the criterion.

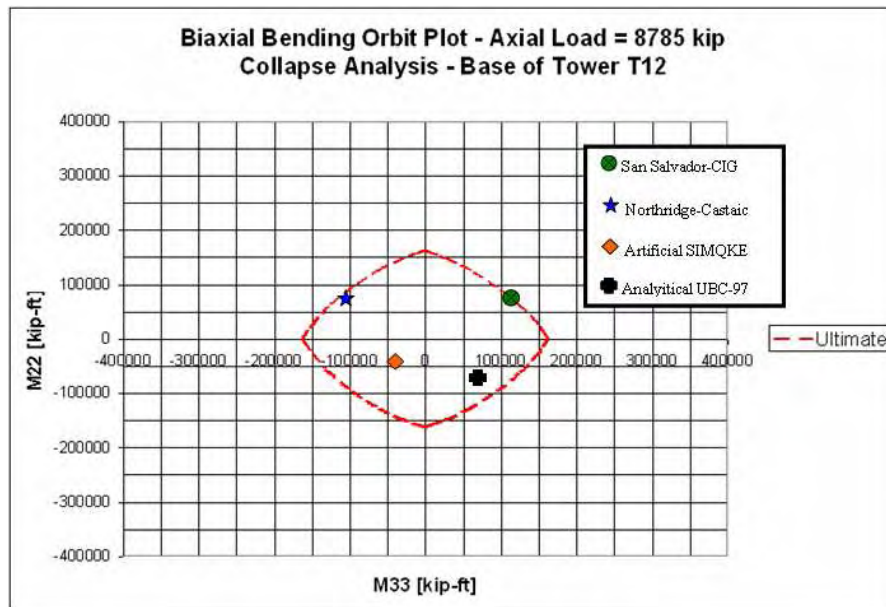


Figure 8.23. Orbit plot for likelihood of collapse – Base of T12

Figure 8.24 shows the results for the base of tower T8. Here it can be seen that all cases fall comfortably within the orbit plot.

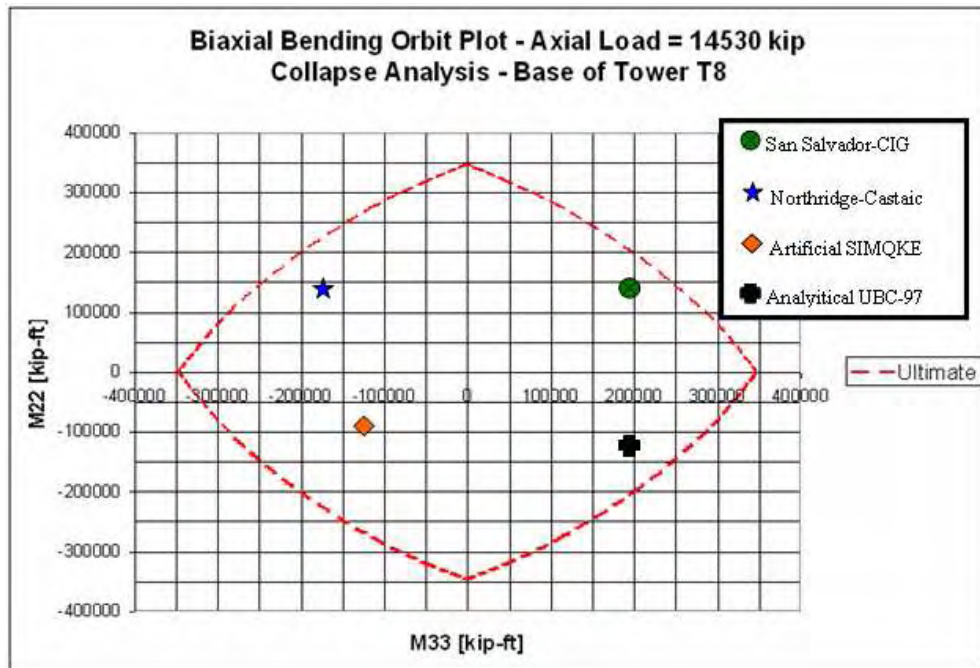


Figure 8.24. Orbit plot for likelihood of collapse – Base of T8

Figure 8.25 shows the results for the base of tower T4. As in the previous towers, all (M_{22} , M_{33}) points fall within the orbit plot.

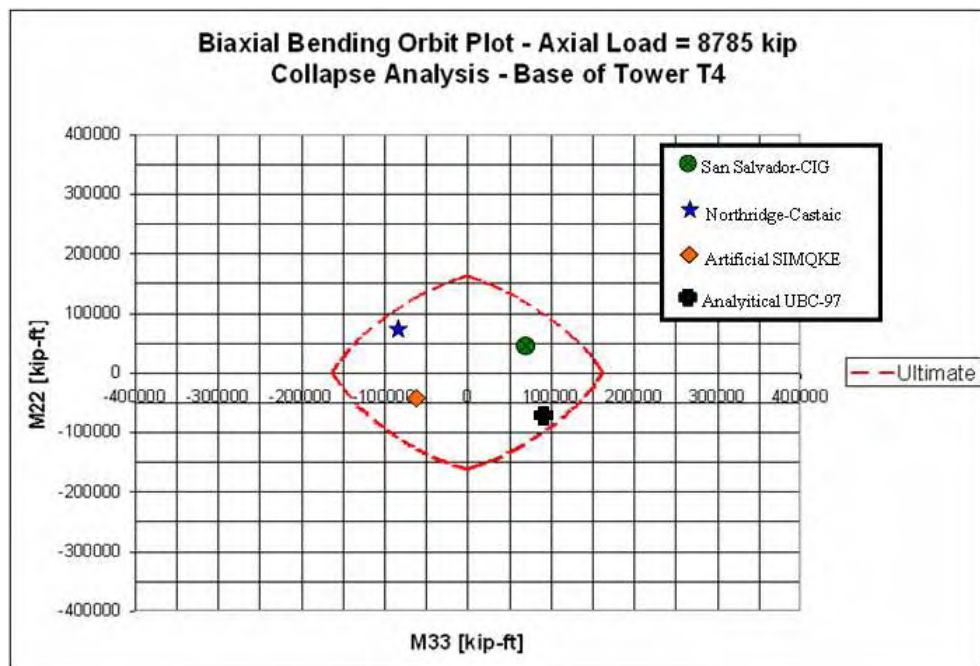


Figure 8.25. Orbit plot for likelihood of collapse – Base of T4

The top tower segment (section TSEC1) is now examined. This is one of the two segments with only one layer of 11#11 bars. The halved values (R-factor = 2) are summarized in Table 8.5. As for Table 8.4, the biaxial component is assigned a value equal to 70% of the maximum moment.

Table 8.5 Reduced bending moments (R=2) at TSEC1 (bottom)

	San Salvador-CIG	Northridge-Castaic	Artificial-SIMQKE
TSEC1 (Bottom) of T12			
Max abs(M) [kip-ft]	24775	-16965	-8225
0.7*Max abs(M) [kip-ft]	17343	11876	-5758
Dead Axial Force [kip]	-3610	-3610	-3610
TSEC1 (Bottom) of T8			
Max abs(M) [kip-ft]	29490	-22270	-11985
0.7*Max abs(M) [kip-ft]	20643	15589	-8389.5
Dead Axial Force [kip]	-3610	-3610	-3610
TSEC1 (Bottom) of T4			
Max abs(M) [kip-ft]	15685	-15055	-10950
0.7*Max abs(M) [kip-ft]	10980	10539	-7665
Dead Axial Force [kip]	-3610	-3610	-3610

The results are plotted in the next three biaxial orbit diagrams (one per quadrant). Also in these plots, the axial force corresponds to the dead load case. Figure 8.26 shows the results at the bottom of TSEC1 of tower T12 and it can be observed that the San Salvador-CIG record does not meet the criterion.

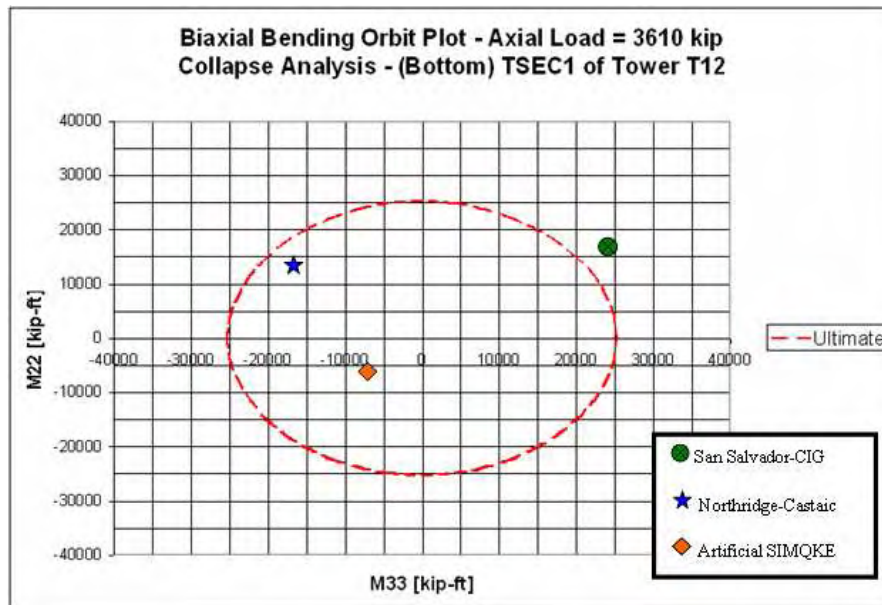


Figure 8.26. Orbit plot for likelihood of collapse – (bottom) TSEC1 of T12

Figure 8.27 shows the results at the bottom of TSEC1 of tower T8. Both the points for the San Salvador-CIG and Northridge-Castaic fall outside the plot.

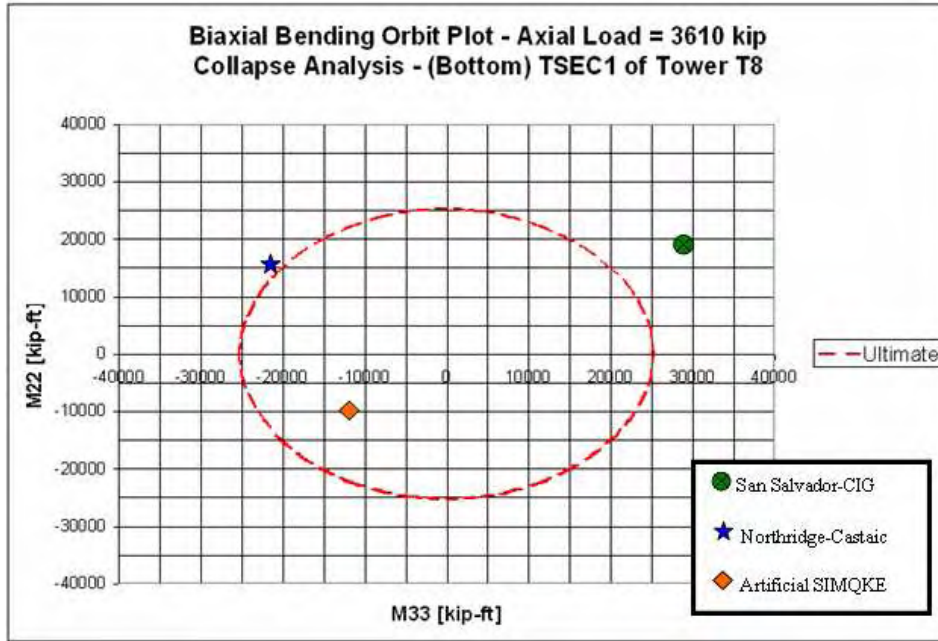


Figure 8.27. Orbit plot for likelihood of collapse – (bottom) TSEC1 of T8

The results for the base of tower T4 are displayed in Figure 8.28. All cases fall comfortably within the orbit plot.

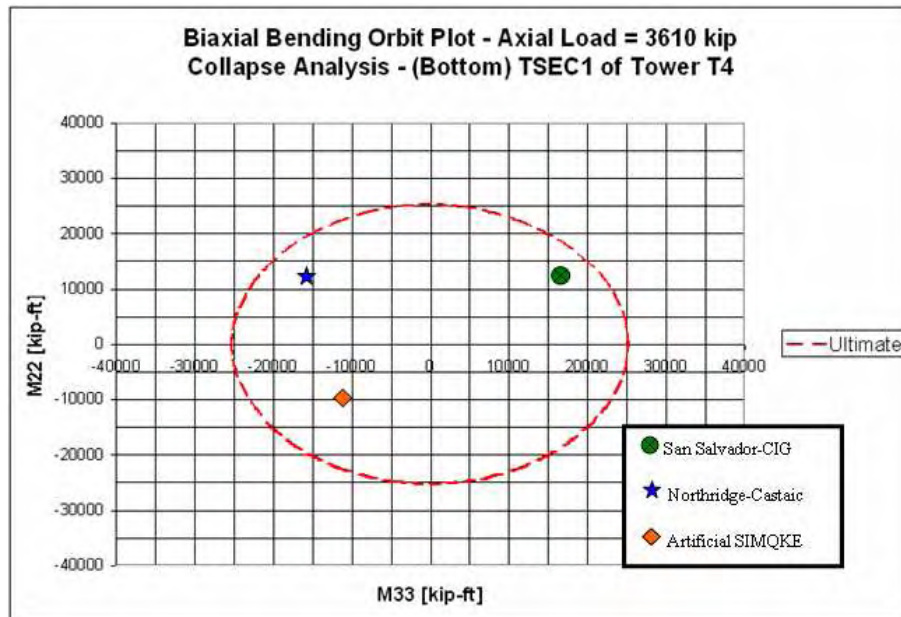


Figure 8.28. Orbit plot for likelihood of collapse – (bottom) TSEC1 of T4

The next-to-top tower segment (section TSEC2) is now examined. This is the other segment (in addition to TSEC1) with only one layer of 11#11 bars. The halved values (R-factor = 2) bending moments are summarized in Table 8.6. As for the previous tables the biaxial component is assigned a value equal to 70% of the maximum moment.

Table 8.6. Reduced bending moments (R=2) at TSEC2 (bottom)

	San Salvador-CIG	Northridge-Castaic	Artificial-SIMQKE
TSEC2 (Bottom) of T12			
Max abs(M) [kip-ft]	30395	-27525	-15130
0.7*Max abs(M) [kip-ft]	21276.5	19267.5	-10591
Dead Axial Force [kip]	-4735	-4735	-4735
TSEC2 (Bottom) of T8			
Max abs(M) [kip-ft]	50100	-34090	-15280
0.7*Max abs(M) [kip-ft]	35070	23863	-10696
Dead Axial Force [kip]	-4735	-4735	-4735
TSEC2 (Bottom) of T4			
Max abs(M) [kip-ft]	28205	-29340	-19845
0.7*Max abs(M) [kip-ft]	19743.5	20538	-13891.5
Dead Axial Force [kip]	-4735	-4735	-4735

The results are plotted in the next three biaxial orbit diagrams. The axial force corresponds to the dead load case. Figure 8.29 shows the orbit plot and (M₂₂, M₃₃) points at the bottom of TSEC2 of tower T12. All points fall within the orbit.

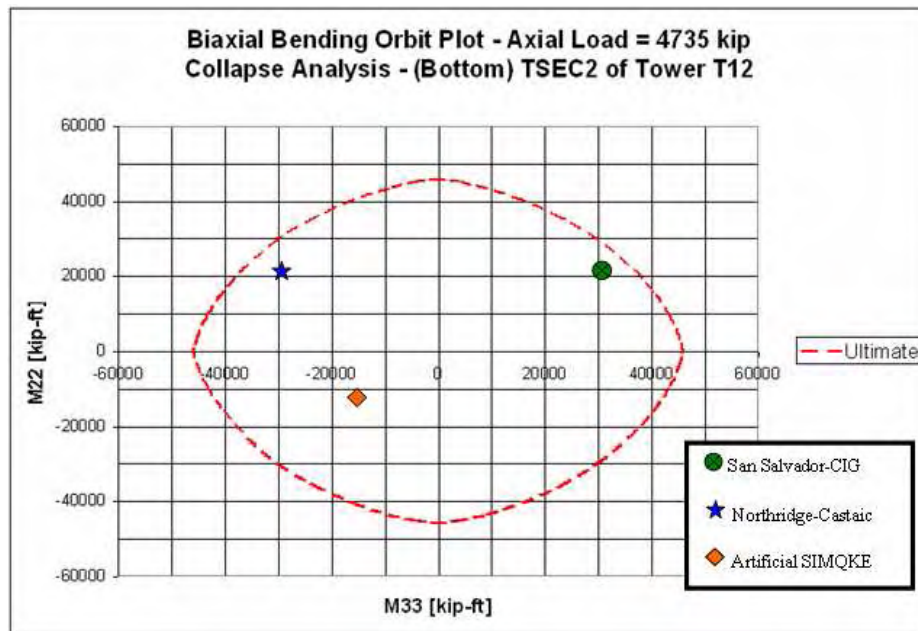


Figure 8.29. Orbit plot for likelihood of collapse – (bottom) TSEC2 of T12

Figure 8.30 shows the results at the bottom of TSEC2 of tower T8. The San Salvador-CIG point falls outside the orbit while the Northridge-Castaic point falls right on the curve.

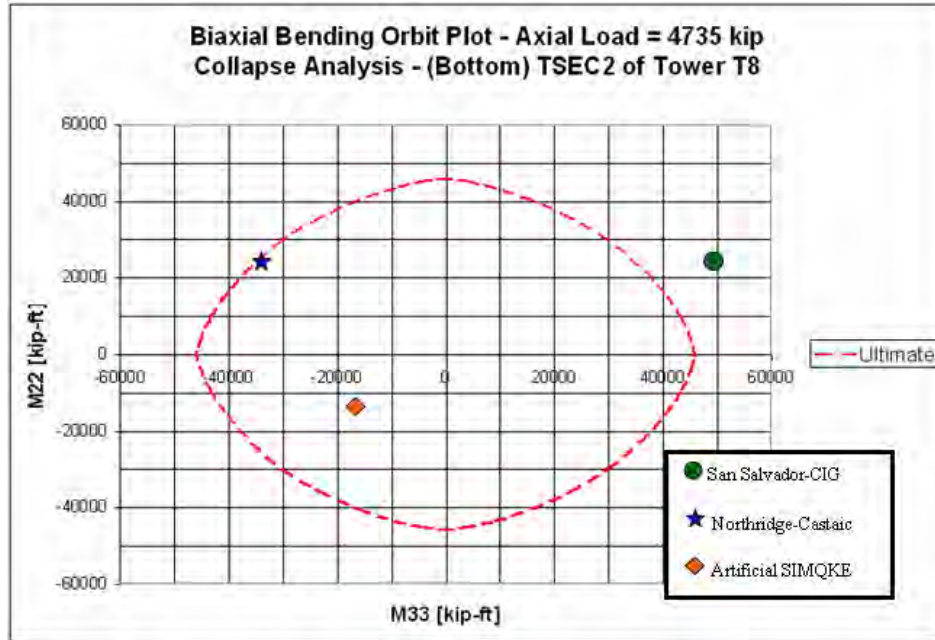


Figure 8.30. Orbit plot for likelihood of collapse – (bottom) TSEC2 of T8

The results for the base of tower T4 are shown in Figure 8.31. All cases fall within the orbit plot.

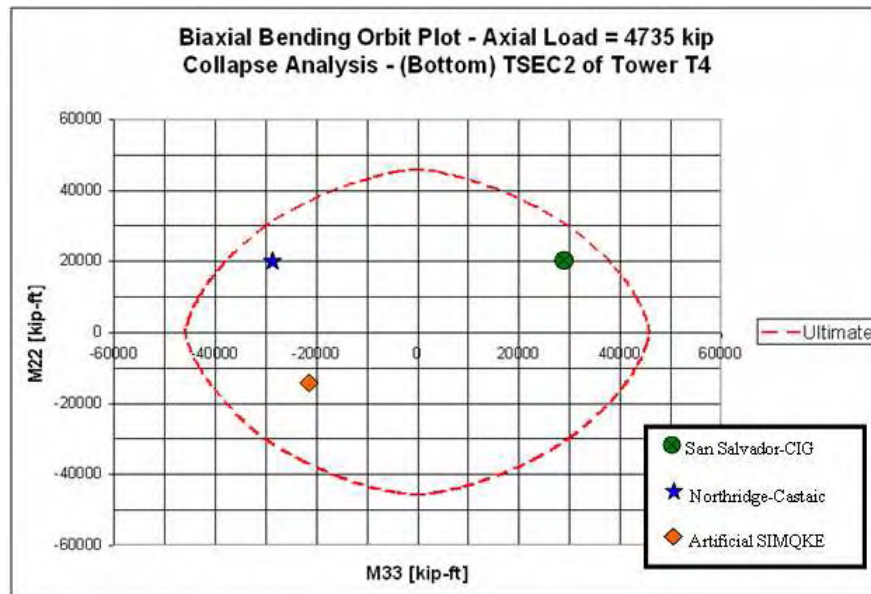


Figure 8.31. Orbit plot for likelihood of collapse – (bottom) TSEC2 of T4

The results are qualitatively summarized in Table 8.7. All the tower bases passed the collapse criterion. However, the top segment (TSEC1) of the towers failed the collapse criterion in towers T12 and T8. The San Salvador-CIG record participated in both towers while the Northridge-Castaic record participated only in tower T8. The next-to-top segment (TSEC2) failed the collapse criterion in tower T8 with the San Salvador earthquake. These results do not necessarily mean that the top two segments of the towers are going to collapse but rather that there is a likelihood that they could fail during an improbable event defined by the San Salvador-CIG and Northridge-Castaic records. The San Salvador record was the strongest of the two records.

Table 8.7. Qualitative summary of collapse likelihood in towers

CASE	<u>PASS</u> (Collapse Likelihood)	<u>FAIL</u> (Collapse Likelihood)
BASE OF T12		
San Salvador-CIG	X	
Northridge-Castaic	X	
Artificial-SIMQKE	X	
Analytical-UBC97	X	
BASE OF T8		
San Salvador-CIG	X	
Northridge-Castaic	X	
Artificial-SIMQKE	X	
Analytical-UBC97	X	
BASE OF T4		
San Salvador-CIG	X	
Northridge-Castaic	X	
Artificial-SIMQKE	X	
Analytical-UBC97	X	
(Bottom) TSEC1 OF T12		
San Salvador-CIG		X
Northridge-Castaic	X	
Artificial-SIMQKE	X	
(Bottom) TSEC1 OF T8		
San Salvador-CIG		X
Northridge-Castaic		X
Artificial-SIMQKE	X	
(Bottom) TSEC1 OF T4		
San Salvador-CIG	X	
Northridge-Castaic	X	
Artificial-SIMQKE	X	

Table 8.7. Continuation

CASE	PASS (Collapse Likelihood)	FAIL (Collapse Likelihood)
(Bottom) TSEC2 OF T12		
San Salvador-CIG	X	
Northridge-Castaic	X	
Artificial-SIMQKE	X	
(Bottom) TSEC2 OF T8		
San Salvador-CIG		X
Northridge-Castaic	X	
Artificial-SIMQKE	X	
(Bottom) TSEC2 OF T4		
San Salvador-CIG	X	
Northridge-Castaic	X	
Artificial-SIMQKE	X	

8.4 Second Run. Scaled San Salvador-CIG and Northridge-Castaic

8.4.1 Elastic Criterion at Base of Towers – Second Run

This section investigates the response for the two powerful earthquakes while scaled to a more probable value of 0.3g PGA. The orbit plots for the scaled earthquakes are shown in Figures 8.32 through 8.37. A total of six figures, which correspond to the six cases shown in Table 7.9, are included. The bases of the three towers (T12, T8 and T4) are examined for the two scaled earthquakes considered in the study. The first three figures correspond to the San Salvador earthquake.

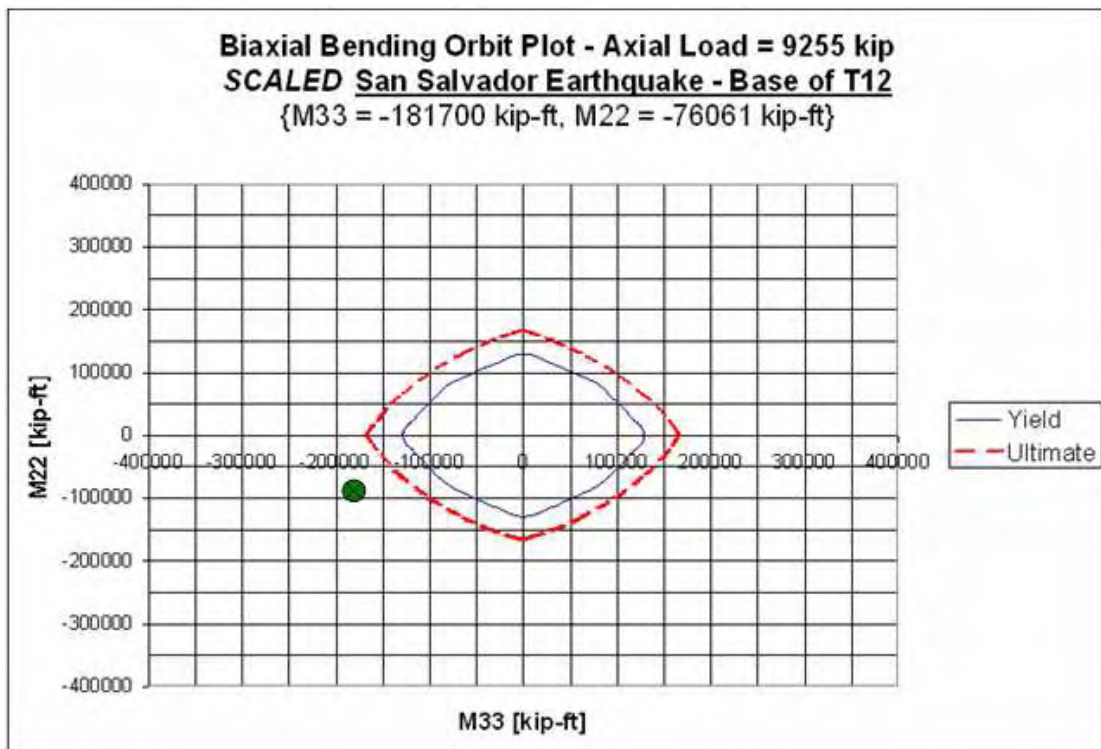


Figure 8.32. Orbit plot –scaled San Salvador earthquake – Base of T12

This first orbit plot (Figure 8.32) shows that the base of tower T12 still does not have sufficient capacity even for a scaled San Salvador earthquake. The margin has been reduced by approximately one-half (compared to the unscaled earthquake) but it still does not meet the elastic criterion. However, compliance is achieved in the other two towers (see Figures 8.33 and 8.34).

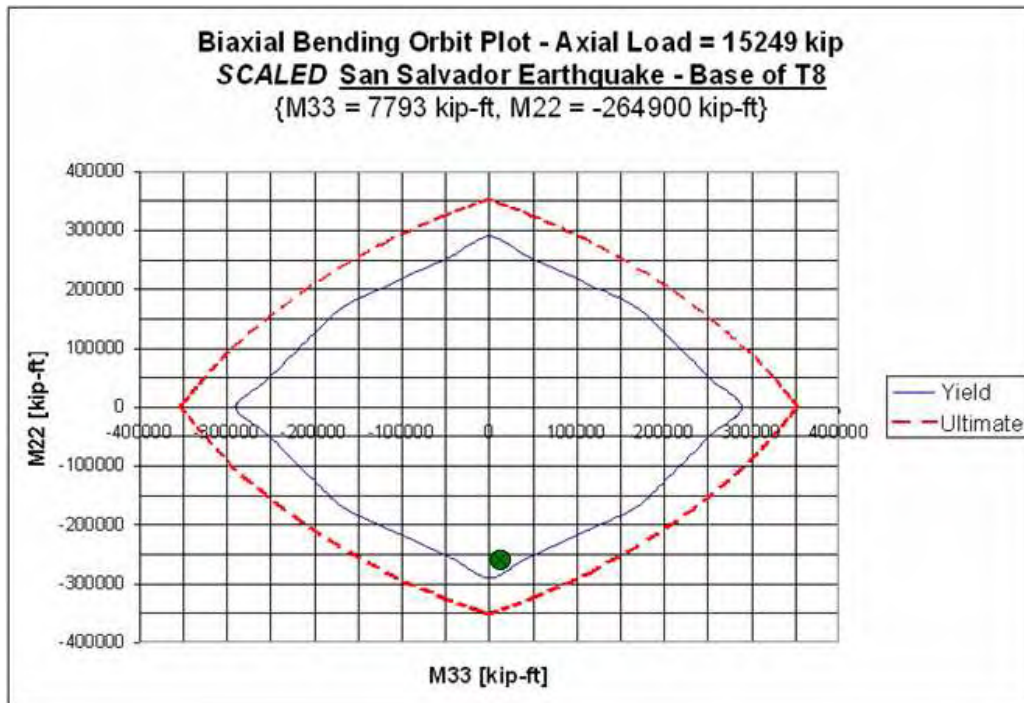


Figure 8.33. Orbit plot –scaled San Salvador earthquake – Base of T8

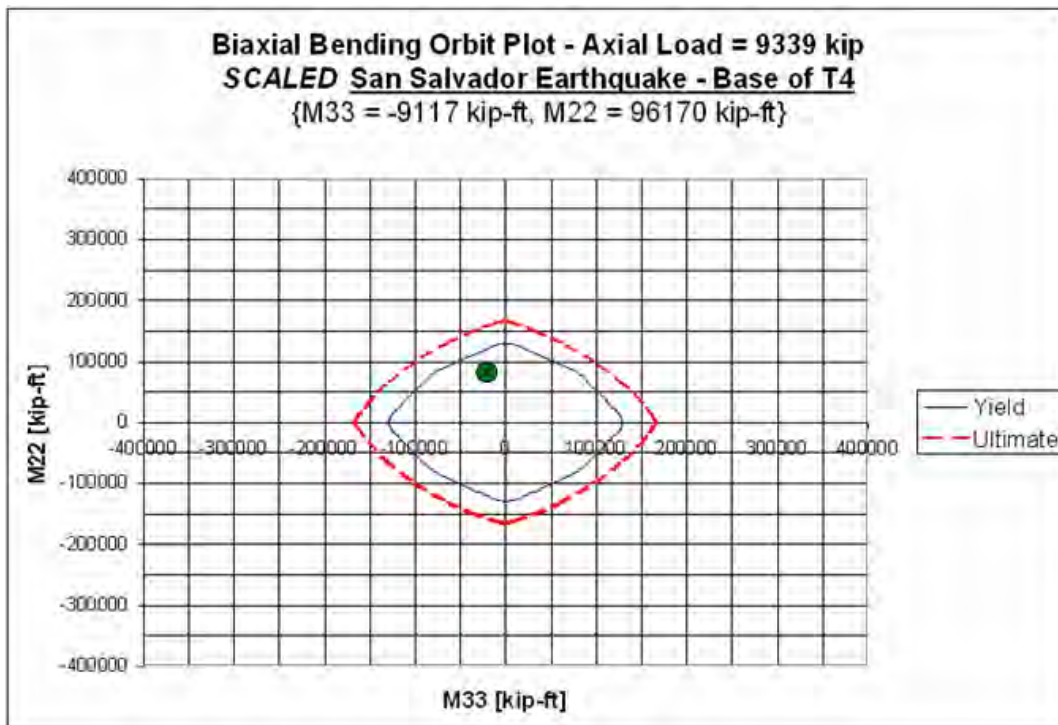


Figure 8.34. Orbit plot – unscaled San Salvador earthquake – Base of T4

The results for the scaled Northridge-Castaic earthquake are shown in Figures 8.35 through 8.37. As in the San Salvador case, the base of tower T12 (Figure 8.35) does not meet the elastic criterion by a significant margin. The base of tower T8 (Figure 8.36) barely meets the criterion.

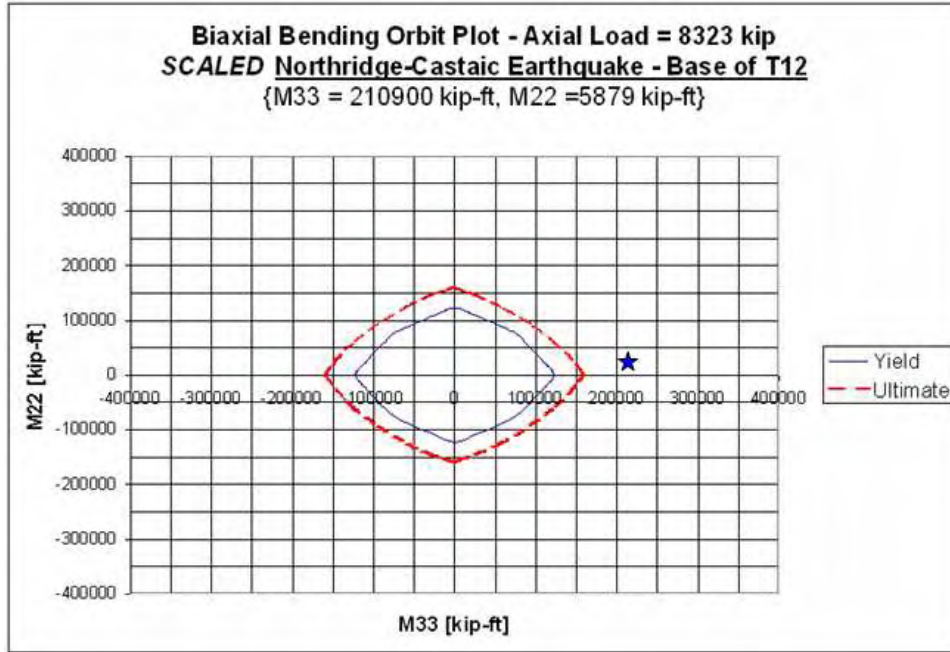


Figure 8.35. Orbit plot –scaled Northridge-Castaic earthquake – Base of T12

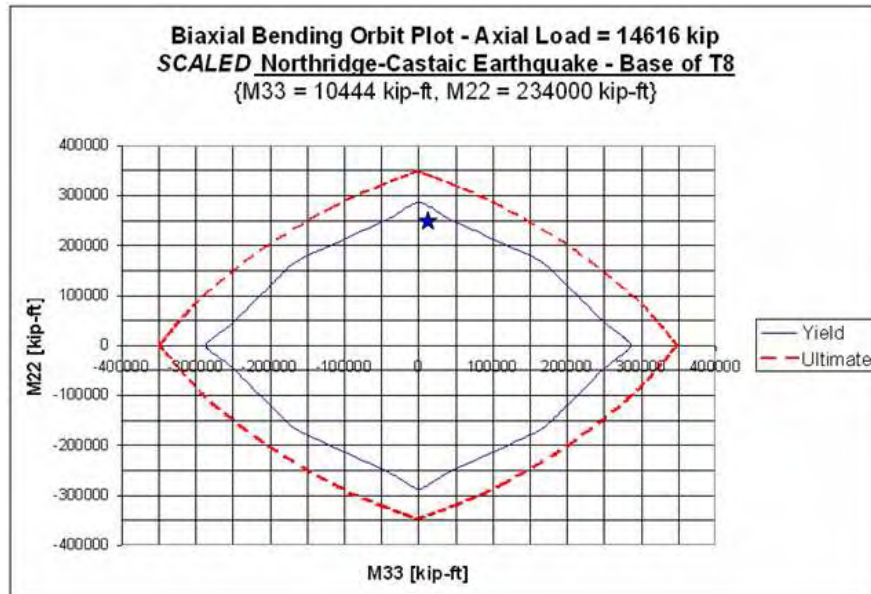


Figure 8.36. Orbit plot –scaled Northridge-Castaic earthquake – Base of T8

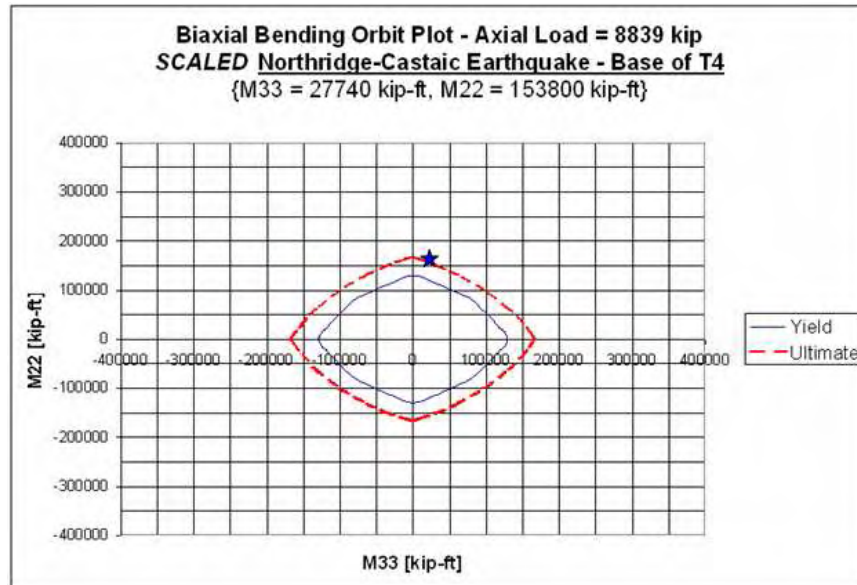


Figure 8.37. Orbit plot –scaled Northridge-Castaic earthquake – Base of T4

The base of tower T4 is also incapable of meeting the elastic criterion with the scaled Northridge-Castaic earthquake. The results are qualitatively summarized in Table 8.8. There is an improvement over the unscaled cases but the towers are still not capable of withstanding the onslaught of these powerful records. It is interesting to compare results between Tables 6.9 and 7.9. It shows that San Salvador and Northridge-Castaic are worst-case for towers T4 and T12. For tower T8, however, Loma Prieta, El Centro, and Kocaeli are worst with moments reaching 350,000 kip-ft. Quite clearly, the towers of the observatory are not capable of resisting these very powerful earthquakes in the elastic regime.

Table 8.8. Qualitative summary of elastic criterion test in tower bases (Unscaled earthquakes)

Earthquake and Tower Number	Pass (Elastic Criterion)	Fail (Elastic Criterion)
San Salvador-CIG, Base of T12		X
San Salvador-CIG, Base of T8	X	
San Salvador-CIG, Base of T4	X	
Northridge-Castaic, Base of T12		X
Northridge-Castaic, Base of T8	X	
Northridge-Castaic, Base of T4		X

8.4.2 Elastic Criterion at All Tower Segments – Second Run

Table 8.9 shows the maximum moments recorded at the base of each of the tower segments. These were read from Table 7.8. Note that there is non-compliance in all the higher segments of the towers. Note that a ~350,000 kip-ft from Loma Prieta, El Centro or Kocaeli would fail the criterion at the base of T8 (section TSEC6).

Table 8.9. Max scaled moments at the bottom of each tower segment

Section	Yield Capacity [kip-ft]	Scaled to 0.3g San Salvador-CIG		Scaled to 0.3g Northridge-Castaic	
		M_max [kip-ft]	Yield Pass or Fail	M_max [kip-ft]	Yield Pass or Fail
TSEC1	20220	-35360	Fail	32720	Fail
TSEC2	35530	74160	Fail	-59300	Fail
TSEC3	73320	102400	Fail	98650	Fail
TSEC4	125400	-181700	Fail	210900	Fail
TSEC5	191300	157700	Fail	143500	Pass
TSEC6	285700	-264900	Pass	234000	Pass

8.4.3 Likelihood of Tower Collapse – Second Run

This section is similar to 8.3.3. The objective is to reduce the bending moments by an R-factor = 2 to evaluate the likelihood of collapse. In this section only one orbit plot will be shown for each of the six tower segments. Only the axial force due to dead load is considered. The orbit plot shows the maximum moment combination for each of the two earthquakes. The Artificial earthquake is also included in the plots.

A table with the moment values (Tables 8.10 through 8.15) is placed above each graph (Figures 8.38 to 8.43) for reference.

Table 8.10. Reduced moments at TSEC1 – Second Run

	Scaled San Salvador-CIG	Scaled Northridge-Castaic	Artificial-SIMQKE
TSEC1 (Bottom) of T12			
Max abs(M) [kip-ft]	17680	-16360	-8225
0.7*Max abs(M) [kip-ft]	12376	11452	-5757.5
Dead Axial Force [kip]	-3610	-3610	-3610
TSEC1 (Bottom) of T8			
Max abs(M) [kip-ft]	14750	-13795	-11985
0.7*Max abs(M) [kip-ft]	10325	9656.5	-8389.5
Dead Axial Force [kip]	-3610	-3610	-3610
TSEC1 (Bottom) of T4			
Max abs(M) [kip-ft]	9835	-12165	-10950
0.7*Max abs(M) [kip-ft]	6884.5	8515.5	-7665
Dead Axial Force [kip]	-3610	-3610	-3610

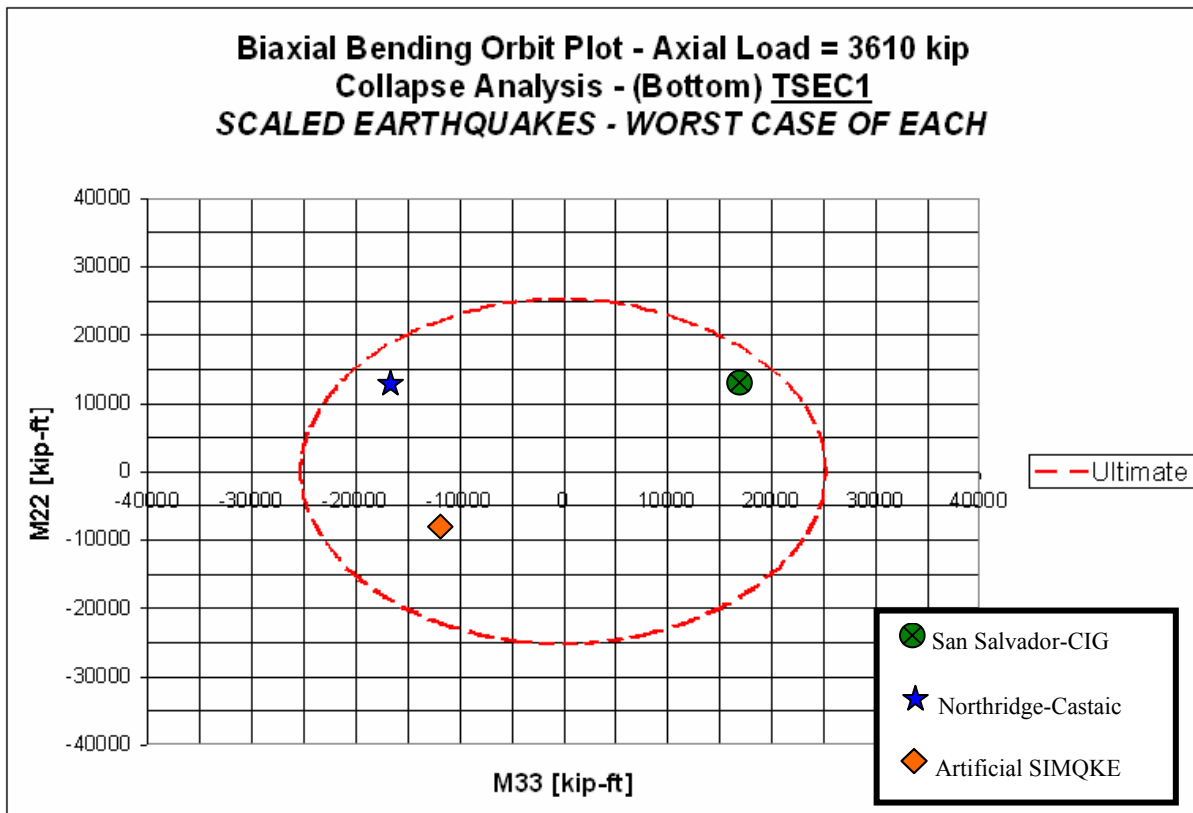


Figure 8.38. (Scaled) Orbit plot for likelihood of collapse of TSEC1

Table 8.11. Reduced moments at TSEC2 – Second Run

	Scaled San Salvador-CIG	Scaled Northridge-Castaic	Artificial-SIMQKE
TSEC2 (Bottom) of T12			
Max abs(M) [kip-ft]	13140	-17120	-15130
0.7*Max abs(M) [kip-ft]	9198	11984	-10591
Dead Axial Force [kip]	-4735	-4735	-4735
TSEC2 (Bottom) of T8			
Max abs(M) [kip-ft]	37080	-29255	-15280
0.7*Max abs(M) [kip-ft]	15000*	20479	-10696
Dead Axial Force [kip]	-4735	-4735	-4735
TSEC2 (Bottom) of T4			
Max abs(M) [kip-ft]	18455	-27385	-19845
0.7*Max abs(M) [kip-ft]	12919	19170	-13892
Dead Axial Force [kip]	-4735	-4735	-4735

* Used actual value of M33

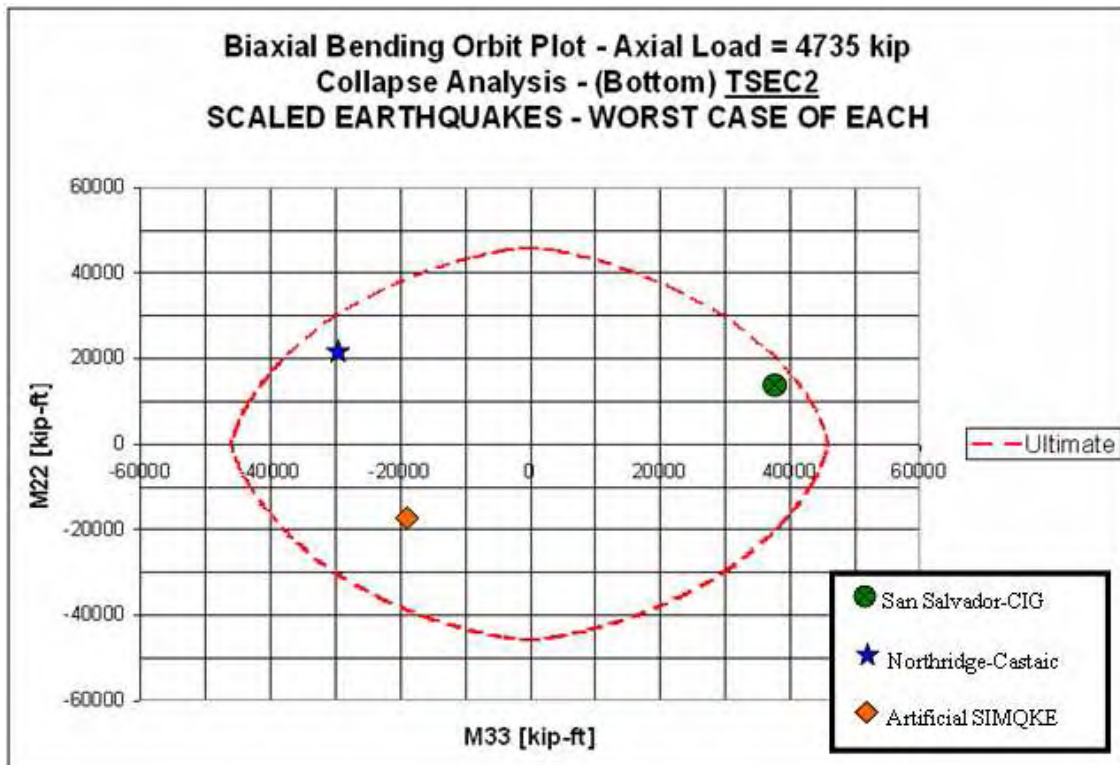


Figure 8.39. (Scaled) Orbit plot for likelihood of collapse of TSEC2

Table 8.12. Reduced moments TSEC3 – Second Run

	Scaled San Salvador-CIG	Scaled Northridge-Castaic	Artificial-SIMQKE
TSEC3 (Bottom) of T12			
Max abs(M) [kip-ft]	43040	-47755	-21680
0.7*Max abs(M) [kip-ft]	30128	33428.5	-15176
Dead Axial Force [kip]	-6425	-6425	-6425
TSEC3 (Bottom) of T8			
Max abs(M) [kip-ft]	51200	-38280	-19430
0.7*Max abs(M) [kip-ft]	35840	26796	-13601
Dead Axial Force [kip]	-6425	-6425	-6425
TSEC3 (Bottom) of T4			
Max abs(M) [kip-ft]	27130	-49325	-28850
0.7*Max abs(M) [kip-ft]	18991	34528	-20195
Dead Axial Force [kip]	-6425	-6425	-6425

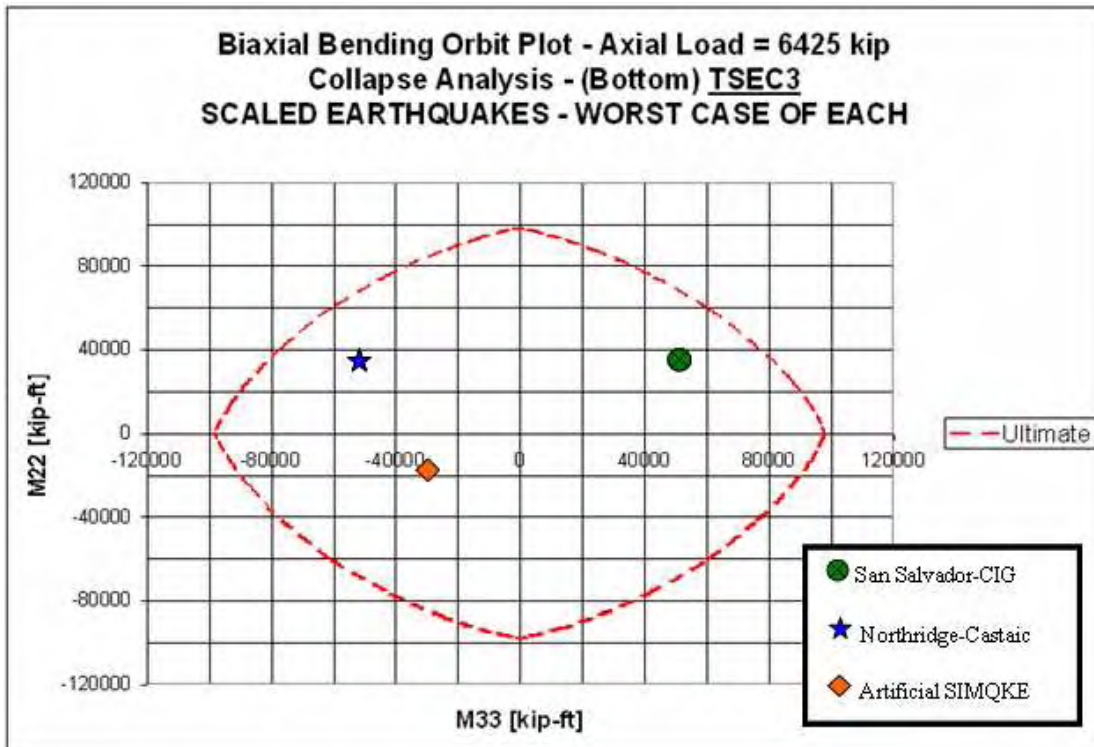


Figure 8.40. (Scaled) Orbit plot for likelihood of collapse of TSEC3

Table 8.13. Reduced moments at TSEC4 – Second Run

	Scaled San Salvador-CIG	Scaled Northridge-Castaic	Artificial-SIMQKE
TSEC4 (Bottom) of T12			
Max abs(M) [kip-ft]	90850	-105450	-48190
0.7*Max abs(M) [kip-ft]	63595	73815	-33733
Dead Axial Force [kip]	-8785	-8785	-8785
TSEC4 (Bottom) of T8			
Max abs(M) [kip-ft]	54050	-52600	-32605
0.7*Max abs(M) [kip-ft]	37835	36820	-22823.5
Dead Axial Force [kip]	-8785	-8785	-8785
TSEC4 (Bottom) of T4			
Max abs(M) [kip-ft]	48085	-76900	-62450
0.7*Max abs(M) [kip-ft]	33659.5	53830	-43715
Dead Axial Force [kip]	-8785	-8785	-8785

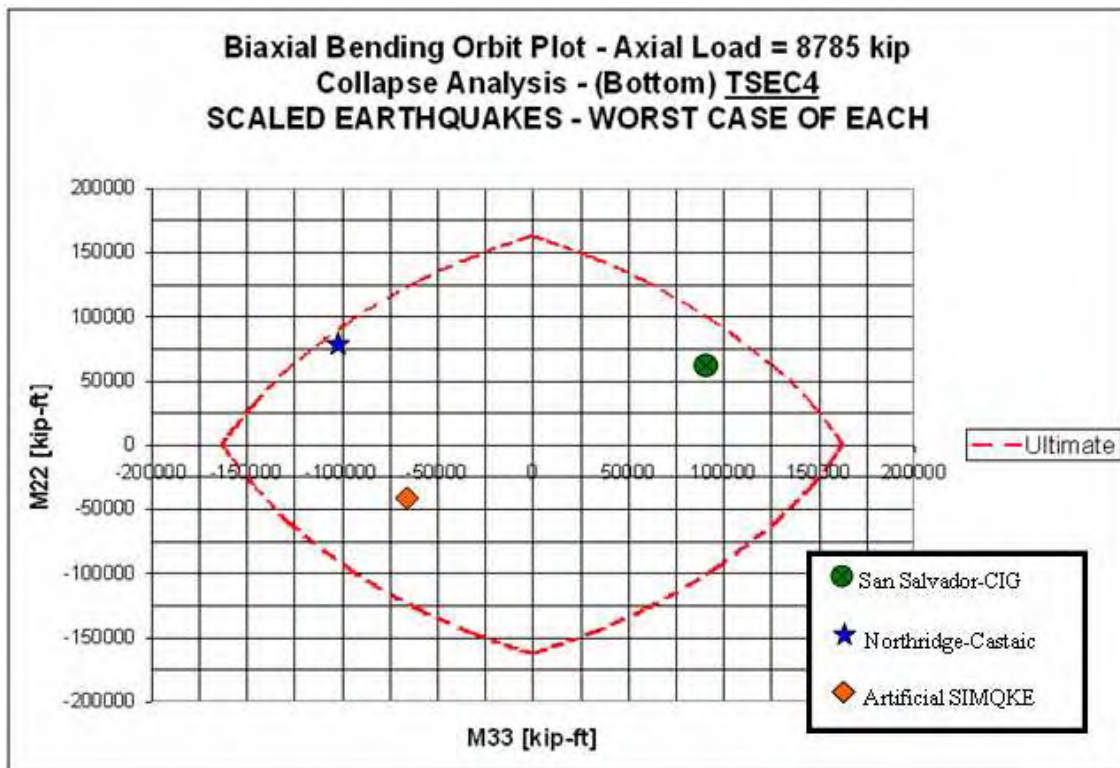


Figure 8.41. (Scaled) Orbit plot for likelihood of collapse of TSEC4

Table 8.14. Reduced moments at TSEC5 – Second Run

	Scaled San Salvador-CIG	Scaled Northridge-Castaic	Artificial-SIMQKE
TSEC5 (Bottom) of T8			
Max abs(M) [kip-ft]	78850	-71750	-66500
0.7*Max abs(M) [kip-ft]	55195	50225	-46550
Dead Axial Force [kip]	-10910	-10910	-10910

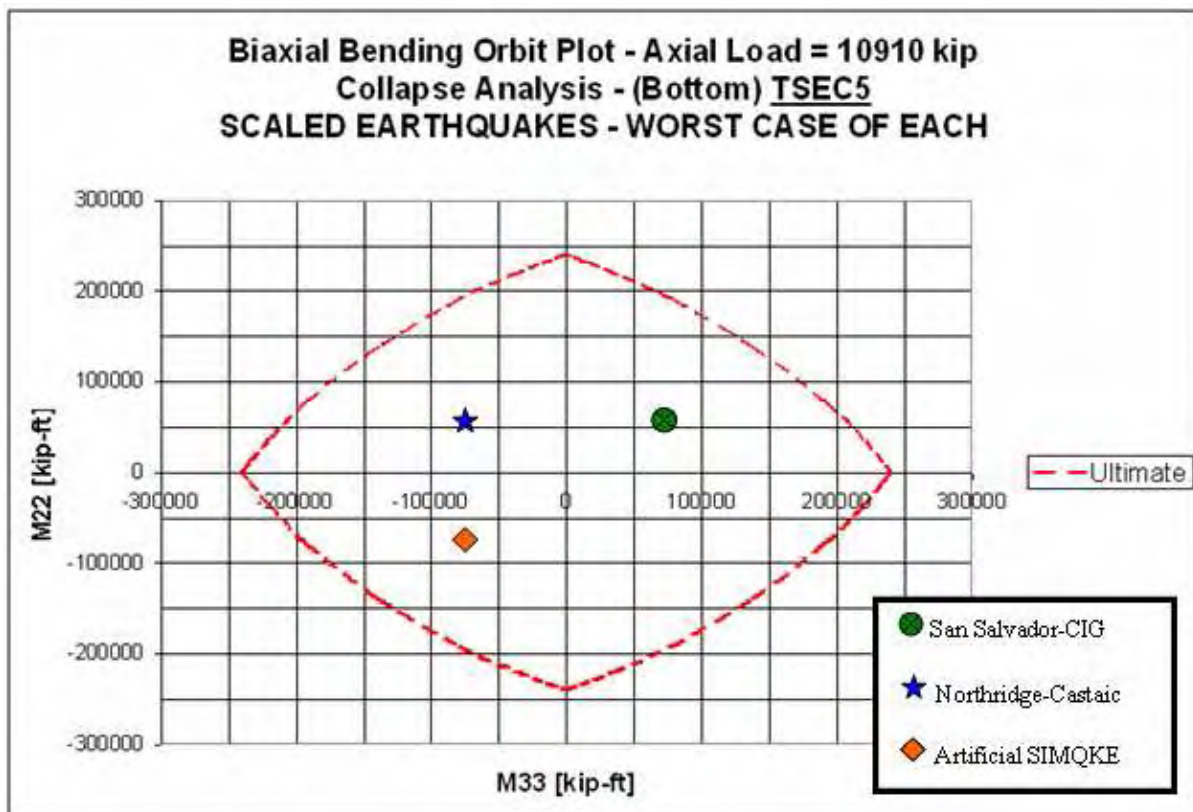


Figure 8.42. (Scaled) Orbit plot for likelihood of collapse of TSEC5

Table 8.15. Reduced moments at TSEC6 – Second Run

	Scaled San Salvador-CIG	Scaled Northridge-Castaic	Artificial-SIMQKE
TSEC6 (Bottom) of T8			
Max abs(M) [kip-ft]	132450	-117000	-113500
0.7*Max abs(M) [kip-ft]	92715	81900	-79450
Dead Axial Force [kip]	-14530	-14530	-14530

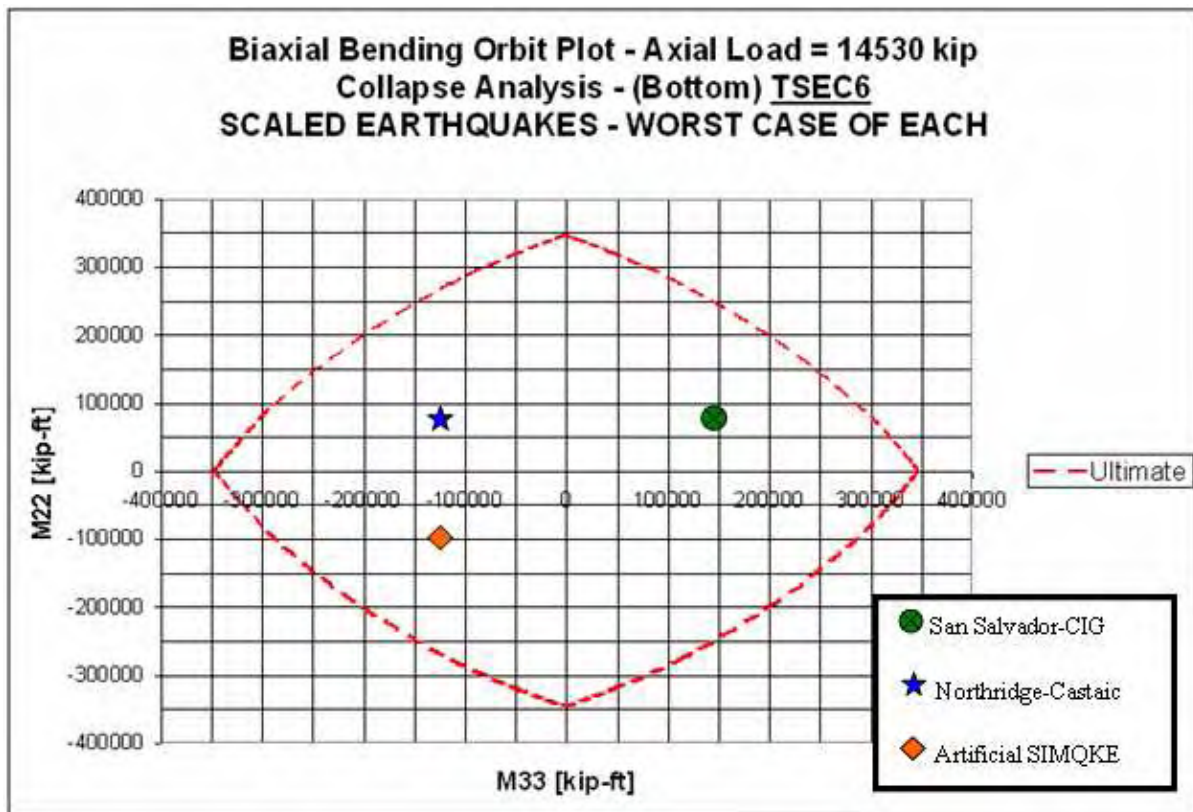


Figure 8.43. (Scaled) Orbit plot for likelihood of collapse of TSEC6

In summary, all the tower segments meet the failure criterion and show there is no likelihood of collapse when the records of San Salvador-CIG and Northridge-Castaic are scaled to 0.3g PGA.

8.5 Third Run. Parkfield and Morgan Hill

It has been shown that the very strong earthquake records of San Salvador-CIG, Northridge-Castaic and others from Chapter 6 such as Loma Prieta, El Centro and Kocaeli, surpass the elastic capacity of the Arecibo Observatory towers even when the record is scaled down to 0.3g PGA. On the other hand, the Artificial earthquake compatible with the UBC-97 design spectrum has met the elastic criterion for all tower segments except for the top two which have a single layer of 11#11 bars. This section considers the Parkfield and Morgan Hill earthquakes. Parkfield is the weaker of the two (Figure 7.10) while Morgan Hill (Figure 7.13) has strong long-period components which exceed the UBC-97 design spectrum.

8.5.1 Elastic Criterion at Base of Towers – Third Run

The results for both earthquakes have been summarized in Figures 8.44 and 8.45. An average axial load is used as there is not a large difference in values. In both cases the elastic criterion is met. As expected, the Morgan Hill earthquake was the stronger of the two as it has strong long-period components which tend to activate the strong modes of the structure.

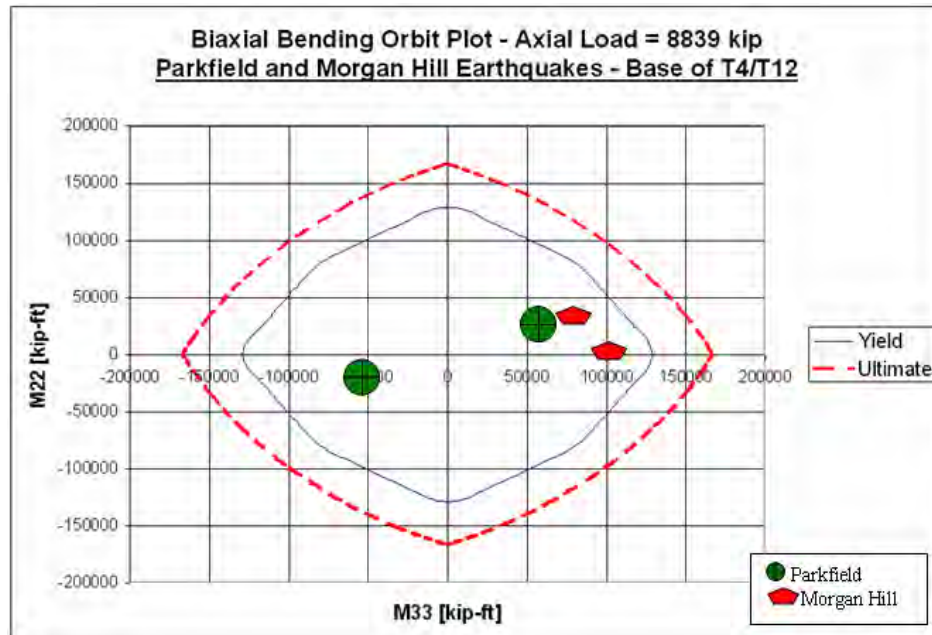


Figure 8.44. Orbit plot for base of towers T4 and T12 – Third run

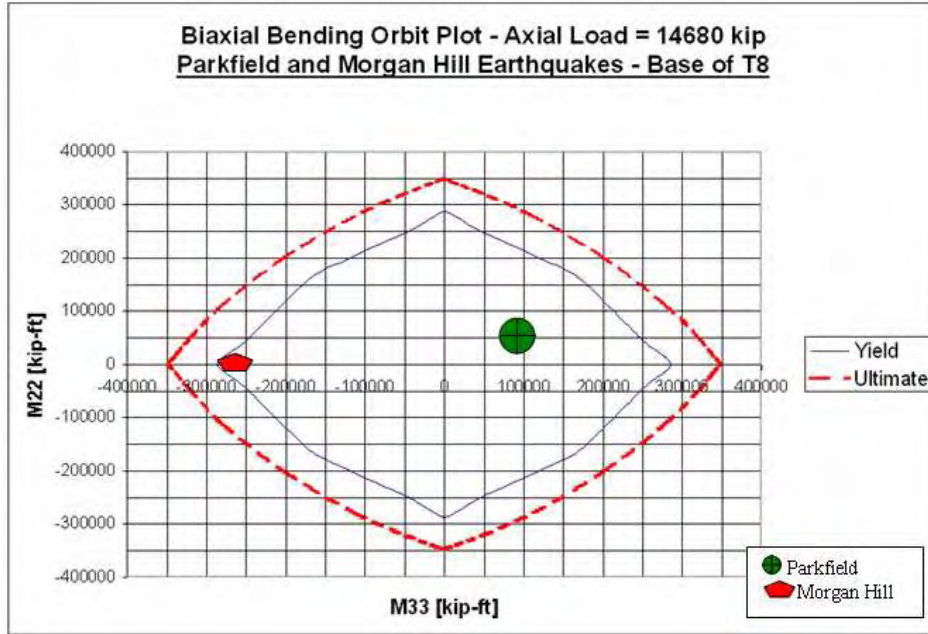


Figure 8.45. Orbit plot for base of tower T8– Third run

8.5.2 Elastic Criterion at All Tower Segments – Third Run

Note from Table 8.16 that the Parkfield record is able to meet the elastic criterion in all the tower segments while the Morgan Hill record shows failure of the top two segments as was the case for the Artificial earthquake. The top two segments are quite clearly the weak links in the towers.

Table 8.16. Maximum moments recorded at the bottom of each tower segment

Section	Yield Capacity [kip-ft]	Parkfield-Sta097		Morgan Hill - Gilroy6	
		M_max [kip-ft]	Yield Pass or Fail	M_max [kip-ft]	Yield Pass or Fail
TSEC1	20220	14440	Pass	32900	Fail
TSEC2	35530	20440	Pass	38240	Fail
TSEC3	73320	26000	Pass	50010	Pass
TSEC4	125400	56400	Pass	103400	Pass
TSEC5	191300	53340	Pass	165000	Pass
TSEC6	285700	97100	Pass	275900	Pass

8.5.3 Likelihood of Tower Collapse – Third Run

A comparison between Tables 8.16 and 8.9 shows that all the values in Table 8.16 are lower, therefore, Parkfield and Morgan Hill meet the collapse criterion in all tower segments.

8.6 Consideration of Shear Forces in the Towers

The minimum shear strength of concrete is given by the following equation:

$$\phi V_c = \phi 2\sqrt{f'_c}bd, \text{ where}$$

$$\phi = 0.65 \text{ (shear strength reduction factor) [adim]}$$

$$f'_c = 3,000 \text{ (concrete compressive strength) [psi]}$$

$$b = \text{width of the cross section [in]}$$

$$d = \text{effective height of the cross section [in]}$$

The area “ bd ” may be conservatively taken as the area of the “web” of the tower’s cross section, i.e., “ b ” is equal to 6 ft = 72 inches in all cases and “ d ” is the effective height of each of the tower segments (TSEC1, TSEC2, etc.). Table 8.17 shows the data and the results of the calculations for the concrete shear capacity. It also shows the maximum shears recorded in all the segments of tower T8 for the probable earthquakes (Parkfield, Morgan Hill and Artificial) as well as for the improbable earthquakes considered in this chapter (scaled and unscaled San Salvador and Northridge). The shear steel reinforcement has been ignored as a conservative assumption.

Table 8.17 Shear capacity and shear forces in the concrete towers

Section	b [in]	d [in]	Phi*Vc [kip]	Max Shear Force (Probable earthquakes) [kip]	Max Shear Force (Improbable earthquakes) [kip]
TSEC1	72	97	497	52	140
TSEC2	72	145	743	290	994
TSEC3	72	205	1051	340	1020
TSEC4	72	277	1420	632	1747
TSEC5	72	349	1789	745	2387
TSEC6	72	421	2158	1036	3110

As can be observed from Table 8.17, the concrete shear capacity is sufficient to meet the shear demands from the probable earthquakes. Consideration of the steel shear reinforcement capacity, as well as the contribution of the transverse concrete section, could increase the shear capacity of the sections (particularly the upper sections) so as to meet the demands of even the improbable earthquakes. Since it has been shown that the moment capacity is exceeded for the improbable earthquakes, this calculation will not be pursued.

8.7 Consideration of Cable Failure

The allowable breaking strength of the cables, obtained from the drawings, and the maximum tensions experienced by the cables during the seismic motions are included in Table 8.18. Since the breaking strength of the cables is comfortably above the maximum tensions experienced during the earthquakes, the cables are not a concern.

Table 8.18. Cable breaking strength and maximum tensions

Cable Description	Nominal Tension (Dead Load Only) [kip]	Max Tension Variation (Seismic Loading) [kip]	Max Total Tension [kip]	Breaking Strength [kip]	Factor of Safety [adim]
Main	480	175	655	1044	1.59
Auxiliary	602	217	819	1314	1.60
Backstay - Main	543	192	735	1212	1.65
Backstay - Auxiliary	728	234	962	1614	1.68
Tiedown	24	30	54	290	5.37

CHAPTER 9

Consideration of Retrofit Alternatives

The results from the last chapter show that any record with at least the same intermediate-period frequency content specified by the UBC 97 spectrum will result in plastic deformations of the upper two segments of the towers. This is a result of having only a single layer of 11#11 bars for those two segments. However, collapse is not likely unless the earthquake is very much stronger than specified in the code. This chapter initiates an investigation on retrofit alternatives. It serves as an introduction for a future investigation on this subject.

9.1 Retrofit Alternatives

Table 9.1 presents several retrofit alternatives with comments on their appropriateness for the Arecibo Observatory.

Table 9.1. Retrofit alternatives

Retrofit Alternative	Comments
Base isolation	Impractical. Free motion associated with base isolators is not tolerable for the observatory due to preciseness of instrumentation. Installation in Arecibo site is also impractical.
Dampers	Impractical. Damper systems interconnect portions of the structure which move relative to each other. The single-column towers do not provide for practical interconnections.
Tuned mass dampers	Impractical to place a tuned mass damper at the top of the towers
External post tensioning	Possible. However, the anchorage of the tendons will be subjected to very high forces. The tendons will also be subject to corrosion attack and thermal strains.
Steel plate bonding	Possible. Works as a steel jacket that strengthens the towers. However, the exposed steel plates are prone to corrosion attack including at the epoxy-steel interface which may affect the bond strength. Kachlakev (1998) indicates that European research studies have shown that the most critical failure mode was bond failure accompanied by separation of the plate from the concrete.
Adding cables at different heights	Possible. The addition of cables would stiffen the towers and will tend to diminish the large bending moments generated in the towers. It is the same concept used for guyed radio towers. However, the cables will spread over a large area and may interfere with the primary reflector. Relatively large concrete anchorages will be required for the cables.
Additional reinforcement	Possible. Additional rebars may be placed on the exterior of the tower cross sections as an additional layer and covered with concrete. The steel rebars are protected from corrosion attack by the concrete. Represents conventional technology. Concrete may be cast or sprayed.
Fiber Reinforced Polymers (FRP)	Possible. Unidirectional FRP strips or sheets may be bonded to the exterior of the tower cross sections to strengthen and stiffen the towers. The 7,350 ft span Jamestown-Verrazano bridge over the Narragansett Bay In Rhode Island completed a retrofit in Feb. 2006. Very low inertia is ideal for seismic applications. FRP represents advanced technology. Cost may be too high.

The most promising alternatives from Table 9.1 are the use of additional reinforcement bars covered with cast or sprayed concrete, and the use of FRP materials. Both would be placed on the exterior faces of the towers.

9.2 Feasibility of Retrofitting with Additional Reinforcement

Rebars would be placed adjacent to the 6 ft wide faces of the cruciform shape as shown schematically in Figure 9.1.

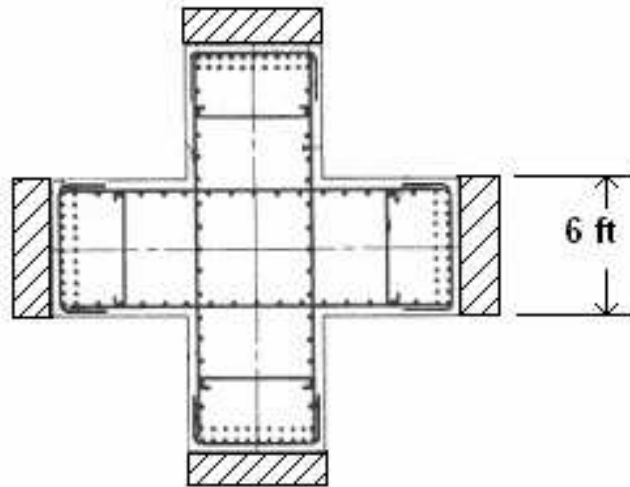


Figure 9.1. Schematic of reinforced areas (hatched zones)

This section may be modeled with the program XTRACT to obtain the retrofitted section capacity. Sections TSEC1 (top of all towers) and TSEC4 (base of towers T4 and T12) were modeled assuming a 12 inch concrete cover with a layer of 11#11 bars placed in the middle. The original section specifies the same arrangement; however, the additional layer is modeled with a yield strength equal to 60 ksi. The original rebar has a specified yield strength of 40 ksi.

Since the objective of this analysis is to determine feasibility of the proposal, it is assumed that the bending moments will be equal to those obtained with the original model.

Figure 9.2 shows the orbit plot at ultimate strength of section TSEC1. An axial force of 3610 kip is used which represents the reaction to dead loading only. The worst combinations of moments due to the unscaled San Salvador-CIG and Northridge-Castaic earthquake records, as well as the Morgan Hill and the Artificial accelerograms are superimposed in Figure 9.2. The figure shows that the unscaled San Salvador earthquake still does not meet the collapse criterion. The Morgan Hill seismic input barely meets the criterion. The alternative of retrofitting with additional rebars is barely feasible just from a technical standpoint because the additional layer of 11#11 barely increases capacity.

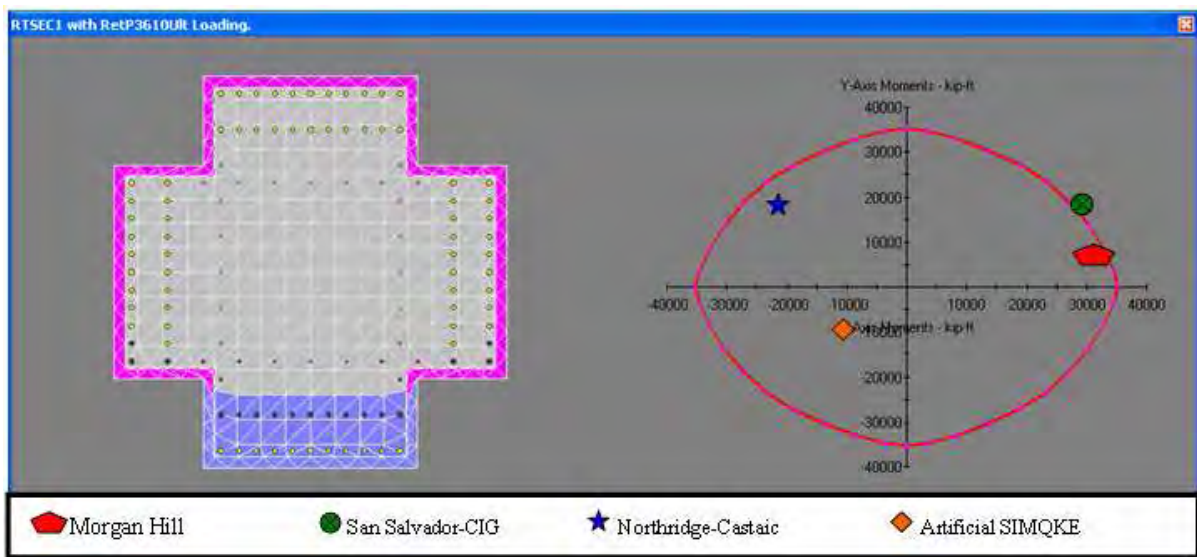


Figure 9.2. Orbit plot (at ultimate) of retrofitted TSEC1 with additional rebars

The next-to-last upper segment (TSEC2) will probably also show a modest increase in capacity with the additional layer of 11#11 bars. Rather than examining segment TSEC2, section TSEC4 which represents the base of towers T4 and T12 will be considered.

Figure 9.3 shows the orbit plot (at yield) of section TSEC4. An axial force of 9460 kip is used which corresponds to the worst loading condition for this section (San Salvador earthquake at the base of T12). Note that the capacity is still very much below the demands placed by both the unscaled San Salvador and Northridge earthquakes. If the intent were to increase the capacity significantly beyond the UBC-97 code (to comfortably assure elastic behavior), this retrofit scheme would be inadequate.

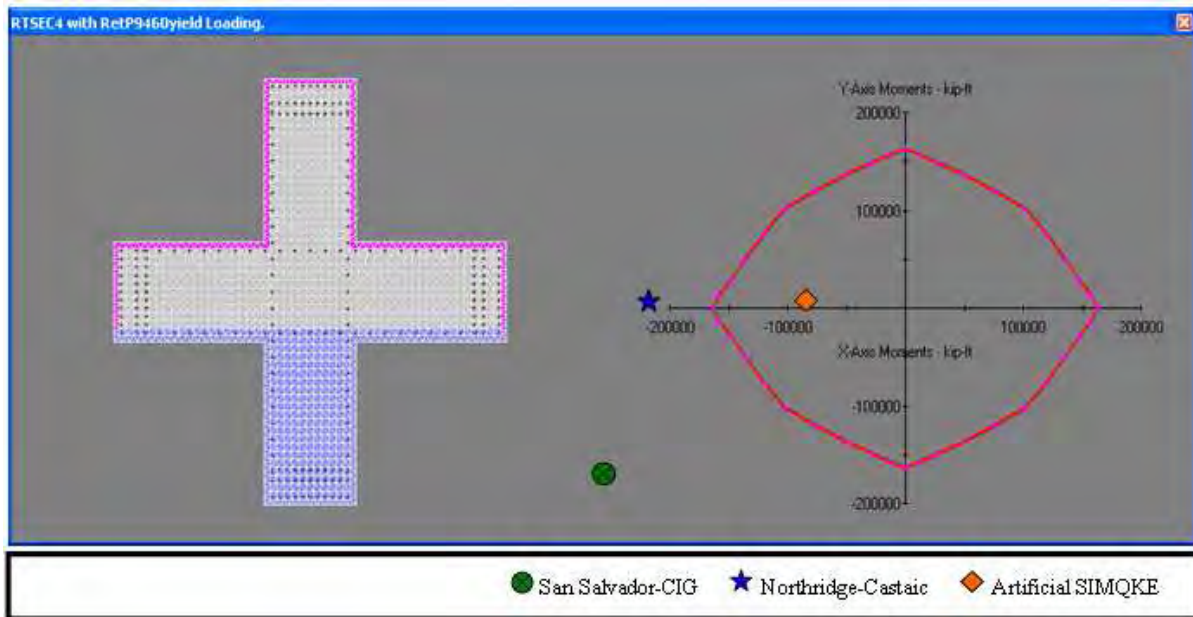


Figure 9.3. Orbit plot (at yield) of retrofitted TSEC4 with additional rebars

9.3 Feasibility of Retrofitting with Fiber Reinforced Polymer (FRP)

It was shown in the previous section that adding a layer of 11#11 rebars of $f_y = 60$ ksi barely provides enough boost for the top section (TSEC1) to meet the demands of the Morgan Hill earthquake which is one of the probable earthquakes for the Arecibo Observatory. The same scheme at the bottom of towers T4 and T12 is completely inadequate to meet demands from very strong earthquakes such as San Salvador. Additional layers of rebars could be considered but the inertia of the structure will start changing substantially and should be taken into account. Still, that scheme does not seem capable of achieving a 2x to 3x boost in capacity if the desire was to meet the San Salvador earthquake demand. The only feasible alternative seems to be the use of FRP.

An additional simulation was carried out with the program XTRACT. The original section was modified and the concrete cover was reassigned using the properties of carbon fiber. The yield stress was augmented to 400 ksi and the modulus of elasticity was also increased to 43000 ksi (Kachlakev 1998). The thickness of the cover was reduced from 4 inches to only 1/16 inch to simulate a sheet wrapping of the material. This simulation assumes that the FRP is wrapped around the entire perimeter of the cross section.

As shown in Figure 9.4 the capacity at yield increases by the required factor of approximately 3x and the demand of the San Salvador earthquake is met.

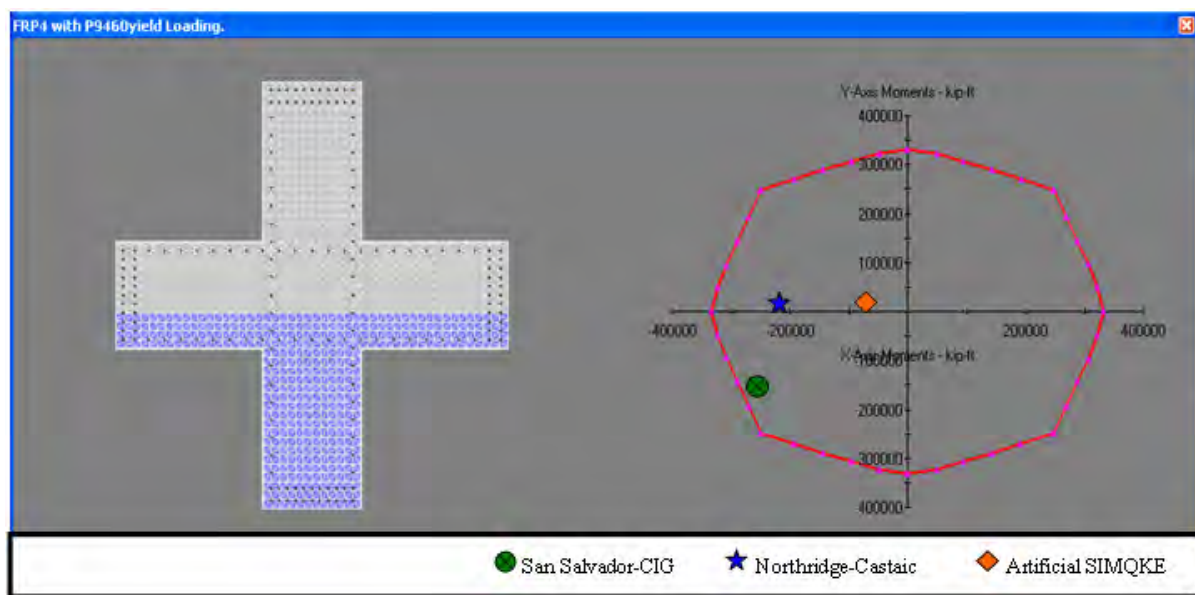


Figure 9.4. Orbit plot (at yield) of retrofitted section TSEC4 with FRP all-around wrap

9.4 Summary

The work on this chapter shows that wrapping with FRP layers has the potential to boost the bending capacity of the towers to very comfortable levels. Elastic response would be assured even for the improbable cases represented by the unscaled San Salvador-CIG and Northridge-Castaic records. Additional studies are required to continue investigating and optimizing this possibility.

CHAPTER 10

Conclusions and Recommendations

All the objectives listed in Chapter 1 have been met. These are:

1. To create a three-dimensional finite element model of the Arecibo Observatory capable of revealing the dynamic properties and the seismic response of this unique structure. This includes the establishment of the deformed equilibrium state due to dead load which serves as the basis from which all further studies are performed.

Three basic finite element models of increasing complexity were built. The models were thoroughly validated at all stages to assure reliability of results. The establishment of the deformed equilibrium state due to dead load was achieved using the nonlinear p-delta analysis option of SAP2000. The process was iterative. Three criteria had to be met after the dead load was applied: 1.) Verticality of towers, 2.) Correct platform elevation, and 3.) Correct tensions in the cables. Sensitivity studies revealed the natural response is not very sensitive to preload values in the cables once the dead load is applied. It was shown that the model responds linearly, as predicted by the literature that documented the behavior of cable-stayed bridges and suspension bridges, two similar types of structures. The results of this investigation into the unique structure of the Arecibo Observatory should be publishable in, among others, the Journal of Bridge Engineering, a transaction journal by the American Society of Civil Engineers which provided much of the literature used for this investigation.

2. To determine the dynamic properties (mode shapes and natural periods) of the Arecibo Observatory using computational experiments.

In this investigation three different types of modes were uncovered. These are platform modes, tower modes and cable modes. Results for each type of mode were given for the three models used in the investigation. In addition, the investigation revealed strong interactions between these modes. Based on the magnitudes of the modal participation mass

ratios it was found that the strongest interactions occur when towers T4 and T12 are in first mode while tower T8 is approaching its 2nd mode of vibration. The platform exhibits very strong rotation about its vertical axis or very strong rotation about its centroidal N-S axis depending on whether towers T4 and T12 are vibrating in-phase or out-of-phase. Several of these types of interaction modes are grouped together in the range of periods between 1.8 seconds down to 0.7 seconds. Model B, which includes tiedown cables and models the platform as two equilateral triangles, was modified to include the service cables, the pedestrian bridge and the cable-car cable, and the results confirm that these components are effectively decoupled from the platform. The modes obtained from this phase of the investigation were used to run transient time-history modal analysis with acceleration records from various world-wide recorded earthquakes.

3. To computationally determine the bending moments and forces at the towers, and the tension in the cables, due to maximum-probable earthquakes expected at the site of the Arecibo Observatory.

In the absence of strong motion acceleration records for Puerto Rico, this investigation used earthquake records recommended by Irizarry (1999) and Llop (2002) as well as an artificial earthquake accelerogram compatible with the UBC-97 Zone 3, Rock Type Sb design spectrum. The unscaled 1986 San Salvador – CIG station record and the 1994 Northridge – Castaic station record, recommended for Mayaguez and Ponce, are used as upper-bound cases. Scaled versions of these records (to 0.3g PGA) were also considered. In addition, the study considered a record from the 1966 Parkfield earthquake that represents the seismic hazard for San Juan. Finally, a record from the 1984 Morgan Hill earthquake is considered, as recommended by Llop (2002) for the Dos Bocas and the Guajataca Dams which are very near the observatory.

4. To determine if the towers are capable of resisting the maximum-credible earthquake demands in the elastic regime. This stringent requirement (maintaining the elastic regime) is based on the required positional accuracy of the instrumentation housed in the suspended platform. Plastically deformed towers would result in misalignment of

the instrumented platform and would defeat the scientific mission of the Arecibo Observatory. As a result, the towers shall be considered an integral component of the precise instrumentation systems used for astronomic and ionosphere research. The possibility that reinforcement-development lengths may be inadequate according to present structural codes will be addressed. Additionally, in the instance that the elastic criterion is not met, a preliminary analysis to investigate the likelihood of collapse of the towers will be performed.

From the UBC-97 code calculations it was determined that the 5 ft lap splices of the main reinforcement provide an adequate development length in both the linear as well as nonlinear (plastic deformations) regime of the towers.

It was shown that the towers of the Arecibo Observatory are capable of elastically resisting a code-level earthquake record, except for the two top segments of the towers. The top two segments are likely to plastically deform if exposed to the intermediate-period content of a code-specified seismic input. The only record (of the five considered) that passed the elastic criterion in all the tower segments was Parkfield which has a very low intermediate-period content. For stronger, though improbable earthquakes such as San Salvador-CIG and Northridge-Castaic, all the segments of the towers would undergo plastic deformations. In addition, the upper two segments might collapse. These two cases were run as upper-bound cases. Similar records (scaled to 0.3g PGA) of very strong earthquakes such as Loma Prieta, El Centro and Kocaeli, as well as the scaled down records of San Salvador-CIG and Northridge-Castaic, were also shown to place demands on the towers which they can not meet elastically. For the scaled versions of San Salvador-CIG and Northridge-Castaic, collapse is not predicted. Further studies in the nonlinear regime of the materials would be interesting since the higher modes of the towers are activated. The modeling of the plastic deformations of the towers in the 3rd or 4th mode of vibration should be a worthy research project.

5. To consider, if necessary, alternatives for retrofitting the structure and to conduct preliminary feasibility studies to determine appropriateness of the most promising alternatives.

Several retrofit alternatives were considered of which only two were deemed feasible. These are the addition of steel reinforcement bars with a new concrete cover, and the use of Fiber Reinforced Polymers (FRP) wrapping. Regarding the first alternative, a preliminary analysis showed that an additional layer of 11#11 bars of grade 60 steel reinforcement barely meets the collapse criterion at the uppermost segment of the towers and fails by a wide margin to satisfy the elastic criterion at the base of tower T12 for the upper-bound case of the San Salvador-CIG and Northridge-Castaic records. FRP wrapping, on the other hand, was preliminarily shown to be the only choice capable of satisfying the demands of the unscaled San Salvador-CIG record at the base of tower T12. The analysis considers wrapping the entire perimeter of the lowest tower segment with 1/16" thick carbon fiber wrap. These preliminary results should be extended with further research into the capacity, durability and cost of the FRP option.

6. To recommend the location of accelerometer transducers in the structure for a future research study being planned by Dr. José Martínez-Cruzado, Director of the Strong Motion Program and member of the graduate committee.

Several interesting investigations could be performed with the gathered data, and each investigation depends on the location where the accelerometers are placed. Some of these research possibilities were presented in the thesis to provide a context upon which to base the recommendations. First of all, the triaxial accelerometer type was recommended at all locations since all the strong motion records researched during this investigation invariably contained three orthogonal directions. By generating data in three orthogonal directions, the records from Puerto Rico would join world-wide earthquake record databases on equal terms. In the context of an investigation regarding soil structure interaction, the hill on which tower T12 is founded was selected as the optimal platform. An accelerometer should be placed on the tower foundation and another grounded on rock approximately two hundred feet away near the access road to the pedestrian bridge. If, as expected, there is negligible soil-structure interaction, then the two records should be nearly identical. This would validate the fixed-tower-base assumption used in this work. For research on topographic amplification effects in karstic geology, an additional accelerometer should be placed at a convenient spot near the

base of the same hill. If the topographic effect is negligible, the records from the base as well as from the top of the hill (away from foundation) should be nearly identical. Otherwise, the record from the top of the hill should be in an amplified state. For experimental research on the fundamental periods of the towers, the ideal location for accelerometer placement is at the top of the towers where the largest displacements take place. For additional experimental research on the higher modes and natural periods of the towers, accelerometers should be placed at each step of the towers. These would provide excellent data to plot and validate several of the higher flexural modes of the towers predicted by the finite element model. In addition, negligible differences in the up-down records at each step would confirm the minimal response in the vertical (axial) direction predicted by the finite element models. Finally, accelerometers placed at each corner of the platform would shed light on the response of the platform and could be used to validate the platform modes predicted by the finite element model.

REFERENCES

- Astaneh-Asl, A., and Gary Black, R. (2001). "Seismic and Structural Engineering of a Curved Cable-Stayed Bridge", *Journal of Bridge Engineering*, ASCE, Vol. 6, No. 6, November/December. pp. 439-450.
- Button, M.R., Cronin, C.J., and Mayes, R.L. (2002). "Effect of Vertical Motions on Seismic Response of Highway Bridges", *Journal of Structural Engineering*, ASCE, Vol. 128, No. 12, December. pp. 1551-1564.
- Chang, C.C., Chang, T.Y.P., and Zhang, Q.W. (2001). "Ambient Vibration of Long-Span Cable-Stayed Bridge", *Journal of Bridge Engineering*, ASCE, Vol. 6, No. 1, January/February. pp. 46-53.
- Chopra, A. (2000). *Dynamics of Structures, Theory and Applications to Earthquake Engineering*, 2nd edition, Prentice Hall.
- Cook, R.D. (2002). *Concepts and Applications of Finite Element Analysis*, 4th edition, John Wiley & Sons.
- Cunha, A., Caetano, E., and Delgado, R. (2001). "Dynamic Tests on Large Cable-Stayed Bridge", *Journal of Bridge Engineering*, ASCE, Vol. 6, No. 1, January/February. pp. 54-62.
- Dames & Moore (1999). "*Probabilistic Seismic Hazard Analysis of Puerto Rico and Recommended Revisions to the Seismic Coefficients of the ANSI/ASCE 7-95 Standard*", Final Report, D&M Job No. 39150-001-004. 500 Market Place Tower, 2025 First Avenue, Seattle, Washington 98121
- El-Tawil, S. and Kuenzli, C. (2002). "Pushover of Hybrid Coupled Walls. II Analysis and Behavior", *Journal of Structural Engineering*, ASCE, Vol. 128 No. 10, October. pp. 1272-1281.
- Fleming, J.F. (1979, cited from Ren, 1999b). "Nonlinear Static Analysis of Cable-Stayed Bridge Structures", *Computers and Structures*, Vol. 10, No. 4. pp. 621-635
- Fleming, J.F., and Egeseli, E.A. (1980, cited from Chang, 2001). "Dynamic Behavior of a Cable-Stayed Bridge", *Earthquake Engineering and Structural Dynamics*, Vol. 8. pp. 1-16.
- Hangai, Y. and Wu, M. (1999). "Analytical Method of Structural Behaviours of a Hybrid Structure Consisting of Cables and Rigid Structures", *Engineering Structures*, Elsevier, Vol. 21. pp. 726-736.
- Irizarry, J. (1999). "*Design Earthquakes and Design Spectra for Puerto Rico's Main Cities Based on Worldwide Strong Motion Records*", MS Thesis, University of Puerto Rico, Mayagüez, PR.

Jansma, P.E. and Mattioli, G.S. (2002). “GPS Results from Puerto Rico and the Virgin Islands: Constraints on Tectonic Setting and Rates of Active Faulting”, Proceedings of the American Geophysical Union Spring 2002 Conference, held at the Washington Convention Center, Washington D.C.,

Kachlakev, D. (1998). “*Strengthening Bridges Using Composite Materials*”, FHWA-OR-RD-98-08 Technical Report.
<http://www.oregon.gov/ODOT/TD/TP_RES/docs/Reports/StrengtheningBridgesUsingCom pMat.pdf>

Llop, E.L. (2002). “*Seismic Safety Assessment of a Typical Concrete Dam in Puerto Rico*”, MS Thesis, University of Puerto Rico, Mayagüez, PR.

Main, J.A., and Jones, N.P. (2002). “Free Vibrations of Taut Cable with Attached Damper. I: Linear Viscous Damper”, *Journal of Engineering Mechanics*, ASCE, Vol. 128, No. 10, October. pp. 1062-1071.

MacGregor, J.G. (1996). *Reinforced Concrete: Mechanics and Design*, 3rd edition, Prentice Hall

Mylonakis, G., Papastamatiou, D., Psycharis, J., and Mahmoud, K. (2001). “Simplified Modeling of Bridge Response on Soft Soil to Nonuniform Seismic Excitation”, *Journal of Bridge Engineering*, ASCE, Vol. 6, No. 6, November/December. pp. 587-597.

Nazmy, A.S. and Abdel-Ghaffar, A.M. (1990, cited from Ren, 1999b). “Three-Dimensional Nonlinear Static Analysis of Cable-Stayed Bridges”, *Computers and Structures*, Vol. 34, No. 2, pp. 257-271.

Reddy, J.N. (1993). *An Introduction to the Finite Element Method*, 2nd edition, McGraw Hill

Ren, W.X. (1999a). “Ultimate Behavior of Long-Span Cable-Stayed Bridges”, *Journal of Bridge Engineering*, ASCE, Vol. 4, No. 1, February. pp. 30-37.

Ren, W.X., and Obata, M. (1999b). “Elastic-Plastic Seismic Behavior of Long Span Cable-Stayed Bridges”, *Journal of Bridge Engineering*, ASCE, Vol. 4, No. 3, August. pp. 194-203.

Ren, W.X., Chen, G., and Hu, W.H. (2005). “Empirical formulas to estimate cable tension by cable fundamental frequency”, *Journal of Structural Engineering and Mechanics*, Vol. 20, No. 3. pp. 363-380

Roebeling (1997). “*Suspension Bridge Technical Data*”,
<<http://www.inventionfactory.com/history/RHAbridg/sbtd>>

Salmon, C.G. and Johnson, J.E. (1996). *Steel Structures: Design and Behavior*, 4th edition, Harper Collins.

Vázquez, D. (2003). “*Seismic Behavior and Retrofitting of Hillside and Hilly Terrain R/C Houses Raised on Gravity Columns*”, PhD Thesis, University of Puerto Rico, Mayagüez, PR.

Volokh, K.Y., Vilnay, O. and Averbuh, I. (2003). “Dynamics of Cable Structures”, *Journal of Engineering Mechanics*, ASCE, Vol. 129, No. 2, February. pp. 175-180.

Wilson, E. (2000). “*Geometric Stiffness and P-Delta Effects*”,
<http://www.csiberkeley.com/support_technical_papers.html>

Xu, Y.L., Ko, J.M., and Zhang, W.S. (1997). “Vibration Studies of Tsing Ma Suspension Bridge”, *Journal of Bridge Engineering*, ASCE, Vol. 2, No. 4, November. pp. 149-156.

Zhang, Q.W., Chang, T.Y.P, and Chang, C.C. (2001). “Finite-Element Model Updating for the Kap Shui Mun Cable-Stayed Bridge”, *Journal of Bridge Engineering*, ASCE, Vol. 6, No. 4, July/August. pp. 285- 293.